Reconfigurable Wearable Antennas for Body-Centric Communications

by

Quoc Hung Dang

B. Eng. (Electrical & Electronic Engineering),
Le Quy Don Technical University, Vietnam, 2010
M. Eng. (Electronic Engineering),
The University of Adelaide, Australia, 2018

Thesis submitted for the degree of

Doctor of Philosophy

in

School of Electrical & Electronic Engineering
Faculty of Engineering, Computer & Mathematical Sciences
The University of Adelaide

2022

Supervisors:
Prof. Christophe Fumeaux
School of Electrical & Electronic Engineering, The University of Adelaide

Dr. Shengjian Jammy Chen
School of Electrical & Electronic Engineering, The University of Adelaide
College of Science and Engineering, Flinders University

Assoc. Prof. Damith Chinthana Ranasinghe
School of Computer Science, The University of Adelaide

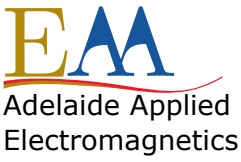

THE UNIVERSITY of ADELAIDE

To my better half, Hoang Anh
my son (BFF) Nhat Quang, my little princess Chau Anh
with all my love.

Contents

Abstract

IN the last two decades, wireless body area networks (WBANs) have seen a rapid development to support a wide range of applications in our daily life. Fostered by this development, wearable textile antennas, as potential components of such networks, have attracted more and more research interests. Furthermore, several practical realizations of reconfigurable wearable antennas have been proposed aiming to maintain the required antenna performance of flexible devices under disadvantageous conformal conditions and changing operating environments. In this context, a number of reconfigurable wearable antennas, as well as several passive wearable antennas with additional functionalities, are proposed in this thesis. These designs will be presented in three main parts.

The first main part of the dissertation will discuss the techniques and components used to realize reconfigurable wearable antennas. Starting with Chapter 3, the pros and cons of four different shorting strategies realized using standard components in wearable antenna designs are investigated. The comparison between these four shorting methods is conducted comprehensively aiming at guiding designers in selection of the most appropriate shorting method for their specific application. Chapter 4 proposes a novel reconfiguration module to provide a stable and repeatable electrical connection between rigid electronics and flexible textile conductors in a coplanar arrangement.

Chapter 5 through Chapter 7 form the second main part of the thesis, which focuses on reconfigurable wearable antenna designs utilizing the proposed techniques and components. A wide range of reconfigurable wearable antennas is proposed in this part including frequency-, radiation pattern- and polarization-reconfigurable antennas. The chapter also includes reconfigurable wearable antennas designed with the combination of these tunability. The proposed antennas have significant improvement in their versatility compared to passive wearable antennas reported in the literature. More importantly, the practicability of the proposed antennas is successfully demonstrated.

The last main part of the thesis presents wearable antennas integrated with radio frequency identification (RFID) sensor modules. Chapter 8 proposes a wearable textile antenna with a computational battery-less RFID module fully integrated in the antenna cavity. The antenna and the RFID module form a complete device which is

demonstrated to work well in practical situations. In Chapter 9, a dual-band reconfigurable ultra high frequency (UHF) wearable antenna and a dual-band dual-port reconfigurable textile antenna for wearable UHF applications are presented.

In summary, this dissertation provides new concepts, techniques and components to design reconfigurable wearable antennas. Based on the proposed techniques and components, a wide range of novel reconfigurable wearable antennas with promising practicability are presented.

Originality Declaration

I certify that this work contains no material which has been accepted for the award of any other degree or diploma in my name, in any university or other tertiary institution and, to the best of my knowledge and belief, contains no material previously published or written by another person, except where due reference has been made in the text. In addition, I certify that no part of this work will, in the future, be used in a submission in my name, for any other degree or diploma in any university or other tertiary institution without the prior approval of the University of Adelaide and where applicable, any partner institution responsible for the joint award of this degree.

The author acknowledges that copyright of published works contained within the thesis resides with the copyright holder(s) of those works.

I give permission for the digital version of my thesis to be made available on the web, via the University's digital research repository, the Library Search and also through web search engines, unless permission has been granted by the University to restrict access for a period of time.

Signed

Date

Acknowledgments

This doctoral thesis would not have been possible without many people, who have supported and encouraged me during my doctoral journey.

"The mediocre teacher tells, the good teacher explains, the superior teacher demonstrates, the great teacher inspires" (William Arthur Ward, an American motivational writer). I have understood this statement thoroughly since I had an opportunity to meet and work with Prof. Christophe Fumeaux. He has become my inspiration to pursue the antenna research field with a great enthusiasm. It was a pleasure to have Prof. Christophe Fumeaux as a supervisor of my Master thesis in Electronic Engineering at the University of Adelaide. He accepted me as his Ph.D student after I successfully completed the master course, which has changed my life forever. Prof. Christophe Fumeaux, with his profound and comprehensive knowledge in electromagnetic and microwave systems, always knew ways to encourage and support me to overcome various challenges during my Ph.D candidature. I have not ever had a supervisor/teacher who is responsible, approachable, and supportive as Prof. Christophe Fumeaux. His guidance led me to go deeper on every research topic to gain as much knowledge as possible before solving any problem or issue. Moreover, his adorable attitude and great passion in researching is a model and a motivation for me to work harder each day. Although words cannot express my appreciation and gratitude for Prof. Christophe Fumeaux, I still want to express my deepest acknowledgment for his selfless supports and encouragement to me during my research journey.

I would like to express my extreme gratitude to Dr. Shengjian Jammy Chen, my co-supervisor who has also greatly assisted me to build the very first bricks for my research journey since I started up with my Master project to become a researcher. With his outstanding research knowledge in electromagnetic and antennas, he encouraged me with numerous novel ideas to improve my designs. I was always able to head to his office to seek for his advice and discussion on any issue, not only in research, but also in my life. Thus, I could say that my PhD candidature would not be undertaken without his extensive supports.

Since one of the main focuses of my thesis is on practicability of wearable antenna, Assoc. Prof. Damith Chinthana Ranasinghe provided invaluable guidance in most of my

designs which demonstrated his comprehensive knowledge on the relation between wearable antenna and RFID-base applications. His critical comments and suggestions developed my confidence to improve my designs to the highest practical quality. I am grateful to be a student of Assoc. Prof. Damith Chinthana Ranasinghe.

Additionally, I would like to acknowledge the office and academic staffs of the School of Electrical & Electronic Engineering for their excellent supports during my Ph.D candidature. I specially thank Mr. Alban O'Brien who patiently helped me to transform all "tricky" designs from ideas to reality. I am also thankful for Mr. Norio Itsumi and Mr. Danny Di Giacomo for their prompt support and assistance on fabrication and material or- dering. I would also like to acknowledge the school staffs who enthusiastically facilitated my PhD course, namely Assoc. Prof. Wen Soong, Prof. Nelson Tansu, Mr. David Bowler, Ms. Laura McNamara and Ms. Tayla Allison.

Furthermore, I would like to give thanks to all members in the Applied Electromagnetic Group and Terahertz Engineering Laboratory at the University of Adelaide, including Dr. Withawat Withayachumnankul, Dr. Nghia Nguyen-Trong, Dr. Sree Pramod Pinapati, Dr. Weijie Gao, Dr. Seyed-Ali Malakooti, Dr. Siti Nailah Mastura Zainarry, Dr. Xiaolong You, Dr. Xiaojing (Alex) Lv, Dr. Morteza Shahpari, Mr. Purna Bdr. Samal, Mr. Xiaoyang Yin, Mr. Baoqi Zhu, Ms. Grace Yuan. I would like to send a special thanks to Dr. Withawat Withayachumnankul who always gave me critical comments and feedbacks throughout my candidature where I could earn and learn from his deep knowledge in electromagnetics, microwave and terahertz engineering.

I sincerely acknowledge the financial support from the University of Adelaide with Adelaide Graduate Research Scholarship, without this I would not have been able to take the Ph.D study. I was grateful to the School of Electrical & Electronic Engineering, the University of Adelaide for the annual travel grant; and it was also great a honor to me to receive the IEEE AP-S C. J. Reddy Travel Grant for Graduate Students from the IEEE Antennas and Propagation Society. Thanks to these financial supports, I was enabled to attend national and international conferences, had chances to communicate and exchange knowledge and experience with experts in the field.

I would like to send the greatest appreciation to my parents who have been unconditionally loving and supporting for all my decisions. I am also grateful to my parents-in-law who have always treated me as their biological son and offered me as much support as they can. I would not have been me today as a PhD researcher without

them. I also want to extend sincere thanks to my sister, who has supported me and my young family.

My special love goes to my son (my BFF), **Nhat Quang**, who has always been joyfulness and motivation for me to overcome all difficulties in work and life. My big love is sent to my daughter, **Chau Anh** who gives me strength to fight for my dreams.

Lastly, my endless loves and appreciation go to the most important person in my life, my wife **Hoang Anh**. She has brought out the best in me, given me strength by supporting and standing by me through all my ups and downs. She was the only one who always says: "I believe you can do it, honey", the words that have opened and motivated for all of my successes. Our journey together is fantastic, wherever it is, she is my destination after all.

Quoc Hung Dang
July 2022
Adelaide, Australia

Thesis Conventions

The following conventions have been adopted in this Thesis:

Typesetting

This document was compiled using LaTeX2e. TeXstudio is used as text editor interfaced to LaTeX2e. Inkscape was used to produce schematic diagrams and other drawings.

Referencing

The referencing and citation style adopted in this thesis are based on the Institute of Electrical and Electronics Engineers (IEEE) Transaction style.

System of units

The units comply with the international system of units recommended in au Australian Standard: AS ISO 1000-1998 (Standard Australia Committee ME/71, Quantities, Units and Conversions 1998).

Spelling

American English spelling is adopted in this thesis.

Abbreviation

CW	Continuous Waveform
CPW	Coplanar Waveguide
EBG	Electromagnetic Band-Gap
EM	Electromagnetic
HMSIW	Half-Mode Substrate-Integrated Waveguide
ISM	Industrial, Scientific and Medical
IC	Integrated Circuit
IoT	Internet of Things
LP	Linear Polarization
PCB	Printed Circuit Board
PDMS	Polydimethylsiloxane
PIFA	Planar Inverted-F Antenna
RF	Radio Frequency
RFID	Radio Frequency Identification
UWB	Ultra-Wide Band
SIW	Substrate Integrated Waveguide
WBAN	Wireless Body Area Network
WISP	Wireless Identification and Sensing Platform
W^2**ISP**	Wearable Wireless Identification and Sensing Platform

Awards and Scholarships

2022

- Best Student Paper Award, 2022 International Symposium on Antennas and Propagation (ISAP 2022)
- IEEE AP-S C. J. Reddy Travel Grant for Graduate Students

2021

- Applied Electromagnetics Industrial Supplementary Scholarship, The University of Adelaide

2019

- ARC Grant Funded Supplementary Scholarship, The University of Adelaide

2018

- Adelaide Graduate Research Scholarship, The University of Adelaide

Publications

Journal Articles

Q. H. Dang, S. J. Chen, D. C. Ranasinghe, and C. Fumeaux, "Modular integration of a passive RFID sensor with wearable textile antennas for patient monitoring," *IEEE Trans. Components, Packag. Manuf. Technol.*, vol. 10, no. 12 pp. 1979 – 1988, 2020.

Q. H. Dang, S. J. Chen, D. C. Ranasinghe, and C. Fumeaux, "A frequency-reconfigurable wearable textile antenna with one-octave tuning range," *IEEE Trans. Antennas Propag.*, vol. 69, no. 12 pp. 8080 – 8089, Dec. 2021.

Q. H. Dang, S. J. Chen, B. Zhu, and C. Fumeaux, "Shorting strategies for wearable textile antennas: a review of four shorting methods," *IEEE Antennas Propag. Mag.*, vol. 64, no. 1 pp. 84 – 98, Feb. 2022.

Q. H. Dang, S. J. Chen, D. C. Ranasinghe, and C. Fumeaux, "Dual-Band Reconfigurable Flexible Antenna with Independent Frequency Tunability," *IEEE Antennas Wirel. Propag. Lett.*, (Early Access, DOI: 10.1109/LAWP.2022.3217256).

Conference Articles

A. Jayatilaka, **Q. H. Dang**, S. J. Chen, R. Visvanathan, C. Fumeaux, and D. C. Ranasinghe, "Designing batteryless wearables for hospitalized older people," in *Proceedings of the 23rd International Symposium on Wearable Computers - ISWC '19*, pp. 91–95, Sep. 2019. **(Three first authors)**

Q. H. Dang, S. J. Chen, D. C. Ranasinghe, and C. Fumeaux, "A Reconfiguration Module with Coplanar Snap-On Connection for Wearable Textile Antennas," in *2019 Asia-Pacific Microwave Conference (APMC)*, pp. 12–14, Dec. 2019.

Q. H. Dang, S. J. Chen, D. D. Zhang, D. D. Kimtai, and C. Fumeaux, "Flexible substrate materials for wearable antennas," in *Australian Microwave Symposium, Sydney, Australia*, Feb. 2020.

Q. H. Dang, S. J. Chen, B. Zhu, and C. Fumeaux, "Dual-band dual-mode wearable textile antennas for on-body and off-body communications," in *2021 IEEE Asia-Pacific Microw. Conf.*, pp. 64–66, Nov. 2021.

S. J. Chen, **Q. H. Dang**, and C. Fumeaux, "Textile planar wideband omnidirectional antenna for wearable applications," in *2021 IEEE Asia-Pacific Microw. Conf.*, pp. 392–394, Nov. 2021.

Q. H. Dang, S. J. Chen, D. C. Ranasinghe, and C. Fumeaux, "Body-to-Antenna Gap Effect on a UHF Wearable Textile Antenna Performance," in *2021 IEEE Int. Symp. Antennas Propag. Usn. Radio Sci. Meet.*, pp. 1271–1272, Dec. 2021.

Q. H. Dang, S. J. Chen, and C. Fumeaux, "Thermographic Investigation of Frequency-Reconfigurable Wearable Antennas," in *Proc. 16th Eur. Conf. Antennas Propag., Madrid, Spain*, Mar. 2022.

Q. H. Dang, S. J. Chen, and C. Fumeaux, "Dual-Band Frequency-Reconfigurable Flexible Wearable Textile Antenna," in *2022 IEEE Int. Symp. Antennas Propag. Usn. Radio Sci. Meet., Denver, Colorado, USA*, Jul. 2022. **[IEEE AP-S C. J. Reddy Travel Grant for Graduate Students]**

Q. H. Dang, S. J. Chen, and C. Fumeaux, "Modular Wearable Textile Antenna with Pattern-Interchangeability using Snap-on Buttons," in *The 2022 International Symposium on Antennas and Propagation, Sydnet, Australia*, Oct. 2022. **[The Best Student Paper Award]**

Q. H. Dang, S. J. Chen, D. C. Ranasinghe, and C. Fumeaux, "Utilization of RF-switch ICs and PIN diodes in Reconfigurable Wearable Textile Antennas," in *2022 Asia-Pacific Microwave Conference (APMC)*, Dec. 2022 (Accepted for presentation).

Journal Articles in Preparation

Q. H. Dang, S. J. Chen, D. C. Ranasinghe, and C. Fumeaux, "Multi-Funtional Reconfigurable Wearable Textile Antennas using Coplanar Reconfiguration Modules," *IEEE Trans. Antennas Propag.*, in preparation for submission.

Q. H. Dang, S. J. Chen, D. C. Ranasinghe, and C. Fumeaux, "Dual-Band Dual-Port Reconfigurable Textile Antenna for Wearable UHF Applications," *IEEE Antennas Wirel. Propag. Lett.*, in preparation for submission.

List of Figures

List of Tables

Chapter 1

Introduction

THIS introductory chapter provides an overview of reconfigurable antennas in general and reconfigurable wearable antennas in particular. This includes the applications of reconfigurable wearable antennas, design strategies and challenges. An overview of the thesis objectives and motivation is then given, with a list of original contributions associated with the research work. The thesis outline is presented to conclude the chapter.

1.1 Introduction and motivation

Wearable antennas have attracted more and more interests from both industry and academia due to the increasing popularity of body-centric wireless communications. Various types of wearable antennas have been developed to satisfy the stringent requirements of the harsh on-body operating environment. To cope with the dynamic change of the human body in movement, numerous passive wearable textile antennas with noticeable characteristics of flexibility and light weight have been demonstrated in the recent literature [1–5]. Because of the growing requirements for multi-functional wireless communications, several additional functionalities have been added to passive wearable antennas to provide versatile modularity for various communications standards. These functionalities include but are not limited to operating in multi-band [6–9] or ultra-wide band [10–14] modalities. Furthermore, to keep the operation of wearable textile antennas stable in a dynamically changing body-centric wireless communications scenario, antennas with some degree of agility in their radiation property are desirable.

The recent literature has demonstrated a significant number of active components-based reconfigurable antennas which offered an agility in resonance frequency [15–17], radiation patterns [18–20], polarization [21–23] and combination of these reconfigurable characteristics [24–27]. However, these antennas were implemented on rigid material substrates which might be inappropriate for wearable applications. By contrast, there have been a very limited number of reconfigurable wearable textile antennas reported in the literature [28–30]. This is because wearable textiles antennas often need to satisfy more requirements of mechanical and electrical robustness, body-to-antenna isolation, easy-to-fabrication, than corresponding rigid antennas. The other crucial reason that limits the realization of reconfigurable wearable antennas is the challenge from realizing robust connections between the rigid active components and flexible conductive layers that form the basis of textile wearable antennas.

In the context of the stated challenges, several techniques and components to design reconfigurable wearable textile antennas will be discussed. After that, the dissertation will propose various passive and reconfigurable wearable antenna designs.

1.2 Objectives of the thesis

There are three main investigation areas in this thesis which are described in details in the following.

1. **Techniques and components for reconfigurable textile antennas**

   Microstrip antennas have been widely used since decades in many applications of our life such as health-care, sport and mobile communications [31–34]. This is because microstrip antennas usually exhibits advantageous characteristics such as low profile, low cost and mechanical robustness. In order to further expand the microstrip antennas' functionalities, several design methods have been reported in the literature including introducing slots, shorting vias or implementing reconfigurability through addition of tuning components. These design methods are usually convenient to implement in standard technologies for rigid-material-based antennas, for example by drilling and then metalizing the substrate to realize shorting vias, and/or by using soldering to assemble active components on the antennas aiming to provide reconfigurability. Nevertheless, in the context of wearable textile antennas, implementation of shorting methods or realization of robust connection between active components and conductive textile materials are challenging tasks. In this context, the first objective of this thesis is divided into two parts:

   (i) Several methods to implement a connection between wearable textile antenna conducting layers and their ground planes have been proposed in the literature such as embroidered walls [35, 36], folded strips of metalized fabric [28] and snap-on buttons [37]. However, a comprehensive analysis of pros and cons of these shorting methods has been lacking, especially in regards to simulation challenges, fabrication complexity, radiation performance, mechanical stability and modularity. As a result, the first part of this thesis area aims to investigate the strengths and weaknesses of four popular shorting methods used in wearable textile antenna designs, including embroidered vias, folded strips of metalized fabrics, eyelets, and snap-on buttons.

   (ii) As mentioned, there has been a challenge in realizing robust connections between lumped electronic passive and active components and textiles material to

be used in reconfigurable wearable textile antennas. There have been two methods reported in the literature to overcome this challenge which are using polydimethylsiloxane (PDMS) substrates to immobilize lumped components [29, 30] or utilization of a reconfiguration module [28]. In this second part of the first objective of this thesis, a novel reconfiguration module with coplanar snap-on connections is proposed for reconfigurable wearable textile antenna designs.

2. **Multifunctional wearable textile antennas**

   Flexibility, light weight and low cost are must-have characteristics that need to be considered while designing wearable antennas. Recently, in order to enhance the functionality of wearable antennas, reconfigurability has been increasingly considered to satisfy requirements of the raising complex of wireless communications systems. Nevertheless, the number of practical wearable antennas has still remained limited due to the challenges in realization of reconfigurability on textile materials. Based on the techniques and components presented in the first research area, the second objective of this thesis is to design several novel reconfigurable wearable antennas. The antennas included in this part not only can be agile in resonance frequency, but also radiation pattern and polarization.

3. **Passive RFID sensor integration with wearable antennas**

   Radio Frequency Identification (RFID) technology has become increasingly important in our daily life. Simple RFID chips can be found in numerous applications such as structural monitoring, item tracking and health care. RFID chips are usually integrated with their host antennas to communicate with an external reader system. However, for advanced functionalities in human activity monitoring where computational RFID modules are required, the integration of RFID modules with wearable antennas is challenging. There have been several methods reported in the literature to integrate the antenna and the electronics into a single package [38–40]. However, none of these solutions provide a secure protection for the electronic module which is crucial in a dynamically changing environment, as encountered in wearable applications. In this context, the third objective of the dissertation is to propose a novel integration method to completely incorporate a bulky battery-less computational RFID module inside the resonant cavity of a wearable antenna.

1.3 Summary of original contributions

There are several original contributions to the field of flexible and reconfigurable wearable antennas included in this dissertation, as listed in the following.

1.3.1 Techniques and components for reconfigurable textile antennas

This section lists the original contributions on several techniques and components used to design passive and reconfigurable wearable textile antennas.

- Four main shorting methods usually used in wearable antenna designs have been comprehensively analyzed. These shorting strategies include embroidered vias, folded strips of metalized fabric, eyelets and snap-on buttons. Two antenna structures including a Planar Inverted-F Antenna (PIFA) and a monopole patch antenna with edge shortings utilizing the investigating shorting methods have been designed and fabricated for experimental characterization. The extensive results gathered in this study indicate that each shorting method exhibits different advantages and disadvantages with respect to simulation, fabrication, antenna performance, mechanical stability and modularity. Depending on the particular application requirements, this investigation will help designers to select the most appropriate shorting method. This investigation has been published in the *IEEE Antennas and Propagation Magazine* under the tile of "Shorting Strategies for Wearable Textile Antennas: A review of four shorting methods " [41]. A summary of the antenna designs reported in [41] was presented at the *2021 IEEE Asia-Pacific Microwave Conference (APMC)* under the title of "Dual-Band Dual-Mode Wearable Textile Antennas for On-Body and Off-Body Communications " [42].

- Exploiting the detachable connections offered by metallic snap-on fasteners, a modular wearable textile antenna with pattern-interchangeability is designed, fabricated and experimentally characterized. The antenna can simultaneously cover the 2.45 and 5.8 GHz Industrial, Scientific and Medial (ISM) radio bands. The proposed antenna can switch between broadside and monopole-like radiations at 2.45 GHz , while the radiation characteristics at 5.8 GHz remain unchanged. This design has been submitted to the *2022 International Symposium on Antennas and Propagation* under the tile of "Modular Wearable Textile Antenna with Pattern-Interchangeability using Snap-on Buttons ".

- A coplanar reconfiguration module based on a small printed circuit board and metallic snap-on buttons is proposed for reconfigurable wearable antenna designs. The module concept can be used to realize a stable and repeatable connection between lumped components and conductive textiles in coplanar agreement. Based on the simulation results, the proposed reconfiguration module is predicted to provide a promising solution to design reconfigurable wearable antennas. This design was presented at the *2019 IEEE Asia-Pacific Microwave Conference (APMC)* under the tile of "A Reconfiguration Module with Coplanar Snap-On Connection for Wearable Textile Antennas" [43].

- A reconfiguration solution based on switching components including RF-switch ICs and PIN diodes is proposed for reconfigurable wearable textile antennas. A vertical reconfiguration module is used to integrate the switching components into wearable texitle antennas. A simple PIFA structure is designed, fabricated and measured to demonstrate the feasibility of the design concept. This design has been submitted to the *2022 IEEE Asia-Pacific Microwave Conference (APMC)* under the tile of "Utilization of RF-switch ICs and PIN diodes in Reconfigurable Wearable Textile Antennas ".

1.3.2 Multifunctional wearable textile antennas

In this section, a summary of the original contributions in relation to reconfigurable wearable textile antennas is presented.

- A frequency-reconfigurable antenna with very wide tuning range of approximately 70% is proposed. To realize an octave tuning range, the antenna is designed to provide a continuous transition between a quarter-wave mode and a half-wave patch mode. This radiation mode transition is achieved by combining an antenna structure and an optimized coplanar reconfiguration module. The wide frequency tuning range principle is analyzed using equivalent circuit model before the proposed antenna is designed, fabricated and measured. Experiment results of the fabricated antenna validate the design concept. This antenna design was published in *IEEE Transactions on Antennas and Propagation* under the tile of "A Frequency-Reconfigurable Wearable Textile Antenna with One-Octave Tuning Range" [44].

- A dual-band frequency-reconfigurable antenna designed to simultaneously operate in the 2.45 and 5.8 GHz ISM radio bands is presented. The antenna structure is based on a PIFA structure combined with a reconfiguration module reported in [44]. The antenna performance in both bands is validated through measurement results of a fabricated antenna, demonstrating a wide frequency tuning range of 48.6% at the lower band and 18.3% at the higher band. This antenna design was presented at the *2022 IEEE International Symposium on Antennas and Propagation and USNC-URSI Radio Science Meeting (APS/URSI)* under the tile of "Dual-Band Frequency-Reconfigurable Flexible Wearable Textile Antenna" [45].

- Using advanced infrared thermography, the thermal behavior of a frequency-reconfigurable wearable antenna in dependence of tuning frequency and antenna input power level is investigated. The results suggest that the hottest spot on the reconfigurable antenna is located at the lumped components positions. The investigation also suggests that the antenna input power level might be a more stringent limitation than the specific absorption rate (SAR) in reconfigurable wearable antenna designs. This investigation was presented at the *16th European Conference on Antennas and Propagation* under the tile of "Thermographic Investigation of Frequency-Reconfigurable Wearable Antennas" [46].

- A dual-band frequency-reconfigurable flexible textile and foam antenna with independent tunability is proposed. The proposed antenna is able to simultaneously operate in two different modes with independent frequency tunability at 2.45 and 5.8 GHz ISM bands. The frequency tuning range at the lower band and higher band are 41.1% and 29.9%, respectively. The antenna is designed, fabricated and experimentally characterized in flat and various bending configurations to validate its practicability for conformal applications. This antenna design was published to the *IEEE Antennas and Wireless Propagation Letters* under the tile of "Dual-Band Reconfigurable Flexible Antenna with Independent Frequency Tunability" [47].

- Two reconfigurable wearable antennas with frequency- and pattern-agility and frequency- and polarization-reconfigurability are proposed. The two proposed antenna share similar structure of using three co-planar reconfiguration modules

to implement the required reconfigurability. The first antenna is able to simultaneously work in dual-band where the radiation patterns at the lower band frequency can be switchable between monopole-like and broadside patterns while the pattern in the higher band remains unchanged. In the lower band, the frequency tuning range at the monopole mode is 27.2% while at the broadside mode, the frequency tuning range is 57.3%. The second antenna can provide a wide tuning range of 31.9% with its linear polarization can be switched between 0°, 120° and 240°. The antenna working principle is analyzed using equivalent circuit models and then prototypes of the antennas have been fabricated and measured to validate the concept. The antenna designs are in preparation for submission to the *IEEE Transactions on Antennas and Propagation* under the tile of "Multi-Functional Reconfigurable Wearable Textile Antennas using Coplanar Reconfiguration Modules".

1.3.3 Passive RFID sensor integration with wearable antennas

The following list provides the details of the original contributions in the third part of the thesis, dedicated to wearable textile antennas and electronics integration.

- A novel integration solution to completely include relatively large electronic components into a resonant cavity of a wearable antenna is proposed. A system-in-package sensor constructed by a computational battery-less RFID module and a modular wearable antenna is designed and fabricated using the proposed integration solution. The antenna and the whole sensor are experimentally characterized with excellent performance. This antenna design was initially presented in the perspective of the system at the *23rd International Symposium on Wearable Computers - ISWC '19* under the tile of "Designing Batteryless Wearables for Hospitalized Older People" [5]. The specifics of the antenna design were then published in the *IEEE Transactions on Components, Packaging and Manufacturing Technology* under the tile of "Modular Integration of a Passive RFID Sensor with Wearable Textile Antennas for Patient Monitoring" [48].

- Considering typical health-care monitoring applications where wearable antennas would be usually mounted on an one-size-fit-all hospital gown, the body-to-antenna gap is identified as having a significant impact on antenna performance. Using the complete sensor including RFID module and wearable antenna

reported in [48], the effect of gaps in-between a human body and a wearable textile antenna operating at 923 MHz is investigated. It is found that the antenna gain and communications range are increased with gaps upto a quarter-wave length distance at 923 MHz. This investigation was presented at the *2021 IEEE International Symposium on Antennas and Propagation and USNC-URSI Radio Science Meeting (APS/URSI)* under the tile of "Body-to-Antenna Gap Effect on a UHF Wearable Textile Antenna Performance" [49].

- A reconfigurable wearable textile antenna aiming to be combined with a computational RFID module to form an advanced sensor package is proposed. The antenna is initially designed with a single feeding port with the ability to work in dual-band where the lower band can be tuned ($0.86 - 1.59$ GHz) while the higher band frequency remains fixed at 2.45 GHz. In a second realization, the antenna design is modified to become a dual-port antenna, aiming of using one port (corresponding to the reconfigurable band) for RFID application while the other port (corresponding to the fixed frequency band) is dedicated for other applications such as Bluetooth or communications to mobile devices. The antenna is optimized to provide good isolation between its two ports and competitive antenna performance. A manuscript gathering the two design variations is in preparation for submission to the *IEEE Antennas and Wireless Propagation Letters* under the tile of "Dual-Band Dual-Port Reconfigurable Textile Antenna for Wearable UHF Applications ".

1.4 Thesis structure

The thesis structure is illustrated in Fig. 1.1 where ten chapters are listed. The first two chapters and the last chapter are dedicated to introductory chapters and conclusion, respectively. The original contributions of the thesis are categorized into three main parts corresponding to seven chapters.

I. **Introduction (Chapter 1& 2)**

The initial introductory chapter provides a brief summary of the context of reconfigurable wearable antennas and lists the objectives of the thesis. Chapter 2 presents a literature review on three main topics. The first topic concerns the current materials frequently used to design wearable textile antennas. Numerous

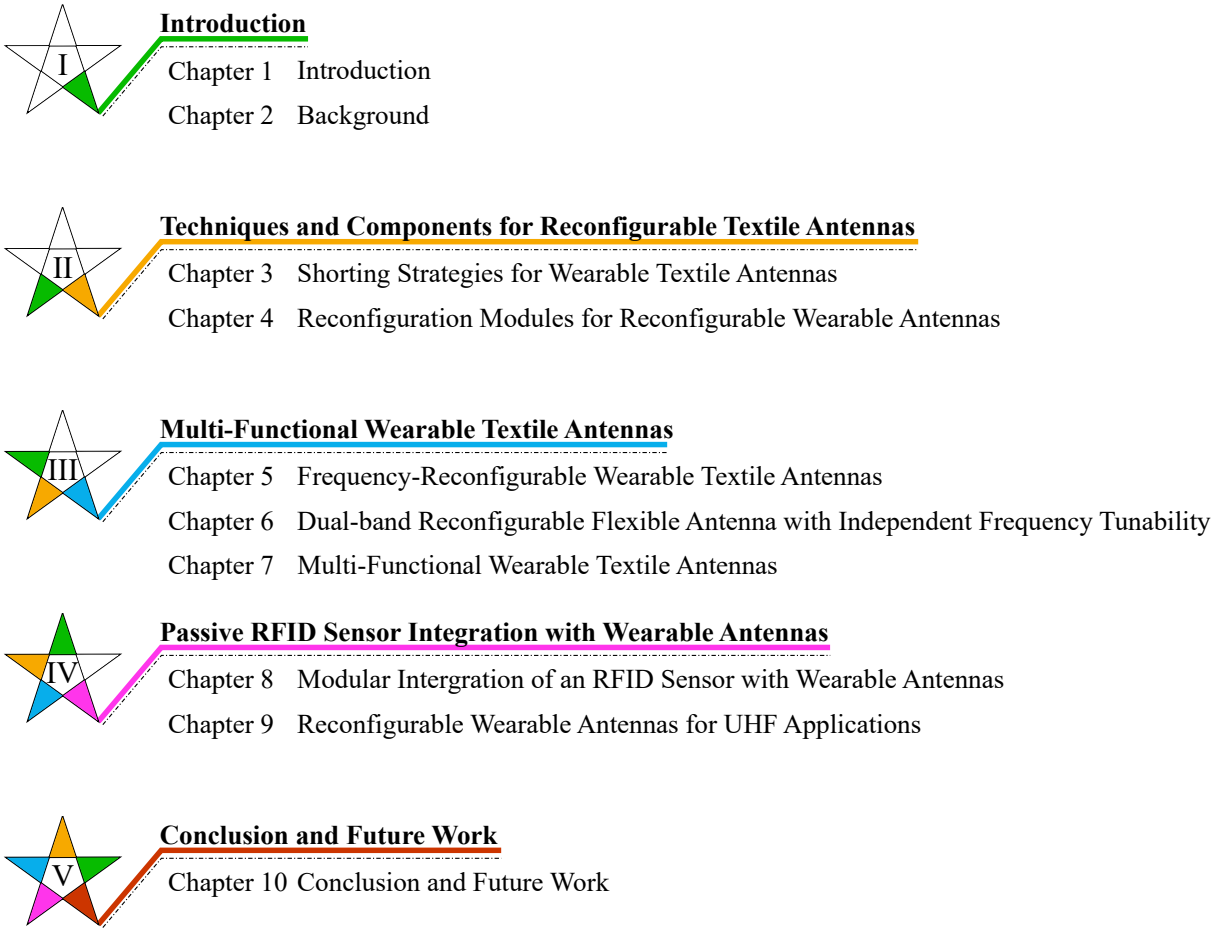

Figure 1.1. Thesis outline. The thesis consists of 10 chapters divided into 5 primary parts. The first part includes introduction and literature review while the last part is the thesis conclusion. The major original contributions are divided into three main parts: i) techniques and components for reconfigurable textile antennas; ii) multi-functional wearable textile antennas and iii) passive RFID sensor integration with wearable antennas.

passive flexible body-worn antennas as well as corresponding design techniques are discussed in the second topic. Lastly, current practical techniques proposed to design reconfigurable wearable antennas are presented.

II. **Shorting strategies and reconfiguration modules for wearable textile antennas (Chapter 3 & 4)**

The second part of the thesis reviews and proposes several generic techniques and components used to design passive and active wearable textile antennas. Chapter 3 comprehensively reviews four popular shorting methods used in wearable

textile antenna designs. The investigation suggests best practices for selection of appropriate shorting methods according to different desired application requirements. In Chapter 4, a novel reconfiguration module used to form a robust connection between electronics and textile conductors in a coplanar agreement is proposed. Additionally, the utilization of switching components including RF-switch ICs and PIN diodes in reconfigurable wearable antennas using reconfiguration module is presented in the second part of the Chapter.

III. **Multi-functional wearable textile antennas (Chapter 5, 6 & 7)**

Several reconfigurable wearable textile antennas are presented in this part of the thesis. Chapter 5 shows a frequency-agile wearable antenna with a very wide tuning range of approximately 70%. The operation principle of the antenna consists in a continuous transition between a quarter-wave mode and half wave patch mode. This reconfiguration modality is analyzed through an equivalent circuit. The practicability of the antenna in conformal applications is suggested by excellent experimental results in various conditions. Also in the chapter, an extended version of this antenna with dual-band frequency-reconfigurable characteristics is presented. The dimensions of the one-octave tuning range antenna are re-optimized to create a dual-band antenna, which can simultaneously cover 2.45 and 5.8 GHz ISM bands with the frequency tuning range in each band being 48.6% and 18.3%, respectively. Chapter 6 depicts a dual-band frequency-reconfigurable wearable antennas with independent tunability. Utilizing four co-planar reconfiguration modules, the flexible antenna exhibits robust performance in various bending configurations which suggests its practicability in conformal applications. Chapter 7 presents a multi-functional wearable antenna design, with two design variations. The first antenna provides frequency- and pattern-agility while the second antenna exhibits frequency- and polarization-reconfigurability. The antenna design principle is confirmed using equivalent circuit models before being validated by experimental results.

IV. **Wearable antennas with integrated RFID sensor (Chapter 8 & 9)**

Passive and active wearable antennas with integrated computational battery-less RFID module dedicated to patient-monitoring applications are shown in this part of the thesis. Chapter 8 proposes a novel method to completely integrate a large

size battery-less RFID sensor into the resonant cavity of a flexible wearable antenna. Additionally, modularization of the RFID module and wearable antenna is introduced which allows customizable modular antenna designs for different application requirements. Furthermore, to cope with the dynamic changes of on-body operating environment, two designs of dual-band reconfigurable wearable antennas for UHF applications are introduced in Chapter 9. The dual-band antennas are designed with frequency-reconfigurability in lower band centered at 923 MHz while the resonance frequency at higher band of 2.45 GHz is fixed.

V. **Conclusion and future work (Chapter 10)**

The last chapter summarizes all the investigations included in this dissertation and provides suggestions of future works.

Chapter 2

Background

THIS chapter presents a literature review of wearable flexible antennas in terms of their desired characteristics and the corresponding design strategies, including material selection and antenna topology development. The most widely used materials including conductive and non-conductive types for body-worn flexible antennas are first reviewed. After that, various passive flexible textile antennas and the corresponding design techniques are presented. At the end, several dominant strategies used to design practical reconfigurable wearable antennas are discussed.

2.1 Introduction

Antennas were invented in the XVIII century and are key components of wireless communications systems. As a converter between guided electromagnetic (EM) waves inside the system and radiated EM waves in free space, a vast variety of antennas have been developed during the last century, from simple designs such as linear wire antennas and log-periodic antennas to more advanced ones including aperture antennas, reflector antennas, microstrip antennas, traveling antennas and reconfigurable/smart antennas. To meet the requirements of diverse modern wireless communications applications such as in aircraft, satellite, Internet of things (IoT), and Wireless Body-Area Networks (WBANs), specialized antennas with dedicated characteristics are required. Because of the great potential to have numerous applications in our daily lives, WBANs have become one of the most dominant applications in which human-body worn computing sensors and devices are wirelessly connected together. As a result, wearable antennas, as vital parts for this type of wireless communications systems have attracted significant research and engineering attention recently.

Considering the users' wearing experiences as well as the influences on the antenna performance due to the wearers' body, the body-worn antennas for wearable applications are usually challenging to design. Firstly, the wearable antennas are supposed to be operating in a dynamically changing environment where mechanical deformation of the antennas including bending and crumpling are very likely to happen, especially in moving conditions. Therefore, the body-worn antennas are expected to be flexible, lightweight and able to cope with these dynamic changes. Secondly, the isolation between the wearable antennas and the human body needs to be maintained to keep acceptable antenna performance with the wearers in vicinity. This is because the human body, as a lossy medium, can interact with the body-worn antennas and consequently change the antenna performance.

To overcome these challenges, a wide variety of passive wearable antennas based on flexible and lightweight materials have been developed. Popular conductor materials include conductive fabrics [50–52], conductive polymer [11, 53, 54] and conductive threads [35, 55], whereas predominant dielectric materials include PF-4 foams [37, 56, 57], polydimethylsiloxane (PDMS) [58, 59] and commercial felts as substrates [12, 60]. Most of these wearable antennas were designed with a full ground plane structure which provides a good isolation between the antenna and the human body. Furthermore, in order to cope with the increasing complexity and functionality of

body-centric wireless communications systems while retaining the antenna compactness, multi-functional wearable flexible antennas are the essential solutions. To this end, various wearable textile antennas were designed to be multi-band [61], ultra-wide band [10] or electrically reconfigurable [28,29].

In this chapter, a general review on the-state-of-the-art wearable antenna designs in terms of their materials, topologies and practicalities will be given, to reflect the research gaps that this thesis is addressing. Firstly, several popular conductive and dielectric materials widely used to realize body-worn flexible antennas will be reviewed. Secondly, typical passive wearable flexible antennas and their corresponding design strategies will be examined in detail. The last section of this chapter will present dominant approaches and strategies used to realize practical reconfigurable flexible textile antennas reported in the literature.

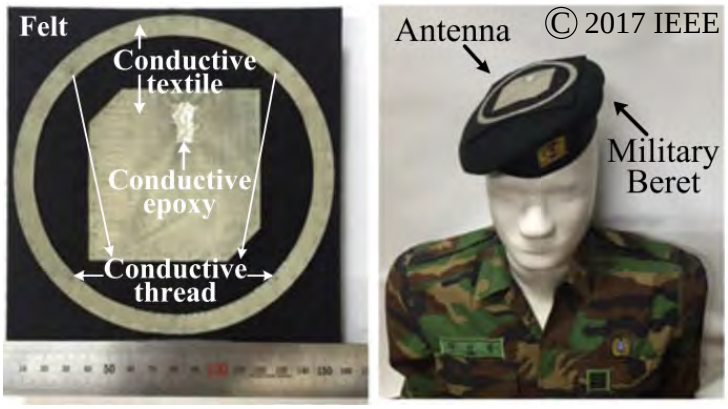

Figure 2.1. Wearable textile antenna. Example of wearable textile antenna mounted on a beret. This image was adopted from [62].

2.2 Wearable antenna materials

Nowadays, body-centric communications are mainly used in health-care monitoring, personal communications and securities applications [63], where the systems are worn by the human subjects. Consequently, considering the wearing experience of the user, flexible, light-weight and robust antennas are highly desirable. Therefore, appropriate antenna materials are essential to fulfill these specialized requirements. For instance, Fig. 2.1 illustrates a very practical wearable textile antenna mounted on a military beret for indoor/outdoor navigating system [62]. In comparison with rigid antennas used in convenient communications systems, this conductive-textile-based body-worn antenna can offer unobtrusive wearing experience while maintaining mechanical and

electrical robustness. These distinct merits were obtained through the utilization of appropriate antenna materials and design strategies, which are the critical differences between wearable flexible antennas and conventional rigid-material-based counterparts. For this reason, the most widely utilized conductive and non-conductive materials for wearable flexible antenna designs will be first reviewed and compared in terms of their mechanical and electrical properties.

2.2.1 Conductive materials

Copper tape

Copper tape has been used as popular conductive material for wearable antenna designs [64, 65]. Copper tape is usually flexible, light weight and easy to be used for antenna fabrication. It also allows high antenna radiation efficiency due to its low surface resistivity (less than 0.05 Ω/square). It also permits direct soldering of lumped electronic components which can simplify the fabrication process of reconfigurable or active antennas. Two typical wearable antennas fabricated using copper tape are shown in Fig. 2.2, the first antenna being a PIFA antenna and the second one being a folded dipole antenna designed for on-body and off-body communications links, respectively. However, copper tape exhibits some mechanical weaknesses while being used in body-worn contexts. Firstly, its mechanical resilience is low, therefore it is irreversibly deformed after being bent and/or crumpled, which may lead to changes in the antenna performance. A crumpled copper tape surface can be observed in both antennas displayed in Fig. 2.2. Secondly, copper tape is not bio-compatible and breathable which can significantly limit its practicability.

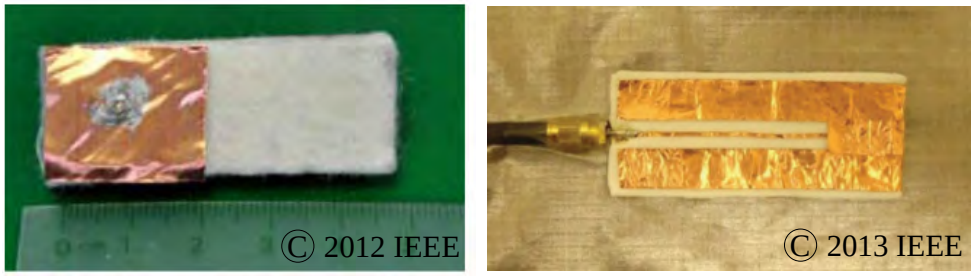

(a) (b)

Figure 2.2. Wearable antennas using copper tape. (a) PIFA and (b) folded dipole antennas fabricated using copper tape with the images were adopted from [64] and [65], respectively.

Conductive ink

Wearable antennas based on conductive ink have also been widely used, as reported in the literature [66–68]. In this method, conductive ink is loaded into a commercial ink-jet printer and is then printed directly onto flexible substrates. With the advances in this printing technology, the fabrication processes can be easily scaled for mass production with continuously improving printing accuracy and speed. For example, a wearable antenna printed on paper substrate which consists of a monopole antenna and a miniaturized artificial magnetic conductors are shown in Fig. 2.3. It can be observed that, the artificial magnetic conductors were fabricated with complicated conductor patterns at very high printing resolution of 150 μm, demonstrating excellent printing quality. Nevertheless, the majority of ink-jet printed conductive layer does not provide very high conduction/radiation efficiency due to the relatively low electrical conductivity of the available inks. Furthermore, the thickness of ink-jet printed layer is usually much smaller than a skin depth, resulting in a relatively high sheet resistance. This current issue may be solved with the development of 3D printing and material technologies which could permit a thicker printing layer with more conductive links on flexible substrates.

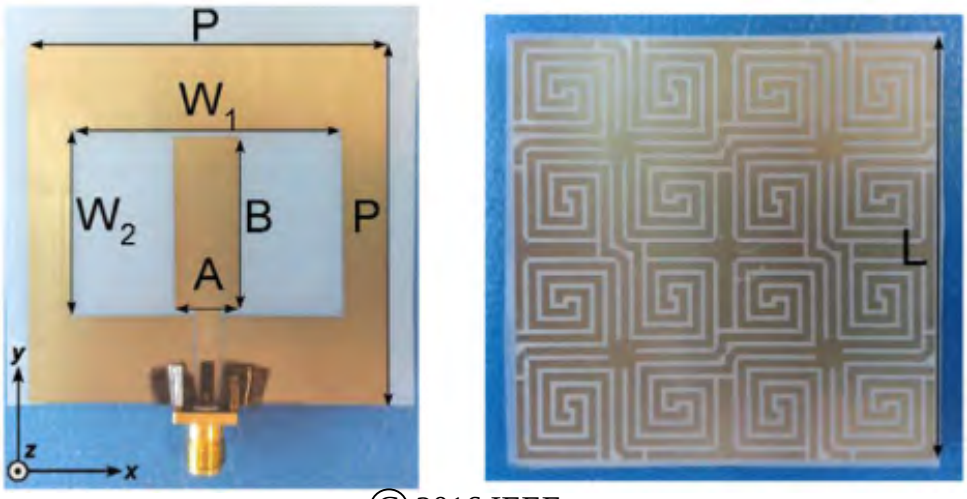

Figure 2.3. Wearable antennas using conductive ink. (a) A monopole antenna and (b) a miniaturized artificial magnetic conductors fabricated using conductive ink. These images were adopted from [68].

2.2.1 Conductive materials

Non-metallic conductors

With the advantages of increasingly enhanced electrical conductivity and exceptional mechanical flexibility, conductive polymers have been considered as another possible choice to design wearable antennas [11,53,54,69,70]. A typical example of highly flexible ultra-wide band (UWB) antenna using conductive polymer [11] is illustrated in Fig. 2.4. It was demonstrated that, the antenna can be bent to 180° upward and downward without any mechanical damage. The antenna was tested to be able to maintain good performance in a conformal test while being bent not greater than 90° [11] angle. Nevertheless, utilization of conductive polymers as antenna conductors is also suffering relatively low antenna efficiency when applying to resonant antennas due to the higher RF current density developed during the resonance process, when compared to non-resonant antennas. It is worth mentioning that, the antenna efficiency can be high for non-resonant antennas through deploying various design techniques [54].

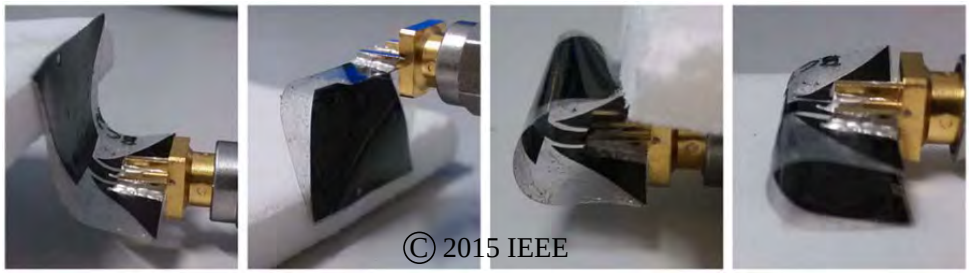

Figure 2.4. Wearable antenna using conductive polymer. A highly flexible ultra-wide band antenna fabricated using conductive polymer as adopted from [11].

Graphene has been also well-known as a promising candidate to design wearable antenna conductor due to high thermal and electrical conductivites [71, 72]. A ultra-wide band flexible antenna with high efficiency fabricated using graphene is shown in Fig. 2.5 (a). After being treated through several fabrication steps of filtering and thermal treatment at 900°C for 1 hour under protective environment, the final graphene film with very high electric conductivity of 3.3 x 10^4 S/m and a thickness of approximately 100 μm [73] has been produced. This value of material thickness is higher than a skin depth, even at lower frequency (δ_s = 50.6 μm at 3 GHz). Therefore, this graphene conductive material can be used to design microwave antennas with high efficiency of approximately 80 % [72] (see Fig. 2.5 (b)). The limitation of using graphene is the complicated fabrication processes which usually require significant amount of time.

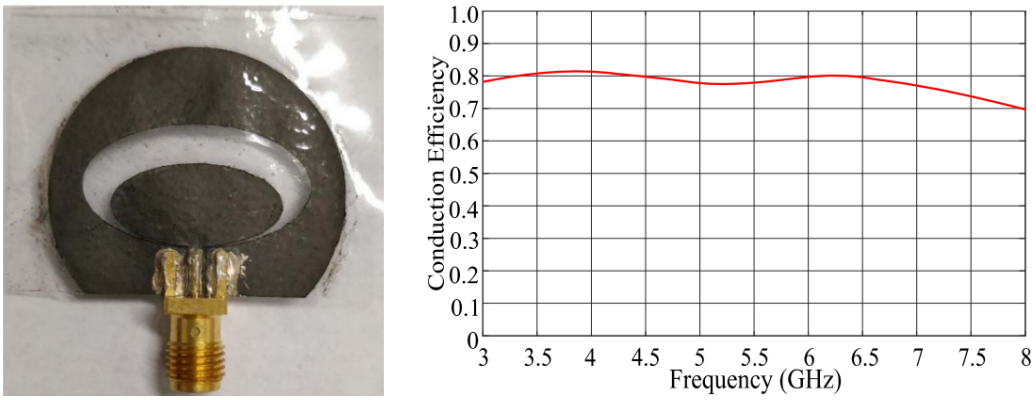

Figure 2.5. Wearable antenna using graphene. A high-efficiency microwave graphene antenna as adopted from [72]. (a) The fabricated antenna and (b) measured conduction efficiency of the antenna.

Conductive textile

So far, conductive textile is one of the most widely used conductors for wearable flexible antennas due to its advantages of high mechanical flexibility, low sheet resistance, substantial thickness of more than 100 μm and bio-compatibility [12, 35, 56, 74]. Conductive textiles are metallized fabrics which generally consist of 3 layers of materials including a nylon fabric in the middle sandwiched by two layers of a copper or nickel over silver. With these coated metal layers, the fabric exhibit very high electrical conductivity, leading to a sheet resistance being as small as 0.01 Ω/square. As a result, wearable antennas based on conductive fabrics usually exhibit very high radiation efficiency of more than 90% [35]. Conductive fabrics are ready-to-use materials which come with a very big size sheet which can be accurately cut to required patterns using a laser milling machine. Several typical examples of wearable antennas using conductive fabric reported in the literature are displayed in Fig. 2.6. Two UWB wearable textile antennas using conductive textile reported in [10] and [12] are shown in Fig. 2.6 (a) and Fig. 2.6 (b), respectively. They both possessed radiation efficiency of more than 90%. It can be observed that, the radiation patch patterns are complicated and affixed well on the rough surface of a felt substrate. Conductive textiles also demonstrate robust mechanical stability which can be used as interchangeable patches for modular antennas [37], as shown in Fig. 2.6 (c). A common drawback of conductive fabrics is the limitation of minimum cuttable geometry. It is empirically found that silver fabrics may be trimmed down to a minimum dimension of approximately 2 mm to maintain

its mechanical robustness. Unlike copper tapes, it is very challenging to electrically connect lumped electronic components to conductive textiles in a robust manner. This disadvantage is one of the biggest barriers to design reconfigurable textile antennas.

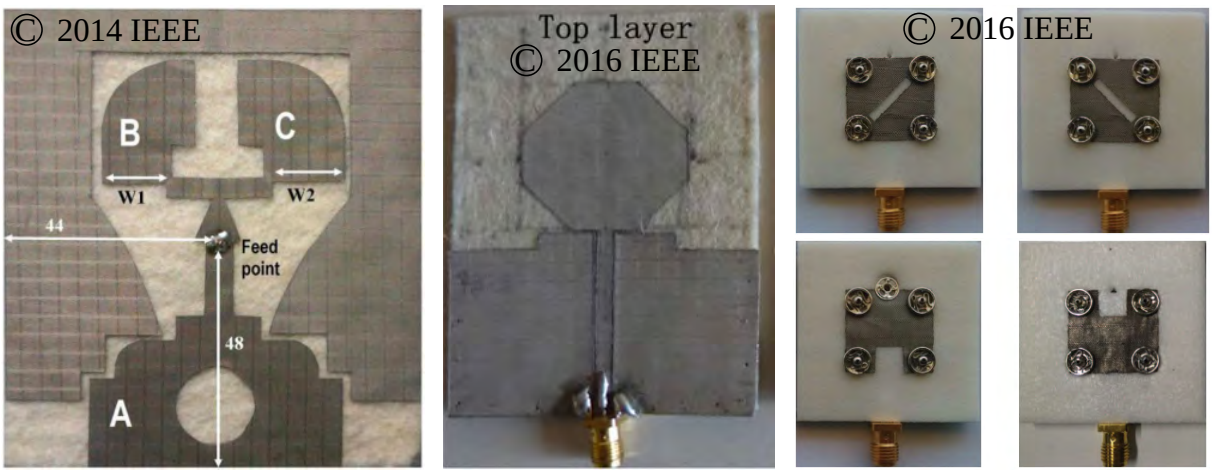

Figure 2.6. Wearable antennas using conductive textile. Examples of wearable textile antennas fabricated using conductive textile. (a) A UWB antenna with full ground plane, (b) a planar monopole UWB antenna and (c) a modular antenna with different radiation modules as reproduced from [10], [12] and [37], respectively.

Summary on conductive materials for wearable antennas

In general, it can be concluded that, conductive textiles can be considered as one of the the most appropriate conductive materials for wearable antenna designs, due to its high electrical conductivity and exceptional mechanical resilience. With rapid development of printing and material technologies, the other conductive materials such as conductive polymers and graphene will also offer increasingly improving electrical and mechanical characteristics for body-worn devices.

2.2.2 Non-conductive materials

Most antennas require dielectric substrate materials to hold the conductors and thus form the geometry. These dielectric materials are very important as they can influence the antenna performance such as efficiency, size and bandwidth. It is even more important for wearable antennas, as the antenna substrates have significant effects on the flexibility and weight characteristics of the wearable antennas. Therefore, the choice of

wearable antenna substrate materials is crucial to achieve the expected antenna performance while keeping the required mechanical properties. In term of mechanical characteristics, suitable body-worn antenna substrates are expected to be highly flexible, light weight and easy for antenna fabrication. To obtain satisfactory antenna efficiency, the substrates are also required to be low lost.

Felts

Felts have been used as substrate materials in wearable textile antenna designs for more than a decade [1,10,75–79]. Since felts are generally highly flexible, easy-to-find, easy-to-fabricate and affordable, they are the most popular wearable antenna substrate materials. Some of reported wearable textile antennas constructed on felt substrate including a substrate integrated waveguide (SIW) cavity-backed circular ring-slot textile antenna, a copper foil tape wearable antenna and a wideband wearable all-textile PIFA are illustrated in Fig. 2.7 (a), (b) and (c), respectively. Although these antennas all feature excellent mechanical flexibility, felts have some drawbacks that can limit its applications in practical body-worn scenarios. Firstly, felts usually have a relatively high loss tangent (tanδ) ranging from 0.02 to 0.04, which consequently leads to a modest antenna efficiency in a range between 30% and 70%. Regarding the corresponding antenna fabrication processes, since felts usually come with a rough surface, it is difficult to maintain a robust connection to the conductive parts. However, felts are very practical for applications where one-time-use or disposable antennas are needed, since they provide a balanced trade-off between antenna performance and the cost.

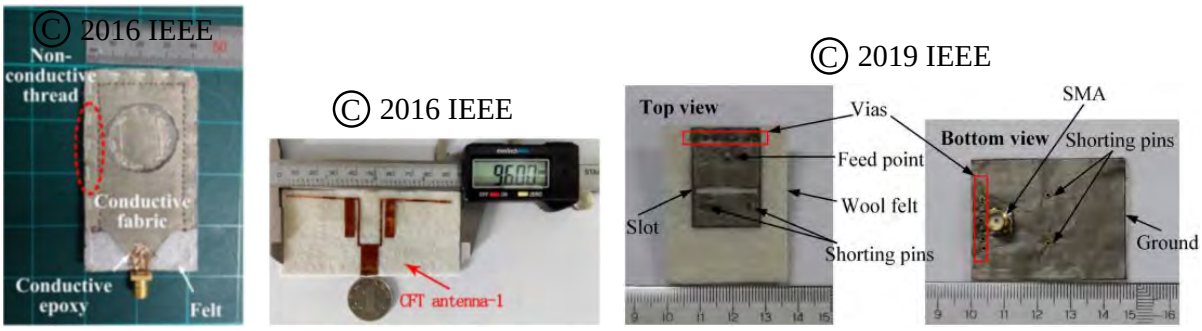

(a) (b) (c)

Figure 2.7. Wearable antennas using felt substrate. Examples of wearable textile antennas fabricated using felt substrate. (a) A substrate integrated waveguide (SIW) cavity-backed circular ring-slot textile antenna, (b) a copper foil tape wearable antenna and (c) a wide-bandwidth wearable all-textile PIFA as reproduced from [76], [77] and [78], respectively.

Polydimethylsiloxane (PDMS)

Another popular substrate material that has been widely used for body-worn antennas is polydimethylsiloxane (PDMS) [13, 61, 80–82]. The advantageous characteristics of PDMS include high mechanical flexibility, modest dielectric constant (ε_r = 2.7) and versatile geometry plasticity. On top of that, two noticeable features of PDMS namely water resistance and transparency make PDMS a practical solution to realize protective layers for body-worn antennas [13]. However, like felts, PDMS is not a very low-loss material with a similar loss tangent around $0.02-0.04$ [61, 81] which will have an impact undermining the antenna radiation efficiency. Furthermore, its fabrication process usually requires several steps as shown in Fig.2.8, which is more complicated and time-consuming than other ready-to-use substrate materials. As mentioned in [81], the process of making a single layer of PDMS substrate for a textile microstrip line involved five steps. It began with preparing composites by mixing different ingredients with correct ratios. The mixture was then carefully poured into a dedicated mold to be cured, forming the desired geometry. When the mixture was partially cured, conductive layers were very carefully adhered on that before being fully cured. Although the curing processes can be accelerated with a higher temperature, it would still take a large amount of time. In summary, although the fabrication process of PDMS-based antennas usually requires a multi-step procedure, a dedicated mold, and a significant amount of time, PDMS still has been used broadly in body-worn antenna designs due to its unique advantages such as high mechanical flexibility, bio-compatibility and plasticity.

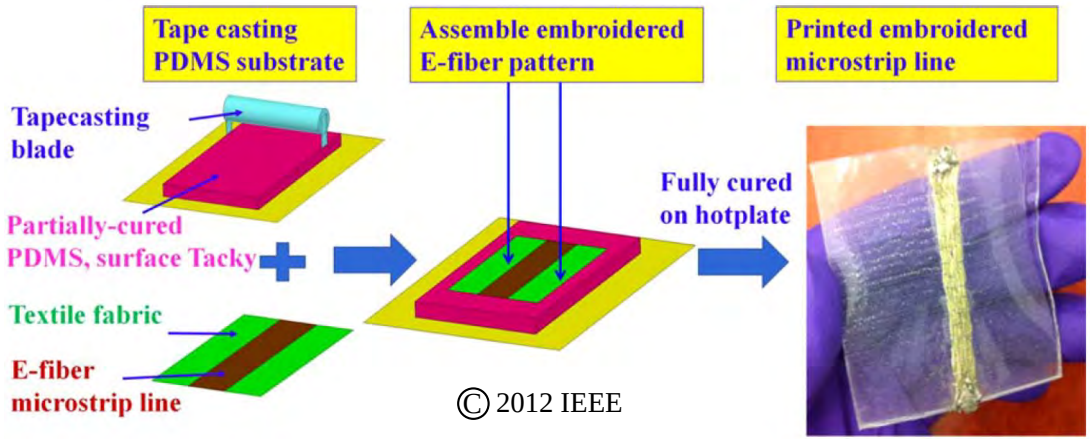

Figure 2.8. PDMS-based microstrip line fabrication process. Fabrication process of single layer PDMS with RF microstrip line made from E-fiber. The image was adopted from [81].

Foam

Foam can be considered as one type of the most conventional dielectric materials for flexible body-worn antenna designs, since it was first utilized almost two decades ago [83]. Recently, a specialized foam dedicated for microwave application named Cuming Microwave C-Foam PF-4 (PF-4 foam) has been used for realizing wearable antennas [35–37, 56, 57], thanks to its exceptional advantages including high flexibility, high mechanical resilience, low loss and light weight. Two examples of wearable textile antennas realized on PF-4 foam substrate including a wearable textile half-mode substrate-integrated cavity antenna and a polarization/frequency interchangeable patch modular wearable textile antenna are illustrated in Fig. 2.9 (a) and (b), respectively.

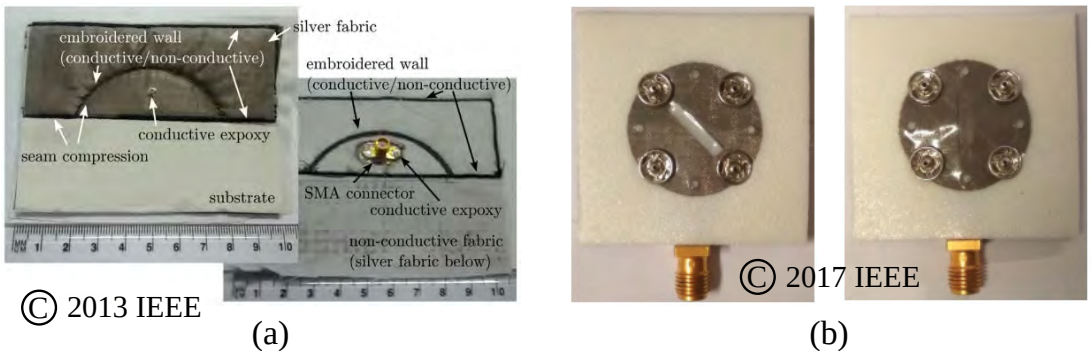

Figure 2.9. Wearable antennas using PF-4 foam substrate. (a) A wearable textile half-mode substrate-integrated cavity antenna and (b) a polarization/frequency interchangeable patch modular wearable textile antenna using PF-4 foam substrate, as adopted from [35] and [84], respectively.

In comparison with felt and PDMS, PF-4 foam has several unique strengths in both mechanical and RF features. In term of physical characteristics, the foam is highly flexible with excellent mechanical resilience which is highly desirable for conformal applications. It is also very light, breathable and bio-compatible, which allows the antennas to be very comfort to wear. From the fabrication process perspective, PF-4 foam is ready-to-use and can be easily cut into the required shape and dimension. Owing to its very smooth surface, it is convenient to attach conductive materials onto these foams using fabric glue [35]. In term of RF characteristics, PF-4 foam has very low lost with a loss tangent $\tan\delta = 0.0001$ which can permit a very high antenna radiation efficiency of more than 95%, as reported in [35]. However, a possible limitation of PF-4 foam comes from its low relative permittivity ($\varepsilon_r = 1.06$) which makes the antennas size larger than

the counterparts made using higher permittivity materials. Additionally, PF-4 foam is an expensive material which limits its applicability in cost-focused applications.

Summary on dielectric materials for wearable antennas

In this part, several widely used non-conductive materials for wearable flexible antenna designs have been discussed. Considering the pros and cons of these substrate materials, PF-4 foam can be the best choice to design wearable textile antennas when high radiation performance is required, provided the antenna cost is not the main concern. By contrast, felt is more suitable for one-time-use applications due to its acceptable electrical performance and affordable price. PDMS shows the strengths of mechanical flexibility and plasticity which provides excellent design versatility for wearable textile antennas.

2.3 Passive flexible wearable antennas

In this section, typical state-of-the-art passive flexible wearable antennas as well as their corresponding design techniques will be discussed. The considered body-worn antennas will be categorized into four main groups regarding their significant features including basic passive, multi-band, ultra-wide band and modular antennas. All the considered wearable antennas are designed with flexible characteristics which allow the antennas to conform to the shape of wearers, especially in moving conditions.

2.3.1 Basic passive textile antennas

This section describes some representative examples of basic passive textile antennas selected from the literature.

Flexible textile PIFA antenna

A flexible textile E-shaped shorted PIFA design [83] can be considered as one of the first wearable flexible antenna reported in the literature. The antenna was designed to operate in a frequency range of $360 - 460$ MHz. As illustrated in Fig. 2.10 (a), the proposed antenna is constructed on a low loss ($\tan\delta$ = 0.004) and flexible foam substrate, a thin copper layer patch and a conductive non-woven fabric ground plane. To overcome a challenge of narrow bandwidth of low-profile microstrip patch antennas [85], the E-shaped radiation patch is employed to support multiple resonances. Three arms of the

antenna E-shape patch are shorted to ground plane to further increase the bandwidth. The simulated antenna reflection coefficient under bending condition is depicted in Fig. 2.10 (b) which predicts the possibility of antenna utilization in conformal applications. The reflection coefficient parameters of the flat antenna was measured in free space and on human body (as displayed in Fig. 2.10 (c)), in which a slight frequency shift is observed. This antenna design demonstrated that the PIFA structure in combination with slots is an effective approach for antenna miniaturization and bandwidth enhancement.

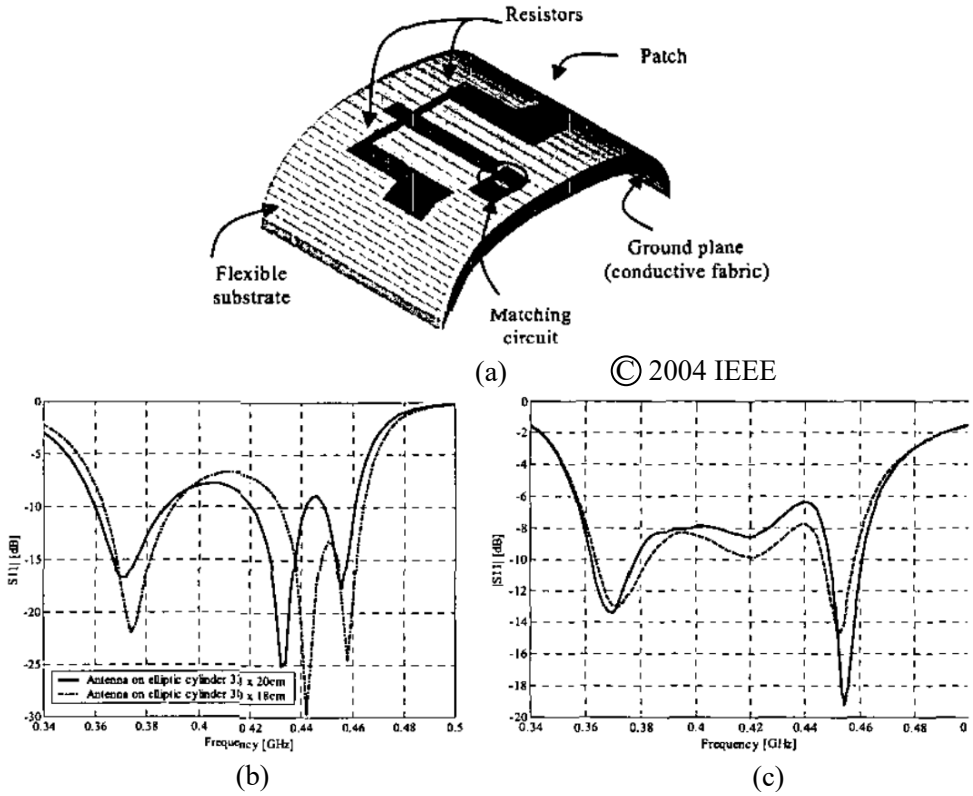

Figure 2.10. A flexible wearable E-shaped shorted PIFA antenna. A flexible wearable E-shaped shorted PIFA antenna. (a) Simulated antenna under bending condition, (b) simulated reflection coefficients of the antenna under bending and (c) measured reflection coefficients of the antenna in free space and on-body conditions. The images were adopted from [83].

UHF wearable textile cavity antenna

In [36], the authors utilized a multilayer cavity structure with a slot-monopole and embroidered walls to realize a UHF wearable textile antenna operating at 923 MHz. Conductive yarn as an effective technique in wearable textile antenna manufacturing [35, 81, 86, 87], was used to realize cavity walls. The proposed antenna structure

is shown in Fig. 2.11 (a) where two layers of substrate and three layers of conductive textiles are illustrated. A full ground plane was used in the design to maximize a human-to-antenna isolation. A slot-monopole radiation patch was placed on top of the antenna while a feeding layer was accommodated in the middle of two substrates. A H-shape slot and cavity walls dimensions were optimized to miniaturize antenna size, increasing a bandwidth and to pull the operating frequency to 923 MHz as targeted. The cavity walls were realized using computerized embroidery technology to enhance the antenna robustness. In the design, substrate compression caused by embroidered structure was taken into account to accurately simulate the proposed antenna structure. The proposed antenna exhibited good antenna performance with a fractional bandwidth of 3% centered at 923 MHz and a radiation efficiency of 78%. The antenna resonance frequency shift under various setups of bending test is also appreciable as illustrated in Fig. 2.11 (b). In this wearable antenna design, the utilization of conductive yarn in realization of cavity wall and improving antenna antenna robustness was demonstrated.

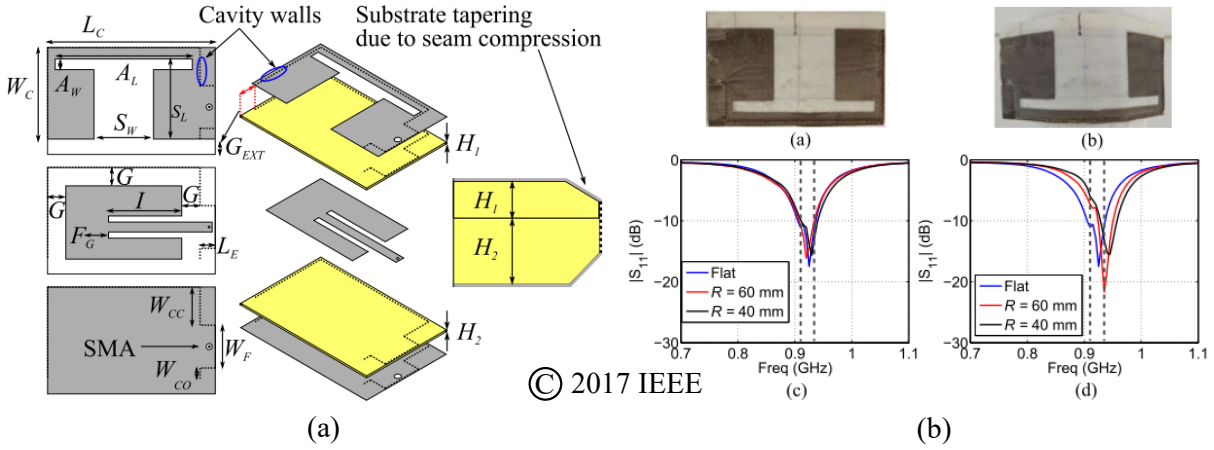

Figure 2.11. Multilayer cavity slot wearable textile antenna. A textile multilayer cavity slot monopole antenna under bending test. (a) Antenna structure and (b) measured reflection coefficients of the proposed antenna under flat and bending conditions. These images were reproduced from [36].

Flexible textile dipole antenna using snap-on buttons

An textile elliptical dipole antenna with wideband performance designed for RFID-based fall detection system was presented in [88]. Especially, pairs of metallic snap-on buttons were utilized to realize the connections between the antenna and the electronics. The two dipole elements were made of conductive textiles with elliptical shape

to enhance a bandwidth. A highly flexible, low loss and light-weight PF-4 foam was used for the antenna substrate to further maximize the antenna efficiency. Two pairs of snap-on buttons were used to connect the proposed body-worn antenna with a RFID module to form a completed sensor. The RFID module with male snap-on buttons, the proposed antenna with sewed female snap-on fasteners, a 50-to-70Ω impedance balun and the fabricated antenna connected to RFID module worn by human body are shown in Fig. 2.12 (a). The proposed antenna exhibited a wide impedance bandwidth from $783 - 1042$ MHz, as shown in Fig. 2.12 (b). It was also found that, the variation of the gap in-between the male and female snap-on buttons only has a minor effect on the antenna resonance frequency as illustrated in Fig. 2.12 (c). The proposed antenna design suggests a promising approach to integrate the RFID module to the wearable flexible antenna by utilizing the metallic snap-on buttons. However, one drawback of this design is the electronic components are placed on the immediate periphery of the body-worn antenna which leads to a less compact system with no protections for the electronic module. The novel integration method to overcome this weakness will be demonstrated later in Chapter 8.

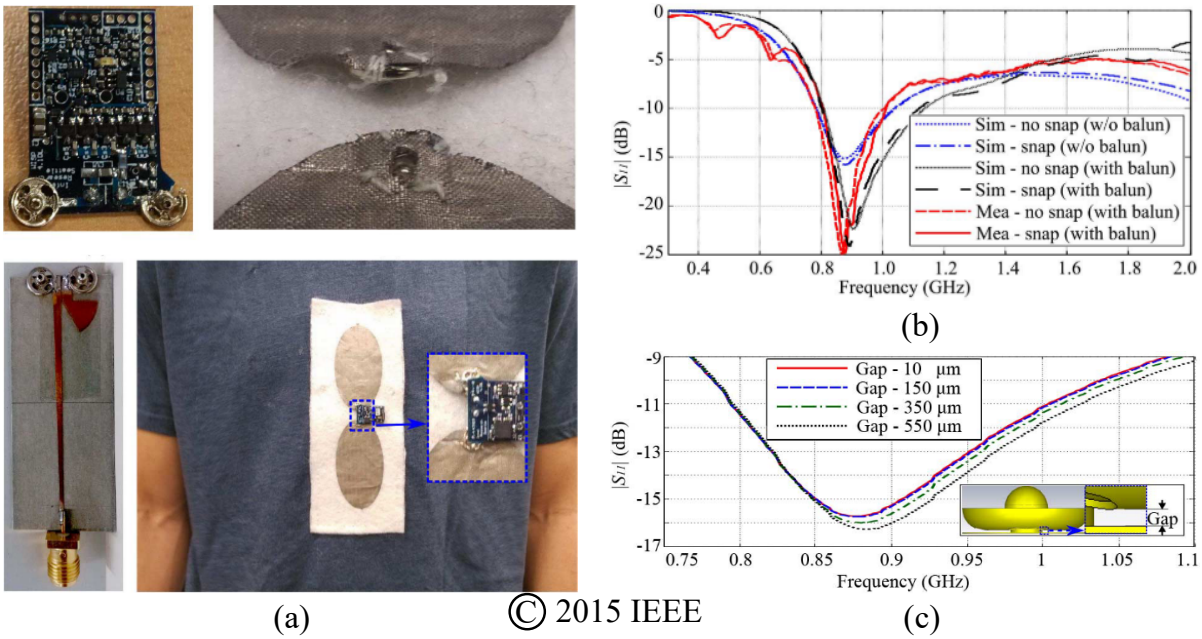

Figure 2.12. Flexible textile dipole antenna for RFID applications. (a) RFID module, the proposed antenna with sewed female buttons, a 50-to-70 Ω impedance balun, the antenna connected to a computational RFID module on human body, (b) simulated and measured reflection coefficient of the antenna and (c) simulated reflection coefficient according to different gap in-between male and female snap-on buttons. The images were adapted from [88].

2.3.2 Multi-band wearable textile antennas

Realizing multi-band modality is a traditional method used in antenna design to extend its functionalities. In body-centric wireless communications, multi-band wearable textile antennas are highly desirable to cope with the increasing system complexity and functionality while retaining the antenna compactness. In this part, several multi-band body-worn antennas realized using textile materials will be discussed.

Compact dual-band textile HMSIW antenna

A compact wearable textile antenna based on a half-wave substrate integrated waveguide (HMSIW) operating simultaneously in the 2.4 and 5.8 GHz ISM bands was proposed in [7]. The proposed antenna was realized on a flexible closed-cell expanded rubber protective foam substrate with low loss tangent ($\tan\delta = 0.016$). The antenna conductors were made from a copper plated polyester taffeta fabric which has a thickness of 80 μm and a surface resistance of 0.18 Ω/square. The antenna size was miniaturized using a half-diamond HMSIW structure constructed by a number of brass eyelets, the fabricated prototype is shown in Fig. 2.13 (a). The resonance frequency at lower band was excited in a fundamental mode of HMSIW structure while the higher order mode was realized by adding a narrow short slot on the antenna radiation patch. The proposed antenna demonstrated good antenna performance in free space and on the human body with the $|S_{11}|$ results shown in Fig. 2.13 (b) and (c). The antenna was also tested under various bending scenarios which indicate a robust wearable antenna for conformal applications with a negligible frequency shift.

Dual-band textile antenna on EBG substrate

A dual-band wearable textile antenna incorporating an electromagnetic band-gap (EBG) surface was reported in [6] demonstrating another method to realize dual-band characteristics as well as a strategy to enhance isolation between wearable antennas and the wearer's body. The proposed antenna consists of a coplanar waveguide (CPW) feeding section, an inner radiating element with rectangular ring elements and a ground plane. The CPW was used to enhance antenna bandwidth to be much wider than a traditional microstrip antenna at a cost of strong back radiation. Therefore, a 3×3 cell array dual-band EBG structure was introduced to reduce the backward radiation toward human body. The antenna and the EBG array substrates were made of a 2.2 mm flexible felt substrate. A high conductivity "Zelt" material with a thickness of 0.06 mm,

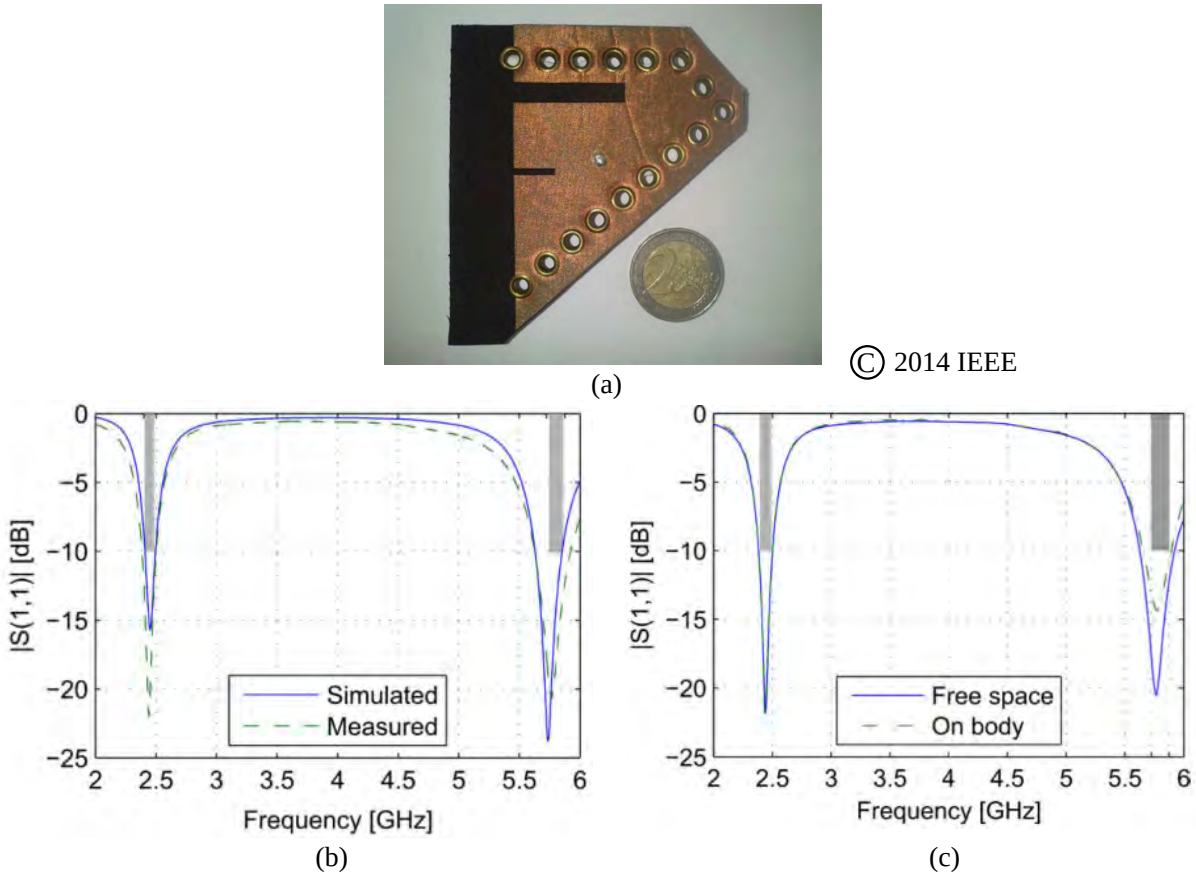

Figure 2.13. Compact half diamond dual-band textile HMSIW antenna. A compact half diamond dual-band textile HMSIW antenna with shorting eyelets, (a) Fabricated prototype, (b) Simulated and measured $|S_{11}|$ of the antenna in free space and (c) measured $|S_{11}|$ of the antenna in free space and on body. The images were reproduced from [7].

surface resistance less than 0.01 Ω/square was dedicated for antenna conductors. The fabricated antenna with EBG cell array is shown in Fig. 2.14 (a). Although the EBG reduce the antenna bandwidth at both resonance bands (see Fig. 2.14 (b)), the final design bandwidths were still appreciable considering the excellent body-to-antenna isolation achieved. A significant reduction of backward radiation was proven in the study by the comparison of radiation patterns in cases of with and without EBG structure. The antenna also exhibited stable performance while placing on human body (arm and leg) and under bending conditions.

Dual-band dual-mode wearable textile antenna

Another dual-band wearable textile antenna targeting off- and on-body communications at the 2.45 and 5.8 GHz ISM bands was reported in [61]. The proposed antenna

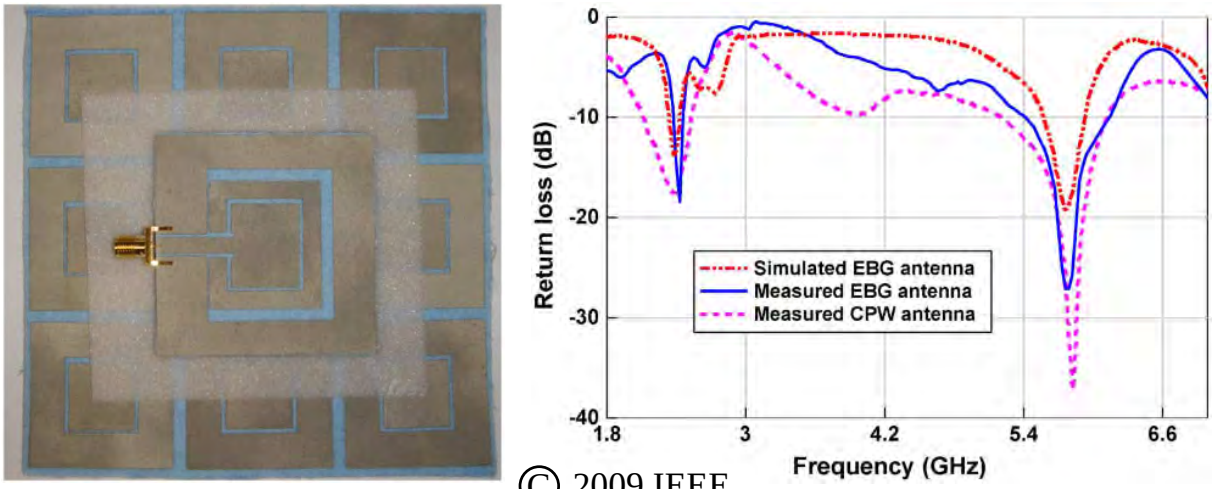

Figure 2.14. Dual-band wearable textile antenna on an EBG substrate. A dual-band wearable textile antenna on an EBG substrate. (a) Fabricated antenna and (b) simulated and measured $|S_{11}|$ of the antenna. The images were adopted from [6].

consists of a full ground plane and a circular patch made of conductive textile which are placed on two sides of a PDMS substrate. The targeted radiation modes are TM^z_{11} and TM^z_{02} corresponded to resonance frequency of 2.45 and 5.8 GHz, respectively. Two arc-shaped slots and a shorting pin were utilized to tune the antenna resonances of the two targeted modes, as shown in Fig. 2.15 (a). Specifically, the slot width was used to tune the lower band resonance frequency while the variation of slot length significantly affected the frequency at higher band. By changing the shorting position with respect to the center of the patch, the frequency at lower band was noticeably affected while the resonance frequency at 5.8 GHz only slightly shifted. The fabricated prototype is shown in Fig. 2.15 (b). The antenna exhibited good performance under various experimental characterizations including on-phantom and bending tests as illustrated in Fig. 2.15 (c) and (d), respectively. However, due to the utilization of high loss PDMS material, the antenna efficiency is limited to around 50% in both radiation bands.

2.3.3 UWB wearable textile antennas

Ultra-wide band (UWB) communications possess distinct advantages such as high data rate capacity and low power spectrum density compared to narrowband communications. As a result, UWB wearable antennas are in high demand for body-centric applications. With an ultra-wide bandwidth, these antennas may be able maintain

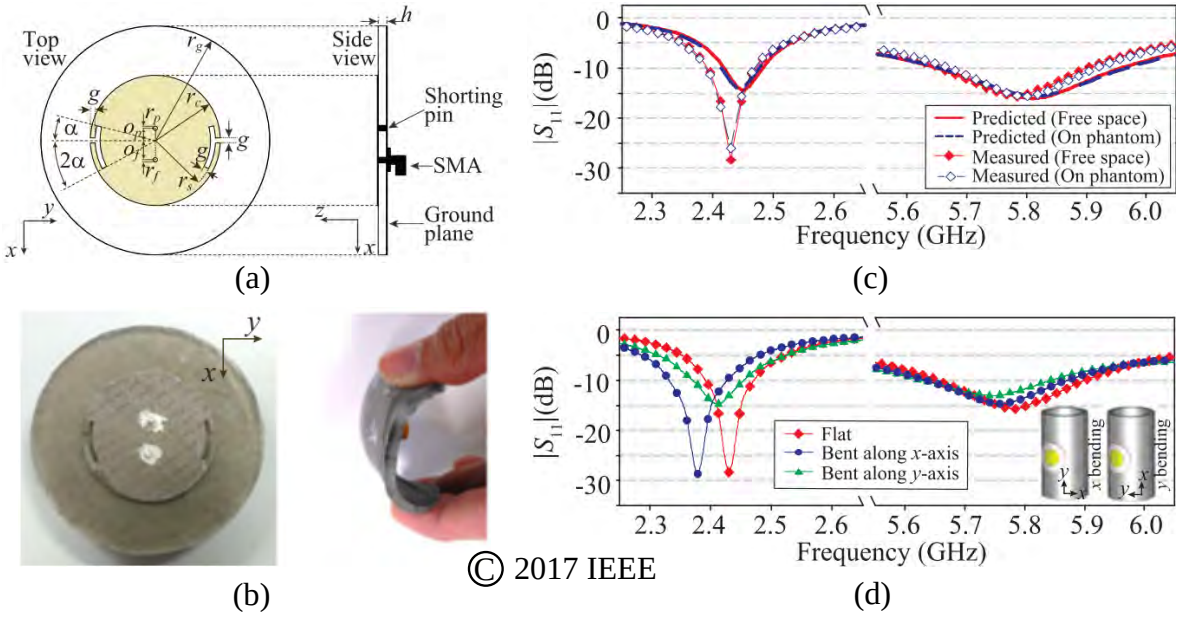

Figure 2.15. Dual-band dual-mode wearable textile antenna on PDMS. A dual-band dual-mode wearable antenna on PDMS substrate. (a) Antenna structure, (b) fabricated prototype, (c) simulated, free-space and on-phantom measured reflection coefficient and (d) measured reflection coefficient under flat and bending conditions in *x*- and *y*-axis. The images were adopted from [61].

their impedance matching when encounter detuning in dynamically changing operation conditions. One of conventional feeding methods for UWB antennas is using CPW structure [11, 89]. However, since CPW structures usually sensitive to the surroundings, it is not suitable for body-worn applications. To enhance body-to-antenna isolation, it is necessary to implement a full ground plane on UWB wearable antennas. In this part, several UWB wearable antennas realized on full ground plane structure will be discussed.

It is well known that, one inherent drawback of microstrip antenna realized on full ground plane is the narrow bandwidth. To overcome this limitation to achieve ultra-wide bandwidth, multiple resonators and slots were utilized in [10, 13]. Both considered antennas had a similar bandwidth ranging approximately from 3.5 to 10 GHz. As shown in Fig. 2.16 (a), the antenna reported in [10] employed three patches namely A, B and C and the surrounding radiator to combine multiple resonance frequencies to form an ultra-wide bandwidth. The patches A, B, C, the surrounding patch shapes, and the gap in-between them were optimized to further enhance the final bandwidth ranging from 3.4 to 10.2 GHz as shown in Fig. 2.16 (b). Using similar techniques of employing multiple resonators, the antenna reported in [13] was also able to exhibit

2.3.3 UWB wearable textile antennas

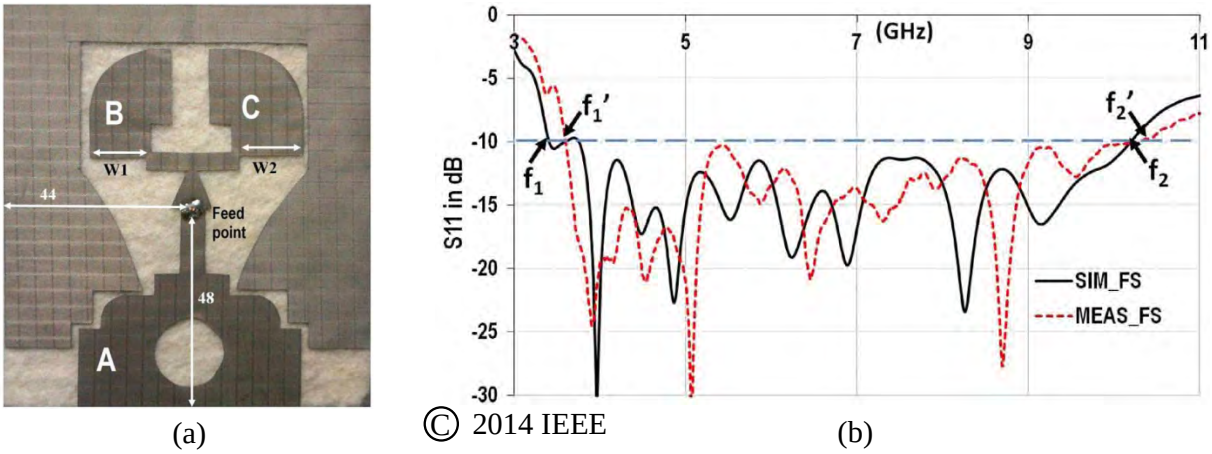

Figure 2.16. UWB wearable textile antenna with full ground plane. A UWB wearable textile antenna with full ground plane. (a) Antenna prototype and (b) simulated, measured reflection coefficient. The images were adapted from [10].

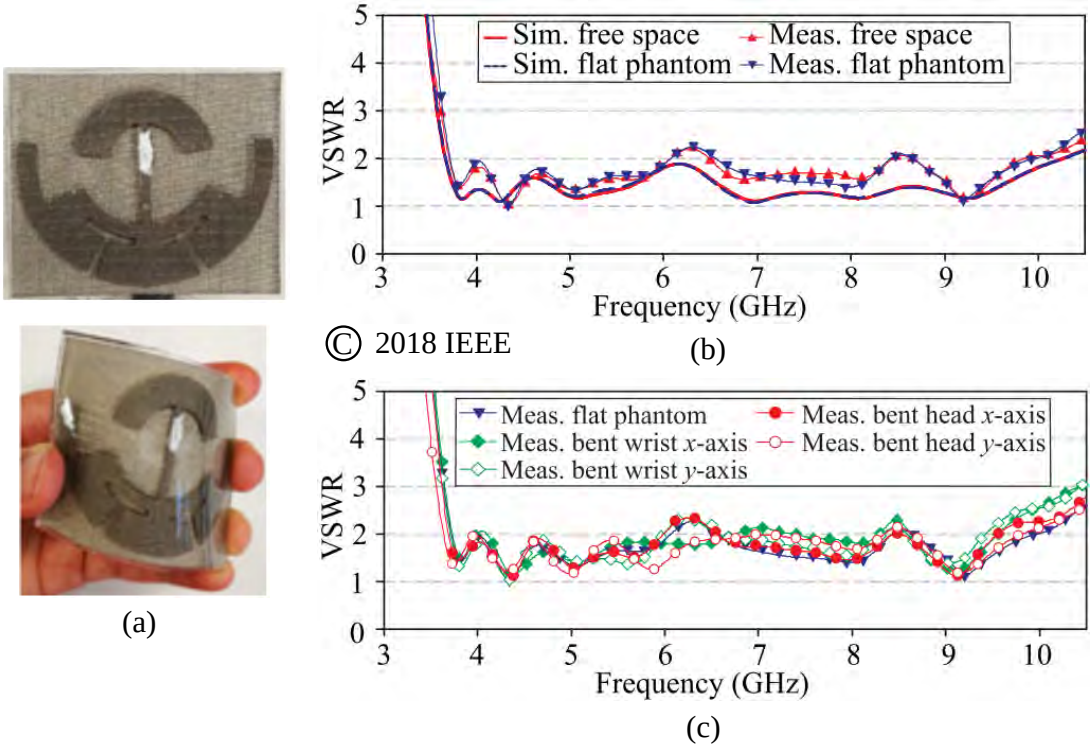

Figure 2.17. UWB wearable textile antenna on PDMS. A UWB wearable textile antenna on PDMS substrate. (a) Antenna prototype in flat and bending conditions, (b) simulated, measured VSWR of the flat antenna in free space and on-phantom and (c) measured VSWR of the antenna under flat and bending conditions in *x*- and *y*-axis. The images were adopted from [13].

similar bandwidth. As illustrated in Fig. 2.17 (a), two arc-shaped patches fed by a small transmission line were used in the design. Furthermore, two T-shaped slots were deployed to enhance the matching at the lower resonance frequencies. By utilizing a PDMS substrate which has a higher permittivity than felt substrate (ε_r = 2.7 for PDMS and ε_r = 1.45 for felt), the antenna reported in [13] is noticeably smaller than the one presented in [10], while exhibiting similar bandwidth (from 3.7 to 10.3 GHz as shown in Fig. 2.17 (b)). Both antennas showed robust performance while being tested under various practical conditions including on-body and bending tests.

2.3.4 Modular textile antenna

Besides multi-band and ultra-wide band modalities, passive wearable textile antennas can be also designed with modularity to effectively enhance the functionalities. In [37], a wearable textile antenna concept designed with detachable radiation patches for different application requirements was proposed. The proposed antenna was constructed on two layers of flexible, light weight and low loss PF-4 foam substrate. Some of the antenna components including a ground plane, a microstrip feed line and modular radiation patches were made from flexible and highly conductivity silver-coated nylon fabric with a thickness of 100 μm and a dc sheet resistance of 0.01 Ω/square. By utilizing metalized snap-on buttons as mechanical and RF connections, the interchangeability of radiation patches to exchange the antenna radiation characteristics was enabled.

In the proposed design concept, the antenna was constructed with a common antenna feed base and exchangeable radiation elements. Four male snap-on buttons were embedded in the common feed base to hold the modular radiation components by engaging with four female counterparts. Using the interchangeability of the snap-on fasteners, pre-designed radiation patches can be swapped according to required radiation characteristics. Several variations of radiation patches were developed in the study to demonstrate the design concept. A circularly polarized patch module allowed the antenna to radiate in either left-hand or right-hand circular polarization at 5 GHz, as illustrated in Fig. 2.18 (a). As shown in Fig. 2.18 (b), a linear-polarization patch module was used to realize a PIFA mode and patch mode operating at 2.45 and 5.3 GHz, respectively. A linearly polarized patch module with rectangular slots was used to adjust the resonance frequency of the half-wave patch radiation mode. The slot length was changed to realize different resonance frequencies, as displayed in Fig. 2.18 (c). In

Fig. 2.18 (d), an X-band patch module was utilized to realize a resonance frequency at 8 GHz.

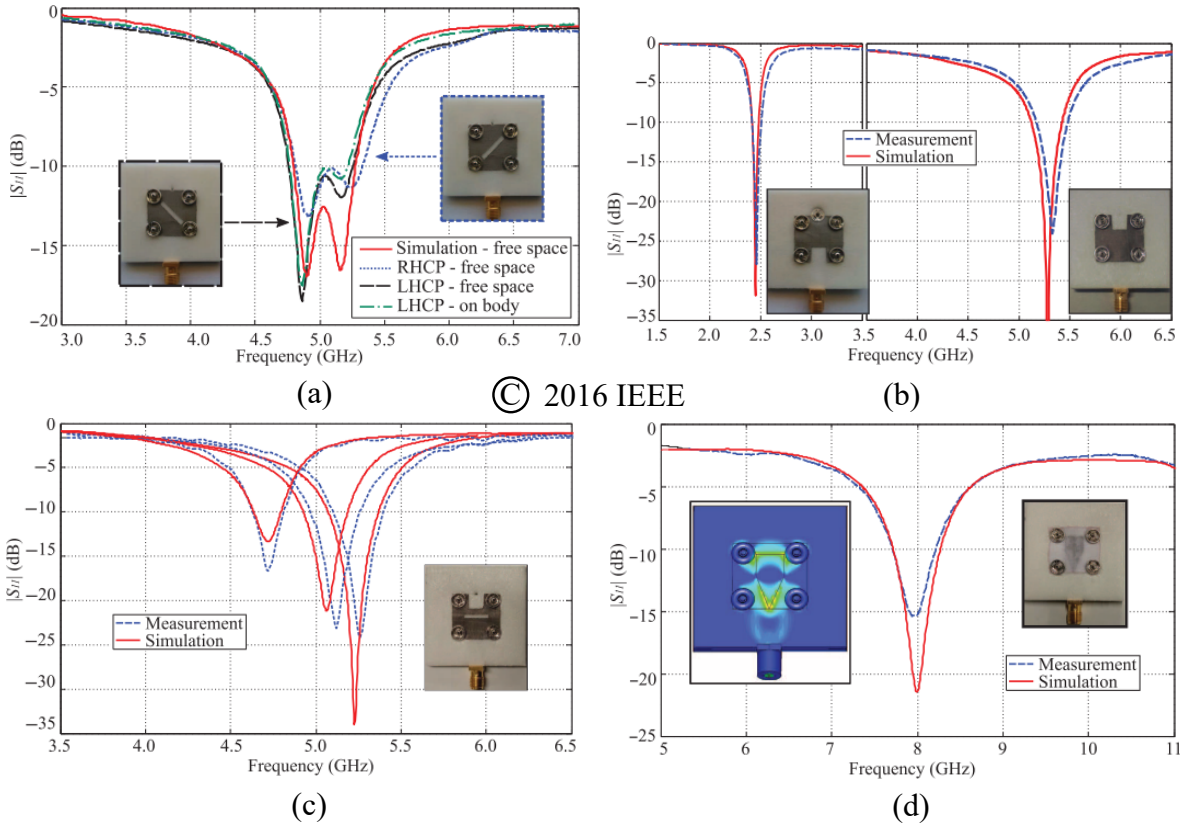

Figure 2.18. Modular wearable textile antenna using snap-on buttons. A modular wearable textile antenna using snap-on buttons. Simulated and measured reflection coefficient of the proposed antenna while using (a) a circularly polarized patch module, (b) a linear-polarization patch module, (c) slot patch modules and (d) an 8-GHz patch module. Inset: fabricated prototype with corresponding patch modules. The images were adopted from [37].

2.3.5 Summary on passive flexible wearable antennas

In this section, typical passive flexible wearable antennas and their design techniques have been reviewed. It is found that, to miniaturize antenna size, common techniques such as introducing slots and deploying quarter-wave structure (e.g., PIFA) were adopted. To increase bandwidth or achieve multiple bands, textile-based components such as eyelets and conductive threads were employed to realize various cavities (e.g., HMSIW) to bring more resonances. With the ability of providing excellent mechanical and RF connections, metallic snap-on buttons were found to be appropriate candidates to provide interchangeability to wearable antenna parts including flexible substrate or conductive parts.

2.4 Reconfigurable wearable textile antennas

Reconfigurable antennas have attracted research and industry interests for almost a century, starting with a concept of beam steering applied for huge antenna systems [90–92]. In these antenna systems, the reconfigurability in antenna radiation characteristics was achieved by using either mechanically movable parts or reconfigurable arrays. In recent decades, thanks to the extensive development of RF electronics, a wide variety of active lumped components such as RF-switch Integrated Circuit (IC), PIN diodes or varactor diodes have been developed and become commercially available. By incorporating these active components into reconfigurable antenna designs, one can develop electronically tunable antennas. By adjusting the control voltages to the active components, the antenna radiation characteristics can be reconfigured accordingly, which is related to the internal parameter change in the active components.

In the literature, numerous reconfigurable antennas have been proposed. These antennas are able to reconfigure their operation frequency [93–96], radiation polarization [21,22,97], radiation pattern [98–100] or combination of these agilities [25,26,101–103]. Examples of frequency-reconfigurable antenna using varactors, polarization-reconfigurable antenna using PIN diodes and pattern-reconfigurable antenna using PIN diodes are shown in Fig. 2.19 (a), (b) and (c), respectively. The connection process of lumped components on rigid PCB materials such as Roger/RT 5880, Rogers RO4003 and FR4 is easy and convenient by using soldering technique.

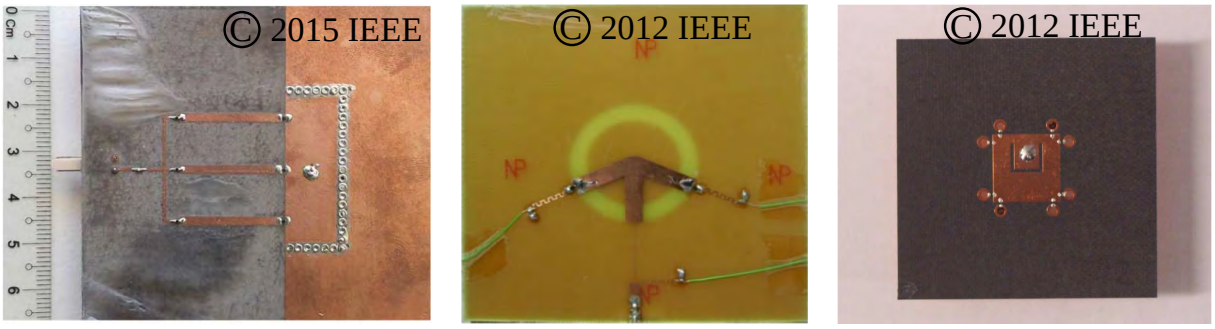

Figure 2.19. Reconfigurable rigid antennas reported in the literature. Examples of reconfigurable rigid antennas reported in the literature (a) frequency-reconfigurable antenna using varactors, adopted from [95], (b) polarization-reconfigurable antenna using PIN diodes, adopted from [97] and (c) pattern-reconfigurable antenna using PIN diodes, adopted from [98].

Since practical wearable antennas are generally constructed on flexible materials such as PF-4 foam, felt and conductive textiles which do not allow direct soldering on their surfaces, the implementation of active components for body-worn antennas is a challenging task. Because of this reason, there exist very limited number of reconfigurable wearable antennas proposed in the literature. To overcome this challenge, various antenna solutions have been proposed and will be discussed in this part.

2.4.1 Conceptual reconfigurable wearable antennas

As mentioned, the challenge in implementation of active components on flexible materials limits the ability of realizing electrically reconfigurable wearable antennas. Due to this challenge, at the beginning, several designs aiming to realize pattern reconfigurable wearable antennas using artificial switches (i.e., not real switches) were proposed [60, 104]. These two fabricated conceptual wearable reconfigurable antennas are shown in Fig. 2.20. In [60], the wearable textile antenna would be able to switch between three beam directions at θ = 0°, 30° and 331° in the yz-plane, if a practical switch could be used. The beam direction switchability was demonstrated by fabricating three antenna prototypes with different connections between a proximity-coupled feed and two sides of antenna patch. The three radiation states (S0, S1 and S2) corresponded to the cases of no connection between the feed and the antenna patch, the feed is connected to the left side of the patch, and the feed is connected to the right side of the patch, as illustrated in Fig. 2.20 (a). Another conceptual reconfigurable wearable antenna was reported in [104]. It could theoretically switch between broadside and omnidirectional radiation patterns, if realistic RF switches could be implemented in the antenna. The antenna includes a full resonance patch, a full ground plane and six shorting vias realized on a flexible felt substrate as shown in Fig. 2.20 (b). By connecting and disconnecting the resonance patch to the six shorting vias, the patch antenna would be able to resonate at a zeroth-order mode (connections ON) or a conventional patch mode (connections OFF). Similar to the first antenna, in order to validate the reconfiguration principle of this antenna, several fabricated antennas corresponding to different switching states were fabricated and measured. Therefore, although the reconfigurable textile antennas discussed above would be conceptually working, their reconfigurabilities could not practically demonstrated.

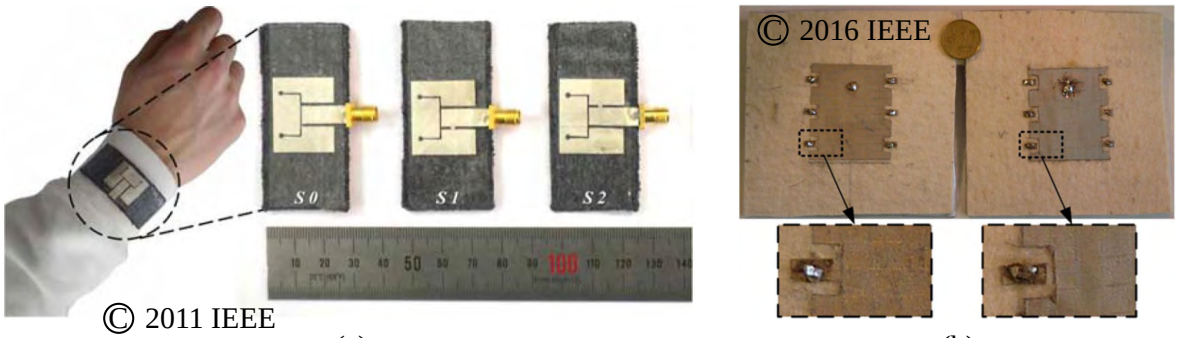

(a) (b)

Figure 2.20. Conceptual reconfigurable textile antennas. Examples of conceptual pattern-reconfigurable textile antennas using artificial switches. The images were adopted from (a) [60] and (b) [104].

2.4.2 Reconfigurable flexible antennas using PDMS

An effective method to maintain the robust connection between rigid electronics and flexible antenna conductors is using PDMS as an encapsulating layer [29, 30]. Double layers of PDMS were utilized to securely immobilize two varactors and an antenna radiation patch and thus make their connection robust. The fabrication process consisted of several steps as illustrated in Fig. 2.21. Three molds with specified thickness were used to accurately shape the antenna substrate layers. After being poured into the mold, each antenna layer needed to be cured in the oven at an exact temperature within a fixed time. An excellent connection between lumped components and antenna parts was validated through various practical experiments including bending and washing. Although the electronic-to-textile connection challenge was solved by using PDMS, this method still has several drawbacks including low antenna efficiency (of approximately 50%), complicated fabrication process and a relatively heavy and bulky structure. Furthermore, since the radiation patch and active components are permanently integrated inside the PDMS substrate, the reconfigurable antenna cannot be maintained or repaired.

2.4.3 Reconfigurable textile antennas using reconfiguration module

Another practical method used to integrate active components into wearable textile antennas is using reconfiguration modules [28]. The first proposed reconfiguration module and its integration solution are illustrated in Fig. 2.22. The module has a dedicated circuitry embedded in a PCB structure in its middle between two back-to-back male snap-on buttons connected at the two terminals of the PCB unit. The completed

2.4.3 Reconfigurable textile antennas using reconfiguration module

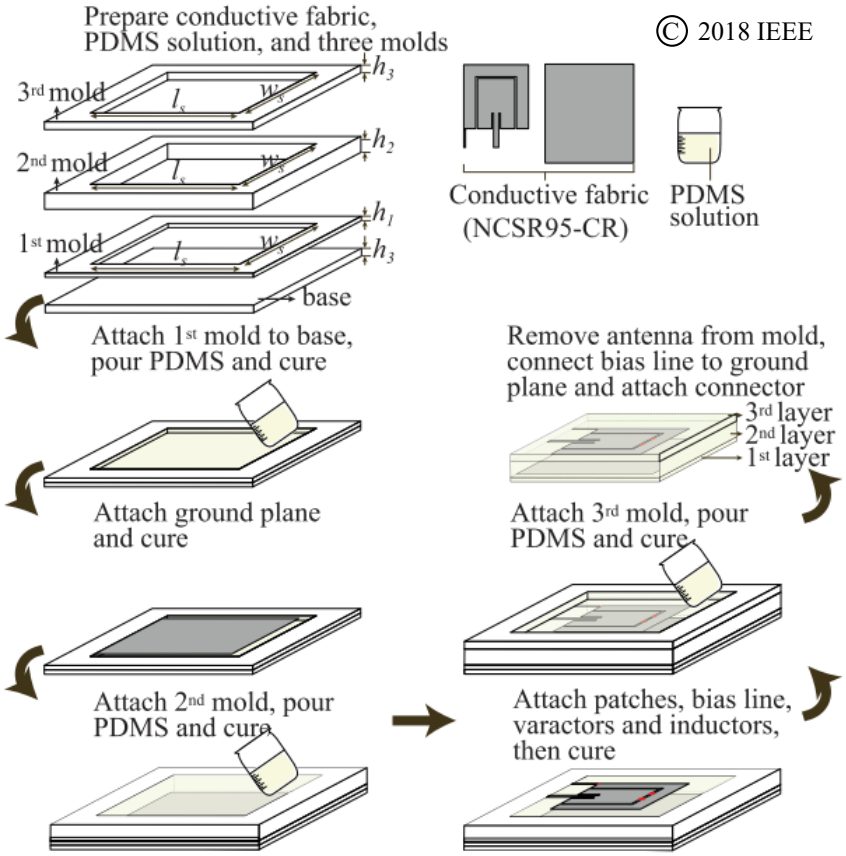

Figure 2.21. Fabrication process of a reconfigurable wearable antenna using PDMS. Manufacturing process to realize frequency-reconfigurable flexible antenna using PDMS. The image was adopted from [29].

module is then placed in the center of a body-worn antenna, the two back-to-back male snap-on fasteners at two sides of the reconfiguration module are engaged with their female counterparts at the other sides of antenna conductive layers. A fabricated PCB module and a completed module prototype are shown in Fig. 2.23. Due to the excellent mechanical and RF connections provided by the snap-on buttons, the proposed reconfiguration module and consequently the loaded active components are well connected to the textile conductors of the antenna. Once the reconfiguration module is manufactured, the antenna fabrication process requires short amount of time. The antenna practicability was validated by a bending test and a loading test with a dielectric disk placed onto the antenna resonant patch. The proposed antenna exhibited a relatively wide frequency tuning range of 32.8% with high radiation efficiency up to 90%. In [28], the authors utilized varactors as tuning components to design frequency-reconfigurable wearable textile antenna aiming to demonstrate the feasibility of the

reconfiguration module concept. It is also possible to use the proposed module to load other types of active components such as PIN diodes or RF-swich IC to realize pattern- or polarization-agile textile antennas. However, since the proposed reconfiguration module design is only dedicated to vertical electronics-to-textile connection, its application is partly limited.

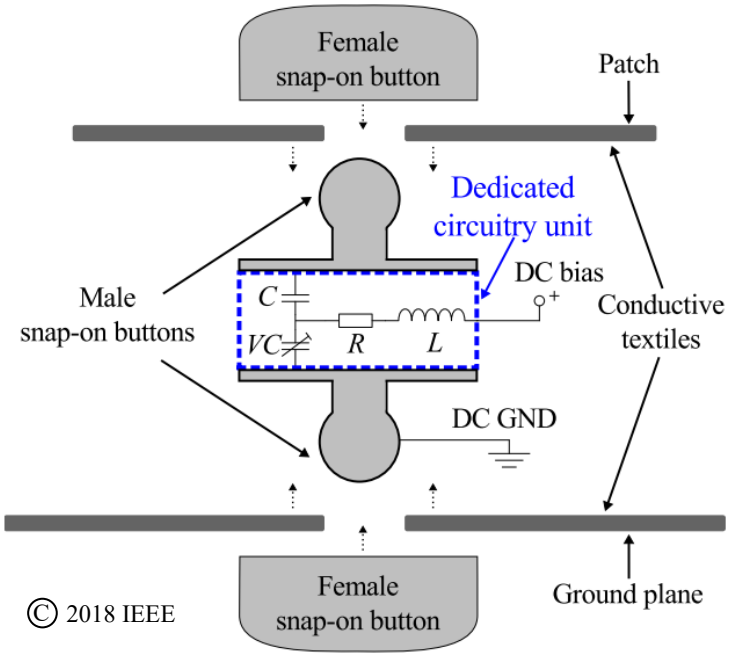

Figure 2.22. Reconfiguration module integration solution. A solution to integrate a reconfiguration module into wearable textile antennas using snap-on button connections. The image was adapted from [28].

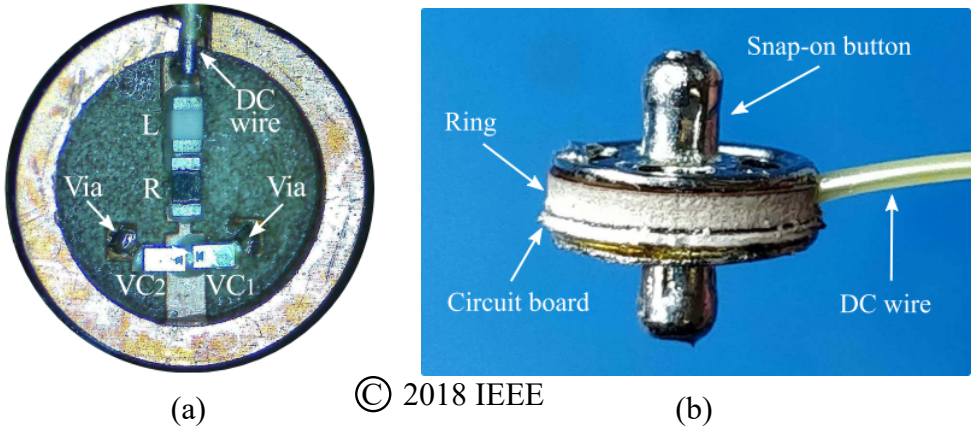

Figure 2.23. Reconfiguration module for wearable textile antennas. Reconfiguration module for wearable textile antennas. (a) PCB board with components loaded and (b) prototype of reconfiguration module. These images were adopted from [28].

2.4.4 Summary on reconfigurable wearable textile antennas

To date, there have been very limited practical solutions for realizing electronic-to-textile connections aiming to implement reconfigurability to wearable textile antennas. Using PDMS as an encapsulating layer [29, 30], the connections between active components and antenna textiles are securely maintained even after extreme tests of bending or washing. However, this method requires complicated fabrication processes which are very time consuming. Furthermore, the antenna radiation efficiency is low due to the high loss characteristics of PDMS. Another promising solution is utilizing reconfiguration modules combining snap-on buttons and dedicated circuitry units. In this solution, active components are assembled onto a small PCB with back-to-back male snap-on fasteners. Excellent mechanical and RF connections between the module and the antenna textile conductors were demonstrated through extreme bending and loading tests. The antenna exhibited wide frequency tuning range and high radiation efficiency. However, the proposed reconfiguration module is only suitable to realize connection between rigid electronics and antenna textiles in a vertical arrangement.

2.5 Conclusion

In this chapter, several aspects of wearable textile antenna technology have been reviewed. Firstly, some widely-used conductive and non-conductive materials in wearable antenna designs have been discussed. Each material exhibits its own advantages and disadvantages which are appropriate for different design requirements. Considering antenna efficiency and fabrication complexity, PF-4 foam and conductive textiles are found to be among the best choices for wearable textile antenna designs. Secondly, some typical passive flexible textile antennas and corresponding design techniques have been reviewed in the second section of this chapter. Several techniques such as utilizing slots, multiple resonators, quarter-wave modes (PIFA structure), and components such as conductive yarns, shorting eyelets and metallic snap-on buttons were employed in realizing flexible body-worn antennas. In the last section of this chapter, some practical solutions used to realize reconfigurable wearable textile antennas have been presented. It is found that, utilization of reconfiguration module is one of the most effective method to realize practical reconfigurable body-worn antennas.

Chapter 3

Shorting Strategies for Wearable Textile Antennas

SHORTING vias are standard components in planar fabrication technologies, but their implementation is not straightforward in wearable textile electronics. There have been broadly four main different shorting strategies for wearable flexible textile antennas, namely those based on embroidered metalized wires, folded strips of metalized fabric, metallic eyelets, and snap-on buttons. Each method exhibits different strengths and weaknesses in terms of complexity, efficiency, mechanical stability, and modularity.

In this chapter, these shorting strategies are applied to design different selected antenna structures, specifically two variations of a quarter-wavelength patch antenna and a monopolar patch antenna with edge shortings. The analysis aims at guiding designers in the selection of the most appropriate shorting method for their specific application, considering the efficiency of the folded strips, the fabrication simplicity of the eyelets, the mechanical stability of the embroidered vias, and the modularity of the snap-on buttons.

3.1 Introduction

As mentioned in Chapter 2, since wearable textile antennas are destined to be mounted on or integrated into clothes, they need to be low-profile, light-weight and flexible. Several prevailing materials, including conductive as well as non-conductive types, have proved their suitability in wearable antenna designs. Typical flexible and light-weight conductive materials have been discussed in Chapter 2 and can be summarized as copper tape [64, 65], conductive ink [66–68], conductive polymers [11, 53, 54, 69, 70, 105, 106], graphene composites [71–73, 107, 108] and conductive textile [10, 12, 28, 35, 56, 61, 74, 78]. Popular non-conductive substrates include felt [1, 10, 64, 75–79, 109], PDMS [13, 58, 61, 80–82, 110] and PF-4 foam [35–37, 56, 57].

Shorting metallic vias are used widely in printed circuit board (PCB) antenna technology to vertically connect metallic layers to the ground plane across the substrate. They are used for example to reduce the size of antennas [111–113], to create substrate-integrated waveguides and cavities [95, 114–118] or to control the current distributions, as illustrated by the monopole-like radiation pattern of centered-fed patch antennas with edge-shortings [119–124]. For rigid antennas, the shorting vias are often implemented by using rivets [95, 118, 121, 122, 125], metallic walls [119, 120] or metalized holes [114, 116] which are illustrated in Fig. 3.1 (a), (b) and (c), respectively. A set of 12 shorting rivets in Fig. 3.1 (a) and 4 shorting walls in Fig. 3.1 (b) are used to generate additional radiation modes. In Fig. 3.1 (c), the metalized holes are utilized to create a substrate-integrated waveguide. Such methods are however not applicable for textile antenna technologies, and thus there is a need for dedicated solutions in this domain.

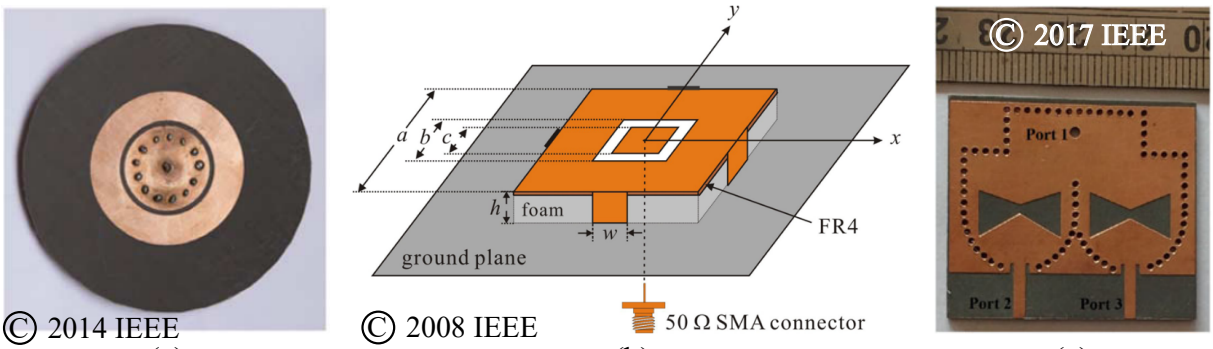

Figure 3.1. Shorting vias for rigid antennas. Examples of shorting vias for rigid antennas, implemented by using (a) rivets, adopted from [122], (b) metallic walls, adopted from [120] and (c) metalized holes, reproduced from [116].

In this context, recent studies have proposed several strategies to realise shortings between a patch and its ground plane for wearable antennas. These include embroidered vias [35,87,126,127], a folded strip of metalized fabric [128,129], eyelets [7,130–132] and snap-on buttons [37, 133]. All the mentioned studies demonstrated ad-hoc utilization of a particular shorting method in its textile implementation. There is however a need for a detailed analysis on the strengths and weaknesses of these prevailing shorting methods, which motivates the present detailed investigation. It is noted that preliminary comparison of three shorting strategies was published in a conference contribution [128], however only based on simulations.

This chapter will firstly present a comprehensive numerical and experimental investigation on the aforementioned four popular shorting methods compatible with textile technologies, which are embroidered vias, folded strips of metalized fabric, eyelets and snap-on buttons. These shorting strategies are briefly described and then applied to construct three antenna topologies including two variations of quarter-wave patch antennas and a planar patch-based monopolar antenna. Simulation, fabrication processes and measurement results are presented before the advantages and disadvantages of each shorting methods are discussed.

To demonstrate the benefit of the interchangeability of the snap-on fasteners, the second part of the chapter will present a dual-band wearable textile patch antenna with modular pattern interchangeability. The antenna simultaneously covers the 2.45 and 5.8 GHz ISM radio bands. By utilizing detachable shorting connections of metalic snap-on buttons, the proposed antenna can be set up to radiate either in broadside or monopole-like radiation patterns at 2.45 GHz, while the radiation characteristics at 5.8 GHz remain unchanged. The proposed modular antenna is fabricated and measured to validate the concept.

3.2 Shorting strategies for wearable textile antennas

In this section, four different shorting strategies for wearable flexible textile antennas, namely based on embroidered metalized wires, folded strips of metalized fabric, eyelets and snap-on buttons are investigated. These shorting methods are applied to design different selected antenna structures, specifically two variations of a quarter-wavelength patch antenna and a monopolar patch antenna with edge-shortings. The simulated and experimental results demonstrate how these four shorting strategies can

be effectively used in flexible wearable textile antenna designs. Each method exhibits different strengths and weaknesses in terms of their complexity, efficiency, mechanical stability and modularity. The analysis aims at guiding designers in selection of the most appropriate shorting method for their specific application, considering the efficiency of the folded strips, the fabrication simplicity of eyelets, the mechanical stability of the embroidered vias and the modularity of the snap-on buttons. The results presented in this section have been published in [41].

3.2.1 Overview

The four mentioned shorting strategies, as illustrated in Fig. 3.2 in cut views, are sequentially introduced in the following, together with general descriptions of their features and expected performance.

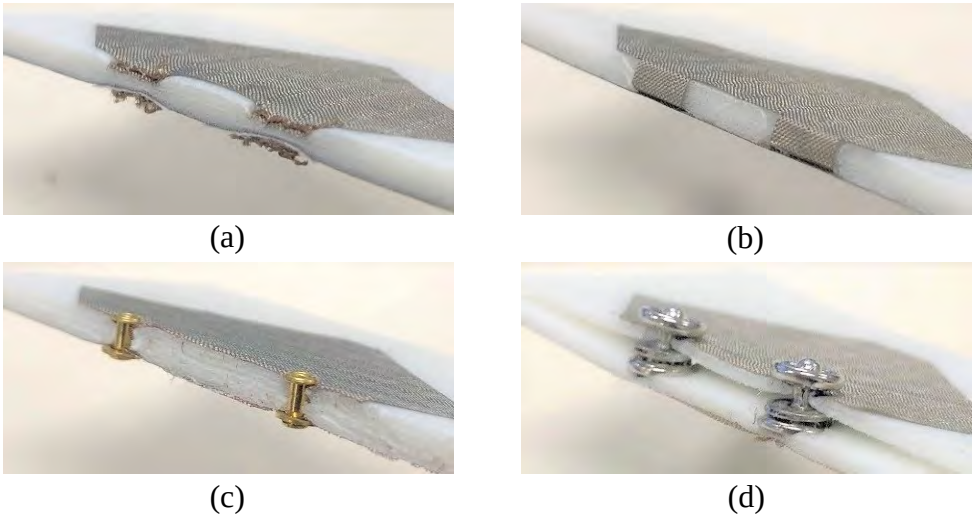

Figure 3.2. Four considered shorting strategies. Four considered shorting strategies, shown in a cut view. (a) Embroidered vias, (b) folded strips of metalized fabric, (c) eyelets and (d) snap-on buttons.

Shorting with embroidered vias

Embroidery techniques have been used widely in textile antenna designs due to their compatibility with textiles and clothing manufacture techniques [35,51,126,134]. Conductive textile planes on different layers can be electrically connected using embroidered stitches realized in silver-coated yarns, as illustrated in Fig. 3.2 (a). This shorting modality is expected to increase the mechanical robustness of the antennas and can be

applied for mass production since the manufacture process is a standard technique in the textile/clothing industry. Nevertheless, the typically modest conductivity of available conductive threads is expected to degrade the antenna performance in terms of gain and efficiency. Furthermore, each stitch causes a local compression of the substrate, which is a critical parameter that increases the complexity of modeling and may affect the antenna performance [35, 56].

Shorting with folded strip of metalized fabric

A thin folded strip of metalized fabric can be used to provide electrical connection between a planar conductor layer and the ground plane. As shown in Fig. 3.2 (b), the strip may be made from the same cut of conductive fabric as the top metallic patch, thus benefiting from a seamless contact and a very low sheet resistance. This particular feature leads to expectation of high antenna performance in terms of radiation efficiency. However, the electrical connection of this folded strip to the ground plane is not necessarily always straightforward, since it may require conductive glue or embroidery technology for some antenna topologies.

Shorting with eyelets

The use of eyelets is very widespread in the clothing industry. Fabric eyelets made of copper or brass can be utilized to realize shorting vias between two conductive textile layers (Fig. 3.2 (c)). This method is in fact very similar to the soldered rivet vias employed in PCB technologies. Shorting with eyelets is expected to be the easiest method for fabrication, since it is based on a standard clothing manufacture process. However, a tight connection between eyelets and the conductive textile need to be maintained to guarantee the antenna performance.

Shorting with snap-on buttons

Snap-on buttons are another type of fixture commonly adopted in the clothing industry. An assembly of two back-to-back metallic male snap-on buttons can be used to build a connection between two conductive textile layers separated by a substrate (Fig. 3.2 (d)). The female snap-on buttons are utilized to affix the back-to-back male buttons with the conductive textile layers. The tightness of the connection between the female and male snap-on buttons highly depends on the substrate thickness. For very

thin substrate this connection is maintained with high level of robustness since a typical disengaging force is approximately 3 N [88]. The main advantage of this shorting method is the modularity of the possible connections [37], however at a cost of a rather complex fabrication process.

3.2.2 Antenna configurations

The two generic antenna topologies employed in this study are a quarter-wave patch antenna (which can be referred to as a type of planar inverted-F antenna - PIFA) and a planar monopole antenna with ground-shorting, since these antenna types both rely on shorting vias, while operating on very different principles. The PIFA design is based on [135], however with an adaptation of a proximity-coupled feed instead of a probe feed. The proximity-fed monopolar patch structure is based on [123], with a circular radiation patch and three single vias instead of a rectangular patch with four multi-vias shorting walls. The antennas are designed to operate simultaneously at 2.45 and 5.8 GHz, i.e. in two of the ISM frequency bands. This dual-band operation will also allow to investigate how diverse modes in the antenna structure may be differently affected by the shorting strategy.

In order to satisfy wearability requirements, the antenna substrate is selected here as a highly flexible and light-weight material, which is Cuming Microwave C-Foam PF-4 with a thickness of 1.6 mm, relative permittivity $\varepsilon_r = 1.06$ and loss tangent $\tan\delta = 0.0001$. Our test indicated that, the PF-4 foam has a compression set of approximately 15% of initial thickness after being compressed by 50% at about 23°C for 72 hours. This measured result is significantly below the suggested maximum compression set of 40% for wearable antenna design from [136]. This type of substrate was empirically found in other works to have satisfactory compressibility [35,36] and flexibility [28,37] for wearable textile antennas. The antenna ground plane, resonant patch and microstrip feed are designed using a highly electrically conductive silver-coated nylon RIPSTOP fabric (referred to as "silver fabric" in the following) with a sheet resistance of 0.01 Ω/square. For brevity and consistency of the results, only one type of substrate and conductive material is considered. However, it is to expect that similar considerations on these shorting strategies can be applied to other flexible substrates such as felt or PDMS as well as other conductive textile materials.

All antenna designs have been refined through parametric full-wave simulations, so that they operate satisfactorily in the mentioned two ISM bands. All simulations were performed using CST Studio Suite 2019.

PIFA structures and operation principle

The PIFA configurations are shown in Fig. 3.3 and the final dimensions are listed in Table 3.1. In order to create the quarter-wave PIFA topologies, the resonant patch can be shorted either on an entire side or at two points at one of its edges. For each shorting method, a specific parametric refinement has to be performed on parameters W_1 - W_4 and L_1 - L_4 to adapt the dual operation bands and maximize the antenna performance. For a PIFA, the quarter-wave patch size is roughly inversely proportional to the width of shorting wall [85]. Therefore, PIFAs using full shorting wall require larger resonant patches than the ones using two shorting posts.

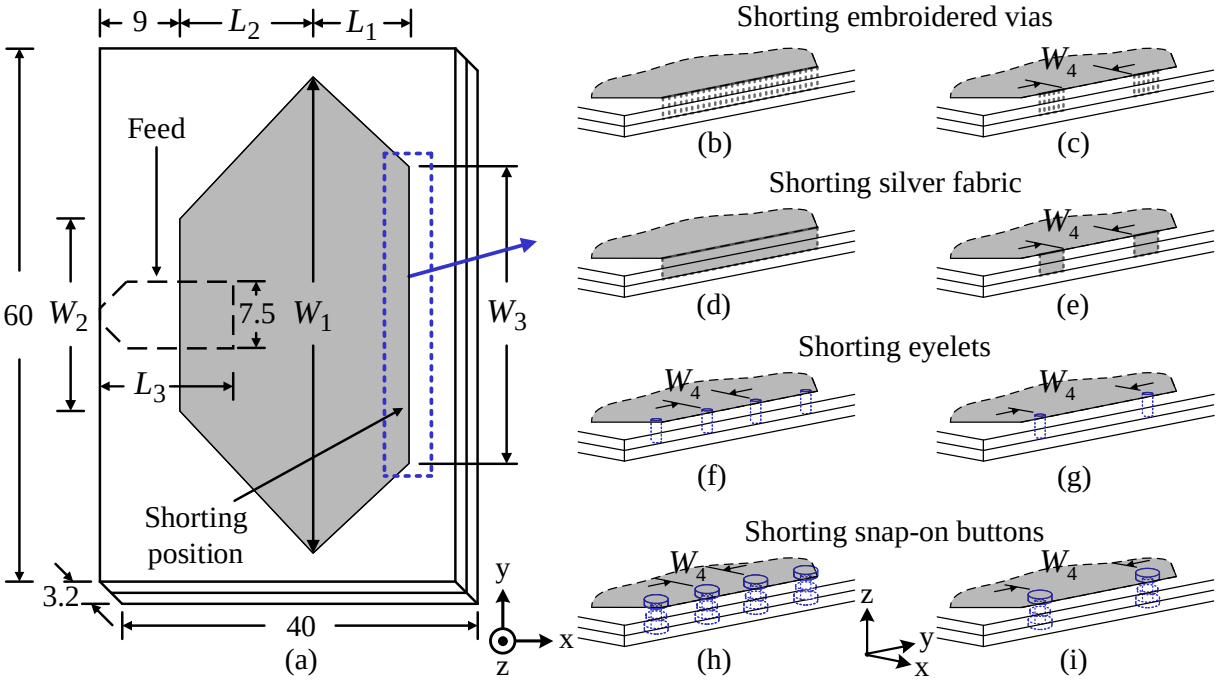

Figure 3.3. PIFA antennas configuration. (a) PIFA configuration with fixed dimensions given in mm while variables W_1 - W_4 and L_1 - L_3 refer to values in Table 3.1. The right-hand side images illustrate the shorting implementations: (b) full embroidered wall, (c) two small embroidered walls, (d) full folded strip of silver fabric, (e) two small folded strips of silver fabric, (f) full wall of 4 shorting eyelets, (g) two shorting eyelets, (h) full wall of 4 snap-on buttons and (i) two snap-on buttons.

Table 3.1. PIFA antennas dimensions. PIFA dimensions (in mm) for the various shorting types

	W_1	W_2	W_3	W_4	L_1	L_2	L_3
Full embroidered via	52.7	21.6	33.8	-	10.2	15.0	14.0
Full silver fabric strip	52.6	21.6	34.4	-	10.2	15.0	14.0
Full eyelet	53.6	21.6	34.4	10.4	10.8	15.0	15.0
Full snap-on buton	54.3	24.0	34.0	10.8	12.0	16.0	14.5
Two embroidered vias	45.7	3.9	28.0	10.0	8.3	17.0	15.0
Two silver fabric strips	45.7	3.9	28.0	10.0	8.1	17.0	15.0
Two eyelets	46.0	3.9	28.0	20.0	8.0	17.0	14.0
Two snap-on buttons	45.6	7.5	26.0	16.0	10.2	17.0	15.0

The antenna radiation patches are shorted to the ground at one resonant patch edge to excite the $TM^z_{0(0.5)0}$ mode, and its instantaneous electric field distribution is shown in Fig. 3.4 (a). A higher-order mode TM^z_{011}, with the instantaneous electric field distribution displayed in Fig. 3.4 (b), is realized by optimizing the patch geometry and consequently the input impedance. An irregular hexagonal shape is used to design the resonant quarter-wave patch instead of a traditional canonical shape, to add degrees of freedom in optimizing the antenna performance. The dual-band characteristics are achieved by exploiting two radiation modes simultaneously. The parameter optimization for important dimensions W_1, W_2 and W_4 for the PIFA using two shorting eyelets are shown in Fig. 3.5 to demonstrate the general design procedure. The PIFA mode ($TM^z_{0(0.5)0}$) resonating at 2.45 GHz is initially excited by choosing an appropriate patch length ($L_1 + L_2$) which is approximately a quarter-wave length. As illustrated in Fig. 3.4 (b), the higher band at 5.8 GHz is mainly determined by the patch width W_1. Therefore, once the quarter-wave mode is excited, the next step is to change the radiation patch width W_1 to obtain the higher band at 5.8 GHz. As shown in Fig. 3.5 (a), the higher band is more sensitive to the radiation patch width W_1 than the lower band. Once the 5.8 GHz is approximately achieved, the narrow feeding end of the resonant patch with width W_2 is varied aiming to tune the lower band while maintain the higher band, as depicted in Fig. 3.5 (b). Lastly, the shorting posts' spacing W_4 (for the PIFAs using two shorting posts) or the dimension W_3 (for the PIFAs using full shorting wall) is optimized for the higher frequency only with minor effect on lower frequency as shown in Fig. 3.5 (c).

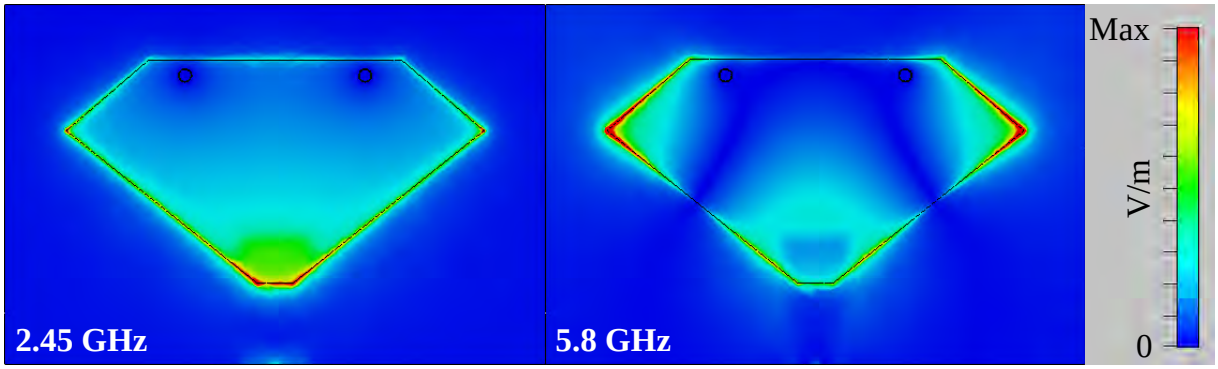

Figure 3.4. Electric field distributions of PIFA. Simulated electric field amplitude distribution in the cavity of the PIFA. (a) PIFA mode at 2.45 GHz and (b) higher-order mode at 5.8 GHz.

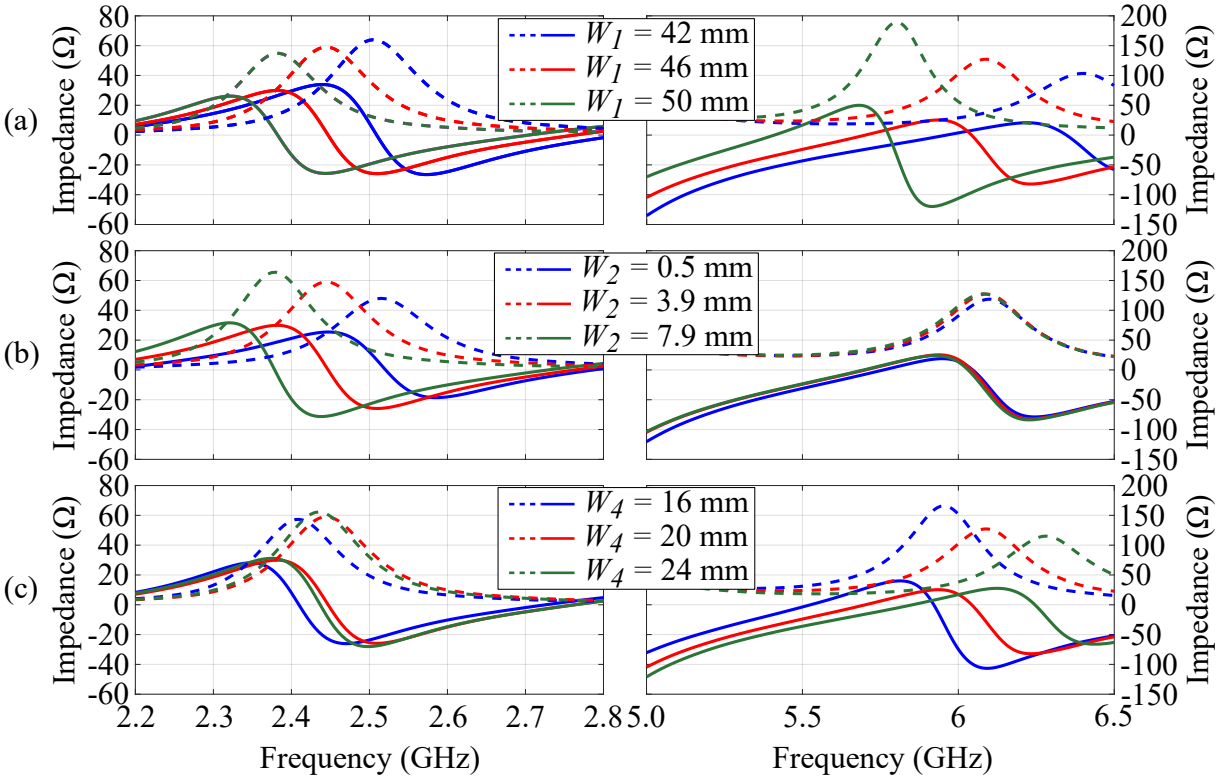

Figure 3.5. Simulated input impedance for the PIFA. Simulated input impedance for the PIFA antenna with various patch dimensions. Solid lines: imaginary part; Dashed lines: real part.

Monopole antenna structures and dimensions

The low-profile shorted-patch monopole antenna structures and dimensions are shown in Fig. 3.6. This antenna topology is based on the generic designs of shorted-patches as presented in [125], and more specifically on derived designs described in [120,124,137]. In this antenna structure, the centered-fed circular patch is shorted at three points on its circumference, where the 120° separation creates three in-phase radiating apertures, which can be observed in the electric field distribution shown in Fig. 3.7 (a). These thin apertures create an equivalent magnetic current loop and have a resonance at a lower frequency of 2.45 GHz. Three PF-4 layers of 1.6 mm thickness are stacked to create the substrate and increase the bandwidth at 2.45 GHz.

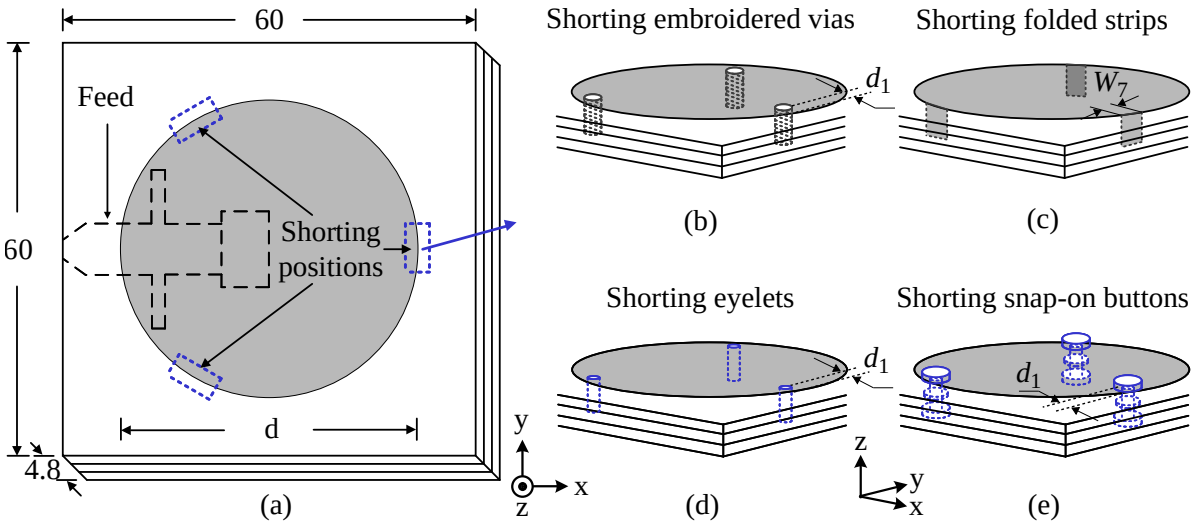

Figure 3.6. Shorted-patch monopolar antenna configuration. (a) Shorted-patch monopolar antenna configuration and dimensions (in mm) with shorting positions, (b) shorting embroidered vias: d = 51.3 mm, (c) shorting folded strips of silver fabric: d = 43.2 mm, (d) shorting eyelets: d = 43.7 mm and (e) shorting snap-on buttons: d = 53.9 mm.

In order to create a higher-order mode operating at the higher resonance frequency at 5.8 GHz and cover the corresponding ISM band, we used a stacked proximity-coupled feed structure which is depicted in Fig. 3.8, with dimensions shown in Table 3.2. The general design procedure is to start from a design achieving its lower-order resonant mode at 2.45 GHz. Since the length of the three apertures influences the resonance frequency at the monopole mode significantly [123], the shorting positions (for the

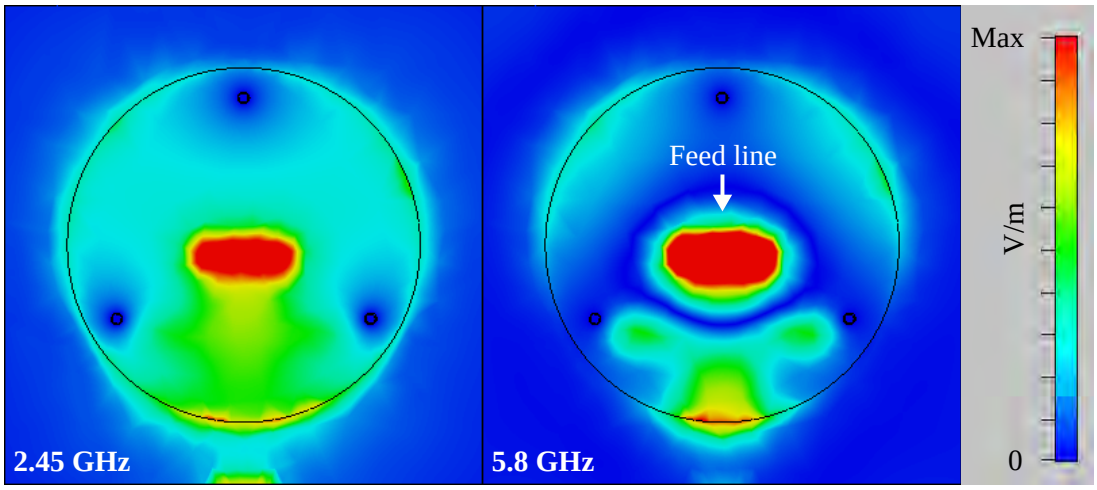

Figure 3.7. Electric field distributions of the monopole antennas. Simulated electric field amplitude distribution in the cavity of the monopole antennas illustrating the three radiating apertures on the circumference. (a) Monople mode at 2.45 GHz and (b) higher-order mode at 5.8 GHz. The hot spots in the center are due to the proximity of the feeding structure.

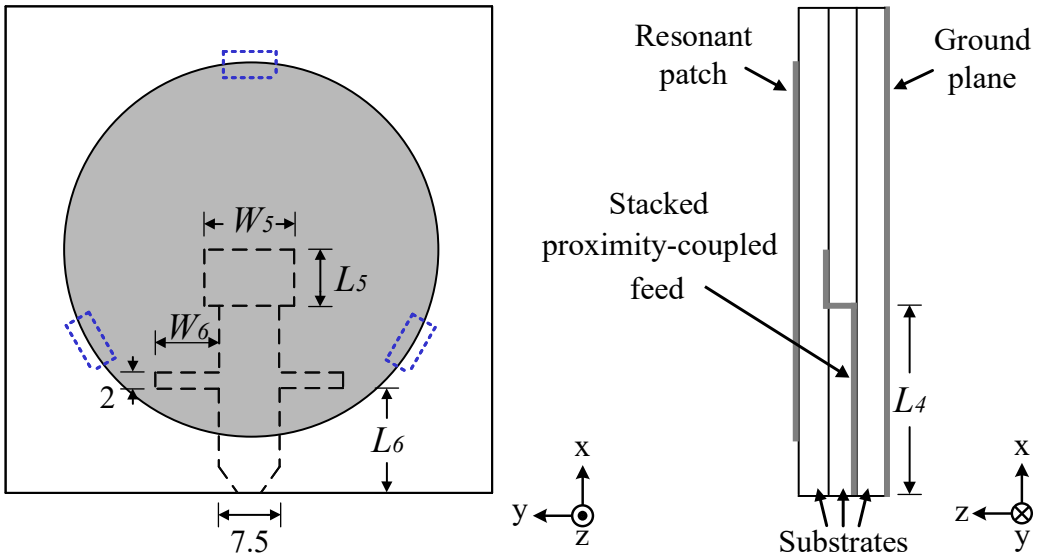

Figure 3.8. Stacked proximity-coupled feed structure and dimensions. Stacked proximity-coupled feed structure and dimensions (in mm).

Table 3.2. Stacked proximity-coupled feed dimensions. Stacked proximity couple feed dimensions (in mm)

	W_5	W_6	L_4	L_5	L_6
Shorting eyelets	11.5	9.0	25.0	2.8	17.9
Shorting snap-on buttons	21.1	0	26.5	3.7	-
Shorting embroidered vias	9.7	0	27.0	3.0	-
Shorting folded strip	11.5	9.0	27.5	2.5	17.4

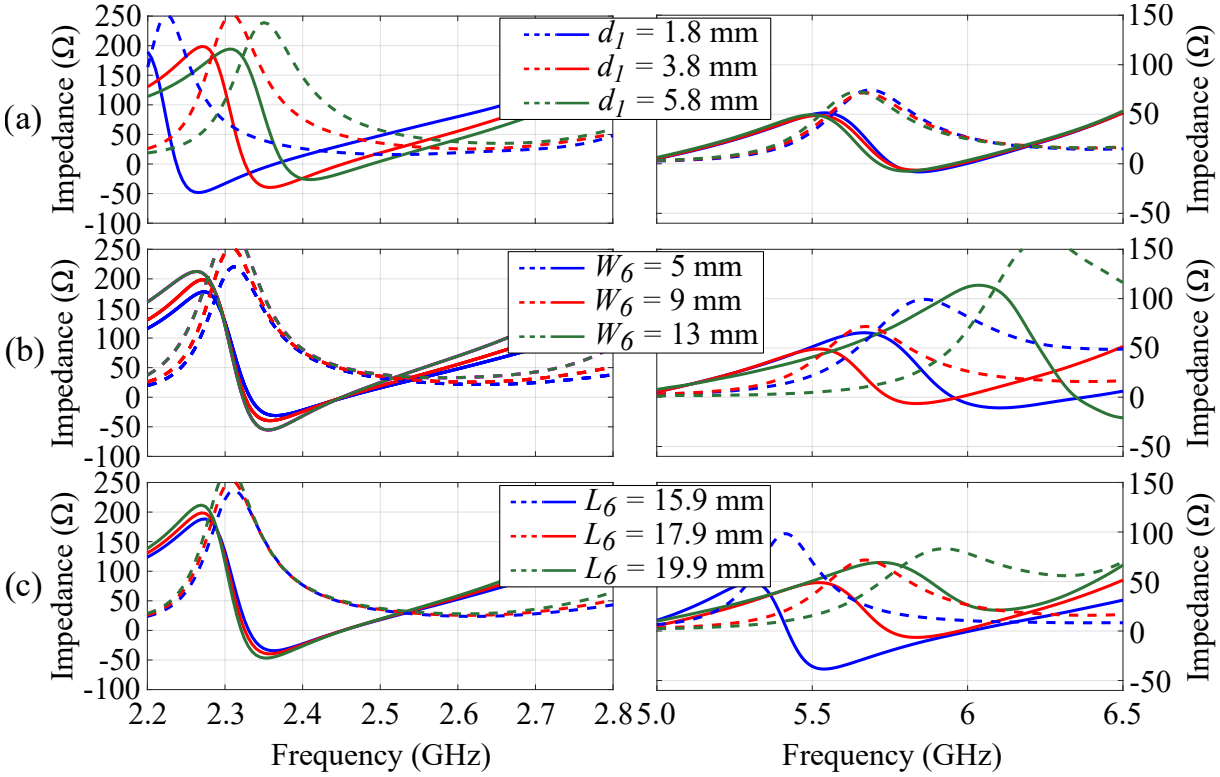

Figure 3.9. Simulated input impedance of the monopole antenna. Simulated input impedance of the monopole antenna for various values of feeding dimensions. Solid lines: imaginary part; Dashed lines: real part.

monople antenna using shorting eyelets and shorting snap-on buttons) or the shorting dimensions (for the monople antenna using shorting folded strips and shorting embroidered vias) are selected to realize the lower band at 2.45 GHz. The parameter optimization for important dimensions d_1, W_6 and L_6 for the monopole antenna using shorting eyelets are shown in Fig. 3.9 to demonstrate the general design procedure. It

can be concluded from Fig. 3.9 (a) that, by varying the gap in-between shorting position and the patch edge (d_1) (the wall width W_7 for shorting by folded strips of silver fabric, see Fig. 3.6), the resonance frequency of the monopole mode is changed with almost no influence to the higher band. For the monopole antennas using shorting folded strips and shorting embroidered vias, it is necessarily to vary the shorting dimensions in stead of shorting position d. The 5.8 GHz band then can be adjusted by varying the two dimensions of the stacked proximity-coupled feed W_6 and L_6. By optimizing the feed dimension, the higher frequency is changed with very minor effect on the lower frequency as shown in Fig. 3.9 (b) and (c).

3.2.3 Antenna simulation and fabrication

Simulation and fabrication methods for different shorting strategies are presented in this section. In order to fabricate the considered antennas, the PF-4 foam substrate and silver fabric pieces are cut to given dimensions, preferably using a laser milling machine for best accuracy. For the antenna shorted using folded strips of silver fabric and embroidered walls, the resonant patches are cut in a different ways which will be explained later. The ground plane, top plane and microstrip feed are attached to the foam substrates using washable fabric glue. Conductive epoxy CW2400 from CircuitWorks is used to mechanically and electrically connect all the conductive parts together including an SMA connector to the microstrip feed and the folded strips of silver fabric to the ground plane.

Embroidered vias

The embroidered via-walls are realized using Statex Shieldex 117/17 dtex 2-ply conductive yarn which has an appropriate diameter of 0.12 mm and linear resistance of R = 40 Ω/cm. There are two critical parameters to be considered: the stitch density and the substrate compression.

The stitch density depends on both the stitch spacing as well as the number of passes, and has been shown to have a significant impact on antenna performance [35, 56, 86, 134, 138, 139]. A higher embroidery density decreases the via effective sheet resistance, and also leads to a higher mechanical robustness of the antenna structure. However, a large number of path may undermine the integrity of the foam substrate, and therefore, a trade-off is required. In this study, a stitch spacing of 2 mm with two repetitions

(passes) of the embroidery is applied to create the shorting vias which is illustrated in Fig 3.10 (a). Due to easier fabrication, instead of using a linear via, a circular embroidered via with a radius of 3 mm is utilized for a shorted-patch monopole antenna (as displayed in Fig 3.10 (d)).

A compression of the flexible substrate is observed at the seam and is a critical parameter to consider while designing embroidered shorting vias or walls. The effective height of the embroidered connection is decreased due to this substrate compression, which is actually beneficial to the antenna performance, as it leads to a shorter resistive path and thus a higher radiation efficiency [35].

In order to precisely simulate the substrate compression, embroidered samples with selected densities are manufactured as shown in Fig 3.10 (b) and (e). On that basis, the substrate compression can be quantified for accurate 3D modelling, allowing inclusion in the 3D simulations as illustrated in Fig 3.10 (c) and (f).

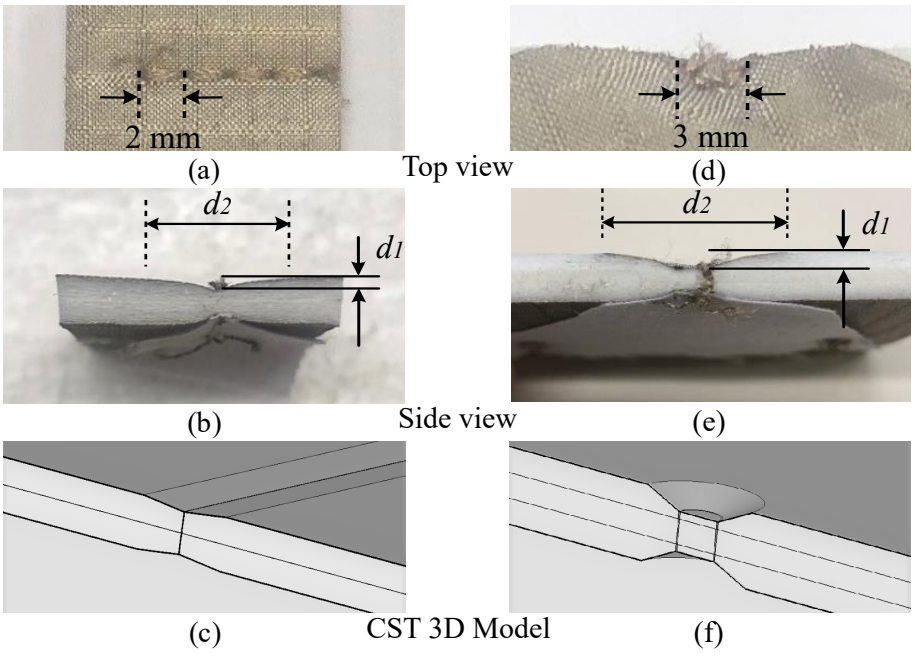

Figure 3.10. Substrate compression caused by embroidery vias. Substrate compression caused by an embroidery wall and a circular embroidered via. Linear wall: (a) fabricated prototype, (b) compression dimensions with $d_1 = 0.4$ mm, $d_2 = 5.8$ mm and (c) CST simulation. Circular via: (d) fabricated prototype, (e) compression dimensions with $d_1 = 1.1$ mm, $d_2 = 8$ mm and (f) CST simulation.

Figure 3.11 shows the embroidery processes for the three different types of antenna considered using a Brother Entrepreneur PR655 Advanced 6-Needle Home embroidery machine. The fabrication challenge for this shorting method lies in the embroidery tolerance. However, once an appropriate embroidery fabrication setup is defined, the process is scalable for mass production.

Since the embroidered walls are placed at the edge of the resonant patch, it is necessary to extent the resonant patch at the shorting position to make sure that the embroidered walls fully contact the patch. Figure 3.11 (c), (d) detail the extended parts which have similar width as the embroidered shorting walls and appropriate length (4 mm in this case). These parts can be cut off after the embroidery process is completed. It is unnecessary to make the extended path for monopole antenna because the circular walls are embroidered fully inside the resonant patch.

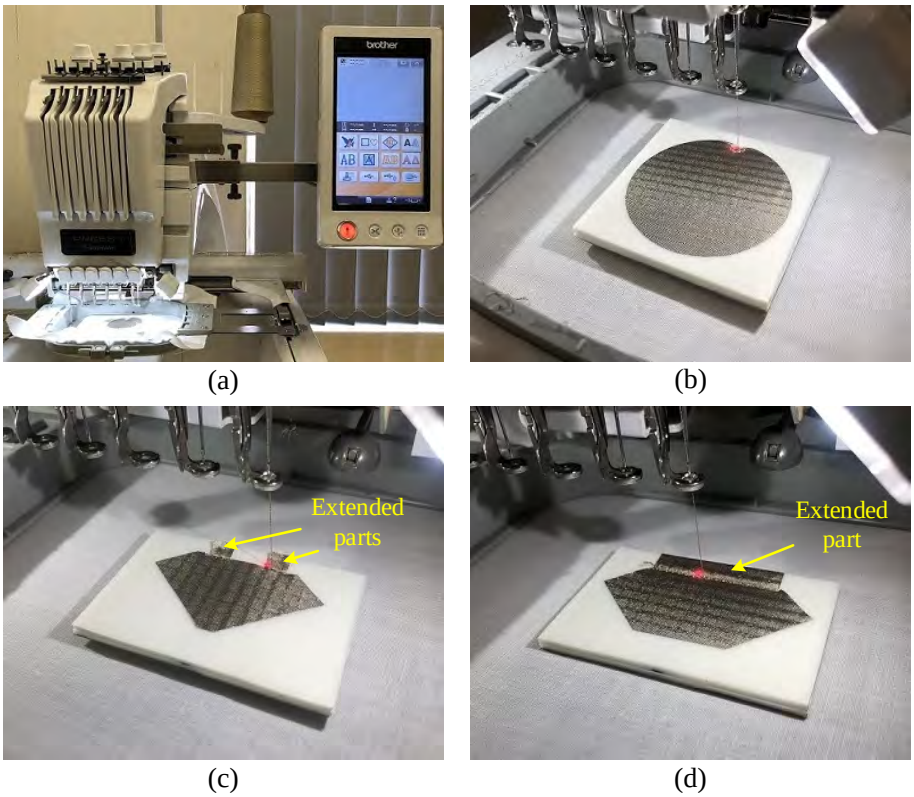

Figure 3.11. Embroidery process. Embroidery process, (a) embroidery machine, (b) planar monopole antenna, (c) PIFA with two small embroidered vias and (d) PIFA with full embroidered via.

3.2.3 Antenna simulation and fabrication

Folded strip of metalized fabric

This method is the simplest shorting strategy since it only requires thin strips of metalized fabric to connect the resonant patch to the ground plane. In simulation, a sheet resistance of 0.01 Ω/square corresponding to the silver fabric characteristic has been used to realize the shorting strips.

The fabrication process to create a shorting wall using folded strip of silver fabric includes the following steps. The resonant patch and the shorting walls with an extra length are cut as one piece of conductive fabric, as illustrated in Fig. 3.12 (a). An extra shorting wall length of 3 mm offers sufficient contacting area for connection to the ground plane. The strips are inserted through made-to-purpose slits in the substrate, as shown in Fig. 3.12 (b), folded as shown on Fig. 3.12 (c) and glued to the later affixed ground plane using conductive expoxy. All the steps of the fabrication procedure can be well controlled, making the process convenient and accurate. Fig. 3.12 (d) shows the fabricated PIFA with two folded strips of silver fabric as an example.

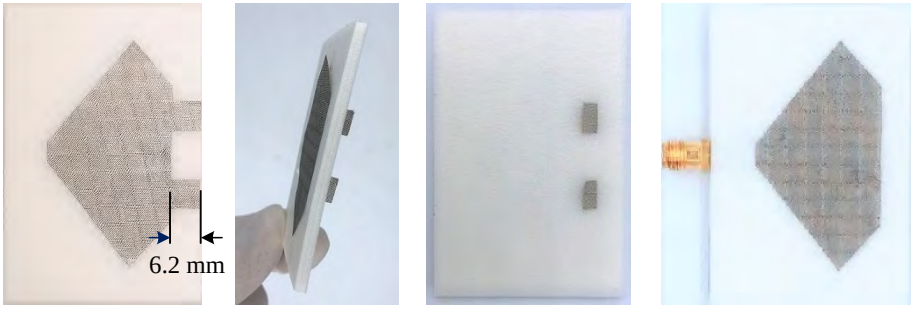

Figure 3.12. Fabrication of shorting with folded strips. Fabrication of shorting with folded strips, (a) resonant patches with shorting strip/walls, (b) shorting strips/wall inserted through the substrate, (c) back side of the substrate before attachment of the ground plane and (d) the fabricated PIFA with two folded strips of silver fabric.

Eyelets

Brass eyelets are selected to implement the shortings due to their high conduction efficiency. A precise modeling of the eyelet dimensions and the observed substrate compression are two important aspects in simulation. A larger eyelet's ring radius will lead to a better textile connection at a cost of a larger antenna size. Considering this trade-off, we select eyelets with an outer cylinder radius of 0.75 mm and a cap radius

of 1.33 mm. Additionally, an intrinsic substrate compression is observed near the eyelet, which strengthens the eyelet-to-textile connection. It is important to note that the level of substrate compression here is controllable through manufacture settings. In the present study, the substrate compression is selected as 0.2 mm.

The antennas with shorting eyelets require some specific fabrication steps. Holes are punched in the substrate to provide a tight fit and cross slits are cut through the conductive textile layers to warrant electrical contact, as shown in Fig. 3.13 (a). A washer is utilized to enhance the contact between the eyelet and the antenna ground plane as shown in Fig. 3.13 (b) and (c). The eyelet riveting process allows a fabrication at high level of accuracy, with potential for automatization. The fabricated PIFA with two eyelets is displayed in Fig. 3.13 (d).

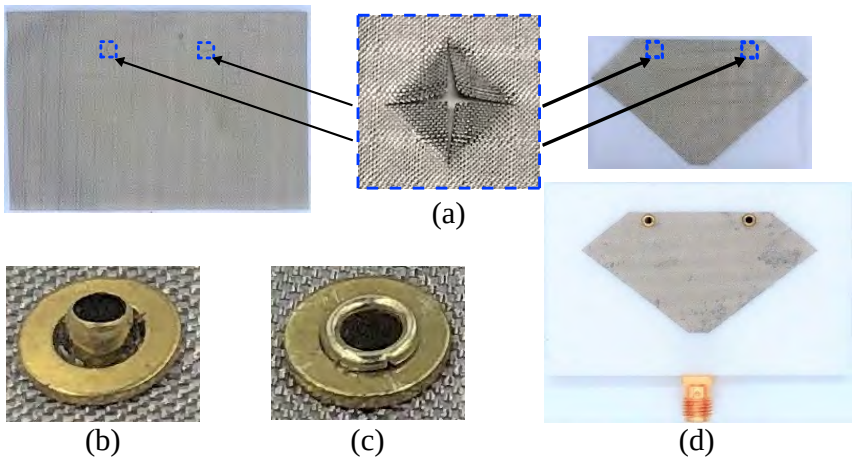

Figure 3.13. Eyelet riveting processes. Eyelet riveting processes, (a) cross slits on the patch and ground plane for accommodating the eyelets, (b) eyelets and washers placement, (c) completed riveting and (d) fabricated PIFA with two eyelets.

Snap-on buttons

Commercial snap-on buttons were utilized as fixtures and RF connectors in [37, 133, 140]. In order to realize a snap-on button shorting strategy, we use back-to-back male nickel snap-on buttons to form a via. Two female buttons provide the counterpart connections and mechanical fixture to conductive textiles [37]. The dimensions of the snap-on configuration in Fig. 3.14 indicate that a maximum gap between two female buttons is 2.6 mm which is still shorter than the substrate thickness of either the PIFA or monopole antenna at 3.3 and 4.9 mm, respectively. This feature consequently introduces a substrate compression and thus enhances the button-to-textile connection

robustness. However, this also leads to potential unwanted detachment of the female buttons in working condition due to the pushing force of the compressed substrate. It is therefore necessary to reduce the substrate compression to an appropriate level, e.g., by sewing the bottom female snap-on button on the ground plane to integrate it into the antenna. In this case, there is almost no substrate compression for the PIFAs and the substrate compression level for monopole antennas is reduced from 1.3 to 0.4 mm.

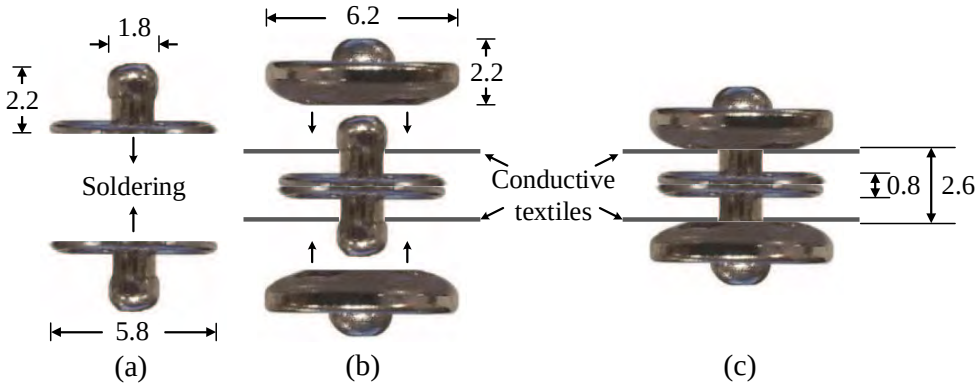

Figure 3.14. Snap-on button via connection. Snap-on button via connection (dimensions in mm). (a) Back-to-back male connection, (b) pair of female snap-on buttons for connection to the back-to-back male buttons and (c) completed connection using snap-on buttons.

The antennas with snap-on button shorting were fabricated in the following steps. Firstly, a back-to-back male snap-on buttons connector is fabricated by soldering two male snap-on buttons together as depicted in Fig. 3.14 (a). A pair of female snap-on buttons are used to form a complete connection as shown in Fig. 3.14 (b) and (c) respectively. As shown in Fig. 3.15 (a), the bottom female snap-on buttons are permanently

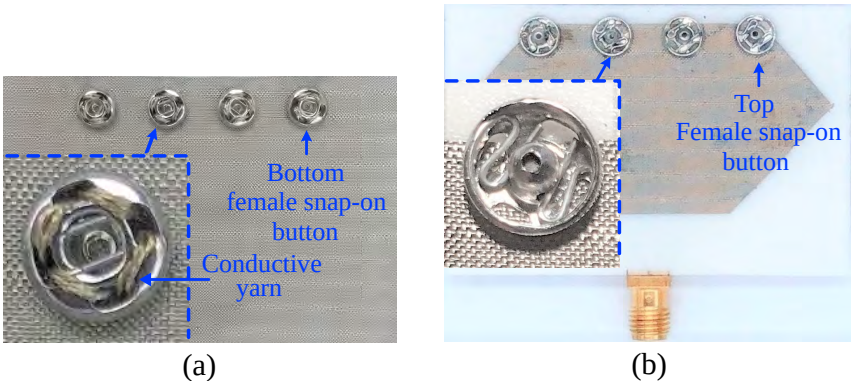

Figure 3.15. Shorting by snap-on buttons. Shorting by snap-on buttons, (a) bottom female snap-on buttons sewed to the ground plane and (b) completed antenna.

sewed to the ground plane using conductive thread to enhance connection robustness. Holes on antenna substrate are also required for accommodating the back-to-back male snap-on buttons connectors. Fig. 3.15 (b) depicts a completed antenna with the female snap-on buttons affixed on the top. For this shorting method, the discrepancy between simulated and manufactured antennas is caused by the inaccuracies inherent to a manual fabrication process.

3.2.4 Measurement results and comparison

This section presents characterization of the performance for all twelve fabricated antenna variations, illustrating and comparing the application of four shorting strategies onto the three types of antennas. The twelve fabricated antennas with various shorting strategies are shown in Fig. 3.16.

Reflection coefficient

Figure 3.17 shows the simulated and measured reflection coefficients ($|S_{11}|$) of the eight PIFAs and four monopole antennas. A good agreement between simulation and measurement results is obtained for all twelve antennas. The bandwidth of all twelve antennas completely covers both the 2.45 and 5.8 GHz ISM bands. It is noticeable that there are discrepancies in simulated and measured reflection coefficients in the higher band for the monopole antennas. This is mainly caused by an imperfection of the manual fabrication of stacked feeding structure, which is not related to the shorting methods.

Radiation patterns

The measured radiation patterns of all twelve antennas at 2.45 and 5.8 GHz are shown in Fig. 3.18. All the antennas have the expected radiation patterns, namely directional patterns for PIFAs and omnidirectional patterns for the monopole antennas. The difference in antenna gains is indicative of different efficiencies among the shorting strategies and will be quantitatively investigated in the next section.

Gain and efficiency

The measured realized gain and efficiency for all antennas are compared in Table 3.3. At 5.8 GHz, small variations in the measured gain and efficiency are mainly attributed

3.2.4 Measurement results and comparison

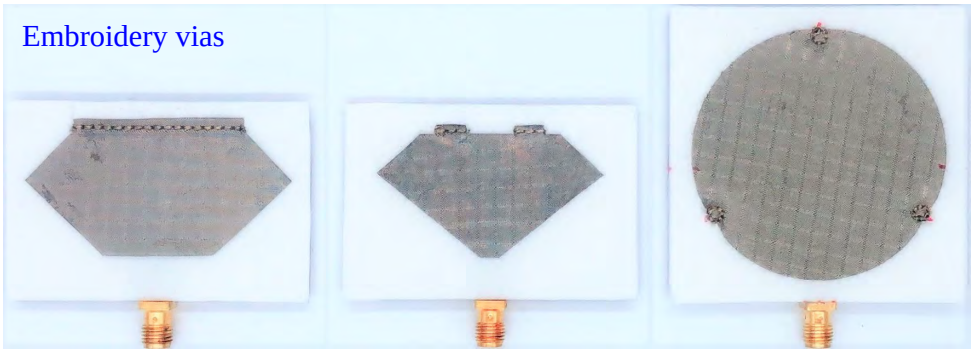

(a)

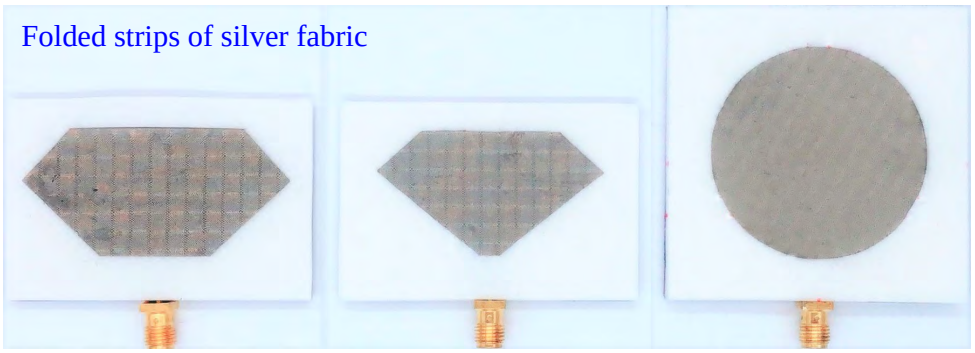

(b)

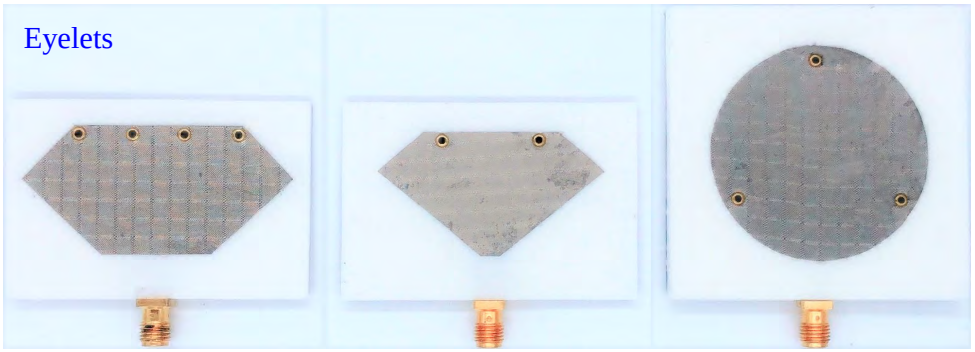

(c)

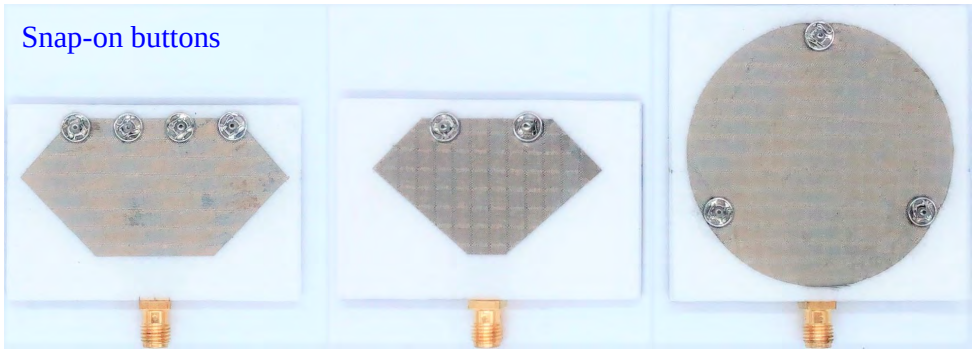

(d)

Figure 3.16. Twelve fabricated antennas with various shorting strategies. Twelve fabricated antennas with various shorting strategies, (a) antennas using embroidery vias, (b) antennas using folded strip of metalized fabric, (c) antennas using eyelets and (d) antennas using snap-on buttons.

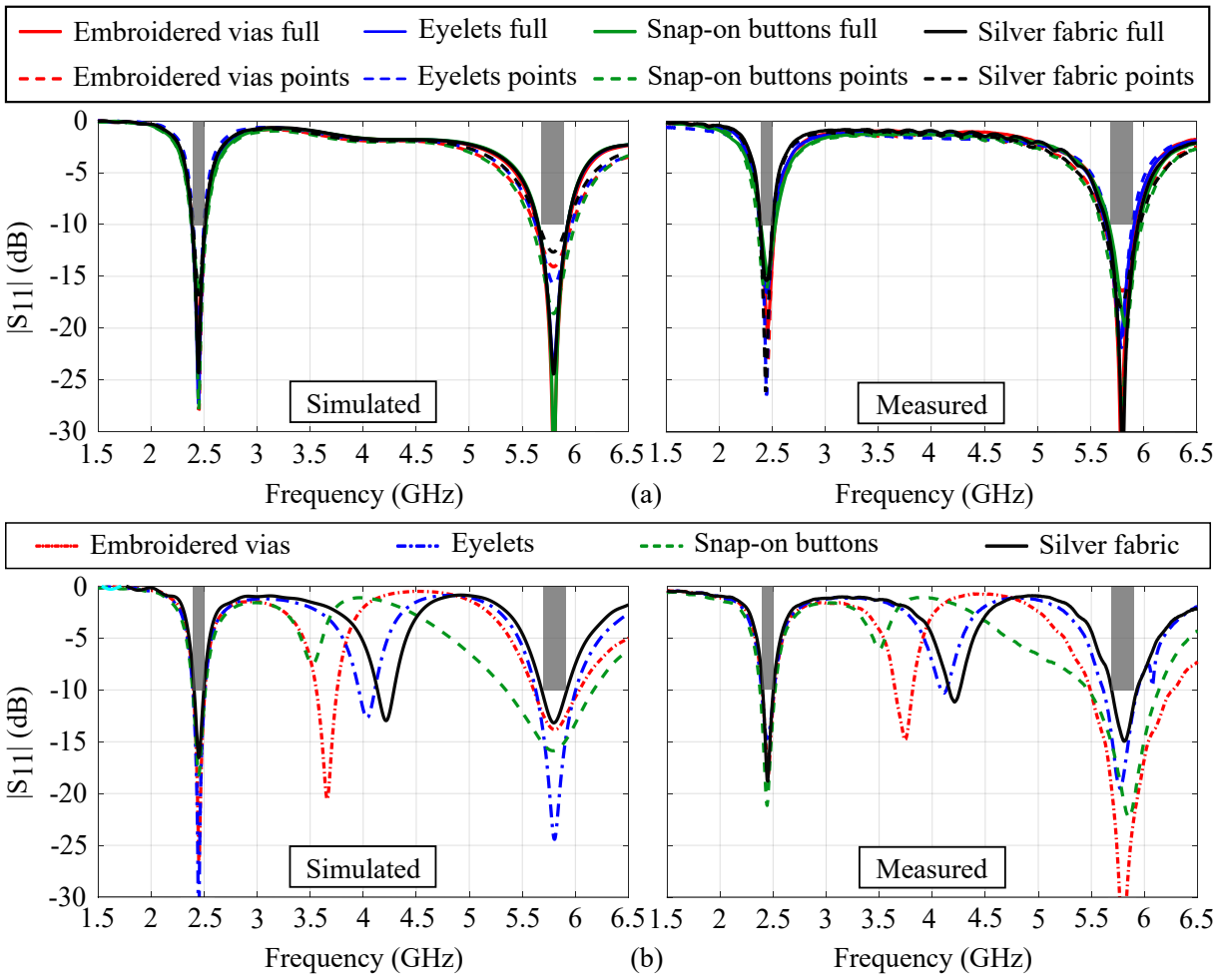

Figure 3.17. Reflection coefficients of the twelve antennas. Simulated and measured reflection coefficient comparison between the twelve antennas with various shorting strategies, (a) eight PIFAs and (b) four monopole antennas. The targeted ISM bands are represented as gray areas.

to imperfect fabrication and measurement, since the design is much more sensitive to the resonant patch dimensions at this frequency. In contrast, at 2.45 GHz, the discrepancies between measured results are mainly due to the different losses arising from the various shorting methods. Due to a smaller patch size, the PIFAs with two shorting posts have slightly lower gain and efficiency than the ones with a full shorting wall. The measured gain of all monopole antennas in the *xy*-plane are low which is attributed to the small size of the antenna and omnidirectional conical radiation characteristics.

The antennas using the folded strips of silver fabric have consistently the highest gain and efficiency as expected due to the highest conductor efficiency of this shorting

3.2.4 Measurement results and comparison

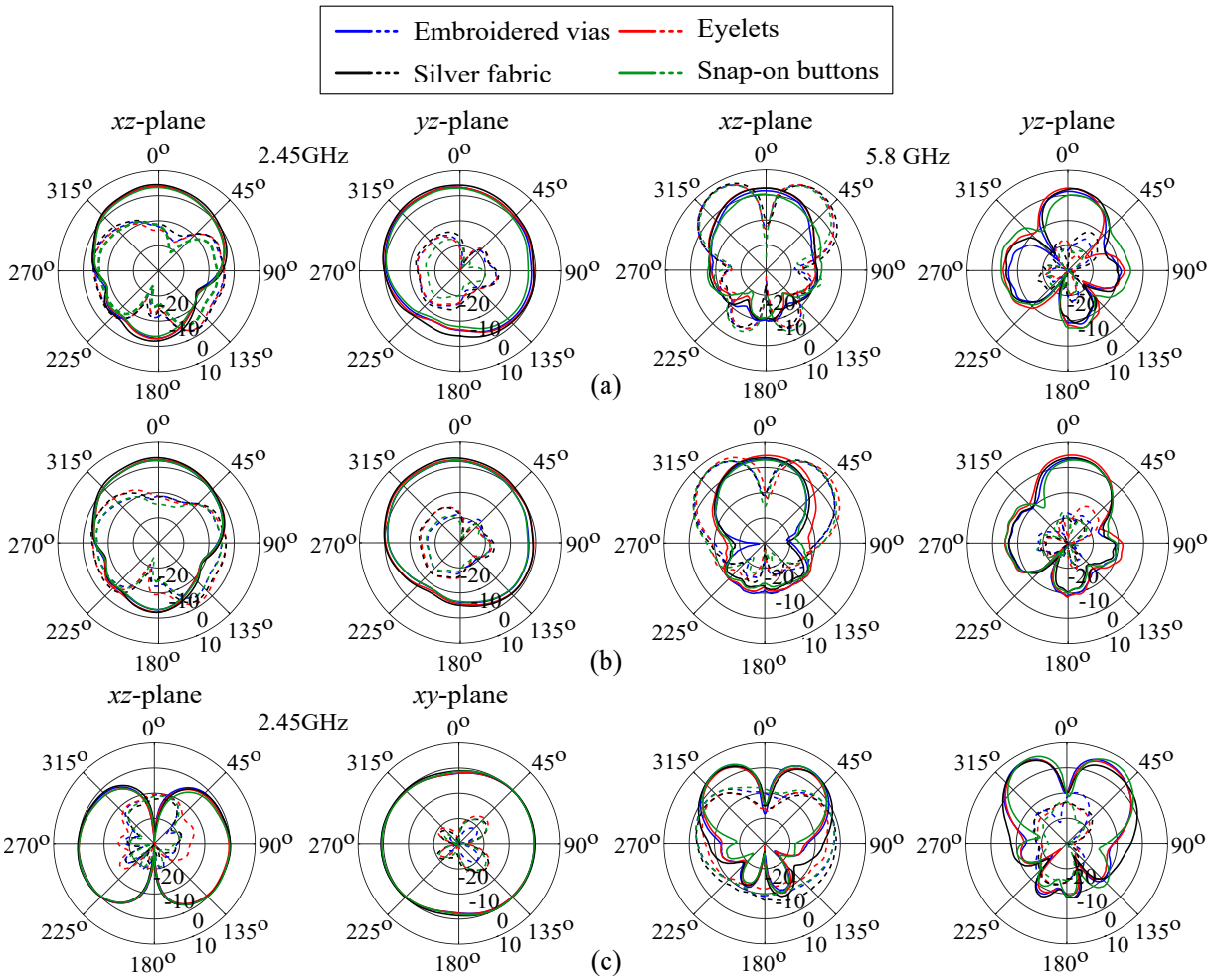

Figure 3.18. Measured radiation patterns of the twelve antennas. Measured radiation patterns (realized gain) of the twelve antennas: (a) PIFAs shorted by full wall, (b) PIFAs shorted by two posts and (c) monopole antennas. Solid lines: co-polarization. Dashed lines: cross-polarization.

method. The high resistance of the embroidered conductive vias or wall lead to the lowest antenna gains and efficiencies. The decrease of antenna gains and efficiencies of the antennas using eyelets and snap-on buttons is likely due to the imperfect connection of eyelets and snap-on buttons with the ground planes and radiation patches.

Impact of bending

Since wearable antennas are mostly mounted conformally on the human body, it is necessary to assess the effect of bending on the antenna performance [141]. All the antennas were bent and the effect of this deformation on the reflection coefficient was measured. The bending radius is chosen at 30 mm to mimic the extreme case when

Table 3.3. Measured antenna gains and efficiencies of the twelve antennas. Measured antenna gains and efficiencies

Antenna	2.45 GHz		5.8 GHz	
	Measured gain (dBi)	Efficiency (%)	Measured gain (dBi)	Efficiency (%)
PIFA with full embroidered wall	3.65	77.80	7.45	92.04
PIFA with full silver fabric strip	4.45	95.06	7.83	96.38
PIFA with full eyelets	3.77	83.75	8.07	93.97
PIFA with full snap-on buttons	3.27	67.76	7.25	88.51
PIFA with two embroidered vias	2.79	65.77	6.28	85.90
PIFA with two silver fabric strips	3.92	92.26	6.65	89.42
PIFA with two eyelets	3.19	82.60	7.06	92.47
PIFA with two snap-on buttons	2.81	66.99	6.54	89.33
Monopole antenna with embroidered vias	0.88	71.45	6.72	92.04
Monopole antenna with silver fabric strips	0.93	76.74	6.48	93.11
Monopole antenna with eyelets	0.79	69.98	6.69	92.47
Monopole antenna with snap-on buttons	0.69	69.34	7.39	94.41

the antennas are mounted on a very small arm. Two bending directions are considered here: along the x-axis and along the y-axis. The measured reflection coefficients at both 2.45 and 5.8 GHz are shifted insignificantly, as shown in Fig. 3.19. In these two bands, the worst reflection coefficients are only observed at the bandwidth limits and reach approximately -6 dB. Considering the extreme bending test conditions, these reflection coefficients are still practically acceptable.

Thermal imaging of the antennas

A lossy shorting via will lead to an increase in the temperature of the operating antenna due to the ohmic loss. In this section, the differences in antenna gain and efficiency between the considered shorting methods is validated qualitatively by comparing the temperature at shorting positions measured using a thermal infrared camera.

3.2.4 Measurement results and comparison

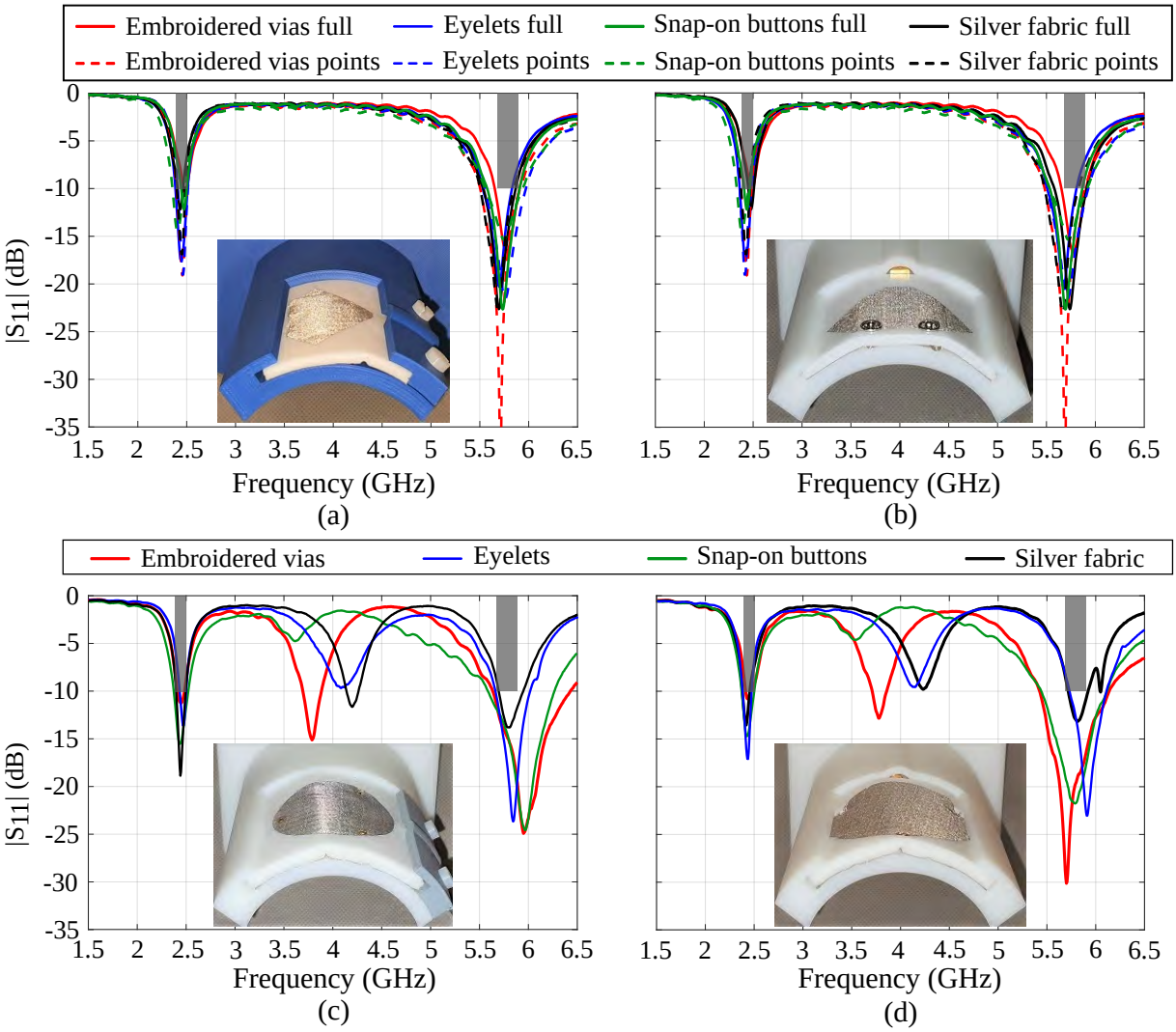

Figure 3.19. Reflection coefficients of antennas under bending conditions. Measured reflection coefficients of antennas under bending conditions. Eight PIFAs were bent along (a) the *x*-axis and (b) *y*-axis. Four monopole antennas were bent along (c) the *x*-axis and (d) *y*-axis. Inset: examples of bending test configurations in 3D-printed holders.

The temperature measurement setup is shown in Fig. 3.20. The temperature is measured using a FLIR E53 Advanced Thermal Imaging Camera with a reading temperature range extending from -20°C to 120°C. A sinusoidal reference signal is generated using an analog signal generator, and then passed through an RF amplifier to reach a power of 1 W before feeding the antennas. In order to reduce the impact of thermal noise, the measurements are taken in an anechoic chamber without any reflecting objects in vicinity and with the light turned off during measurements.

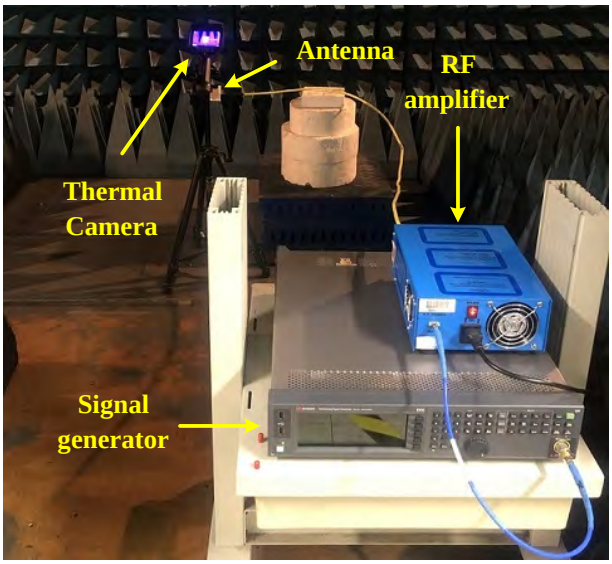

Figure 3.20. Temperature measurement setup. Temperature measurement setup with a thermal infrared camera.

Figure 3.21 illustrates representative thermal images of three typical antennas for the case when the power is first off and then turned on. The antennas are left to reach their equilibrium point sequentially at the two operation frequencies. The overall averaged antenna temperature is measured initially, before recording the temperature at some typical points on the antennas for comparison. The considered points for temperature measurements are three points at the shorting positions for the monopole antennas, six points along the shorting wall for the fully edge-shorted PIFAs, and two points at two shorting positions for the post-shorted PIFAs. According to Fig. 3.21, the temperature on the shorting points for the post-shorted PIFA is higher than for the fully shorted PIFA, which corroborates the differences in the measured gain and efficiency of these two types of PIFA as mentioned in Section 3.2.4. It can be also observed that at 5.8 GHz the antenna temperature does not significantly change while the power is turned on. The reason is that at 5.8 GHz all twelve antennas are radiating in the very efficient patch mode (with higher than 90% efficiency) where nearly no currents are flowing through the shorting posts/wall. Based on the temperature at considered points at 2.45 GHz displayed in Table 3.4, a good correlation between the antenna efficiencies and shorting point temperatures is obtained.

The difference in temperature at shorting points for different shorting methods are shown in Fig. 3.22. For brevity, the represented results are limited to the PIFA antennas with two shorting points. In this case, the antennas using the folded strips of silver

3.2.4 Measurement results and comparison

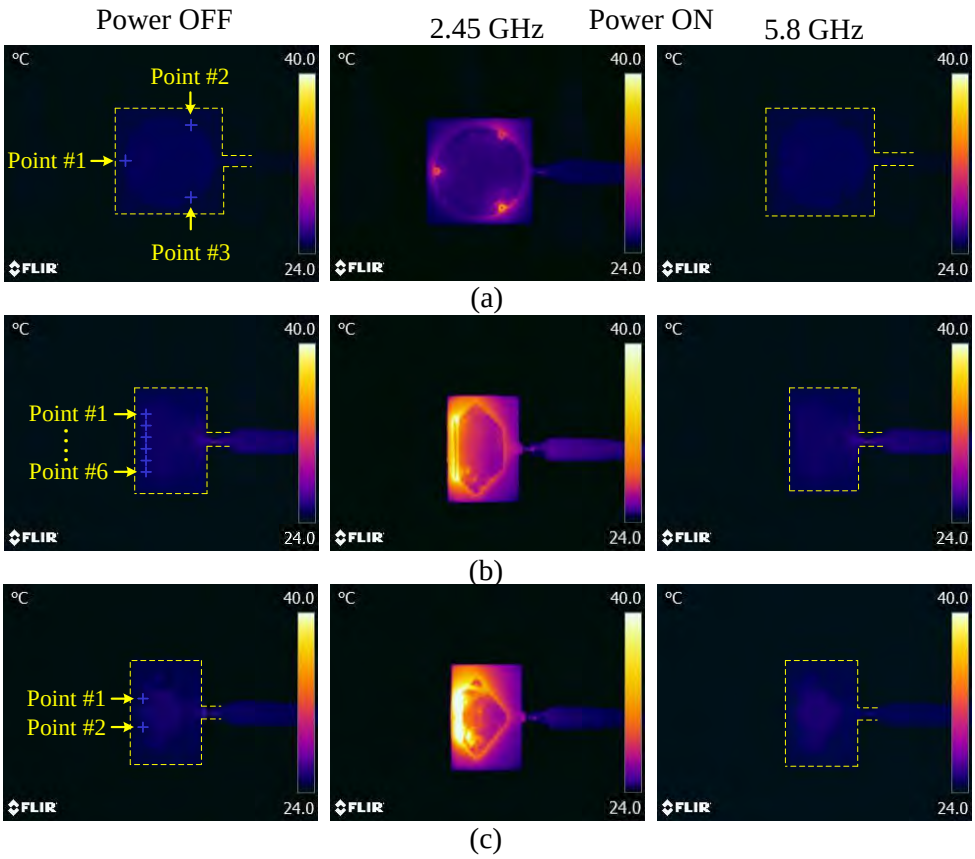

Figure 3.21. Thermal images recorded for all the antennas. Thermal images recorded for all the antennas using embroidered vias without and with excitation: (a) monopole antenna, (b) PIFA shorted using full shorting wall and (c) PIFA shorted using two shorting points.

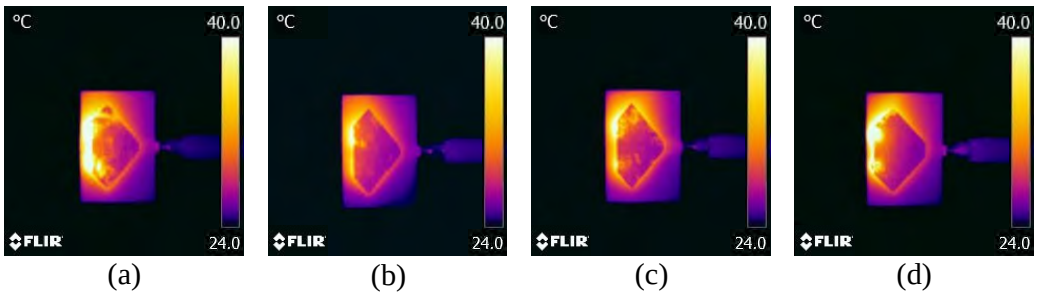

Figure 3.22. Thermal images recorded for the two-spots-shorted PIFAs. Thermal images recorded for all the two-spots-shorted PIFAs at 2.45 GHz: (a) embroidered vias, (b) folded strips of silver fabric, (c) eyelets and (d) snap-on buttons.

fabric have the highest gains and efficiencies and the temperature at the considered points for these antennas remains the lowest. The temperature at the considered points

Table 3.4. Temperature of twelve antennas at considered points at 2.45 GHz. Temperature at considered points at 2.45 GHz

Antenna	Temperature in degree Celsius at 4 minutes after turning the power on						Measured efficiency (%)
	Point #1	Point #2	Point #3	Point #4	Point #5	Point #6	
PIFA with full embroidered wall	39.1	36.6	35.5	35.3	36.4	38.8	77.80
PIFA with full silver fabric strip	34.9	32.6	31.4	31.7	31.4	33.2	95.06
PIFA with full eyelets	39.0	36.6	35.8	34.8	34.8	37.2	83.75
PIFA with full snap-on buttons	47.6	42.4	38.8	40.6	40.7	47.1	67.76
PIFA with two embroidered vias	52.8	53.2	-	-	-	-	65.77
PIFA with two silver fabric strips	37.2	37.6	-	-	-	-	92.26
PIFA with two eyelets	40.1	38.9	-	-	-	-	82.60
PIFA with two snap-on buttons	51.4	50.9	-	-	-	-	66.99
Monopole antenna with embroidered vias	33.1	32.1	35.5	-	-	-	71.45
Monopole antenna with silver fabric strips	33.5	31.9	32.1	-	-	-	76.74
Monopole antenna with eyelets	34.2	35.1	33.1	-	-	-	69.98
Monopole antenna with snap-on buttons	35.6	35.3	35.2	-	-	-	69.34

for the antenna using embroidered vias are the highest as expected, corresponding to the lowest gain and efficiency.

3.2.5 Comparison summary

Based on the experiment results, it can be claimed that all shorting methods considered are applicable to textile antenna design. However, each shorting method has its own advantages as well as weaknesses. The selection of the appropriate shorting method must consider several aspects according to the particular application and designers' purposes. In this section, we extract the critical findings from the comparisons that have been conducted for the four shorting methods and recommend them with respect to fabrication, simulation, antenna performance, mechanical stability and modularity. A broad qualitative comparison between the four considered shorting methods is given in Table 3.5.

3.2.5 Comparison summary

Table 3.5. Shorting strategies comparison. Shorting strategies comparison

Shorting methods	Antenna performance	Simulation	Fabrication	Mechanical stability	Modularity
Embroidered vias	Excellent	Complex, empirical knowledge of compression required	Automated production applicable	Highest level of robustness	No
Folded strip of metalized fabric	Highest	Straightforward	Convenient, high accuracy	Intermediate level of robustness	No
Eyelets	Excellent	Intermediate with predictable compression effects	Convenient, high accuracy	Intermediate level of robustness	No
Snap-on buttons	Satisfactory	Complex, empirical knowledge of compression required	Complex, low accuracy	Lowest level of robustness	Yes

Antenna performance

As mentioned above, the highest gain and efficiency are obtained while using the folded strip of silver fabric due to the highest conductivity of this shorting method. The thermal analysis on the antennas confirms this finding. Hence, this shorting strategy is the best candidate when the design priority is antenna performance.

Simulation

Shortings by folded strip of silver fabric or eyelet are the most convenient methods in the perspective of their accurate modelling with full-wave simulation tools. Indeed, these two shorting methods do not have significant uncertainties with respect to their electrical or mechanical structure. In contrast, shorting by snap-on-buttons and embroidered vias are characterized by uncertainties with respect to their structures. For example, the compression of the substrate needs to be pre-characterized for given embroidery settings, so that a sufficiently accurate prediction in simulations can be obtained.

Fabrication

As mentioned in Section 3.2.3, silver fabric and eyelet vias are straightforward to fabricate with high level of accuracy, since every single manufacture step can be well

controlled. The embroidered via method is more difficult to accurately fabricate than the other methods, since it requires pre-characterization of features for prototyping. However, once the settings are characterized, this method is also scalable for mass production using industrial embroidery machines. Shorting by snap-on buttons is also relatively difficult to manufacture due to the low degree of accuracy of manual fabrication steps including sewing of female buttons to conductive textiles and soldering of back-to-back male connectors. Nevertheless, industrial mass production techniques with high accuracy can be applied to the manufacture of the male-to-male snap-on button connection. The automatic machinery for mass production in the clothing industry can also be applied to diminish the fabrication tolerances.

Mechanical stability

All of four considered shorting methods have been proven to work well under various bending conditions, as mentioned in Section 3.2.4. However, the mechanical effect of bending or crumpling on each shorting strategy is different, as described phenomenologically in the following. Although the embroidered via shorting method is more difficult than the other methods in prototyping stages, this method provides the most robust mechanical connection and can help in the structural stability of the textile antennas. The antennas shorted by folded strips of silver fabric also have high level of robustness, since the shorting wall is fixed in the slit on the antenna substrate and permanently glued to the ground plane. For shorting eyelet, a larger eyelet's cap size results in a more robust construction of the antenna. The antenna shorting by snap-on buttons has a lower degree of robustness compared to the other methods, since the detachment of the top female buttons can be occur in harsh operating conditions such as bending or crumpling.

Modularity

Despite its relatively modest performance and a rather high complexity in fabrication and simulation, the snap-on button shorting method presents a distinct advantage of modularity compared to the other modalities. Indeed, the antenna resonant patch or location of shorts can be interchangeable by simply unfastening/fastening snap-on buttons. This advantage has been used to design a modular antenna as investigated in [37].

3.2.6 Summary on the shorting strategies

Four different practical shorting strategies for flexible wearable antennas have been investigated and compared. Using those shorting methods, twelve antennas including four full-edge shorted PIFAs, four post-shorted PIFAs and four planar shorted-patch-based monopolar antennas have been designed, fabricated and measured. The choices of shorting method depend on the designer purposes and priorities. Folded strips of silver fabric provide the overall best antenna performance. Shorting eyelets are the easiest method of fabrication with high level of accuracy. Embroidered vias enhance the compactness and robustness of the flexible wearable antenna and are also suitable for mass production. Shorting by snap-on buttons offer interchangeability to the antenna resonant patch. It has been demonstrated that the four considered shorting methods are applicable with their strengths and weaknesses to different utilizations in textile antenna technology.

3.3 Wearable modular textile antenna using snap-on buttons

As analyzed in Section 3.2, despite the complexity in simulation and fabrication, the shorting method using snap-on buttons exhibits a distinct strength of interchangeability which is not available in other shorting techniques. Based on this advantageous feature, snap-on button connections can be utilized as manual detachable mechanical and RF connection to modularly change antenna radiation characteristics.

A dual-band wearable textile patch antenna with modular pattern interchangeability is proposed in this section. The antenna simultaneously covers the 2.45 and 5.8 GHz ISM radio bands. By utilizing detachable shorting connections made of metalic snap-on buttons, the proposed antenna can be set up to operate either with broadside or omnidirectional radiation patterns at 2.45 GHz, while the radiation characteristics at 5.8 GHz remain unchanged. The proposed modular antenna is fabricated and measured to validate the concept.

3.3.1 Introduction

Depending on the types of WBANs, the wearable antennas need to have appropriate radiation characteristics to establish efficient wireless communication channels between devices. In particular, for on-body communication channels between body-mounted devices, omnidirectional patterns [142] are preferred. By contrast, broadside radiation patterns [143] are advantageous for off-body communications between body-worn devices and base stations. Aiming to develop versatile systems, it is desirable to investigate wearable textile antennas that can be modularly configured to operate with either ominidirectional or broadside patterns at a fixed resonance frequency.

A pattern-reconfigurable antenna with ability to switch between on-body and off-body modes at 2.45 GHz was presented in [144]. However, this antenna was realized on rigid material which may cause discomfort to wearers. A wearable textile antenna with a similar functionality was proposed in [104]. Nevertheless, there was no practical switching method proposed in the design.

In this section, a dual-band wearable textile antenna with radiation pattern modularity for on-body and off-body communications is presented. The antenna is able to simultaneously operate in the 2.45 and 5.8 GHz ISM radio bands. By utilizing a snap-on button shorting method working as a manually detachable RF connection as mentioned in Section 3.2, the antenna can be configured to operate in monopole-like or broadside patterns at 2.45 GHz, while the radiation pattern at 5.8 GHz remains unchanged. The proposed antenna has been fabricated and experimentally characterized to validate the operation concept.

3.3.2 Antenna design

The proposed antenna configuration is shown in Fig. 3.23 with all the antenna dimensions given in the caption. The antenna is constructed by three layers of foam substrates, a stepped proximity-coupled feed, a circular patch and a ground plane. The snap-on button shortings are created using a pair of female buttons at their ends and an inter-layer connection consisting of a pair of back-to-back male snap-on buttons. Three such shortings are placed on the patch circumference with 120° angular separation (Fig. 3.23). To enhance RF connections between the shortings and the ground plane, the bottom female buttons are permanently sewed onto the ground plane using

conductive threads. Holes are trimmed on the bottom and middle substrates to accommodate the bottom female buttons and male-to-male buttons, respectively. Three small circular holes with a radius of 0.8 mm (size of male button pin) are cut on the top substrate leaving space to accommodate the pins of male buttons. Three holes on the top circular patch are designed to be noticeably bigger than the pin of male snap-on button to ensure that the radiation patch does not connect with the back-to-back male snap-on buttons connection while the top female snap-on buttons are detached. A stepped proximity-coupled feed with optimized dimensions is used to excite the higher-order mode at 5.8 GHz, as discussed in Section 3.2.2.

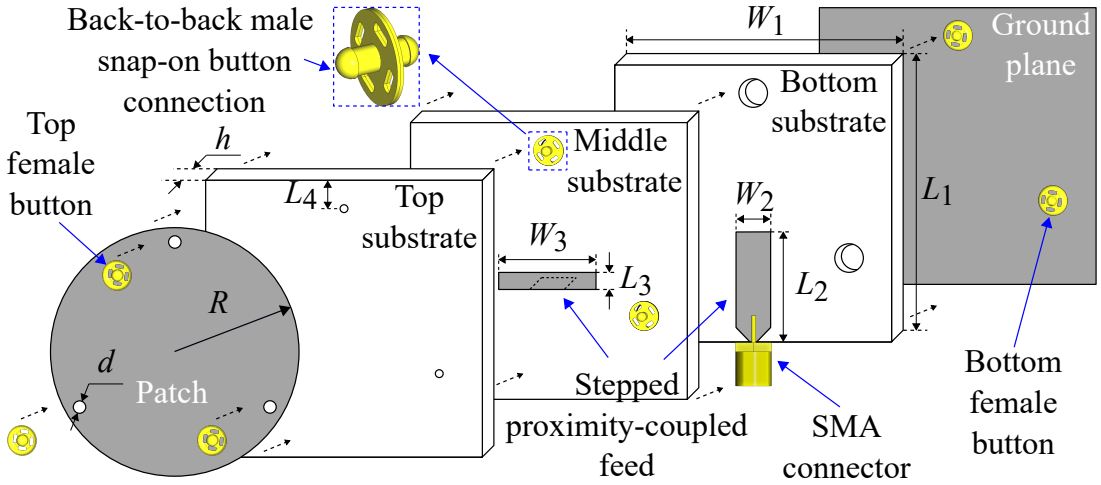

Figure 3.23. Configuration of wearable modular textile antenna. Configuration of the proposed antenna. Dimensions (mm): $L_1 = 60.0$, $L_2 = 26.3$, $L_3 = 3.7$, $L_4 = 6.3$, $W_1 = 60.0$, $W_2 = 7.5$, $W_3 = 9.0$, $h = 1.6$, $R = 27.4$ and $d = 3.0$.

Thanks to the interchangeability of the snap-on fasteners, the button connections can be used as manual RF switches. The ground plane and the radiation patch are connected when the top female buttons are attached to the male-to-male connection (switch ON). In contrast, the connection is OFF with the detachment of the top female buttons (switch OFF). The simulated instantaneous electric field distribution of the proposed antenna in the ON and OFF states is illustrated in Fig. 3.24. In the ON state, three radiation apertures are created between the snap-on button shortings from the patch to the ground, which leads to a monople mode at 2.45 GHz (Fig. 3.24 (a)). In the OFF state, the antenna is working in a half-wave resonant patch mode because the radiation patch is not contacted to the ground plane (Fig. 3.24 (c)). It is worth mentioning that, since

the higher-order mode at 5.8 GHz is realized by manipulating the input impedance through optimization of the feed dimension, it is independent to the switching state of the radiation modes at the lower band. This is confirmed by the stable E-field distribution of the higher-order mode observed at both states in Fig. 3.24 (b), (d).

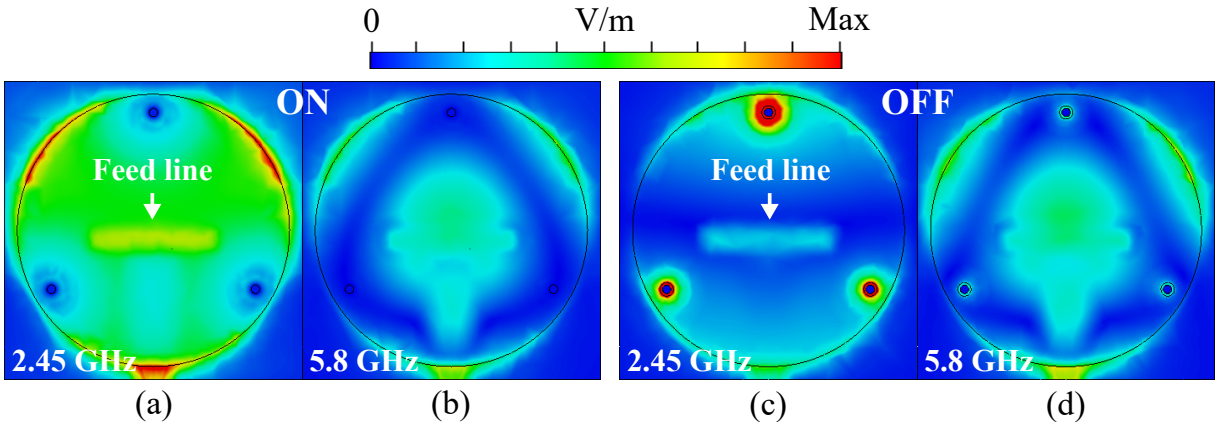

Figure 3.24. Electric field distributions of the modular antenna. Instantaneous electric field distributions of the proposed antenna at (a, b) ON state and (c, d) OFF state.

3.3.3 Experimental results

The proposed antenna has been fabricated (insets of Fig. 3.25) and experimentally characterized to validate the modular operation concept. A highly flexible, light weight and low-loss ($\tan\delta$ = 0.0001) PF-4 foam with relative permittivity of ε_r = 1.06 is utilized as antenna substrates. The ground plane, the patch and the stepped proximity-coupled feed are made of a conductive metallized fabric (with a sheet resistance of approximately 0.01 Ω/square). Antenna conductive and non-conductive parts are glued together using a washable fabric glue while the SMA connector is connected to the microstrip feed and ground plane using conductive epoxy.

A good agreement between the simulated and measured $|S_{11}|$ parameters for different radiation states is observed in Fig. 3.25. The two targeted ISM bandwidths of $2.4 - 2.5$ and $5.725 - 5.875$ GHz are completely covered at both radiation states. The simulated and measured radiation patterns of the proposed antenna at the specified frequencies for ON and OFF states are displayed in Fig. 3.26 (a) and (b), respectively. When the snap-on button connection is ON, an omnidirectional radiation pattern with vertical

polarization at 2.45 GHz can be observed in Fig. 3.26 (a). At the OFF state, the half-wave patch mode with broadside radiation at 2.45 GHz is illustrated in Fig. 3.26 (b). A conical monopole pattern with a tilt angle of 60° remains stable at both ON and OFF states at 5.8 GHz.

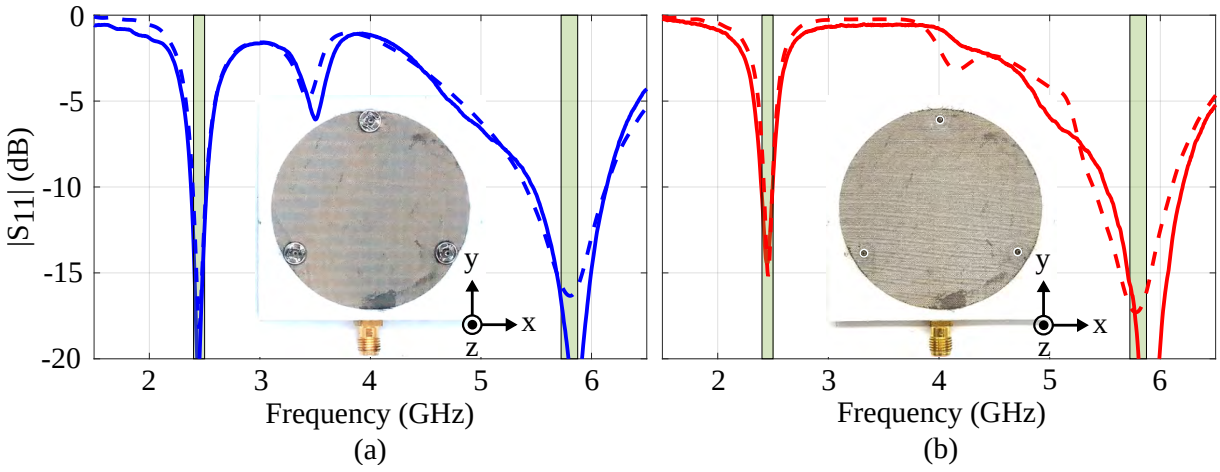

Figure 3.25. Reflection coefficents of the modular textile antenna. Simulated (dash lines) and measured (solid lines) reflection coefficients of the proposed antenna at (a) ON state and (b) OFF state. The targeted ISM bands are represented as green areas. Insets: Fabricated antenna working at ON and OFF states.

The measured antenna realized gain for the monopole mode is 0.75 dBi while at the half-wave patch mode, the realized gain is 7.56 dBi. At 5.8 GHz, the measured antenna realized gain remains at approximately 7.20 dBi for the two radiation states. Estimated radiation efficiencies of the antennas at the monopole mode and the half-wave patch mode are 70.8% and 95.8%, respectively. The actual radiation efficiency estimated based on the measured gain at 5.8 GHz is 96.2%.

3.3.4 Summary on the pattern-interchangeable antenna

A dual-band flexible wearable textile antenna with modular radiation patterns has been presented. The antenna is designed to work simultaneously at 2.45 and 5.8 GHz ISM bands. A snap-on button shorting strategy is ultilized to realize a manual RF switch to connect or disconnect the antenna patch to the ground plane. Consequently, the proposed antenna can be exchanged between omnidirectional and broadside patterns at 2.45 GHz while the 5.8 GHz mode remain unchanged.

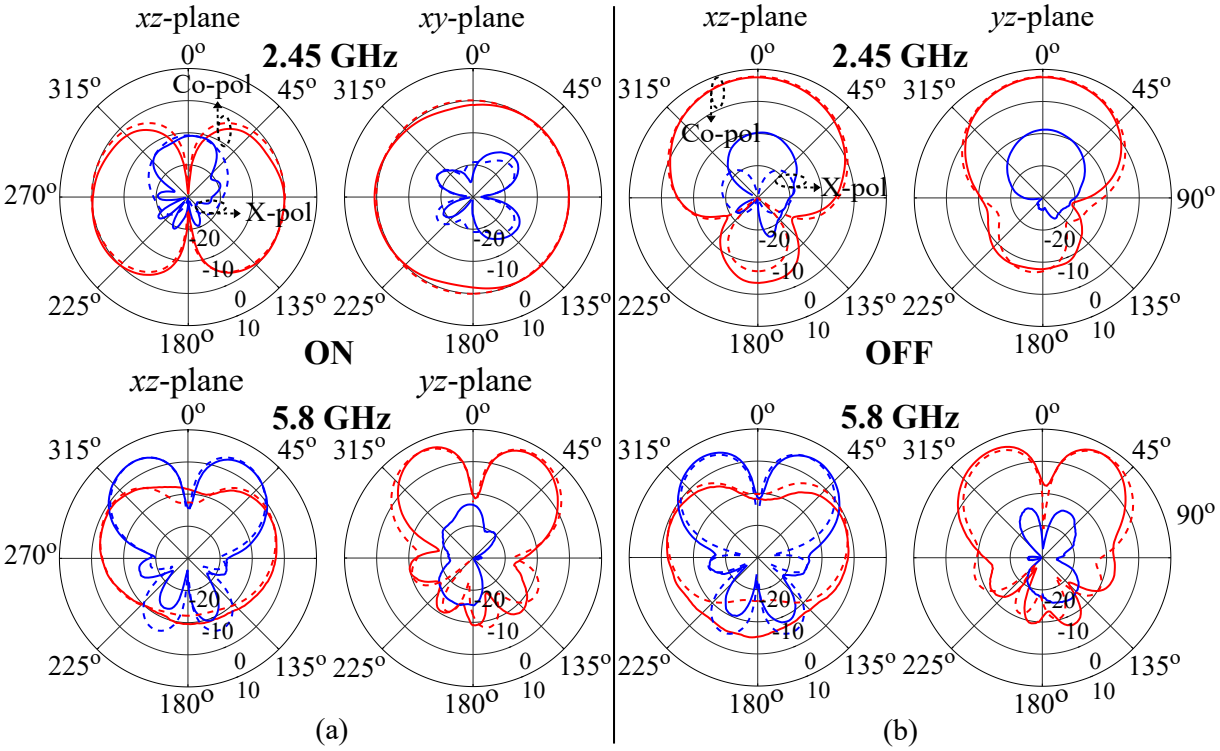

Figure 3.26. Radiation patterns of the modular textile antenna. Simulated (dash lines) and measured (solid lines) radiation patterns of the proposed antennas at (a) ON state and (b) OFF state.

3.4 Conclusion

In the first part of this chapter, four shorting methods for flexible wearable textile antennas including embroidered vias, folded strips of metalized fabric, eyelets and snap-on buttons have been analyzed and compared. Twelve wearable textile antennas including eight PIFAs and four monopolar patch antenna with edge shortings aiming to simultaneously cover the 2.45 and 5.8 GHz ISM radio bands have been designed, fabricated and experimentally characterized. All the fabricated antennas have been shown to exhibit good performance in flat conditions and practically acceptable $|S_{11}|$ in extreme bending test conditions. The selection of appropriate shorting method depends on prioritized features of antenna designs. The best antenna performance can be achieved by using folded strips of metalized fabric. Shorting eyelets are recommended for antenna designs that require a convenient simulation process and a high level of fabrication accuracy. In extremely harsh operation environment, where the compactness and robustness of the wearable antenna are highly prioritized, the embroidered

vias shorting method is the most appropriate candidate. Despite the complicated simulation and fabrication process, shorting by snap-on buttons exhibits the advantage for modular designs, where antenna parts can be interchanged for various functionalities.

The second part of the chapter has proposed a wearable modular textile antenna relying on the mentioned interchangeability of snap-on buttons. Using this advantageous feature of snap-on fasteners, the proposed antenna can be set-up for operation in monopole-like or broadside radiation at 2.45 GHz. The radiation characteristics in the higher band at 5.8 GHz remain unchanged since they mainly depend on the antenna feed dimensions.

Chapter 4

Reconfiguration Modules for Reconfigurable Wearable Antennas

THE utilization of reconfiguration modules has been demonstrated to be an effective strategy to design reconfigurable flexible body-worn antennas. This method using metallic snap-on buttons can provide excellent mechanical and RF connections between lumped components and antenna textiles, which translates in high antenna performance.

This chapter will firstly propose a novel topology of reconfiguration module, which can be used in planar reconfigurable wearable antenna designs. The proposed module can provide a secure and robust coplanar electrical connection between rigid electronics and flexible textile conductors in a coplanar arrangement. The feasibility of the proposed module for wearable reconfigurable antenna designs is investigated by realistic simulations, as building block for future designs implemented in later chapters. The second part of this chapter presents the utilization of RF-switch ICs and PIN-diodes in reconfigurable wearable textile antennas.

4.1 Introduction

As discussed in Chapter 2, there have been mainly two methods reported to date to overcome the challenge of robust electronics-to-textile RF connections in practically realizable reconfigurable body-worn antennas [28, 29]. One used PDMS to cover the whole textile antenna including the lumped elements to achieve robust connections [29], as shown in Fig. 4.1 (a). A different solution to this problem is illustrated in Fig. 4.1 (b) and it makes use of a so-called reconfiguration module as proposed in [28]. This module concept contains a dedicated circuitry for reconfiguration, which is sandwiched between a pair of back-to-back commercial snap-on buttons for vertical textile-to-electronics connections. However, this module configuration was limited for connections in-between two parallel conductive planes.

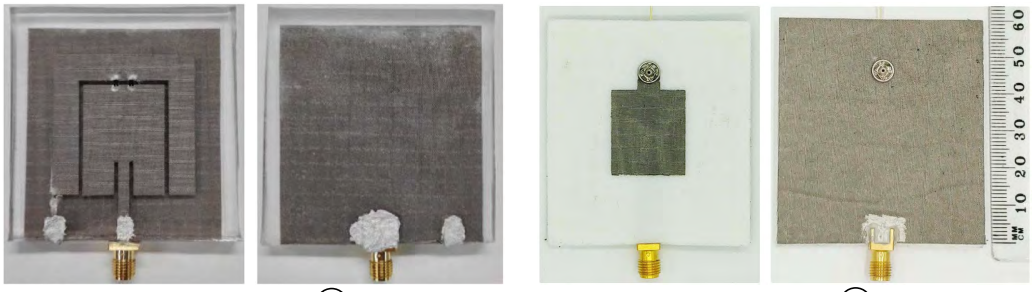

Figure 4.1. Reported reconfigurable wearable antennas. Reported reconfigurable wearable antennas based on (a) Polymer-embedded conductive fabric, adopted from [29] and (b) reconfiguration module, reproduced from [28].

In this context, this chapter initially presents a different reconfiguration concept inspired from [28], in an alternative module configuration tailored for coplanar electronic-to-textile connections. A reconfigurable antenna utilizing a purpose-made reconfiguration module is designed and simulated to investigate the approach. The simulation results suggest that this is a promising implementation of the reconfiguration module concept, which will be experimentally validated with various designs in the later chapters.

The second part of this chapter demonstrates an utilization of RF-switches and PIN-diode in reconfigurable wearable antenna designs. In order to test these components, a simple reconfigurable wearable microstrip antenna is designed, fabricated and experimentally characterized. It is demonstrated that, the RF-switch IC provides a better

antenna performance than the PIN diode at the cost of more complicated design and manufacturing processes.

4.2 Coplanar reconfiguration module

A reconfiguration module based on a small printed circuit board (PCB) and commercial snap-on buttons for reconfigurable flexible textile antennas is proposed in this section. The concept consists of a small PCB loaded with a reconfigurable circuitry including active and lumped components, which is combined with a pair of commercial male snap-on buttons for electrical connection to conductive textiles. The reconfiguration module can provide a secure and robust coplanar electrical connection between rigid electronics and flexible textile conductors, which is usually challenging for textile antennas. To validate this module concept, a frequency-reconfigurable planar inverted-F antenna using a varactor-based module realization is designed and simulated with realistic parameters. The antenna exhibits a frequency tuning range of 24.9% from 2.14 to 2.75 GHz with simulated efficiency from 60.1% to 89.4%. The results presented in this section have been presented as a conference contribution in [43].

4.2.1 Reconfiguration module design

The proposed coplanar reconfiguration module is compared to the vertical one introduced in [28] in Fig. 4.2. As observed in Fig. 4.2 (a), the vertical module has a compact bias circuitry integrated in-between a pair of back-to-back snap-on buttons, which is perfectly suited for vertical connection between two parallel conductors. In contrast, the proposed module with the same functionality has its snap-on buttons now placed in the same plane as the PCB for coplanar connections, as shown in Fig. 4.2 (b).

The proposed reconfigurable module schematic is illustrated in Fig. 4.3 (a). The unit consists of two varactors (MA120H46) connected in parallel between two buttons and a bias circuit containing an RF-choke inductor L = 360 nH and a RF-block resistor R = 1 MΩ. It is noted that the DC-blocking capacitor is not required due to the floating potential of the patch. The MA120H46 varactor equivalent circuit is shown in Fig. 4.3 (b), where L_v = 100 nH and R_v = 2 Ω are the internal inductance and resistance respectively. The tuning range for the varactor capacitance C_v is between 0.15 and 1.3 pF corresponding to the bias voltage varying between 18 and 0 V [28]. The equivalent circuit of the whole module is illustated in Fig. 4.3 (c).

4.2.1 Reconfiguration module design

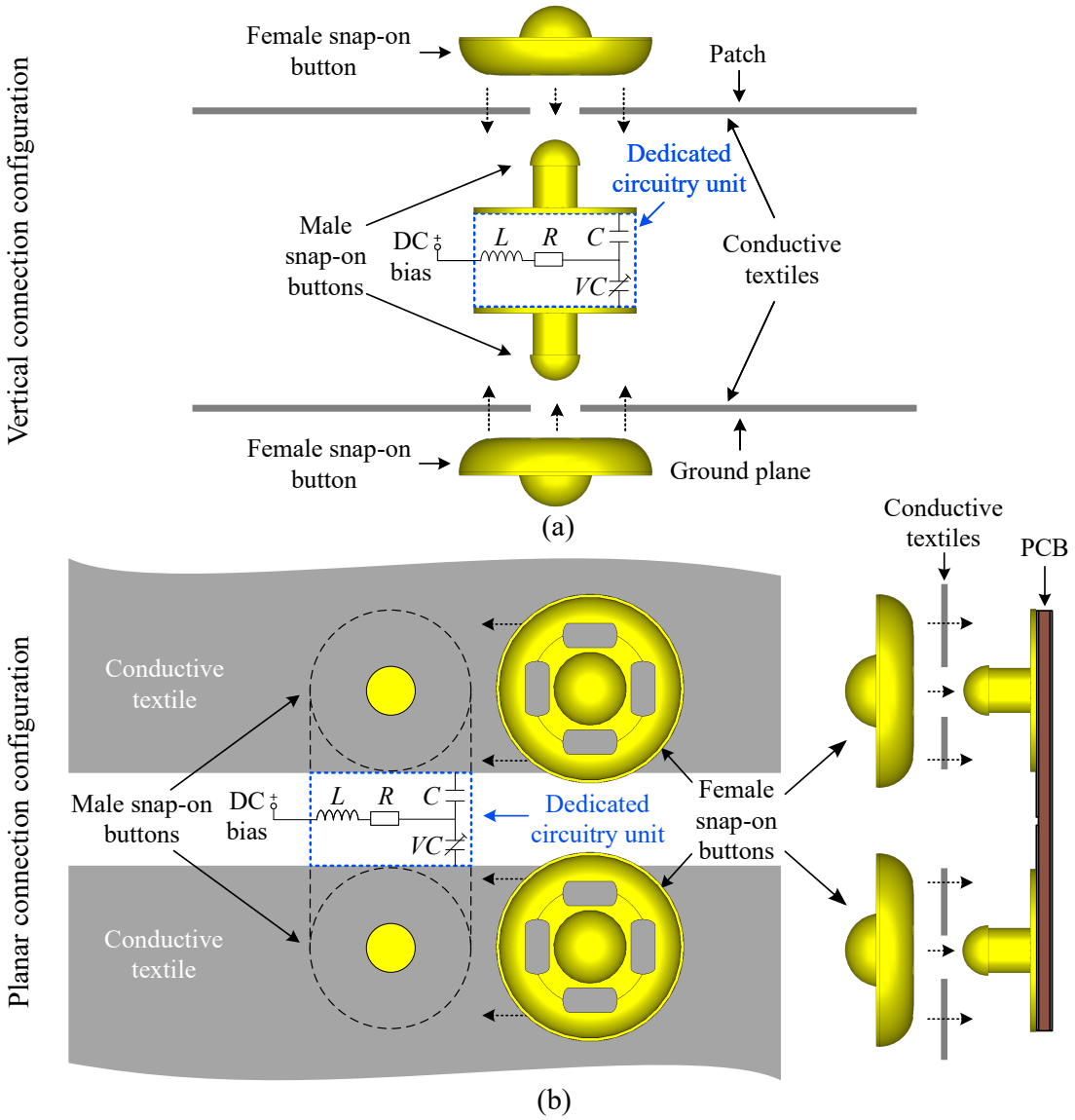

Figure 4.2. Reconfiguration modules. Reconfiguration modules: (a) vertical module reported in [28] and (b) the proposed coplanar module.

The reconfiguration module layout is illustrated in Fig. 4.4. To utilize the PCB space effectively, the RF-choke inductor is placed perpendicularly to the RF-blocking resistor. Two varactors are placed in parallel with their cathodes joined together and connected to a bias voltage through the resistor and the inductor. The PCB is made in Rogers RT/Duroid 6006 with a thickness of 0.64 mm. Two male snap-on buttons are soldered to the PCB.

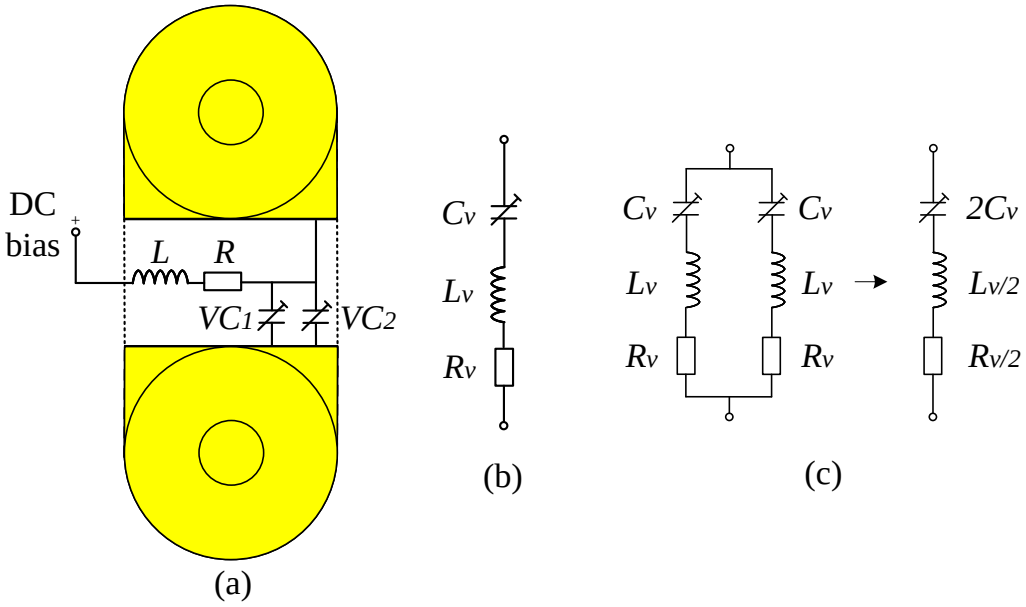

Figure 4.3. The proposed reconfigurable module schematic. (a) Schematic of the proposed reconfigurable module, (b) equivalent circuit of a single varactor and (c) equivalent circuit of two parallel varactors.

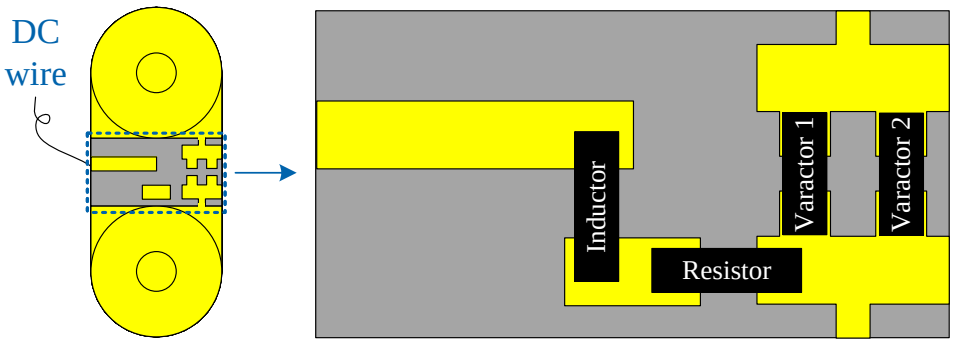

Figure 4.4. Module layout. The proposed reconfiguration module layout showing the placement of the lumped components.

4.2.2 Antenna design

To validate the proposed coplanar reconfiguration module, a planar inverted-F antenna (PIFA) similar to the one implemented in [28] is designed and simulated. The antenna configuration is shown and compared with the one in [28] in Fig. 4.5, while their dimensions are listed in Table 4.1. For convenience, the antenna proposed in this paper is referred as Ant. I whereas the one in [28] is Ant. II. The two antennas have a similar general structure including a ground plane, two substrate layers, a radiation

patch and a microstrip proximity-coupled feed. The vertical reconfiguration module is used as the connection between the ground plane and the radiation patch in Ant. II to form the PIFA whilst Ant. I uses a folded strip of fabric for the same purpose. This folded strip of metallized fabric provides a nearly perfect electrical connection to the ground plane [128].

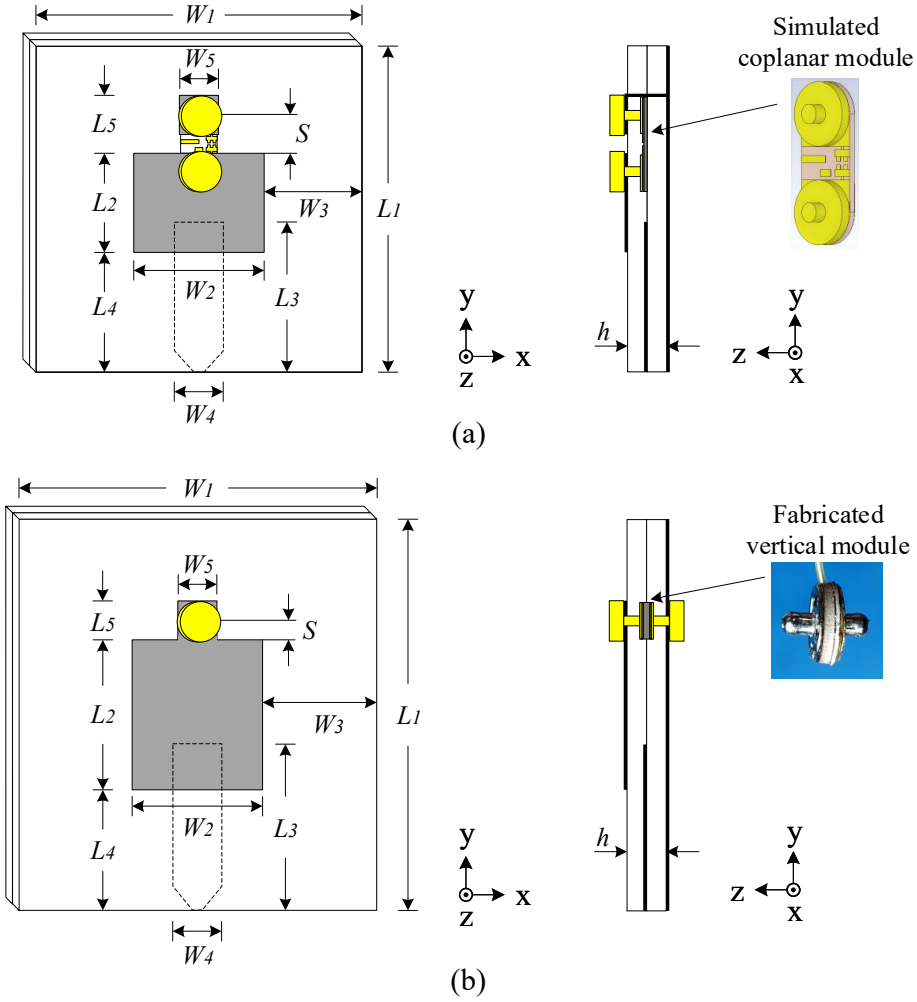

Figure 4.5. Antenna configuration. Antenna configuration: (a) the PIFA (Ant. I) using the proposed coplanar reconfiguration module and (b) the one reported in [28] (Ant. II).

Both antennas use highly flexible Cumming Microwave C-foam PF-4 foam with a thickness of 1.6 mm, relative permittivity ε_r = 1.06 and loss tangent tanδ = 0.0001 as the substrate. A silver-coated nylon RIPSTOP fabric with a sheet resistance of 0.01 Ω/square is selected as the conductor for the ground plane, radiation patches and proximity-coupled feed. Both antennas are optimized to operate at 2.45 GHz with a bias voltage of 2.5 V. This is for the sake of attaining a maximum tuning range when

Table 4.1. Dimensions of antennas. Dimensions of antennas using the vertical and coplanar modules (in mm)

Parameters	L_1	L_2	L_3	L_4	L_5	h
Values (Ant. I/Ant. II)	50/60	15.2/20	23/25.5	18.4/18.5	8.9/6	3.2/3.2
Parameters	W_1	W_2	W_3	W_4	W_5	S
Values (Ant. I/Ant. II)	50/55	20/20	15/17.5	7.5/7.5	6/6	5.7/4.3

a 5 V voltage source is used, taking into account that the available power source in a wearable system is limited.

4.2.3 Simulation results

The simulated reflection coefficients for both antennas are compared in Fig. 4.6. The proposed PIFA antenna can achieve a frequency tuning range of approximately 24.9% from 2.14 to 2.75 GHz, which is slightly lower than the reported value of 32.8% from 2.1 to 2.92 GHz attained with the vertical module [28]. In other words, the frequency tuning range of Ant. I is smaller than the one of Ant. II. However, this can be optimized by adding more varactors to the decicated circuitry unit [96] and/or by increasing the gap between the two male snap-on buttons. This will be investigated in the future to optimize the design for experimental validation.

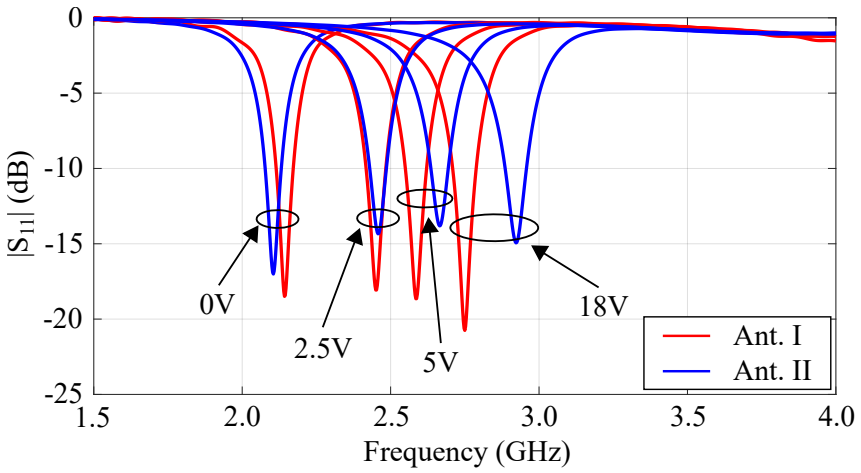

Figure 4.6. Reflection coefficients for both antennas. Comparison of the simulated reflection coefficients for both antennas.

Table 4.2. Radiation performance summary. Antenna gain and efficiency for both antennas

Resonance frequency (GHz)	Ant. I		Resonance frequency (GHz)	Ant. II	
	Gain (dBi)	Efficiency (%)		Gain (dBi)	Efficiency (%)
2.14	1.9	60.1	**2.10**	0.7	43.8
2.45	3.6	79.6	**2.45**	2.7	65.3
2.59	4.0	85.5	**2.67**	3.9	73.2
2.75	4.3	89.4	**2.92**	5.1	75.0

The simulated maximum gain and efficiency of the two antennas at 4 different resonance frequencies within the tuning range are shown in Table 4.2. The proposed module is predicted to yield better antenna efficiency from 60.1% to 89.4% in comparison with the reported values for Ant. II, which ranged from 43.8% to 75%. Ant. I has larger gain and higher efficiency than Ant. II because the coplanar reconfiguration module is less compact and thus the electromagnetic fields are less confined than in the vertical one. This reduces the power losses caused by the reconfiguration module materials in Ant. I compared to Ant. II.

4.2.4 Summary on the coplanar reconfiguration module

This first part of this chapter proposed a reconfiguration module based on a small PCB and snap-on buttons. The proposed concept provides a stable and repeatable electrical connection between rigid electronics and flexible textile conductors in a coplanar arrangement. This configuration facilitates alternative design possibilities compared to a previously reported module in [28] which permitted vertical connections. To illustrate the concept, a frequency-reconfigurable PIFA has been designed and simulated. The antenna is predicted to have a frequency tuning range of approximately 24.9% while its radiation efficiency varies from 60.1% to 89.4%. These simulated results suggest that the proposed module is a promising coplanar connection solution for wearable and flexible reconfigurable antennas.

4.3 Reconfiguration modules with RF-switch ICs and PIN-diodes

There have been numerous reconfigurable microstrip antennas reported in the literature, aiming to extend the antenna versatility and functionalities. To design reconfigurable antennas, two main categories of active components have been utilized in terms of tuning modality, namely continuously tuning and discretely switching components. On the one hand, varactor diodes have been widely used as tuning components to design frequency-agile antennas [20, 94, 103, 145]. On the other hand, PIN diodes are the most frequently used switching components to design pattern- or polarization-reconfigurable antennas [27, 101, 146, 147]. For reconfigurable wearable textile antennas, most of the designs to date are based on varactors [28, 29] and a very limited number use switching components [30].

In this section, the utilization of RF-switch Integrated Circuits (ICs) and PIN diodes to design reconfigurable wearable textile antennas is presented. Two reconfigurable modules, based on either of these two components, are designed for a frequency-reconfigurable wearable microstrip antenna, aiming to compare the impact of these components on antenna performance.

4.3.1 Reconfiguration modules

This section discusses methods used to integrate the RF switch IC and PIN diode into wearable flexible textile antennas with robust connections between components and flexible conductors.

Component characteristics

A PIN diode MA4FC300 from MACOM Technology Solution is used in this study. This type of PIN diode has been utilized in reconfigurable antenna designs [148]. The PIN diode has a forward resistance of 3 Ω in the ON state and a capacitance of 0.04 pF in parallel with a resistance of approximately 20 kΩ in the OFF state [149].

As alternative switch, a pHEMT GaAs IC antenna switch SKY13446-374LF from Skyworks is selected. This RF-switch IC allows switching between the input port and two output ports (or SPDT: Single Pole Double Throw) with two control voltages as low as 1.8 V. To investigate an equivalent circuit and fabrication processes of the RF-switch

IC, an evaluation board has been designed and fabricated. Three SMA connectors have been connected to the three ports of the RF-switch using microstrip lines, as illustrated in the inset of Fig. 4.7. The IC switch is grounded at its back, therefore a small hole is drilled on the board at the IC position to connect the back of the IC to the ground plane of the board. By matching the simulation and measurement results (as shown in Fig. 4.7), it is estimated that, in the OFF state the RF-switch IC is equivalent to a parallel circuit of a capacitance 0.01 pF and a resistance of 20 kΩ. For the ON state, the RF-switch represents a resistance of 0.3 Ω.

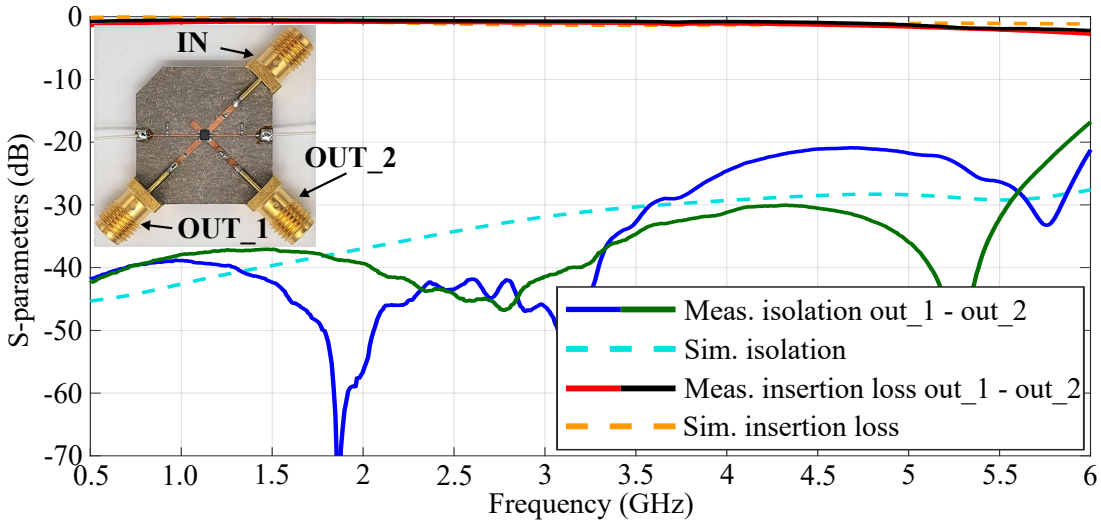

Figure 4.7. S-parameters of the RF-switch IC. Simulated and measured S-parameters of the RF-switch IC on an evaluation board. Inset: fabricated evaluation board.

Reconfiguration module design

An effective strategy to integrate active components such as diodes to flexible textile antennas is the utilization of reconfiguration modules, as demonstrated in the previous Section 4.2. For demonstration, the vertical reconfiguration module proposed in [28] is selected to load the PIN diode and the RF-switch IC. This reconfiguration module consists of two back-to-back male metallic snap-on buttons, with a small circular printed circuit board (PCB) and a spacer ring in between. Schematics of the reconfiguration modules using PIN diode and RF-switch IC are displayed in Fig. 4.8 (a) and (b), respectively. The module using the PIN diode requires one DC control wire, while two DC wires are necessary to control the RF-switch IC. In this study, only one output of the IC is required.

The 3-D exploded views of the reconfiguration module using the PIN diode and the RF-switch IC are depicted in Fig. 4.8 (c) and (d), respectively. It is noticeable that, the

module using the PIN diode has similar structure but with a different PCB layout. The PCB and the ring are made of Roger RT/Duroid 6006 with 0.635 mm thickness. Small holes are drilled through the ring to accommodate the required DC wires.

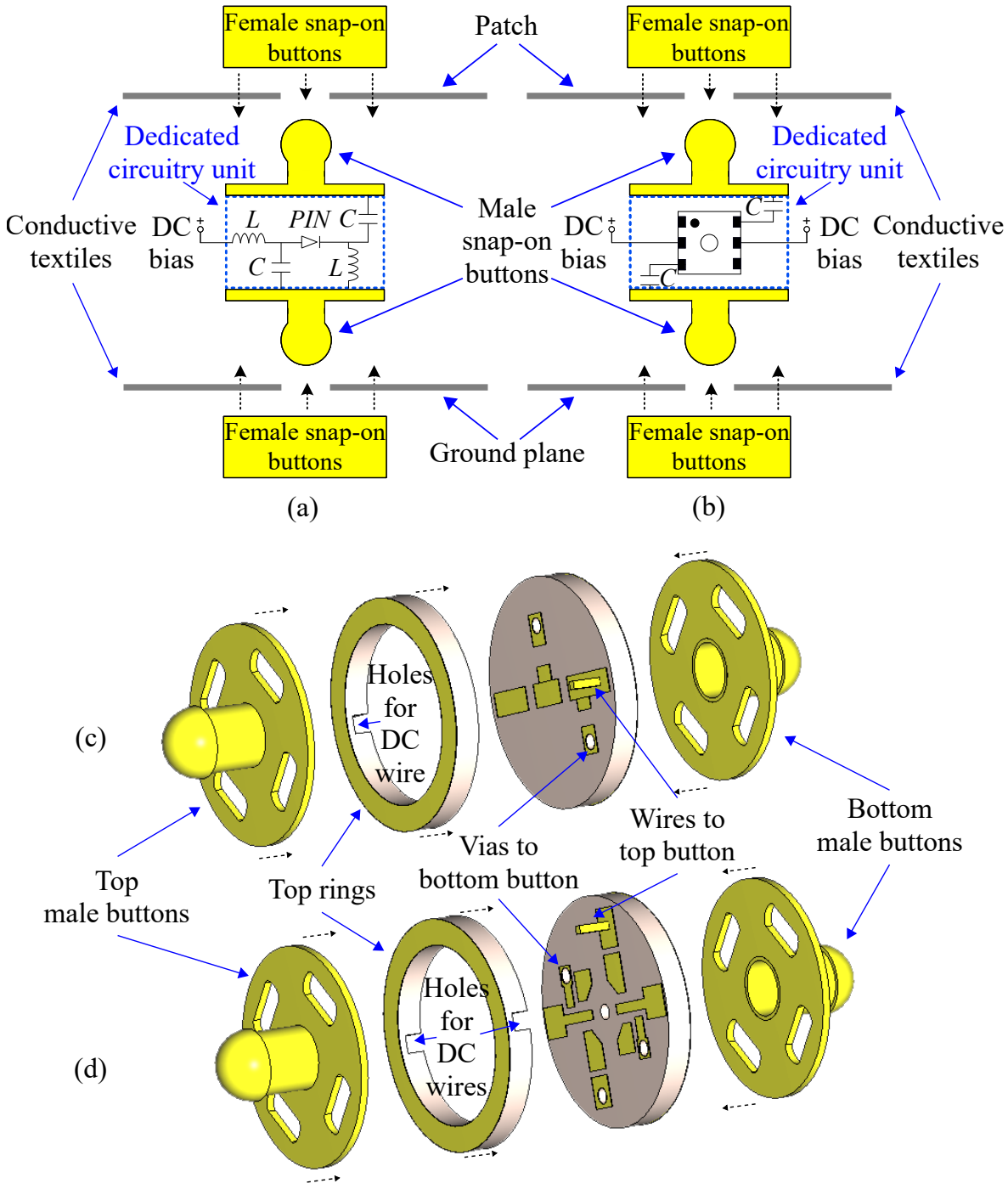

Figure 4.8. Schematics of the reconfiguration modules. Schematics of the reconfiguration modules using (a) PIN diode and (b) RF-switch IC. 3-D exploded views of the reconfiguration modules utilizing (c) PIN diode and (d) RF-switch IC.

The PCB layouts with dimensions and the fabricated PCB boards with lumped components assembled are illustrated in Fig. 4.9 for the modules with PIN diode and RF-switch IC. The ring and PCB board are glued together before soldering to the two male buttons to complete the reconfiguration module. The two assembled reconfiguration module using PIN diode and RF-switch IC are also shown in Fig. 4.9.

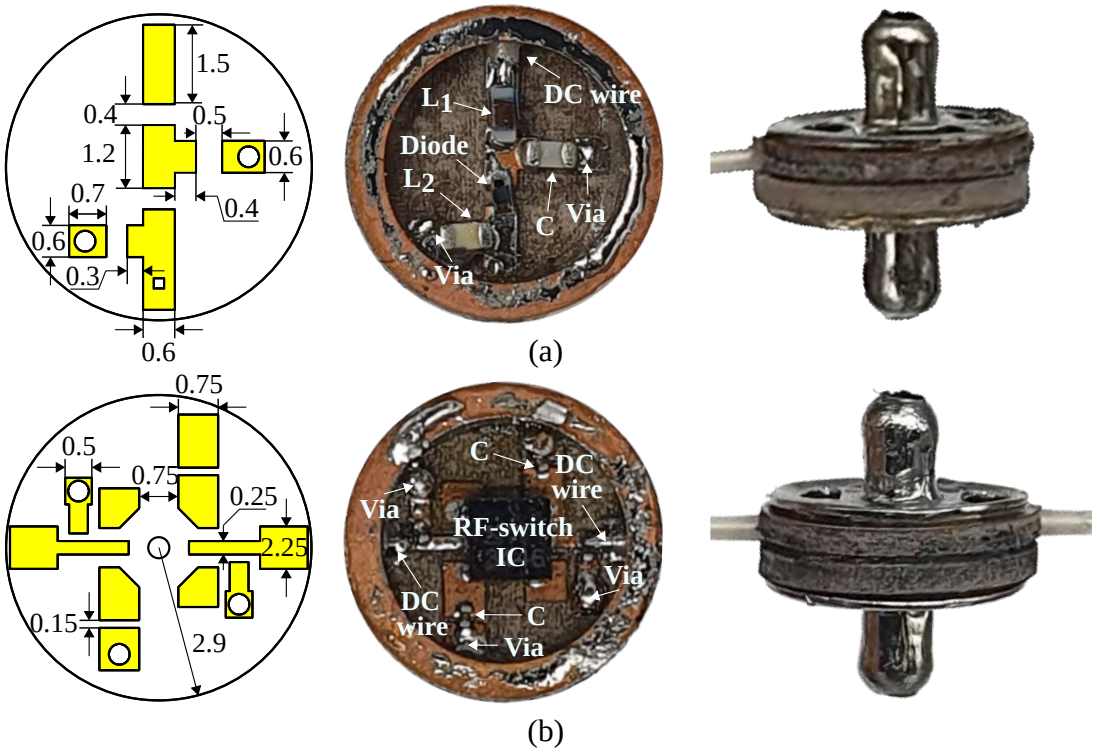

Figure 4.9. Reconfiguration module prototypes. PCB layout with dimensions (mm), zoomed-in reconfiguration module prototypes with lumped components soldered, and assembled reconfiguration modules for (a) PIN diode and (b) RF-switch IC.

4.3.2 Antenna design

To test the reconfiguration modules, a resonant patch antenna structure is selected, as shown in Fig. 4.10 with dimensions detailed in the caption. The antenna includes 2 layers of foam substrate, a full ground plane, a microstrip feed and a square patch with two reconfiguration modules. Holes are trimmed in the two substrate layers to accommodate the reconfiguration modules.

In the ON state of the switching components, they directly connect one side of the patch to the ground plane, thus the antennas work in a quarter-wave resonant mode

as a planar inverted-F antenna (PIFA). In contrast, the antenna will work at a half-wave patch mode in the OFF state because there is no connection between the ground plane and the resonant patch. The instantaneous electric field distributions of the antenna using the RF-switch ICs in ON and OFF states are illustrated in the insets of Fig. 4.11 (a) and (b), respectively. It is worth mentioning that, the E-field distributions of the antenna using PIN diode are almost similar.

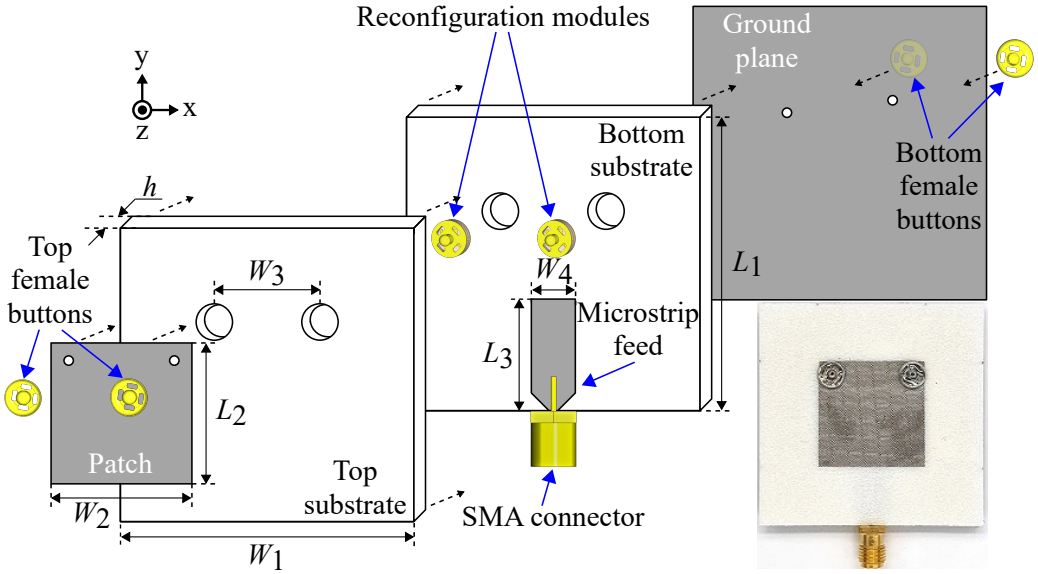

Figure 4.10. Configuration of the antenna. Configuration of the antenna used in the experiment. Dimensions (mm): $L_1 = 50.0$, $L_2 = 22.0$, $L_3 = 19.5$, $W_1 = 50.0$, $W_2 = 22.0$, $W_3 = 18.0$, $W_4 = 7.5$ and $h = 1.6$. Inset: Fabricated antenna using RF switch IC.

4.3.3 Measurement results and comparisons

The selected antenna prototypes have been fabricated and experimentally characterized to compare the performance of the module designs. Antenna substrates have been implemented using a flexible, light weight and low-loss PF-4 foam ($\tan\delta$ = 0.0001, ε_r = 1.06). Conductive parts including the ground plane, the patch and the proximity-coupled feed are made of a conductive fabric with a sheet resistance of approximately 0.01 Ω/square. The fabricated antenna using the RF-switch ICs (similar to the antenna using PIN diode) is shown in the inset of Fig. 4.10.

A good agreement between the simulated and measured reflection coefficients of the antennas using PIN diode and RF-switch IC in ON state and OFF state is observed in Fig. 4.11. For convenience, the antenna using PIN diode and the antenna using

RF-switch IC are called Ant_PIN and Ant_IC, respectively. It can be seen that, the resonance frequency in the ON state of Ant_IC is slightly lower than Ant_PIN. This is because the wire used to connect the PCB with the top male button in the module using PIN diode is closer to the microstrip feed than the module using RF-switch IC. By contrast, in the OFF state, since the RF-switch IC provides better isolation than the PIN diode, the resonance frequency of Ant_IC is higher than Ant_PIN.

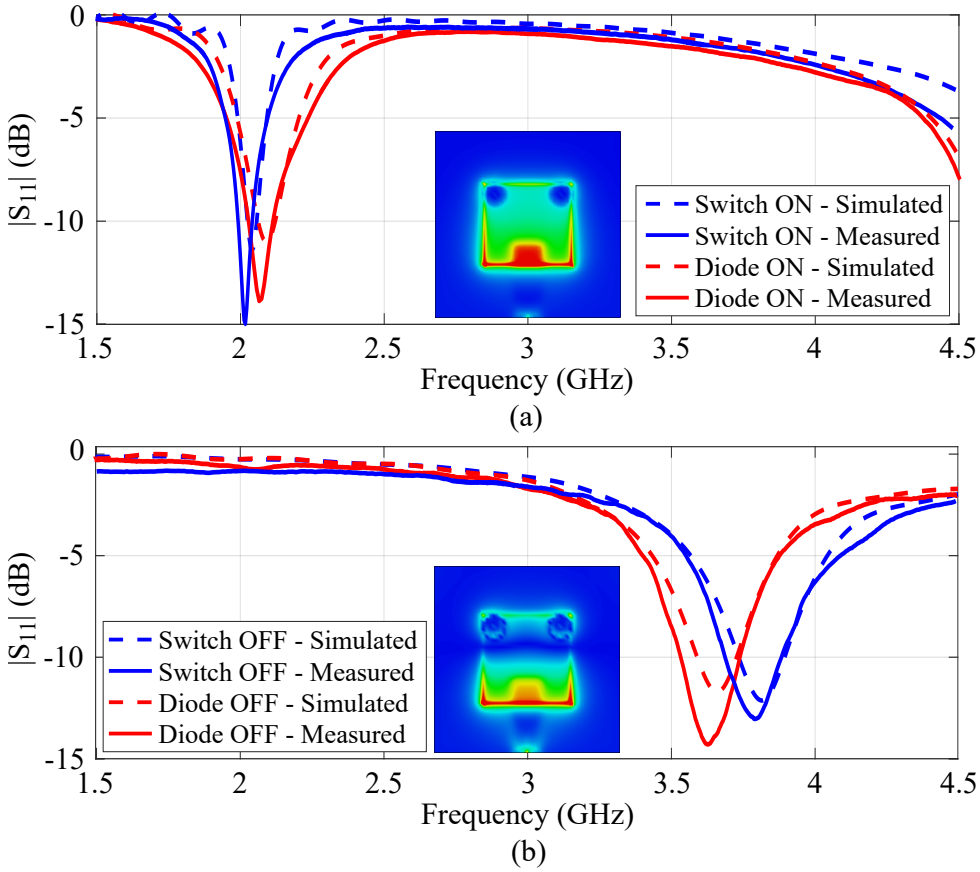

Figure 4.11. Simulated and measured reflection coefficients. Simulated and measured reflection coefficients of antennas using PIN diode and RF-switch IC in (a) ON state and (b) OFF state. Inset: Instantaneous electric field distributions of the antenna using RF-switch IC in ON and OFF states.

The simulated and measured realized gain patterns of Ant_PIN and Ant_IC in the ON and OFF states are shown in Fig. 4.12, where a good agreement can be observed. The small discrepancy can be explained by the imperfection of fabrication and measurement processes. In the ON state, since the forward resistance of the RF-switch is noticeably lower than the one in PIN-diode, the realized gain of Ant_IC is significantly higher than Ant_PIN (-1.3 dBi for Ant_IC and -5.9 dBi for Ant_PIN). In the OFF state, where both antennas operate as half-wave patch mode, the realized gain of Ant_PIN

and Ant_IC are slightly different (4.9 dBi of Ant_PIN and 5.8 dBi of Ant_IC). The estimated efficiencies of Ant_PIN and Ant_IC in the ON state are 15.6 % and 48.3 %. In the OFF state, the predicted efficiency of Ant_PIN and Ant_IC are 65.4 % and 74.7 %, respectively.

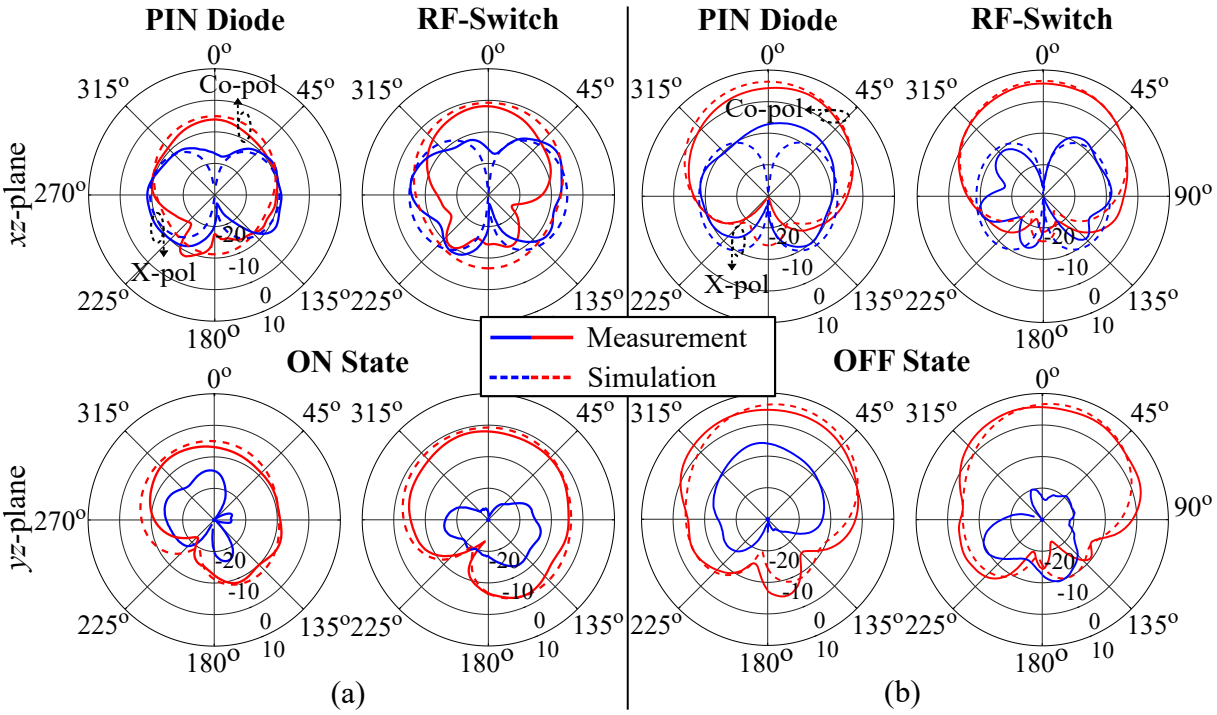

Figure 4.12. Simulated and measured radiation patterns. Simulated and measured realized gain patterns of Ant_PIN and Ant_IC in (a) ON state and (b) OFF state.

The reconfiguration modules using RF-switch IC or PIN diode exhibit different advantages and weakness in term of design, fabrication and antenna performance. First of all, the design and fabrication processes of the reconfiguration module with PIN diode are much simpler than those for the module with RF-switch IC. Only a single DC wire is required to control the working states of the module with PIN diode. By contrast, the module using RF-switch IC needs two DC control wires. In the present study, only one RF-switch output is used, however, both outputs could be exploited to expand the antenna functionality. The RF-switch IC provides a better isolation between the two module terminals in the OFF state and a significant lower insertion loss in the ON state. These merits result in a noticeably better antenna performance while using the RF-switch IC module, especially in the ON state. Furthermore, according to the datasheet of the switching components, the RF-switch IC can be used for an input

power up to +35 dBm (3.2 W). In contrast, the operation the PIN diode is limited to an input power of 150 mW.

4.3.4 Summary on the use of RF-switch ICs and PIN diodes

The use of RF-switch ICs and PIN diodes to obtain reconfigurability for wearable textile antennas, in the form of reconfiguration modules, has been demonstrated and compared. The equivalent circuit and critical fabrication process for the RF-switch IC have been investigated through an evaluation board. It is found that, although the integration of the RF-switch IC is more complicated than that of the PIN diode, it provides a significantly better antenna performance, due to the higher input-to-output isolation in OFF state and the lower insertion loss in ON state.

4.4 Conclusion

In this section, two topologies of reconfiguration modules have been presented, showing their potential for realization of reconfigurable wearable textile antennas. The first part of the section has introduced a novel reconfiguration module aiming to realize robust coplanar connection between electronics and textile antenna conductors. The concept consists of a small PCB loaded with a reconfigurable circuitry including active and lumped components, which is combined with a pair of commercial male snap-on buttons for electrical connection to conductive textiles. To validate this module concept, a frequency-reconfigurable planar inverted-F antenna using a varactor-based module has been designed and simulated.

The utilization of switching components including RF-switch Integrated Circuit (IC) and PIN diodes in reconfigurable wearable textile antennas has been presented in the second part of the chapter. An equivalent circuit and fabrication processes of the RF-switch IC have been established through an evaluation board. It is demonstrated that, the RF-switch IC provides a significantly better antenna performance than the PIN diode at the cost of more complicated design and manufacturing processes.

Chapter 5

Frequency-Reconfigurable Wearable Textile Antennas

BASED on the shorting techniques, snap-on connections and tuning components for reconfigurable wearable antennas discussed in previous chapters, two wearable textile antennas with frequency-reconfigurability are proposed in this chapter. The frequency agility of these two antennas is realized by adding a coplanar reconfiguration module to a planar inverted-F antenna constructed in textile technology.

A frequency-reconfigurable wearable textile antenna with a tuning range of approximately 70% is firstly proposed in this chapter. An one octave tuning range is achieved by exploiting a continuous transition between a quarter-wave and a half-wave radiation modes. The antenna is designed, fabricated and measured to validate the operation concept. An extended version of this antenna with dual-band frequency-reconfigurable characteristic is then presented. In the last part of this chapter, losses in frequency-reconfigurable wearable antenna in relation with input powers will be visualized by using advanced thermal imagery.

5.1 Introduction

As mentioned in Chapter 2, there have been a wide range of passive flexible wearable antennas developed [7,10,61,127,143], aiming to cope with a harsh dynamic operating environment and with deformations occurring in on-body conditions such as bending or crumpling. Besides the mechanical flexibility, an agility of radiation property is desirable for adapting to frequent changes in wearing operating conditions and for multiple wearable systems. To this target, reconfigurable antennas have been developed to improve antenna functionality [150,151]. In recent years, a significant number of planar reconfigurable antennas based on active components such as PIN diodes and varactors has been reported in the literature [24,98,103]. These antennas were mostly implemented on rigid substrates and offered a reconfigurable capability in resonance frequency [15,95,152], radiation patterns [19,99,153] and polarization [146,154,155]. In contrast, due to the challenge in realizing electrically and mechanically strong connections between rigid electronic components and flexible textile conductors, the number of practical reconfigurable textile antennas has been limited [28,29].

In term of frequency agility, a wider frequency tuning range would be beneficial to compensate the variation of on-body operating conditions and environment, as well as to cover diverse communication standards [150]. Frequency-reconfigurable antennas with a wide fractional frequency tuning range above 50% have been reported in the literature [15, 156–158]. However, several of these antennas employed slots in their ground plane, which made them unsuitable for wearable applications. This is due to the compromised isolation from the body and bidirectional radiation patterns. Other frequency-reconfigurable antennas with full ground plane and directional radiation patterns were reported with wide frequency tunability range up to 50% [95,96,147,159, 160]. Nevertheless, these antennas were on rigid substrates and thus not flexible and lightweight. There have been some practical frequency reconfigurable flexible textile antennas reported in literature [28, 29]. However their frequency tuning ranges are still limited at approximately 15.2% [29] and 32.8% [28]. While appreciable, it would be desirable to extend the tuning range in the perspective of wearable applications.

In the first part of this chapter, a reconfigurable wearable textile antenna with a very wide frequency tuning range reaching nearly 70% is designed, fabricated and experimentally validated. The very wide one-octave frequency tuning range is achieved by combining an antenna structure and a coplanar reconfiguration module concept

as introduced in Chapter 4. The coplanar module is optimized electrically, to maximize its frequency tuning range, and physically, to be practical for wearable applications. The operation principle is based on exploiting a continuous transition between a quarter-wave and a half-wave mode, which leads to the wide frequency tuning range. Although the method of combining different modes has been used in reconfigurable antenna designs [24,28,156,157], they are fundamentally different from our design. For instance, previous approaches usually used PIN diodes to switch between different radiation modes which leads to discrete reconfigurability [24, 156]. In other previous implementations based on varactors, the two radiation modes were either simultaneously [28] or separately [157] excited in the proposed designs to achieve a dual-band frequency reconfigurability. By contrast, it is believed that this is the first frequency reconfigurable antenna with a full ground plane that can utilize the continuous transition between two radiation modes to realize an octave frequency tuning range.

In the second part of this chapter, a dual-band frequency-reconfigurable wearable antenna is proposed, as dual-band extension of the frequency-reconfigurable antenna presented in the first part. Utilizing the flexible coplanar reconfiguration module as the antenna presented in the first part, the PIFA structure now is optimized aiming to to simultaneously cover the 2.45 and 5.8 GHz ISM radio bands. The antenna achieves wide frequency tuning ranges of 48.6% and 18.3% in the 2.45 and 5.8 GHz ISM bands, respectively. The proposed antenna is then fabricated and measured to validate the concept.

The thermal behavior of the proposed frequency-reconfigurable wearable antenna is investigated through infrared thermography in the third part of the chapter. The relationship between the temperature of the textile antenna and the input power is experimentally considered to identify the antenna hot spots. It is found that, the highest temperature point is mainly at the tuning component location, which is consistent with the loss predictions from electromagnetic simulation tools. A clear correlation is confirmed between the radiation efficiency and temperature of the varactors used as tuning elements. It is also observed that tuning frequency remains stable despite the antenna input power variations within the range from 21 to 521 mW. The presented preliminary results demonstrate the use of infrared thermography as a valuable tool for characterization of thermal safety margins of wearable devices and for imaging of losses in reconfigurable antenna technology.

5.2 A frequency-reconfigurable wearable textile antenna with one octave tuning range

A reconfigurable wearable textile antenna with wide frequency tuning range is demonstrated. The frequency agility is realized by adding a coplanar reconfiguration module (as introduced in Section 4.2) to a planar inverted-F antenna (PIFA) constructed in textile technology. The reconfiguration module consists of a small flexible printed circuit board (PCB) which integrates a tuning circuitry with commercial snap-on buttons as electronic-to-textile connectors. Using this module equipped with a varactor diode, the frequency reconfigurability of the PIFA is investigated and optimized parametrically for maximum tuning range, exploiting a smooth transition from a quarter-wave to a half-wave patch resonant mode. A fabricated prototype demonstrates a very wide tuning range of approximately 70% (or one octave) with stable directive radiation characteristics, as predicted by simulations. The robust performance and mechanical stability of the reconfigurable antenna in various on-body and bending configurations validates the viability of the antenna tuning concept and the practicality of the proposed coplanar reconfiguration module. The results presented in this section have been published in [44].

5.2.1 Antenna operation principle

This section presents the principle applied to extend the frequency tuning range of a reconfigurable resonant antenna with a full ground plane.

Most frequency-reconfigurable antennas with full ground planes and broadside radiation patterns utilize electronically controlled components to change the effective antenna dimensions, leading to a change in resonance frequency [28, 29, 95, 96, 147, 159, 160]. By doing so, the reported frequency tuning range among these antennas reached up to 50% [147]. A reason for this limited range is that these antennas were designed to work in a single radiation mode throughout the frequency range, including half-wave patch mode [96], quarter-wave patch mode [28, 95], and orthogonal combination of modes for circular polarization [159, 160].

In this study, a smooth transition between two modes of radiation is utilized to extend the frequency tuning range. Namely, a continuous transition from a single-point shorted planar inverted-F antenna (PIFA) antenna, a quarter-wave planar PIFA mode

$(TM^z_{0(0.5)0})$ to a half-wave standard patch mode (TM^z_{010}) is proposed as the principle of tuning, as displayed in Fig. 5.1.

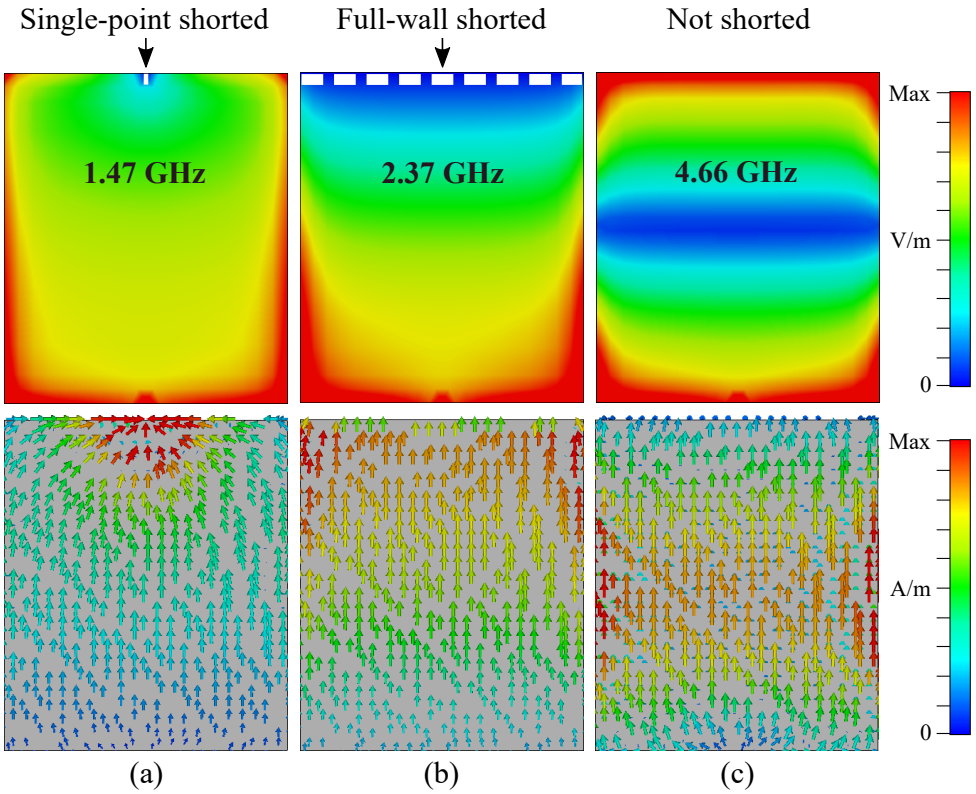

Figure 5.1. Electric field magnitude and current density distribution. Electric field magnitude in the cavity of the antenna and current density distribution under an ideal resonant patch antenna. Quarter-wave resonant patch of a PIFA with (a) one shorting post and (b) full shorting wall. (c) Half-wave resonant patch.

Considering the quarter-wave PIFA modes $(TM^z_{0(0.5)0})$, the resonance frequency f can be approximated using the relation [85]:

$$f = \frac{c_0}{4(L + W - W_s - h)\sqrt{\varepsilon_r}} \tag{5.1}$$

with the speed of light in free space c_0, patch length L, patch width W, shorting wall width W_s, substrate thickness h and substrate relative permittivity ε_r. By placing tunable capacitive components at the resonant patch edge, the effective shorting wall width can be controlled to obtain a variable resonance frequency [28]. Figure 5.1 displays the electric field and current distribution on the antenna resonant patch for the cases where the quarter-wave patch is shorted: (i) at one shorting post (Fig. 5.1 (a); and

(ii) on an entire side of its edge (Fig. 5.1 (b)). The frequency ratio between these two PIFA modes is approximately 1:1.6 which corresponds to a 47% fractional bandwidth.

To further increase the continuous frequency tuning ratio, a smooth transition to an additional radiation mode is needed. A promising solution is offered if the shorting wall can be removed, since the antenna radiation mode would consequently be changed to a standard half-wave patch mode. This resonant mode is shown in Fig. 5.1 (c), where the resonance frequency is increased to nearly three times that of the single-point post-shorted PIFA shown in Fig. 5.1 (a). Along with the additional radiation mode, the achievable frequency tuning ratio can be ideally increased up to 1:3.2 and corresponds to a fractional bandwidth of 100%. However, practical limitations of the tuning mechanism and impedance matching are expected to reduce this potential tuning range, as described in the following Section.

5.2.2 Reconfigurable antenna design

In order to implement a frequency reconfigurability to a wearable textilea antenna, a coplanar reconfiguration module is utilized. The module proposed in the design is based on the coplanar reconfiguration module presented in Section 4.2 - Chapter 4. However, some modifications are applied to enhance the practicality of the antenna as will be discussed in Section 5.2.3.

To provide an example application of the module concept with wide frequency tuning range, a textile antenna based on the proposed PIFA structure with two-mode-transition is adopted as host antenna. The design is simulated using CST Microwave Studio 2019. The antenna geometry is illustrated in Fig. 5.2 with its dimensions detailed in the caption. The antenna is comprised of a full ground plane, a bottom substrate supporting a microstrip proximity feed, a second substrate supporting a main resonant patch and a small strip connected to a shorting wall to form the PIFA structure.

The two stacked antenna substrates are made of a highly flexible, light-weight and low-loss Cumming Microwave PF-4 foam layers with a thickness of 1.6 mm, a loss tangent $\tan\delta$ = 0.0001 and a relative permittivity ε_r = 1.06. The conductive antenna parts including the ground plane, the main resonant patch, the small patch, the shorting wall and the microstrip feed line are made from a silver-coated nylon Rip-stop fabric

(Shieldex® Nora-RS), which is flexible, biocompatible and highly electrically conductive with a sheet resistance of approximately 0.01 Ω/square. The shorting wall realized on conductive strips is utilized here, since it was demonstrated to be an efficient shorting strategy in Section 3.2.

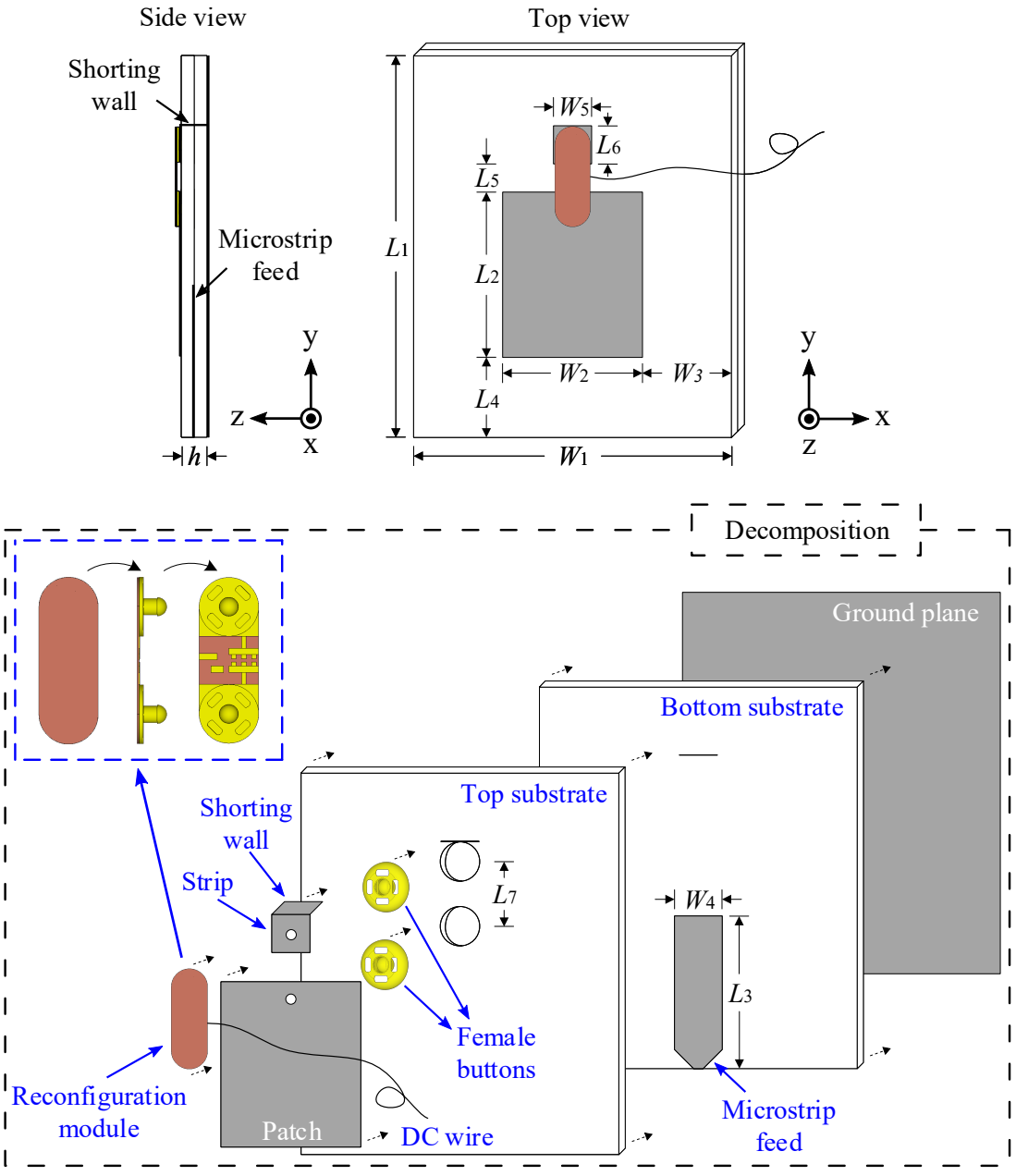

Figure 5.2. Structure of the proposed frequency-reconfigurable flexible antenna. Structure of the proposed frequency-reconfigurable flexible antenna. Dimensions (mm): $L_1 = 60.0$, $L_2 = 26.0$, $L_3 = 24.0$, $L_4 = 18.7$, $L_5 = 21.0$, $L_6 = 6.0$, $L_7 = 10.2$, $W_1 = 50.0$, $W_2 = 22.0$, $W_3 = 14.0$, $W_4 = 7.5$, $W_5 = 6.0$ and $h = 3.2$.

5.2.3 Reconfigurable antenna operation

This section presents an analysis of the antenna through an equivalent circuit model used to understand and demonstrate the operation principle of the wide frequency tuning range. This section also introduces the frequency tuning circuitry unit of the reconfiguration module as well as practical considerations.

Equivalent circuit model

The conceptual diagram and the equivalent circuit model of the antenna are shown in Fig. 5.3. The antenna can be considered as an in-series connection of a shorting wall, a short microstrip line, a reconfiguration module and a resonant patch, as shown in Fig. 5.3 (a). This builds the foundation of the equivalent circuit model of the whole antenna, as illustrated in Fig. 5.3 (b). The impedance Z_{var} of the varactor includes the varactor capacitance C_{var}, the parasitic inductance L_{var} and the internal resistance R_{var} in series, as shown in Fig. 5.3 (c).

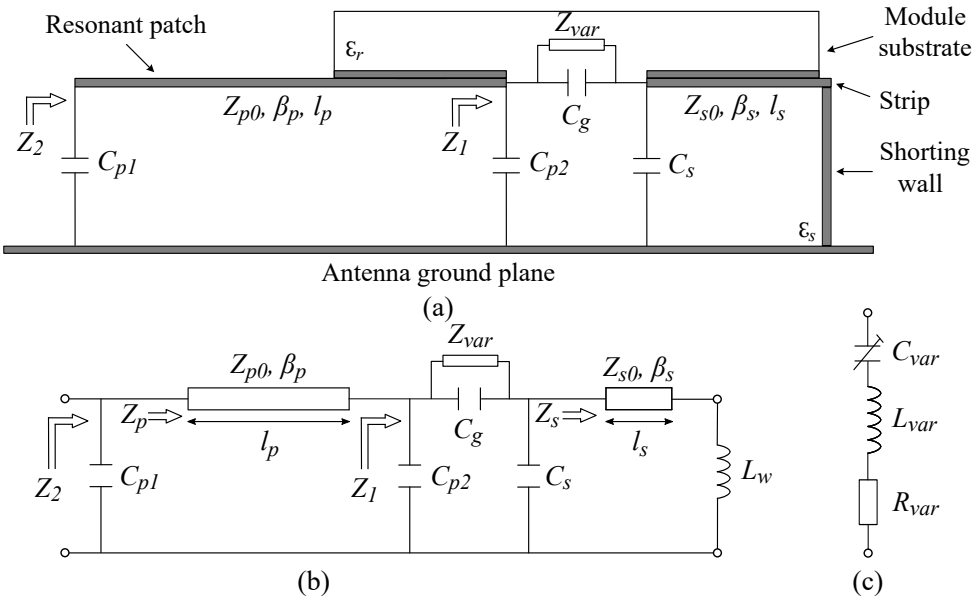

Figure 5.3. Antenna equivalent circuit. (a) Antenna conceptual diagram, (b) equivalent circuit model of the antenna, and (c) equivalent circuit of the varactor (Z_{var}).

The edge shorting wall is modeled using an inductance of L_w which can be calculated following [161] (3rd edition - Chapter 3). The small strip connected to the shorting wall and the antenna resonant patch are represented as two transmission lines. Their impedance Z_s at the varactor position (with the load L_w) and Z_p at the starting point

of the line (with the load Z_1) can be attained using transmission line theory. These calculations are based on the characteristic impedances Z_{s0}, Z_{p0}, the phase constants β_s, β_p and the lengths l_s, l_p of the small strip and the antenna resonant patch, respectively. The capacitance of the gap between the open end of the resonant patch and the shorting strip is denoted as C_g. It can be computed as the gap capacitance between two microstrip lines as demonstrated in [162]. The capacitances of the gap between the antenna ground plane and the open end of the resonant patch (denoted as C_{p1} and C_{p2} respectively) as well as the open end of the small strip (denoted as C_s) can be calculated as [163–166]:

$$C_s = \frac{W_s\sqrt{\varepsilon_s}\xi_{s1}\xi_{s3}\xi_{s5}}{\xi_{s4}cZ_{s0}\frac{W_s}{h}}, \tag{5.2}$$

$$C_{p1} = C_{p2} = \frac{W_p\sqrt{\varepsilon_s}\xi_{s1}\xi_{s3}\xi_{s5}}{\xi_{s4}cZ_{p0}\frac{W_p}{h}}, \tag{5.3}$$

where W_p and W_s are the widths of the resonant patch and the strip to the shorting wall, h and ε_s are the thickness and the relative permittivity of the antenna substrate and the parameters ξ_{p1}, ξ_{p3}, ξ_{p4}, ξ_{p5}, ξ_{s1}, ξ_{s3}, ξ_{s4}, ξ_{s5} can be calculated as given in [164,165].

Using transmission line theory, we are able to calculate the input impedance Z_1 at the input of the reconfiguration module and the input impedance Z_2 at the input of the antenna resonant patch as a function of a hypothetical varactor capacitance C_{var}, yielding

$$Z_1 = [(Z_s||\frac{1}{j\omega C_s}) + (Z_{var}||\frac{1}{j\omega C_g})]||\frac{1}{j\omega C_{p2}}, \tag{5.4}$$

$$Z_2 = Z_p||\frac{1}{j\omega C_{p1}}. \tag{5.5}$$

The calculations of Z_1 can be performed in a thought experiment over several orders of magnitude of the hypothetical varactor capacitance C_{var} to provide a perspective on the transition from open ($C_{var} \to 0$) to short ($C_{var} \to \infty$) [96]. The calculated Z_1 values are plotted on a Smith chart for a capacitance C_{var} varying from 0.001 to 1000 pF, as displayed in Fig. 5.4 (a). As observed in this graph, a nearly open-circuit condition corresponds to the lowest value of C_{var}, while at the highest value of capacitance the input impedance of the reconfiguration module $Z_1 = 0.5 + j57\ \Omega$.

The antenna resonance frequency can be analyzed by calculating the input impedance Z_2 and determining when its imaginary part becomes zero. Figure 5.4 (b) shows the

antenna resonance frequency obtained from the equivalent-circuit analysis and CST full-wave simulation for different values of capacitance of a single (hypothetical) varactor from 0.001 to 1000 pF. A good agreement between these two curves is observed in Fig. 5.4 (b) and when the capacitance is changing from lowest to highest value, the antenna radiating mode is transitioning from a single-point shorted PIFA ① to a quarter-wave resonant mode ② and finally to a half-wave resonant mode ③, as illustrated by the electric field distributions of the antenna.

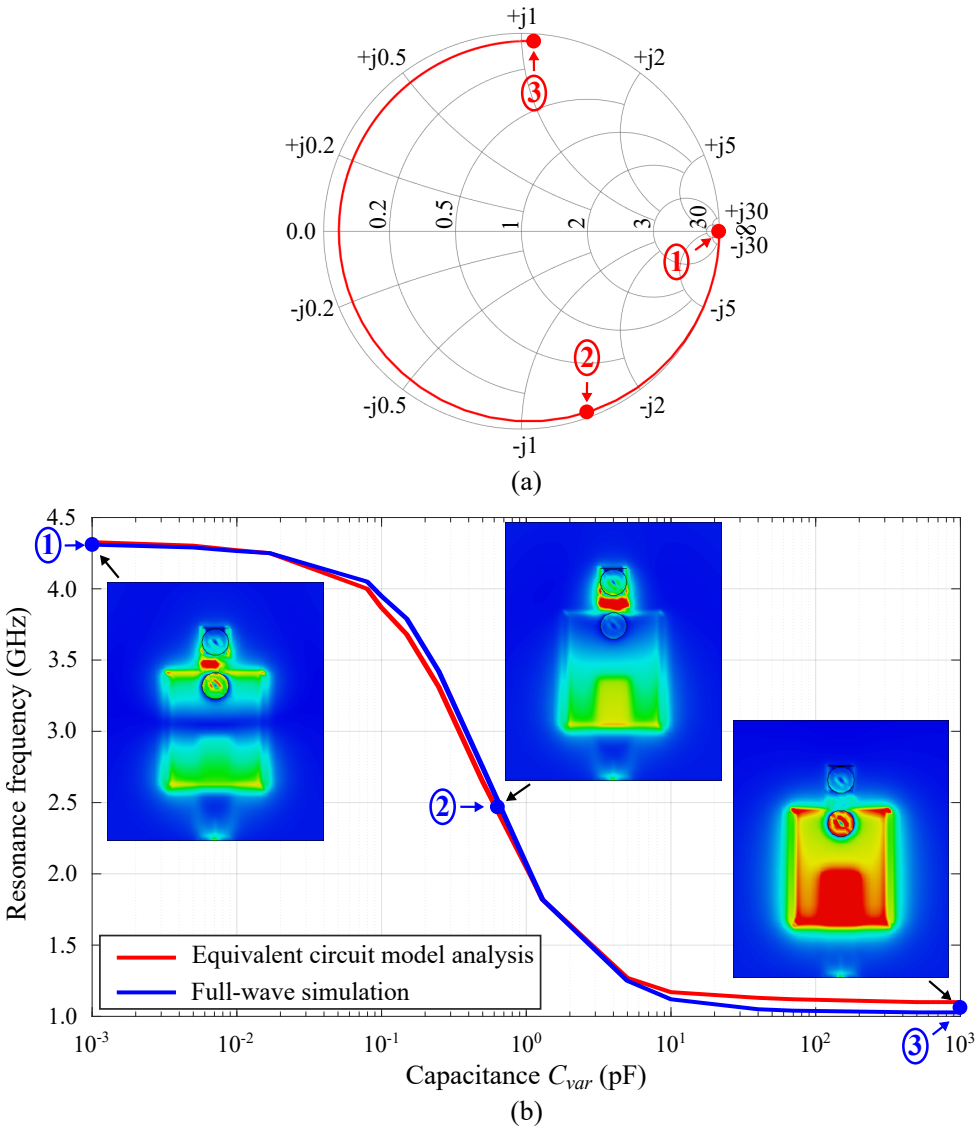

Figure 5.4. Comparision between equivalent circuit analysis and full-wave simulation. (a) Calculated input impedance of the reconfiguration module Z_1 represented in a Smith Chart, and (b) equivalent circuit model analysis and full-wave simulation of the resonance frequency across different values of varactor capacitance. Insets: Simulated electric field distributions in the cavity of the antenna at the lowest, middle and highest resonance frequencies in the ideal tuning range.

Frequency tuning circuitry unit

In order to design an appropriate frequency tuning circuit, it is initially necessary to select an appropriate varactor junction capacitance range since this choice is crucial to maximize the relative frequency tuning range [96]. In this proposed design, the varactor type MA120H46 is used to realize a continuous frequency agility. As investigated in [95], the measured varactor capacitance ranges from 0.15 to 1.3 pF for a bias voltage changing from 0 to 18 V. Additionally, the choice of this high-Q varactor is essential to obtain acceptable antenna efficiency. A wide fractional frequency tuning range amounting to approximately 70% can be achieved using the proposed tuning circuit built with the single varactor. This is illustrated in Fig. 5.5 which is a magnified section of the most frequency-sensitive region in Fig. 5.4 (b), where the potential varactor capacitance values are varied between 0.1 to 5 pF approximately.

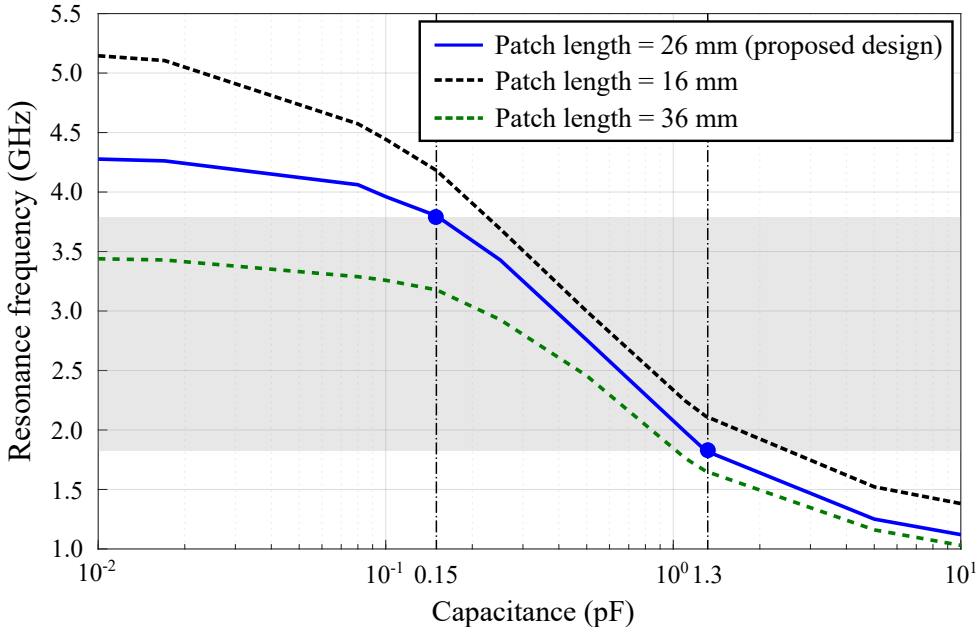

Figure 5.5. Examples from the optimization process. A magnified view of Fig. 5.4 (b) in the region of the interested resonance frequency transition, with two examples from the optimization process under taken to vary the resonance frequency.

From the optimization of the geometry based on the equivalent circuit model, it is found that the patch width has only a minor influence on the resonance frequency at both PIFA mode $TM^z_{0(0.5)0}$ and half-wave standard patch mode TM^z_{010} and therefore, it can be fixed early in the design. In contrast, the resonance frequency range of the antenna can be efficiently controlled by varying the length of the patch: reducing

the patch length increases the resonance frequency and vice versa. This is illustrated in Fig. 5.5 where two resonance frequency curves obtained from a shorter (16 mm long) and longer (36 mm long) patch scenarios are compared with the optimized value (26 mm long). These three cases demonstrate that the antenna tuning range can be adapted through design to exploit a given varactor capacitance span. As shown in the highlighted area in Fig. 5.5, a wide frequency fractional tuning range amounting to approximately 70% can be achieved while using the chosen varactor. Additionally, the operating frequency is simultaneously optimized to be at the center of the ISM frequency bands at 2.45 GHz for a bias voltage of 2.5 V. This is based on the available practical power sources in low-voltage wearable systems with a typical bias voltage ranging from 0 to 5 V.

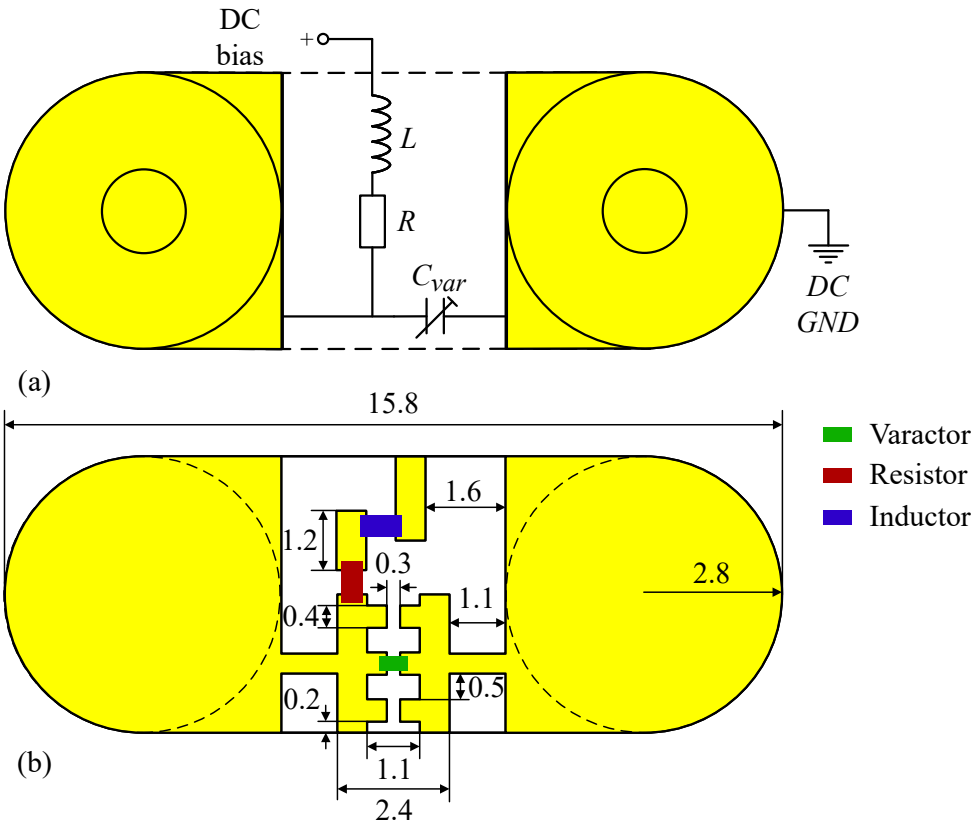

Figure 5.6. Schematic and PCB layout of the proposed reconfiguration module. (a) Schematic and (b) PCB layout with dimensions in mm of the proposed reconfiguration module.

Figure 5.6 (a) shows the schematic of the proposed module designed for the PIFA structure. The circuit consists of one single MA120H46 varactor, as well as a bias circuit including an RF-choke inductor L = 400 nH in series with a large resistor R = 1 MΩ.

A PCB layout with corresponding dimensions is shown in Fig. 5.6 (b). The PCB is designed to accommodate up to 3 varactors to allow the layout to be re-used in different designs where larger capacitance values may be required.

The electric field distributions at the lowest, middle and highest resonance frequencies within the tuning range corresponding to three different varactor capacitance values are shown in Fig. 5.7. At the lowest frequency of 1.82 GHz (C_{var} = 1.3 pF), a PIFA mode is observed, as illustrated in Fig. 5.7 (a). A null in the field distribution (represented by a white dash line) appears at the top of the cavity. This null moves toward the center of the patch with a decreasing varactor capacitance, as shown in Fig. 5.7 (b) and (c). This confirms that the antenna resonant mode is changing from the quarter-wave PIFA mode to a half-wave patch mode. At the lowest capacitance in the varactor range, depicted in Fig. 5.7 (c), the electric field distribution approaches a standard half-wave patch resonant mode (TM^z_{010}).

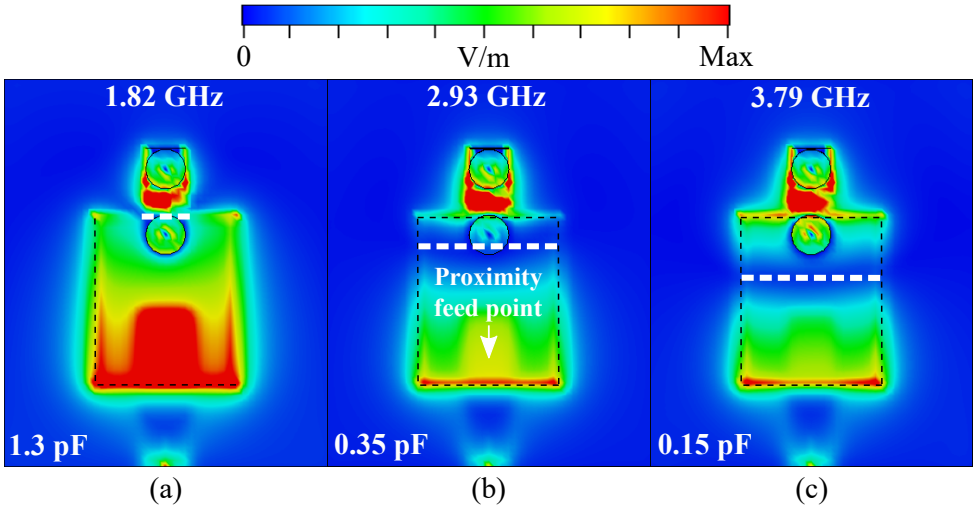

Figure 5.7. Simulated electric field distributions of the proposed antenna. Simulated electric field distributions of the proposed antenna at the resonance obtained for three different varactor capacitances: (a) the lowest frequency 1.82 GHz, (b) the middle frequency 2.93 GHz, and (c) the highest frequency 3.79 GHz.

Practical considerations

This section discusses several crucial aspects to enhance the practicality of the proposed antenna. Considering the size of the reconfiguration module with a total length of 15.8 mm, a rigid printed circuit board (PCB) module would compromise the flexibility of the whole antenna structure. A flexible substrate with a thickness of 0.15 mm,

relative permittivity ε_r = 3.1 and loss tangent tanδ = 0.0079 is therefore used to realize the module. Figure 5.8 (a) shows the fabricated flexible reconfiguration module with components mounted and Fig. 5.8 (b) displays the module under bending condition.

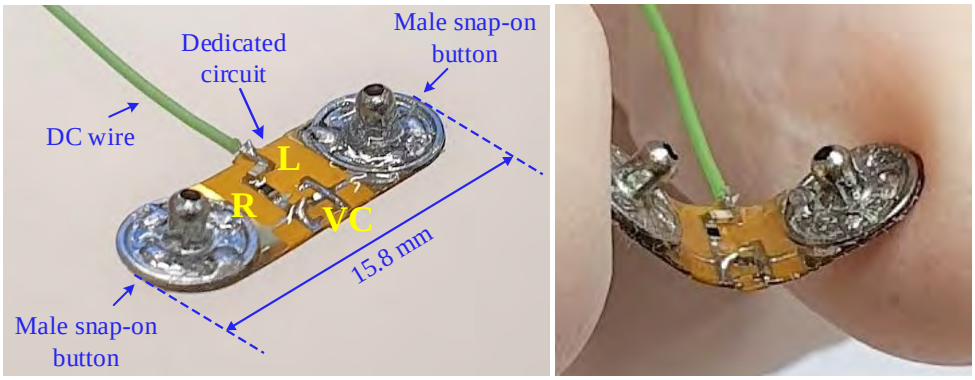

Figure 5.8. Prototype of the proposed coplanar reconfiguration module. Prototype of the proposed coplanar reconfiguration module with lumped components loaded: (a) general view with description of the components, and (b) illustration of possible bending.

In order to integrate the flexible textile antenna to garments, the most convenient method is adding a pocket on clothes to accommodate the antenna [5,48]. This method allows the re-usability of the antenna as well as the washability of clothes at the cost of slightly decreasing the antenna performance, since the antenna is working from within the pocket. Another method is sewing the antenna ground plane onto the inner garment layer and leaving the antenna patch on the outer garment layer [28]. To achieve the washability of the antenna, instead of making the module water-resistant, it is safer to make the module detachable. Therefore, a pair of female snap-on buttons is now integrated into the antenna top substrate instead of the reconfiguration module as represented in [43]. As a consequence of this arrangement, the reconfiguration module can now be interchanged and easily detached for example while washing the garment. To provide more protection to the attached lumped components soldered on the module, a thin layer of PDMS is added on top of the circuitry unit [29].

5.2.4 Experimental results

The proposed antenna as well as the flexible reconfiguration module have been manufactured and measured to validate the proposed reconfiguration concept. The fabrication starts with cutting the PF-4 foam and silver fabric pieces to given dimensions.

Holes on a top substrate are also required for accommodating the female snap-on buttons. All the antenna conductive parts including radiating patches, shorting strip, ground plane and microstrip feed are cut using a laser milling machine (LPKF: Protolaser S) for best accuracy. In order to guarantee an excellent connection between the shorting strip and the ground plane, both parts are realized as one piece of metalized fabric. The substrates and conductive parts are glued together using a washable fabric glue (Tiger Grip from Helmar). An SMA connector is mechanically and electrically connected to the microstrip feed using conductive epoxy CW2400 from CircuitWorks. A fabricated antenna with a reconfiguration module is shown in Fig. 5.9.

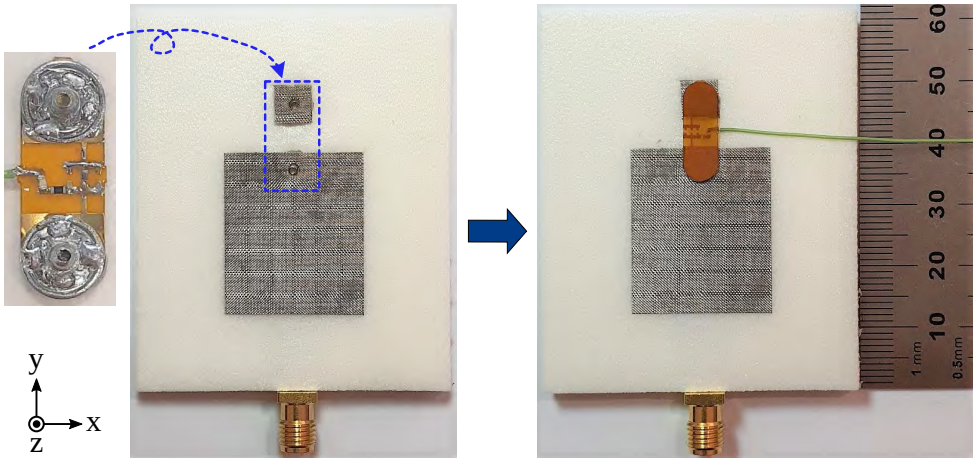

Figure 5.9. Antenna prototype with the flexible reconfiguration module. Antenna prototype with the flexible reconfiguration module. Inset: Zoomed front side of reconfiguration module.

Reflection coefficient and tuning range

Figure 5.10 displays the $|S_{11}|$ parameters obtained from simulation and measurement for different values of the bias voltage, where a very good agreement is observed. As expected, when the bias voltage is tuned from 0 to 18 V, corresponding to the maximum and minimum varactor capacitance respectively, the measured frequency tuning range varies from 1.82 to 3.77 GHz, which yields approximately a 69.7% fractional tuning range. Small discrepancies are due to the imperfect fabrication and measurement processes. When limiting the bias voltage to 0 – 5 V, the approximate 47% fractional frequency agility range from 1.82 to 2.94 GHz is still appreciable. The measured instantaneous impedance bandwidth based on a 10-dB return loss increases from approximately 3.9% to 5.2% as the resonance frequency is tuned from the lowest to the highest values.

5.2.4 Experimental results

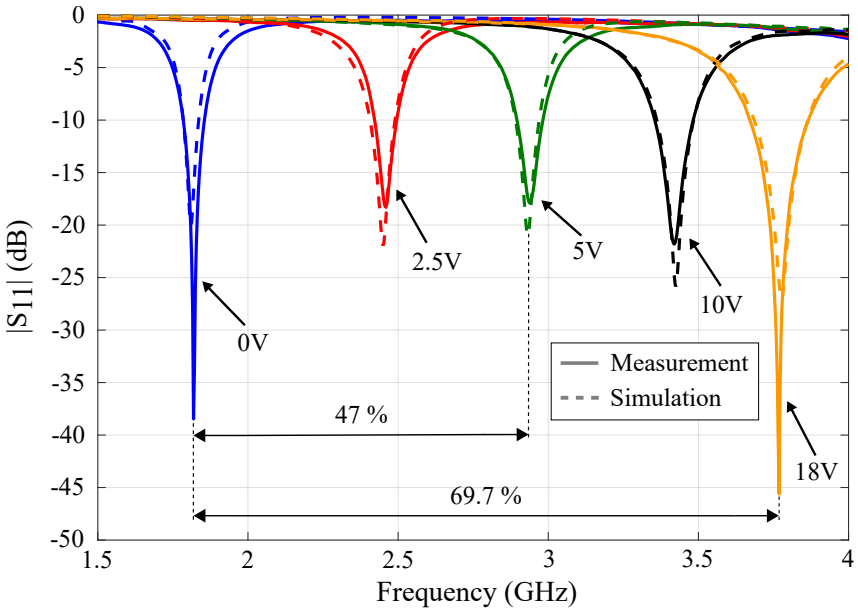

Figure 5.10. Simulated and measured reflection coefficients of the proposed antenna. Simulated and measured reflection coefficients of the proposed antenna for selected values of the bias voltage applied to the varactor.

Radiation pattern, gain and efficiency

Figure 5.11 shows the simulated and measured radiation patterns in the *xz*-plane (H-plane) and the *yz*-plane (E-plane) at 1.82, 2.45, 2.93, 3.42 and 3.77 GHz. A transition of the antenna radiation patterns from a quarter-wave mode to a standard half-wave patch mode is observed. Specifically, up to 2.45 GHz, the antenna radiates in a quarter-wave mode, therefore radiation patterns of a magnetic dipole placed on a finite ground with a maximum gain toward broadside are obtained. At the resonance frequencies which are higher than 2.93 GHz, the radiation patterns resemble more a standard half-wave patch antenna with a noticeable higher gain (by around 3 dB) than a quarter-wave mode in the first two frequencies. The slight discrepancy between simulation and measurement results can be mainly explained by the inherent imperfection of a flexible fabricated antenna as well as the unavoidable misalignment between the transmitter and receiver antennas in measurement setup. Additionally, due to these reasons, the measured cross polarization values are significantly higher than the simulated ones in the *yz*-plane.

The simulated and measured antenna realized gains are compared in Fig. 5.12. The measured realized gain increases from -1.07 to 7.37 dBi when the resonance frequency rises from 1.82 to 3.77 GHz, which is in a satisfactory agreement with the simulated

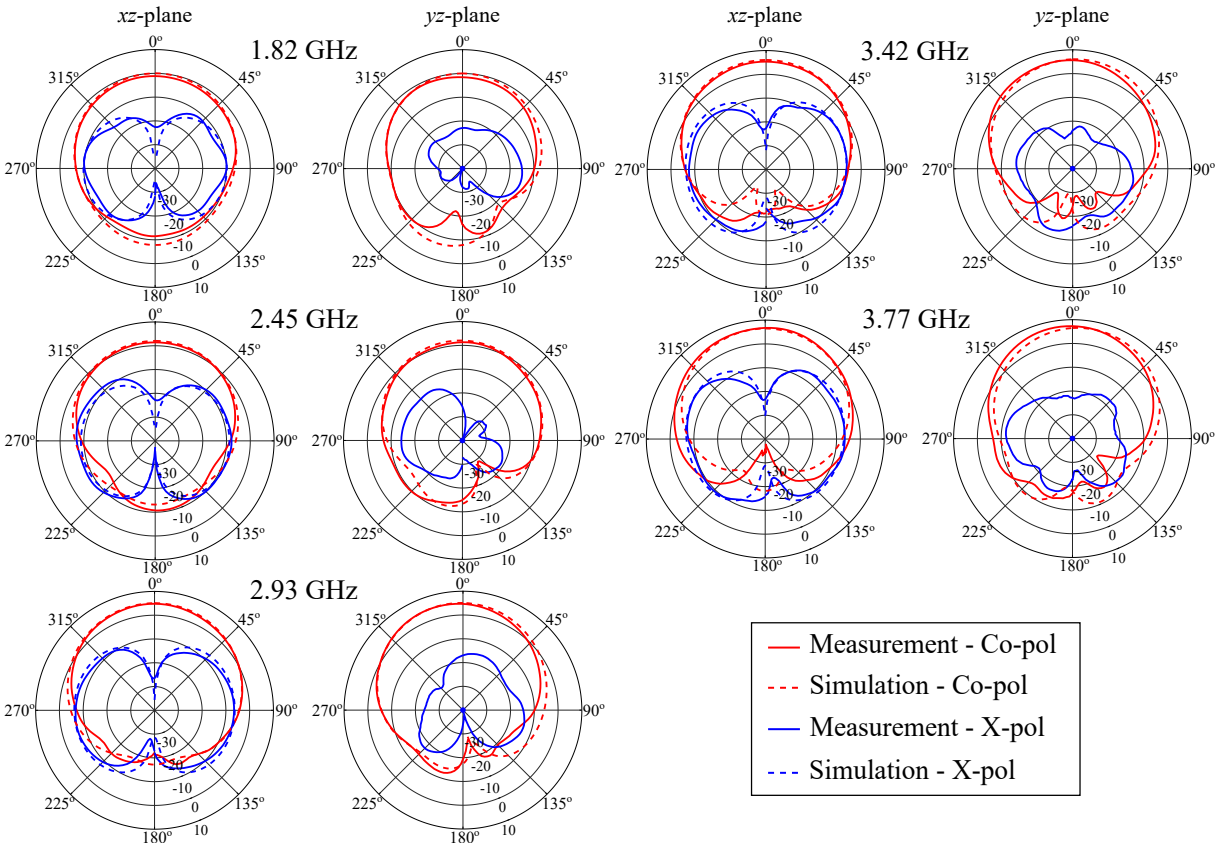

Figure 5.11. Radiation patterns of the proposed antenna. Simulated and measured realized gain radiation patterns of the proposed antenna in the *xz*- and *yz*-planes at 1.82, 2.45, 2.93, 3.42 and 3.77 GHz.

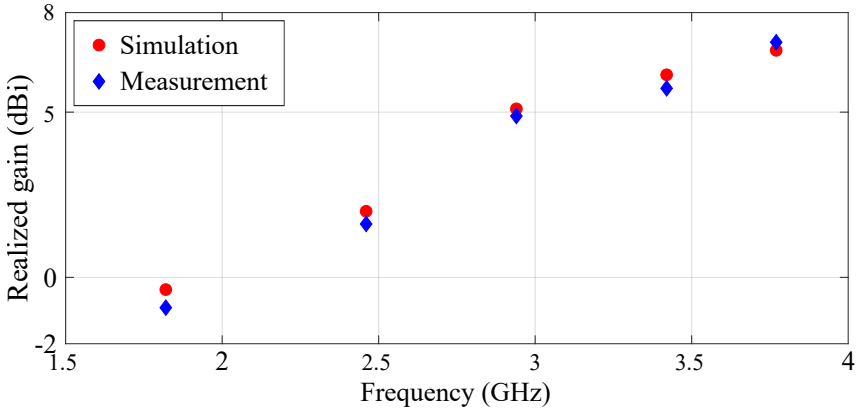

Figure 5.12. Realized gains of the proposed antenna. Simulated and measured realized gains of the proposed antenna.

results. The slight discrepancies are caused by the fabrication and measurement tolerances. The antenna efficiency obtained from simulation rises from approximately

33.1% at the lowest frequency to 90.3% at the highest frequency. Thus, the actual radiation efficiency estimated based on the measured gain is between 29.8% at 1.82 GHz and more than 90% at 3.77 GHz.

Impact of bending and human body

To experimentally characterize the impact of bending on the antenna performance, the flexible antenna is affixed onto a 3-D printed cylindrical base (made by PLA and does not affect the antenna performance) which allows the antenna to be conformal along the x-axis with a bending radius R_b of 30 mm (see inset in Fig. 5.13). The antenna reflection coefficients under flat and bent conditions at different bias voltages are shown in Fig. 5.13. The measured $|S_{11}|$ parameters are lightly shifted upward due to the effective shortening of the patch length under bending conditions. Since the patch length is nearly unchanged while the antenna is bent along the y-axis, the bending effect is less pronounced in that orthogonal direction (which has been proven by simulations not shown here for the sake of brevity).

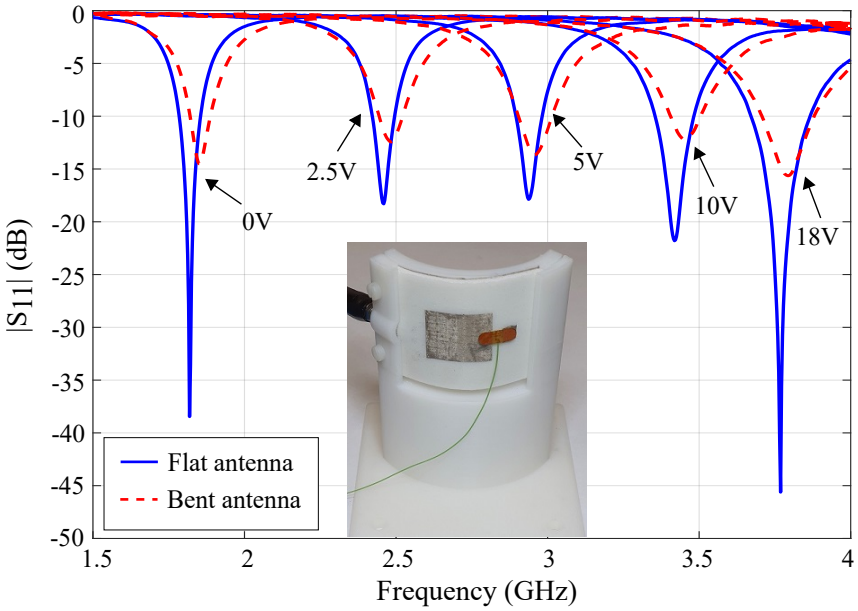

Figure 5.13. Measured reflection coefficients under flat and bent conditions. Measured reflection coefficients of the proposed antenna under flat and bent conditions. Inset: bending measurement setup - the antenna was bent along the x-axis with a bending radius of 30 mm.

Figure 5.14 shows the measured antenna reflection coefficients under two circumstances, namely when the gaps or the materials in-between the antenna and the human body

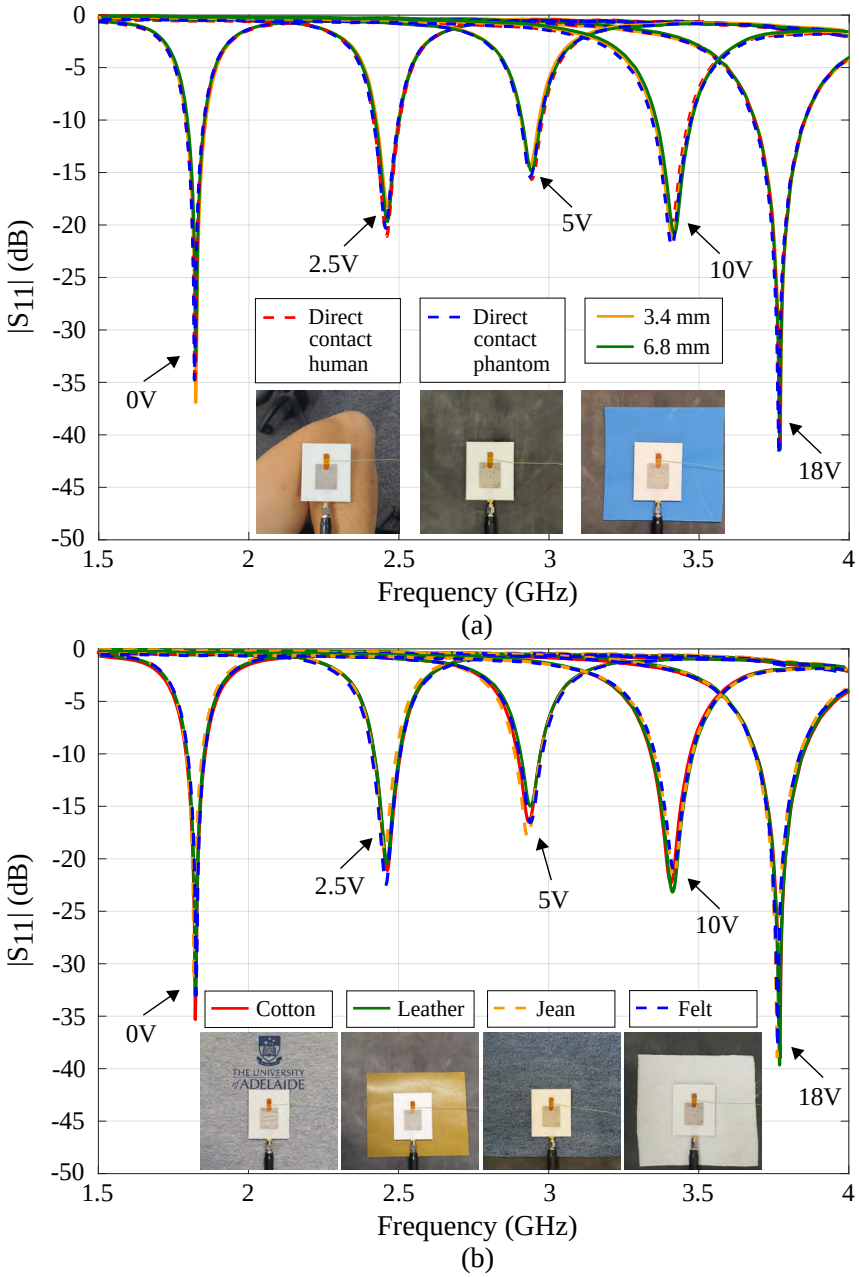

Figure 5.14. Reflection coefficients of the proposed antenna in on-body conditions. Measured refection coefficients of the proposed antenna with (a) different gaps and (b) different clothing materials between antenna and human body.

are varied. A homogeneous human body phantom from SPEAG with a relative permittivity ε_r = 26 and a loss tangent tanδ = 0.3 measured at 5 GHz was used in this test, which is approximately equivalent to an averaged three-layer human body. The distance between the antenna and the human body phantom is adjusted by placing a layer of blue foam (ε_r = 1.02, tanδ = 0.013) with different thicknesses in between.

The reflection coefficient while the antenna is in direct contact with human skin is also measured as the reference. For the second experiment, four popular types of materials used in clothing industry were chosen and measured, which include cotton (ε_r = 1.6, tanδ = 0.04, thickness = 0.5 mm), leather (ε_r = 2.33, tanδ = 0.057, thickness = 2.5 mm), denim jean (ε_r = 1.78, tanδ = 0.085, thickness = 0.8 mm) and felt (ε_r = 1.2, tanδ = 0.025, thickness = 1.8 mm). As illustrated in Fig. 15, the measured refection coefficients remain almost unchanged for all considered experimental circumstances. This result is expected, due to the high isolation provided by the full ground plane of the proposed antenna.

5.2.5 Literature comparison

Table 5.1 displays a comparison of the proposed antenna with other frequency-agile antennas proposed in the literature. All the antennas selected for comparison have similar structure comprising a full ground plane and broadside radiation patterns. The dimensions are given in terms of λ_0, the wavelength in free-space at the center frequency of the tuning range. Additionally, the selected antennas utilize varactors with approximately similar ranges of junction capacitance to provide the continuous frequency tuning capability. It can be seen clearly that the proposed antenna demonstrates a significant improvement in frequency tuning range, especially while comparing to the few available reconfigurable textile antennas. The measured efficiency of the proposed antenna is on the lower side compared to other antennas at the lowest resonance frequency but this can be explained by the large tuning range. The proposed antenna size is comparable to most of the others, noting that the textile implementation with foam substrate does not allow miniaturization using substrate permittivity.

5.2.6 Summary on the wearable antenna with one octave tuning range

A reconfigurable wearable flexible textile antenna with very wide frequency tuning range covering one octave has been proposed. Since the antenna radiating mode continuously changes from a quarter-wave PIFA mode to a half-wave patch mode when decreasing the varactor junction capacitance, a relatively wide frequency reconfigurability is obtained. To validate the concept, the proposed antenna has been designed and optimized with a dedicated flexible coplanar reconfiguration module, based on the

Table 5.1. Comparison between the proposed antenna and antennas reported in the literature. Comparison between the proposed antenna and full ground plane antennas from the literature

Ref.	Material	Size (L × W × h (λ_0))	Tuning range (%)	Efficiency (%)
[160]	Rigid PCB	0.40 × 0.36 × 0.02	26.6	47.0 - 61.0
[95]	Rigid PCB	0.81 × 0.79 × 0.02	41.2	31.0 - 71.0
[96]	Rigid PCB	0.98 × 0.98 × 0.02	41.5	36.0 - 90.0
[147]	Rigid PCB	0.42 × 0.42 × 0.02	50.0	Not given
[29]	Textile	0.50 × 0.50 × 0.05	15.3	40.3 - 46.1
[28]	Textile	0.50 × 0.46 × 0.03	32.8	30.0 - 90.2
This work	**Textile**	**0.56 × 0.47 × 0.03**	**69.7**	**29.8 - 93.7**

equivalent circuit model. The antenna has been fabricated and experimentally characterized. The prototype exhibits a very wide frequency tuning range of 69.7% extending from 1.82 to 3.77 GHz, which confirms the effectiveness of the reconfiguration concept. In the next section, the versatility of the concept will be illustrated by an extension of the design principle from a single-band antenna to a dual-band frequency-reconfigurable realization.

5.3 Dual-band frequency-reconfigurable wearable textile antenna

In order to cope with the increasing complexity of on-body wireless communications systems while retaining the antenna compactness, multi-functional antennas have been investigated to enhance the system ability to cope with multiple standards. To this end, various implementations of wearable textile antennas have been designed to be multi-band [61], ultra-wide band [10] or electrically reconfigurable [44]. Antennas combining multi-band and frequency reconfigurable features were reported previously in the literature [167]. However, the number of flexible wearable textile antennas with this functionality has been very limited to date [28].

As an extended version of the frequency-reconfigurable antenna proposed in Section 5.2, a dual-band wearable textile antenna with frequency agility is presented. The antenna

is designed to simultaneously operate in the 2.45 and 5.8 GHz ISM radio bands. In term of frequency agility, the proposed antenna exhibits wide frequency tuning ranges of 48.6% at its lower band and 18.3% at its higher band. This design extension has been presented as a conference contribution in [45].

5.3.1 Antenna design

The proposed antenna configuration is shown in Fig. 5.15 with all the antenna dimensions listed in the caption. The antenna design is based on a planar inverted-F antenna (PIFA) structure with a frequency tunability achieved by using a varactor (of type MA120H46) integrated on a reconfiguration module similar as reported in the first part of this chapter. A flexible, lightweight, and low-loss PF-4 foam (from Cumming Microwave) with a relative permittivity ε_r = 1.06 and a loss tangent of tanδ = 0.0001 is selected to build a two-layer antenna substrate. A highly flexible and conductive silver-coated nylon Rip-stop fabric is chosen to design all antenna conductive parts including a radiation patch, a small shorted secondary patch and its shorting wall, a microstrip line feed and a ground plane. The proposed antenna is designed and optimized using CST Microwave Studio 2021.

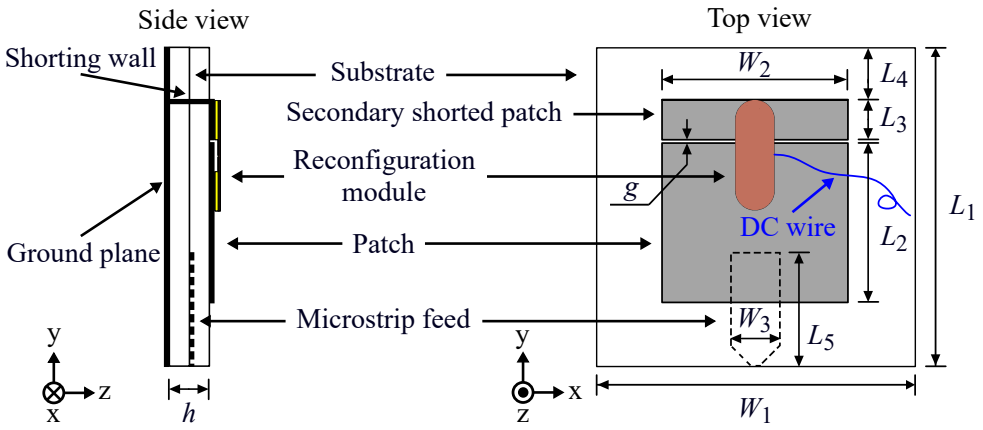

Figure 5.15. Configuration of the dual-band reconfigurable wearable antenna. Configuration of the proposed antenna. Dimensions (mm): $L_1 = 40.0$, $L_2 = 24.0$, $L_3 = 6.0$, $L_4 = 8.7$, $L_5 = 17.0$, $W_1 = 40.0$, $W_2 = 28.0$, $W_3 = 7.5$, $h = 3.2$, $g = 0.5$.

In order to vary the antenna resonance frequencies, the varactor is used to alter the capacitance between the main radiation patch and the shorted secondary patch. The antenna operation can be understood by observing the antenna instantaneous electric field distribution at different values of varactor capacitances as illustrated in Fig. 5.16.

To achieve dual-band operation, the antenna is designed to exploit two radiation modes simultaneously. It can be observed from Fig. 5.16 (a) and (b) that the antenna resonates in a quarter-wave (PIFA) mode ($TM^z_{0(0.5)0}$) at the bottom of its lower band (2.27 and 2.45 GHz).

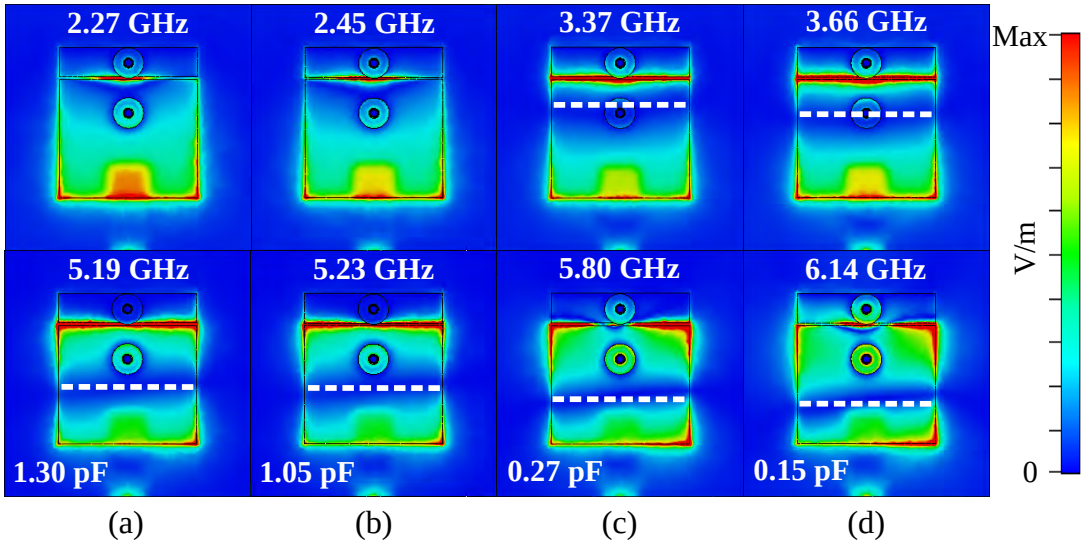

Figure 5.16. Electric field distributions of the dual-band reconfigurable antenna. Instantaneous electric field distributions of the proposed antenna at four different varactor capacitances.

As the varactor capacitance between the main radiating patch and the shorted secondary patch decreases, the mode progressively transitions to a half-wave standard patch mode (TM^z_{010}) at higher frequencies (top row of Fig. 5.16 (c) and (d)). In the higher band (lower row of Fig. 5.16), the antenna only resonates in a half-wave patch mode with the field null progressively moving towards one patch edge with decreasing capacitance, as highlighted by a white dotted line in the figure. It is worth emphasizing that, at lower values of varactor capacitance, the antenna simultaneously radiates in a half-wave standard patch mode (TM^z_{010}) at both bands but with different effective patch lengths. The asymmetrical instantaneous electric field distribution can be observed at the higher band. This is because the components on the reconfiguration module are not assembled in a completed symmetrical agreement. It is also noticeable that, from 5.8 GHz, the radiation mode at the higher band is starting to change from the half-wave standard patch mode to a higher-order mode.

5.3.2 Experimental results

To validate the antenna operation concept, a prototype is fabricated (inset of Fig. 5.18) and experimentally validated. A good agreement between the simulated and measured $|S_{11}|$ parameters for different values of bias voltage is observed from Fig. 5.17 exploiting the full range of accessible varactor capacitance (1.3−0.15 pF). It is noticeable that the measured fractional bandwidths at both bands are slightly higher than the simulated results which are 46.8% and 16.8%. These differences can be explained by the fabrication tolerance. The measured frequency tuning range at lower band reaches a fractional bandwidth of 48.6% (2.29−3.76 GHz). At the higher band, a measured frequency tuning range of 18.3% is achieved (5.17−6.21 GHz).

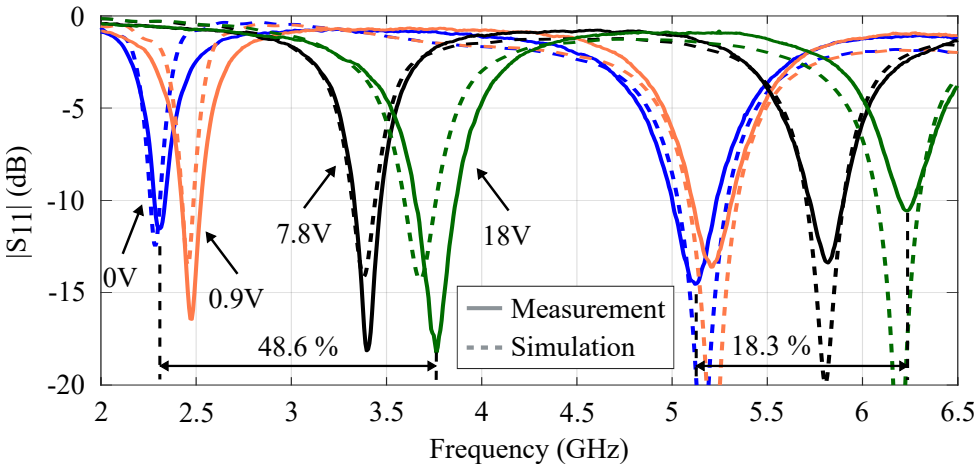

Figure 5.17. Simulated and measured reflection coefficients of the proposed antenna. Simulated and measured reflection coefficients of the proposed antenna at different values of the bias voltage.

The simulated and measured normalized radiation patterns of the proposed antenna at selected frequencies in both bands of operation are displayed in Fig. 5.18. The measured realized gain at 2.29, 2.45, 3.39 and 3.76 GHz are 1.2, 3.1, 5.7 and 6.9 dBi, respectively. In the higher band, the measured realized gain are 8.4, 8.1, 9.0 and 8.0 dBi corresponding to the resonance frequency of 5.17, 5.23, 5.8 and 6.21 GHz. The simulated and measured gain in dBi for the lower band at 2.29, 2.45, 3.39 and 3.76 GHz are (1.8, 1.2), (2.9, 3.1), (6.2, 5.7) and (6.7, 6.6), respectively. For the higher band, the simulated and measured gain at 5.17, 5.23, 5.8 and 6.21 GHz are (8.9, 8.4), (9.0, 8.1), (8.9, 9.0) and (7.2, 7.0). Based on the radiation patterns and the gain of the proposed antenna at the lower band, the transition between the quarter-wave mode to a half-wave patch mode can be confirmed, while the maximum gain remains toward broadside over the

whole band with gain increasing as a function of the frequency. In the higher band, the maximum radiation is also toward broadside with a noticeably higher gain, consistent with a standard half-wave patch radiation pattern on a low permittivity substrate. It can be observed that at 6.21 GHz, the antenna gain is starting to decrease, which is due to a transition from the half-wave patch mode to a higher-order mode.

5.3.3 Summary on the dual-band reconfigurable design

A dual-band frequency-reconfigurable flexible wearable textile antenna with a wide tuning range at both bands has been presented. The antenna exploits two radiation modes simultaneously, namely a quarter-wave mode and a half-wave patch mode. These modes are resonant on a main radiating patch and a secondary shorted parasitic patch, with their effective electrical lengths tuned by a varactor diode between the patches. To demonstrate the concept, the proposed antenna has been optimized, fabricated and experimentally characterized. The antenna exhibits broadside radiation patterns at all resonance frequencies with a relatively wide tuning range of 48.6% and 18.3% around the 2.45 and 5.8 GHz ISM bands, respectively.

5.4 Thermography investigation of reconfigurable wearable antennas

To ensure that the reconfigurable flexible antennas can work well in real on-body operating environments, several environment factors needed to be considered. Investigating a number of detuning effects on passive wearable textile antenna performance, the study [168] suggested that a variation of 5% in the resonance frequency can occur due to bending, human body interaction or moisture uptake. Later, the operation of wearable antennas was disturbed by the presence of some objects in proximity such as human tissues or metal sheets [169]. A tuning range of 8% was recommended for frequency-reconfigurable wearable antenna to keep the $|S_{11}|$ parameters at acceptable ranges.

The temperature of passive flexible textile antennas under working conditions has been investigated through thermographic infrared measurements in the Section 3.2.4 - Chapter 3. Due to the losses in the conductive materials, the temperature of some parts of the antenna can reach more than 50°C at an input power of 1 W even with an

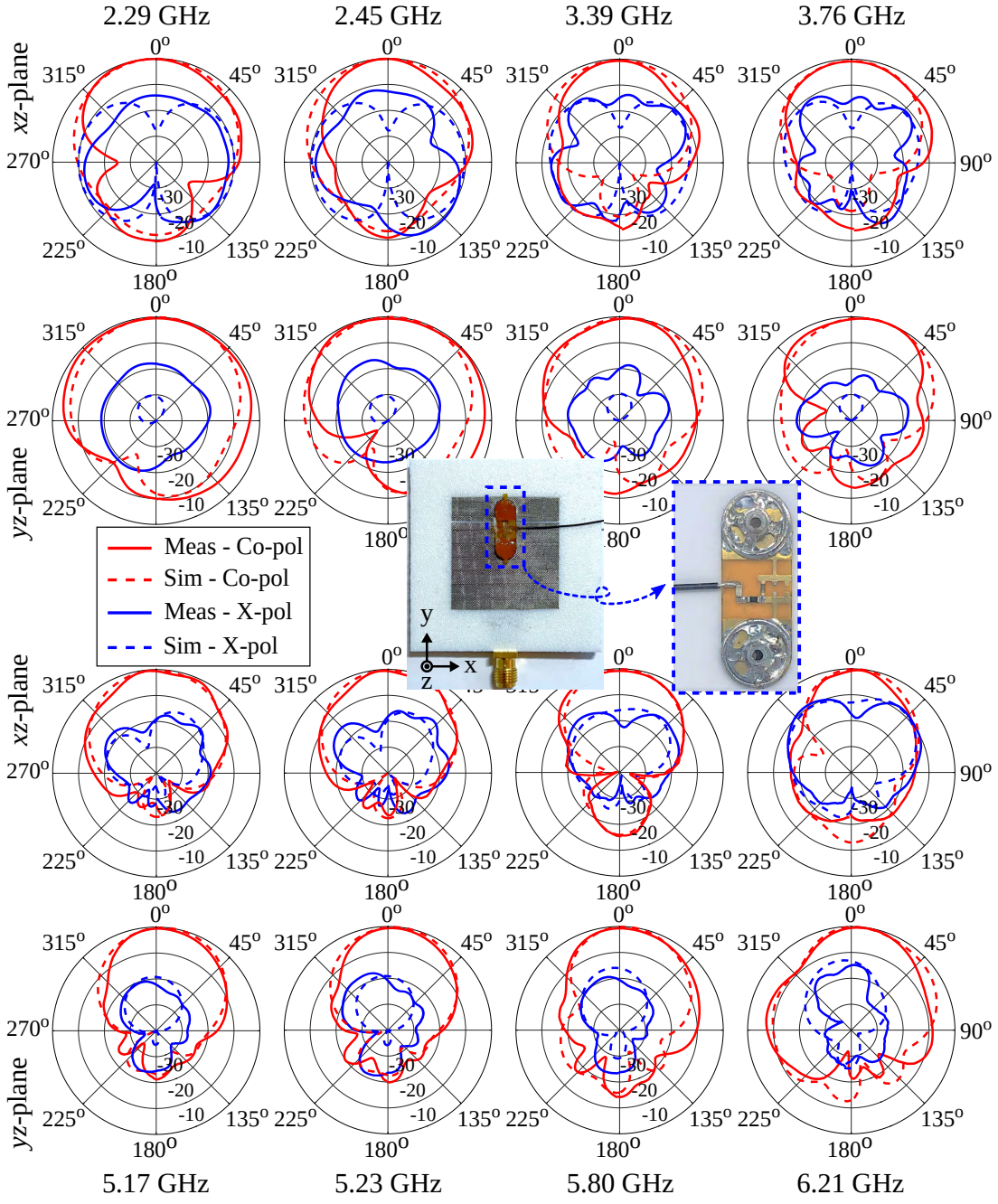

Figure 5.18. Normalized radiation patterns of the proposed antenna. Simulated and measured normalized radiation patterns of the proposed antenna in the *xz*- and *yz*-planes at 2.29, 2.45, 3.39, 3.76, 5.17, 5.23, 5.80 and 6.21 GHz. Inset: the fabricated antenna and zoomed-in front side of the reconfiguration module.

antenna featuring estimated radiation efficiency of 65.8%. This high temperature can possibly cause local skin damage to wearers in about 15 minutes [170]. This risk motivates the present thermography investigation of frequency-reconfigurable wearable

antennas, where changes of resonance frequencies to cope with dynamic changes of the wearable environment affect the radiation efficiency of the antennas.

In this context, thermography investigation of the frequency-reconfigurable antenna presented in Section 5.2 will be discussed in this part. Initially, the increased antenna temperature when operating at various resonance frequencies is investigated through thermal infrared imaging. This measurement identifies the hottest spots on the antenna and also confirms the inverse relation between the radiation efficiency and the antenna highest temperature. This relationship is also confirmed to remain unchanged while the antenna input power is varied from 21 to 521 mW. Finally, the consistency and stability of the tuned frequencies are demonstrated when the input power is set up to 521 mW. The presented preliminary results demonstrate the use of infrared thermography as a valuable tool for characterization of thermal safety margins of wearable devices and for imaging of losses in reconfigurable antenna technology. The results presented in this section has been presented as a conference contribution in [46].

5.4.1 Experimental setup

The frequency-reconfigurable conductive textile antenna with one octave tuning range (approximately 70% fractional bandwidth) presented in Section 5.2 has been selected for this experimental investigation. The relatively wide measured frequency tuning range from 1.83 to 3.77 GHz is possible with a corresponding estimated radiation efficiency ranging from 30 to 93%. The antenna temperature is measured at four different resonance frequencies across the tuning range with approximately 600 MHz spacing, namely at 1.83, 2.47, 3.12 and 3.77 GHz, which correspond to bias voltages of 0, 2.5, 7 and 18 V, respectively.

The thermal measurement setup is shown in Fig. 5.19. A FLIR E53 Advanced Thermal Imaging Camera is employed, allowing a relatively wide temperature reading range extending from –20 to 120°C. An EXG analog signal generator N5173B by Keysight with a frequency range from 9 kHz to 20 GHz is used to generate a continuous waveform (CW) sinusoidal reference signal. An RF amplifier ZHL-42 with a frequency range from 0.7 to 4.2 GHz, minimum gain of 30 dB and a maximum output power of 28 dBm is used to amplify the signal before feeding the antenna. The measurement was taken in an anechoic chamber with the room light turned off and all the antenna connectors

covered by black absorbers. This setup aims to minimize the thermal noise impact caused by reflecting objects.

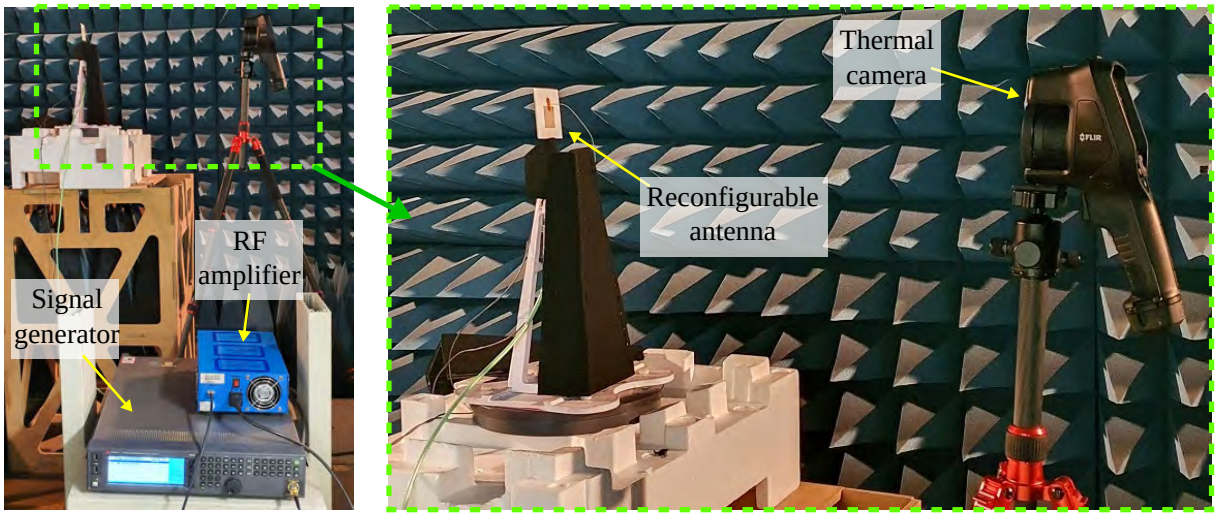

Figure 5.19. Thermal measurement setup for reconfigurable wearable antennas. Thermal measurement setup in the anechoic chamber.

5.4.2 Experimental results

Antenna temperature at different resonance frequencies

The antenna temperature at the four featured resonance frequencies for a fixed input power of 521 mW is shown in Fig. 5.20. The small red triangular in each sub-figure indicates the hottest spot in the antenna which corresponds to the varactor location. The hottest temperature at the resonance frequencies of 1.82, 2.47, 3.12 and 3.77 GHz are 62.1°C, 45.5°C, 36.2°C and 32.6°C, respectively.

It can be observed that higher temperatures are occurring at the lower resonance frequencies. This can be explained by the approximately linearly proportional relationship between the temperature and the power dissipated in a dedicated circuit [171], which is calculated as a multiplication of the square of the current flowing through the varactor and the varactor internal resistance. Since the internal resistance of the MA120H46 varactor is not strongly dependent on bias voltage [95], the temperature is increased mainly due to the raising of the current flowing through the varactor which corresponds to the decreasing of bias voltage. More explicitly, the lowest resonance

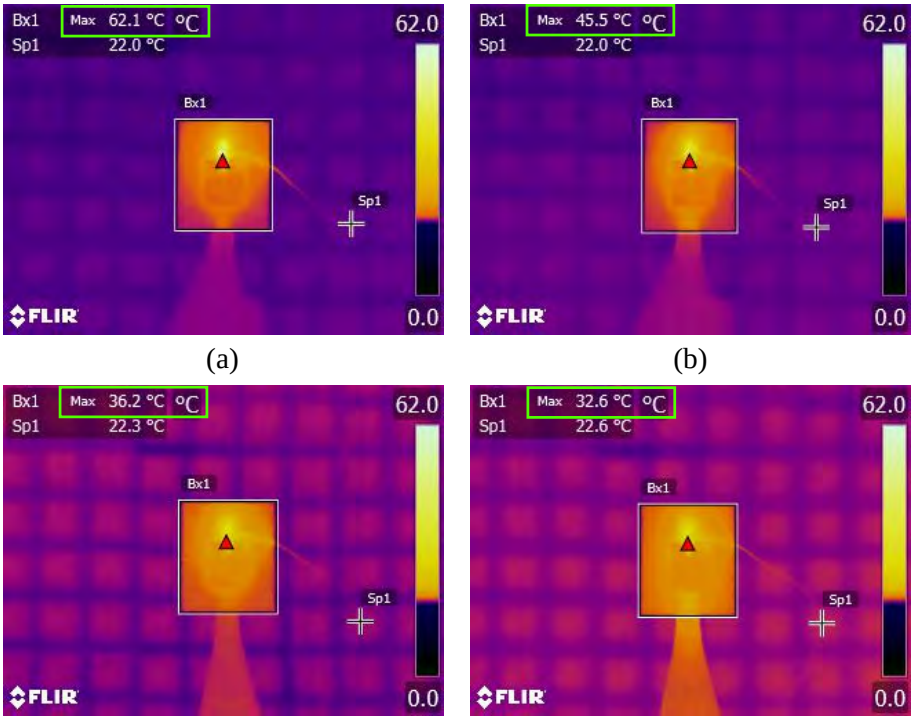

Figure 5.20. The thermal images recorded for the four different resonance frequencies. The thermal images recorded for the four different resonance frequencies when the input power is fixed at 521 mW. (a) 1.83 GHz (max temp. 62.1°C), (b) 2.47 GHz (max temp. 45.5°C), (c) 3.12 GHz (max temp. 36.2°C) and (d) 3.77 GHz (max temp. 32.6°C). Small red triangular indicates the hottest point which is the varactor location with the maximum temperature featured on the top left of each figure. The background temperature was measured at the cross-markers Sp1, and it increased by 0.6°C during the whole experiment.

frequency corresponds to the highest value of varactor capacitance, which leads to the highest current flow through the varactor, where dissipation eventually causes the highest temperature. In contrast, at the high resonance frequency achieved at low value of the varactor junction capacitance, there is only a small amount of current flowing through the varactor which leads to the lower temperature. It is worth to mention that, the environment temperature slightly increased during the experiment by 0.6°C, as indicated by the background temperature measured at the cross-markers (Sp1) in Fig. 5.20.

The measured relationship between the radiation efficiency and the antenna top temperature is shown in Fig. 5.21. It can be seen that the antenna radiation efficiency is

broadly inversely proportional to the antenna temperature. The localized high temperature measured on the tuning module (as illustrated in Fig. 5.20) confirms that the low radiation efficiency at low frequencies is mostly caused by the high current flowing through the varactor. It is also worth mentioning that, at the lower antenna radiation efficiency (from 33% to 44%) the antenna temperature is significantly increased by approximately 20°C. In contrast, at the higher efficiency (more than 80%) achieved above 3 GHz, the temperature is rather stable with the variation remaining below 5°C.

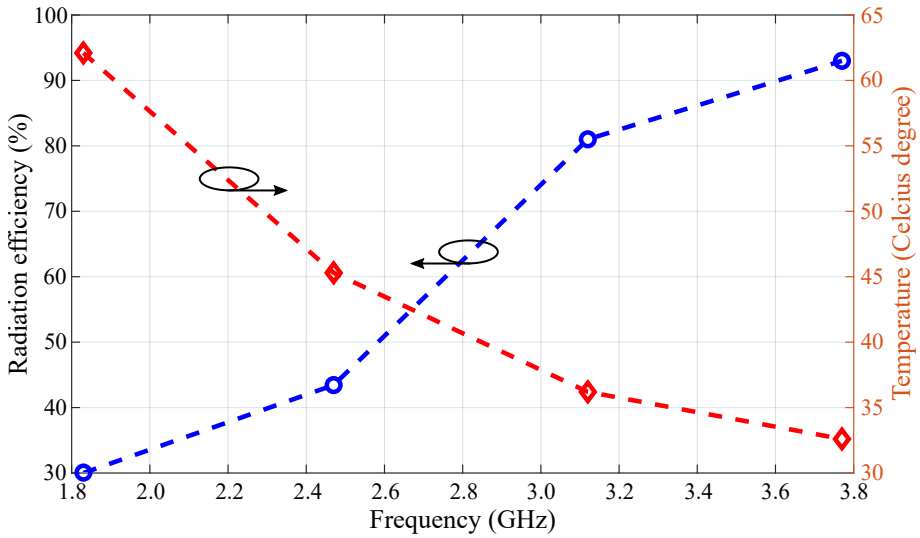

Figure 5.21. Antenna temperature versus radiation efficiency. Antenna temperature versus radiation efficiency across the frequency tuning range.

Antenna temperature at different input powers

In this experiment, the reference signal power (antenna input power) is varied from 21 to 521 mW to investigate the relation between the antenna temperature and input power at the four featured resonance frequencies. It can be observed in Fig. 5.22 that, the highest temperature is obtained at the lowest resonance frequency across the whole range of antenna input power. Since the current flow through the varactor at higher frequency is low, the temperature at higher frequency is only increased by a small amount (9.5°C). In contrast, at the lowest frequency, the module temperature is significantly increased by 37.7°C when the input power is increased by 500 mW. Therefore, it is suggested that at the lowest resonance frequency with the radiation efficiency of approximately 30%, the antenna input power should be limited to 350 mW which corresponds to the reconfiguration module temperature of 50°C to avoid possible skin damage to wearers.

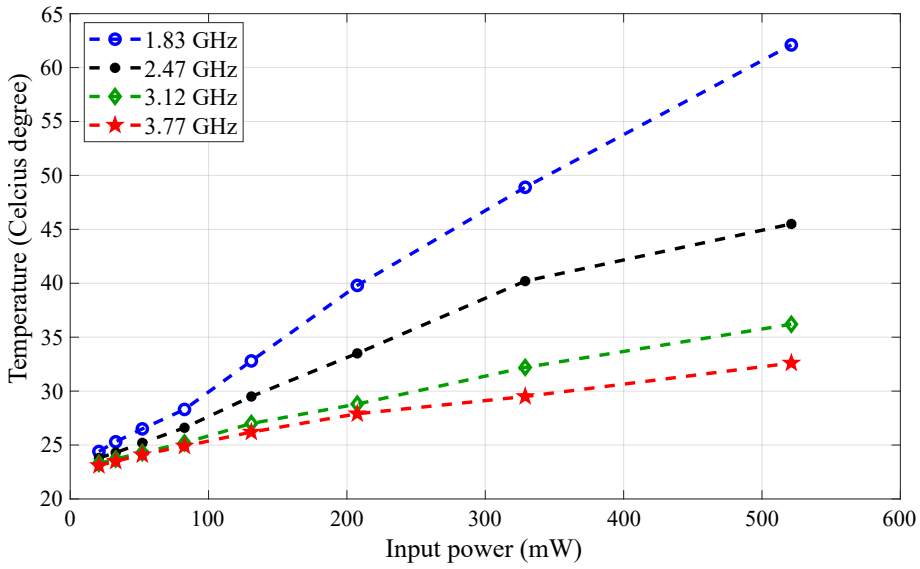

Figure 5.22. Antenna temperature at four different resonance frequencies. The antenna temperature at four different resonance frequencies while the antenna input power is varied from 21 to 521 mW.

Antenna tuning frequency at different input powers

It is known that, when the feeding frequency of the antenna matches the center tuning frequency (controlled by setting the bias voltage), the current flow through the varactor should reach its maximum value. Therefore, by fixing the bias voltage then varying the frequency of the reference signal from the signal generator, it is possible to observe the exact tuning frequency (the best-matched frequency) of the reconfigurable antenna based on the variation of temperature. This experiment was taken at two resonance frequencies corresponding to two extreme bias voltage which are 1.83 GHz (bias voltage of 0 V) and 3.77 GHz (bias voltage of 18 V). The results shown in Fig. 5.23 indicate that the module temperature consistently reaches its highest value at the tuned frequency. It can be also observed that the highest temperature remains at a fixed frequency when the antenna input power is varied from 21 to 521 mW. This suggests that the frequency-reconfigurable antenna is operating at a stable tuning frequency despite input power variations, for a power level reaching up to 521 mW.

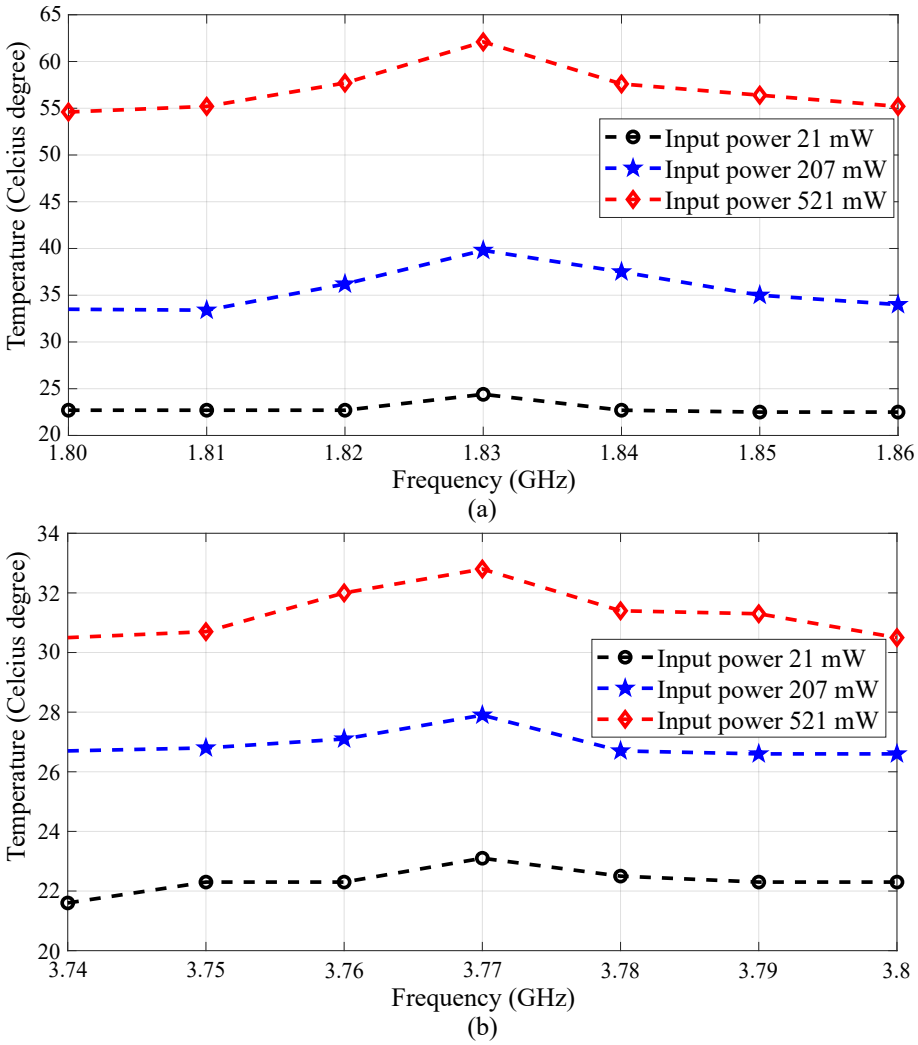

Figure 5.23. Antenna temperature versus frequencies at different input powers. Antenna temperature versus frequencies at different input powers. (a) The lowest and (b) the highest resonance frequency bands.

5.4.3 Summary on thermographic imaging

In this third part of this chapter, the thermographic imaging of a wearable frequency-reconfigurable antenna in dependence of operation frequency and power level has been presented. It is observed that the hottest spot on the reconfigurable antenna is located at the varactor position. The highest temperatures are occurring at the lower resonance frequencies due to the higher current flowing through the varactor. An inverse proportion between the antenna radiation efficiency and the antenna temperature has been demonstrated. It is also suggested that, the threshold of input power for the antenna state with a radiation efficiency of 30% is approximately 350 mW to avoid

potential skin damage to wearers. Finally, the experimental results indicate that for the varactor MA120H46, the antenna resonance frequencies remain unchanged under a CW sinusoidal input power increased upto 521 mW.

5.5 Conclusion

In this chapter, two frequency-reconfigurable flexible textile antennas for wearable applications have been presented. Utilizing the flexible co-planar reconfiguration module with the optimized PIFA structure, the first proposed antenna provides an one octave frequency tuning range of approximately 70%. The antenna was designed following some practical considerations which enhance its practicability in real conformal applications. To illustrate the versatility of the concept, the proposed antenna structure was then re-optimized to become the second antenna with dual-band frequency reconfigurable characteristics. This dual-band antenna can simultaneously cover the 2.45 and 5.8 GHz ISM radio bands with a wide tuning range at both bands of 48.6% and 18.3%, respectively. In the last part of the chapter, a thermal behavior of the first antenna was investigated. Through the presented results, the relationship between antenna temperature and efficiency is experimentally confirmed. It was also suggested that the thermal imaging camera can be a useful tool to characterize thermal safety margins of wearable antennas.

Chapter 6

Dual-Band Reconfigurable Flexible Antenna with Independent Frequency Tunability

THIS chapter presents a dual-band frequency-reconfigurable flexible antenna with independent tunability for wearable applications. The proposed antenna is based on textile and foam, and operates simultaneously in a $TM^{z}_{0(0.5)0}$ mode and a higher-order mode with individual frequency tunability centered at the 2.45 and 5.8 GHz Industrial, Scientific and Medical bands. The relative frequency tuning range at the lower band is 41.1% while that at the higher band is 29.9%. To demonstrate the independent tuning concept, the coplanar reconfiguration module proposed in the previous chapters is utilized. The fabricated antenna prototype operates as expected and can maintain robust performance in various bending configurations through its individual dual-band frequency reconfigurability, which suggests its practicality for wearable applications.

6.1 Introduction

Antennas with multi-band operation and frequency agility can empower communications systems with the ability to work with different standards and in complex electromagnetic environments. There exist several antennas with frequency reconfigurability in multiple bands reported in the literature [17, 157, 167, 172–176]. In particular, some of these antennas exhibit independent frequency tunability which can offer a higher degree of freedom in their adaptability for multiple functionalities. For instance, a monopolar antenna working independently in two reconfigurable frequency bands was proposed in [17]. Additionally, antennas with triple-band independent frequency tuning were reported in the literature providing either omnidirectional [176] or broadside radiation patterns [167, 174]. However, all of those radiators were constructed from rigid materials, which are not suitable for conformal applications demanding flexible antennas.

In this chapter, a flexible, dual-band, reconfigurable antenna with independent frequency tunability is proposed. The antenna is realized based on textile and foam, and it operates simultaneously in a quarter-wave (shorted) resonant mode and a higher-order mode with independent frequency tunability centered at the 2.45 and 5.8 GHz ISM bands. The frequency tuning range at the lower band and the higher band are 41.1% and 29.9%, respectively. The good agreement between simulation and measurement of a manufactured prototype suggests that the antenna performs as designed and can independently correct the detuning due to antenna bending for the two operation bands. The results presented in this chapter was published to the *IEEE Antennas and Wireless Propagation Letters* under the tile of "Dual-Band Reconfigurable Flexible Antenna with Independent Frequency Tunability" [47].

6.2 Antenna design

6.2.1 Antenna geometry

The proposed antenna structure is shown in Fig. 6.1 with the antenna dimensions given in the caption. The antenna is based on the quarter-wave resonance of a Planar Inverted-F Antenna (PIFA) structure which consists of a full ground plane, two foam substrate layers, a microstrip feed, a resonant patch, and four folded shorting stubs. To achieve good mechanical flexibility of the antenna structure, highly flexible

dielectric and conductive materials are selected to construct the antenna. Specifically, a light-weight and low-loss (loss tangent tanδ = 0.0001) PF-4 foam with a thickness of 1.6 mm and a relative permittivity ε_r = 1.06 is used for the two stacked substrates. A highly conductive fabric from Shieldex® Nora-RS with a sheet resistance of approximately 0.01 Ω/square is chosen as the electrical conductor for the ground plane, the resonant patch, the folded shorting stubs and the microstrip feed line.

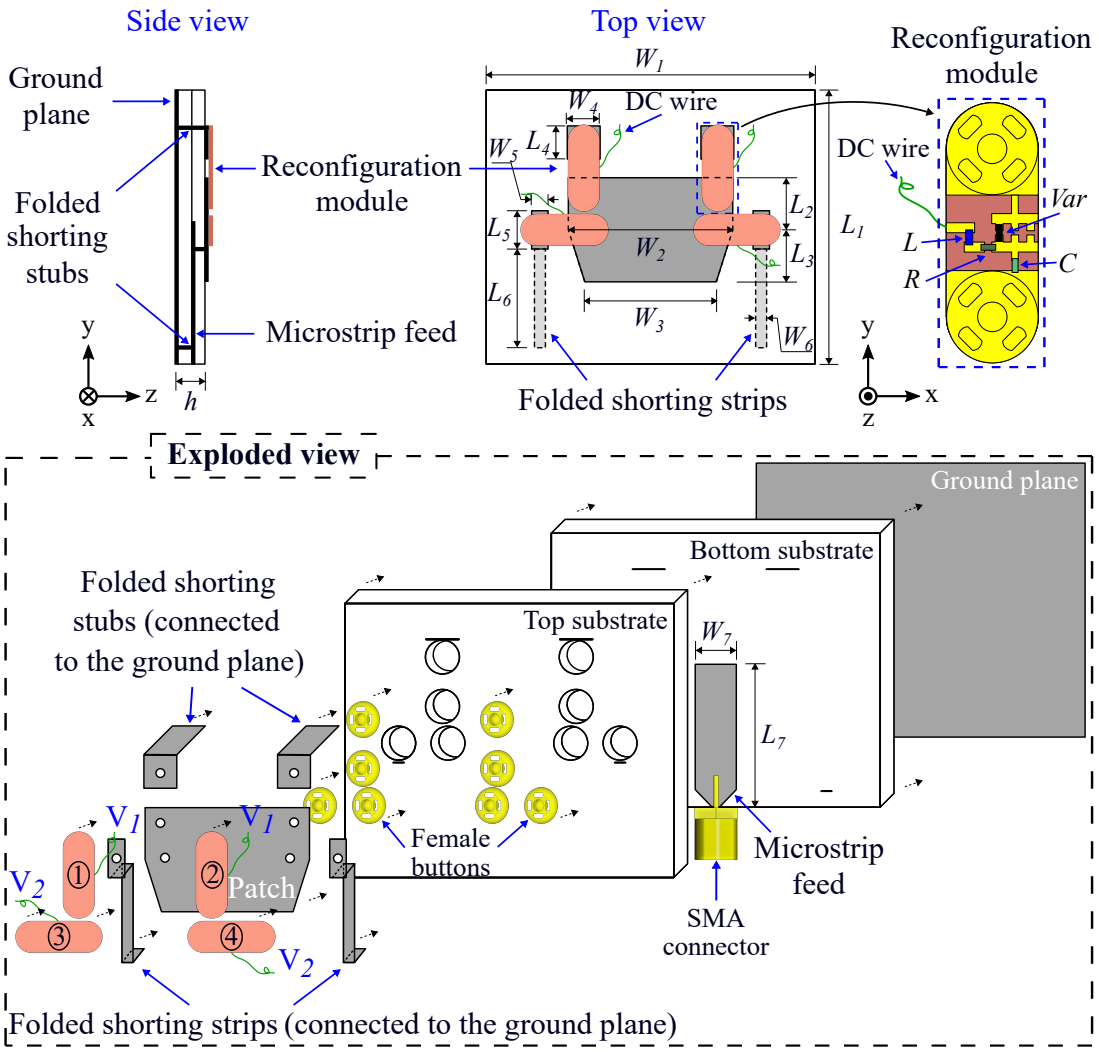

Figure 6.1. Configuration of the proposed antenna. Configuration of the proposed antenna. Dimensions (mm): L_1 = 50.0, L_2 = 9.5, L_3 = 9.5, L_4 = 6.0, L_5 = 7.0, L_6 = 18.0, L_7 = 26.0, W_1 = 60.0, W_2 = 30.0, W_3 = 24.0, W_4 = 6.0, W_5 = 3.0, W_6 = 2.0, W_7 = 7.5 and h = 3.2. Inset: Zoomed-in front side of the reconfiguration module.

Four flexible coplanar reconfiguration modules proposed in Section 5.2 are used in the antenna to obtain reconfigurability. These modules provide a varactor-loaded contact between two metallic snap-on connections at their extremities. They also include the

biasing circuit to control the varactors as shown in an inset in Fig. 6.1. In the present case, the modules are ground-shorted by using shorting stubs connected to metallic female snap-on buttons as shown in an exploded view in Fig. 6.1. The utilization of these detachable reconfiguration modules also makes the antenna straightforward to fabricate and maintain. Two reconfiguration modules are used to connect the radiation patch with folded shorting stubs (module ① and ② as shown in Fig. 6.1) to tune the resonance frequency of the quarter-wave mode in the lower band. The other two modules are placed at the left-hand and right-hand sides of the radiation patch (module ③ and ④ as shown in Fig. 6.1) and connected to folded shorting strips to control the resonance frequency at the higher band. The hexagon shape of the radiation patch is chosen to gain more design flexibility, as presented in Section 3.2. The design is optimized to achieve wide frequency-tuning range at both bands using CST Microwave Studio 2021.

6.2.2 Antenna operation

The lower band centered at 2.45 GHz is based on the fundamental quarter-wave mode ($TM^{z}_{0(0.5)0}$) of the half-patch which is connected to the two folded shorting stubs. By changing the capacitance of the varactors inside the reconfiguration modules ① and ②, the resonance frequency can be tuned. When decreasing the varactor junction capacitance, a transition from quarter-wave mode to half-wave patch mode is observed through the movement of a null in the field distribution in the antenna cavity from the location of the shorting stubs towards the center of the patch, as highlighted by a white dashed line in Fig. 6.2 (a). As a consequence, the operation frequency increases. A wide frequency tuning range of approximately 40% is obtained for this lower frequency mode. It is worth mentioning that, the varactor junction capacitance of the modules ① and ② could be tuned down to 0.15 pF bringing the lower band resonance frequency up to 4.0 GHz. However, the lower bound of capacitance is limited to 0.25 pF to keep a sufficiency gap between the higher end of the lower band (3.53 GHz) and the lower end of the higher band (4.52 GHz) aiming to maintain the independence between both bands.

To open a second band centered at 5.8 GHz, the antenna width is enlarged to excite a higher-order mode with capacitively loaded shorts on both sides, as presented in Section 3.2. It is noted that, the long shorted strips on both sides of the patch also contribute to establishment of the higher-order mode. The varactor junction capacitance of

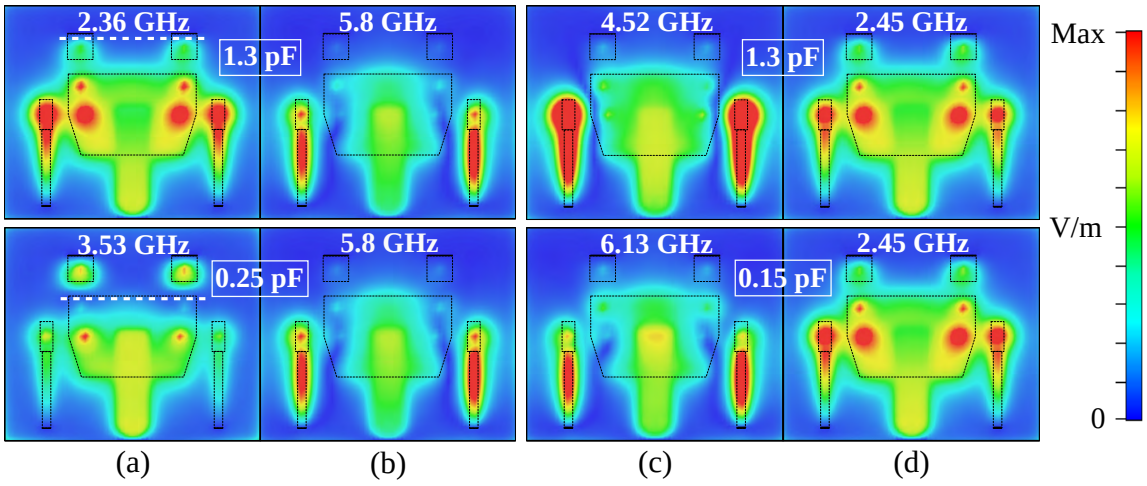

Figure 6.2. Electric field distributions of the proposed antenna. Instantaneous electric field distributions in the cavity of the proposed antenna in (a) lower band tuned to 2.36, 3.53 GHz, (b) higher band fixed at 5.8 GHz while tuning the lower band, (c) higher band tuned to 4.52, 6.13 GHz and (d) lower band fixed at 2.45 GHz while tuning the higher band.

the modules ③ and ④ can be then varied in order to change the effective patch width to tune the resonance frequency at this higher-order mode. The instantaneous electric field distributions for the case of the high band resonance frequencies tuned to 4.52 and 6.13 GHz are shown in Fig. 6.2 (c). It can be observed that, when the varactor junction capacitance of the modules ③ and ④ are decreased from 1.3 to 0.15 pF, the electric field strength at the modules ③ and ④ positions become significantly weaker. This is because of a smaller amount of current flowing through the varactor for a lower value of the varactor junction capacitance, as presented in Section 5.2.3. This means that the RF connection between the patch and the long strips is progressively being lost with decreasing varactor capacitance. This reduces the effective width of the radiating patch, which leads to the increase in resonance frequency.

One can observe that the resonance frequency at the higher band depends mostly on the patch width and the long strips' dimensions, while the resonance frequency at lower band is mainly affected by the patch length. By optimizing the long strips' length, a near complete independence of the lower band from the higher band is achieved, as illustrated in Fig. 6.2 (d) where the resonance frequency in the lower band remains unchanged. Since the modules ① and ② are located at the electric field nulls of the higher-order mode at all resonance frequencies from 4.52 to 6.13 GHz (Fig. 6.2 (c)), the tuning in the lower band has nearly no impact on the higher-band frequency (Fig. 6.2 (b)).

6.3 Experimental results

6.3.1 Antenna fabrication

The proposed antenna has been fabricated and measured to validate the proposed concept. A PF-4 foam sheet is firstly cut into two substrates, and then four slits are manually trimmed to accommodate the folded shorting stubs and the eight holes for female buttons on the top substrate. A laser milling machine (LPKF: Protolaser S) is used to accurately cut all the antenna conductive textile parts. The folded shorting strips and the ground plane are fabricated using one piece of metalized fabric to guarantee a perfect connection between these parts (Fig. 6.3 (a)).

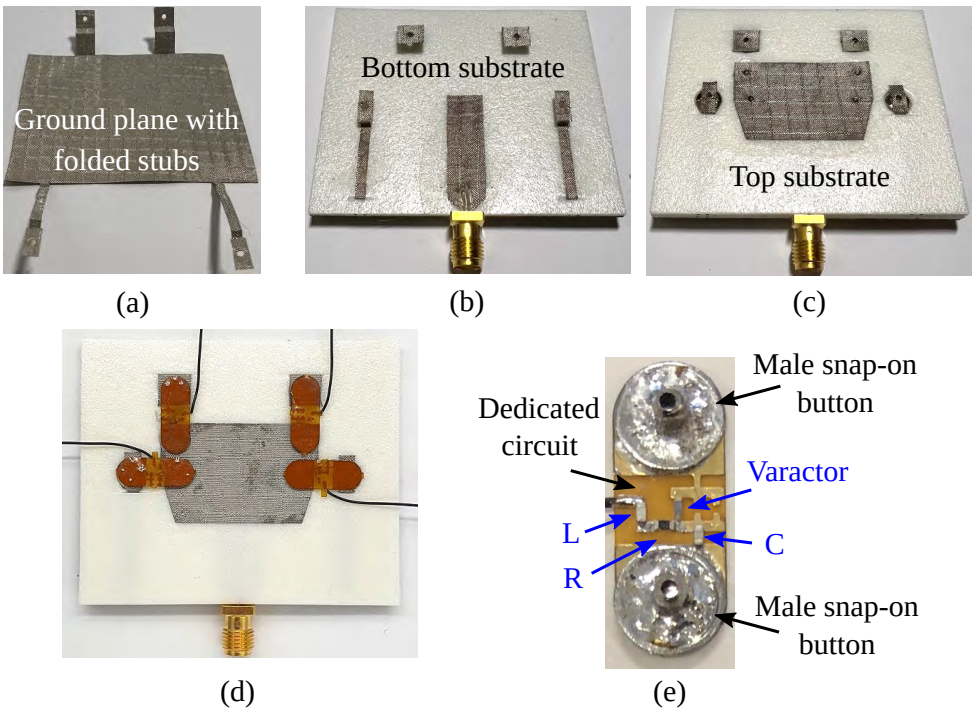

Figure 6.3. Fabricated antenna assembly. Fabricated antenna assembly. (a) Ground plane with folded stubs realized on single piece of silver fabric, (b) bottom substrate, (c) top substrate with antenna patch and top folded stubs, (d) front view of the fabricated antenna and (e) the reconfiguration module.

The folded shorting stubs are passed through the slits on the antenna substrates, and a washable fabric glue (Tiger Grip from Helmar) is subsequently used to affix the conductive parts onto the substrates (Fig. 6.3 (b) and (c)). Conductive epoxy CW2400 (from CircuitWorks) has been used to connect an SMA connector to the microstrip feed and

the ground plane. The full fabricated prototype with its four reconfiguration modules is shown in Fig. 6.3 (d).

A reconfiguration module realized in flexible PCB is shown in Fig. 6.3 (e). The active component used in the design is a varactor MA46H120 from MACOM Technical Solutions. It has an adjustable capacitance ranging from 1.30 to 0.15 pF for a reversed bias voltage varying from 0 to 18 V. The bias circuit consists of a resistor $R = 1$ MΩ in series with an inductor $L = 400$ nH. A DC-blocking capacitor $C = 22$ pF is added to block the DC bias current flowing to the resonant patch. The reconfiguration modules are DC- and RF-grounded through the folded shorting stubs. The bias voltage V_1 controls the varactor capacitances in the modules ① and ②, while the ones in the modules ③ and ④ are adjusted by the bias voltage V_2 (as shown in Fig. 6.1).

6.3.2 Reflection coefficient

A good agreement between the simulated and measured $|S_{11}|$ parameters of the proposed antenna at different values of the bias voltage V_1 and V_2 is illustrated in Fig. 6.4. It can be observed that the frequency tuning of both bands is largely independent from another, that is, only insignificant variations in the operation frequency are observed when tuning the other band. The measured tuning range (defined for $|S_{11}| < -10$ dB) at the lower band varies from 2.34 to 3.55 GHz, which yields approximately a 41.1% fractional tuning range for a bias voltage V_1 varying from 0 to 7.7 V. When the bias voltage V_2 is adjusted from 0 to 18 V, the measured -10 dB tuning range at the higher band varies from 4.55 to 6.15 GHz, corresponding approximately to a fractional tuning range of 29.9%.

6.3.3 Radiation patterns, gain and efficiency

The simulated and measured normalized radiation patterns in the lower band at 2.34, 2.45 and 3.55 GHz and in the higher band at 4.55, 5.8 and 6.15 GHz are displayed in Fig. 6.5. A good agreement between simulation and measurement is obtained, with slight discrepancies mainly due to the mechanical flexibility of the antenna, which can typically cause an imperfect alignment in the measurement. It can be observed that at the lower band the antenna radiates in a quarter-wave mode with a maximum gain toward broadside. One-sided bidirectional radiation patterns are also noticed for all resonance frequencies tuned in the higher band. It can be inferred from the figure

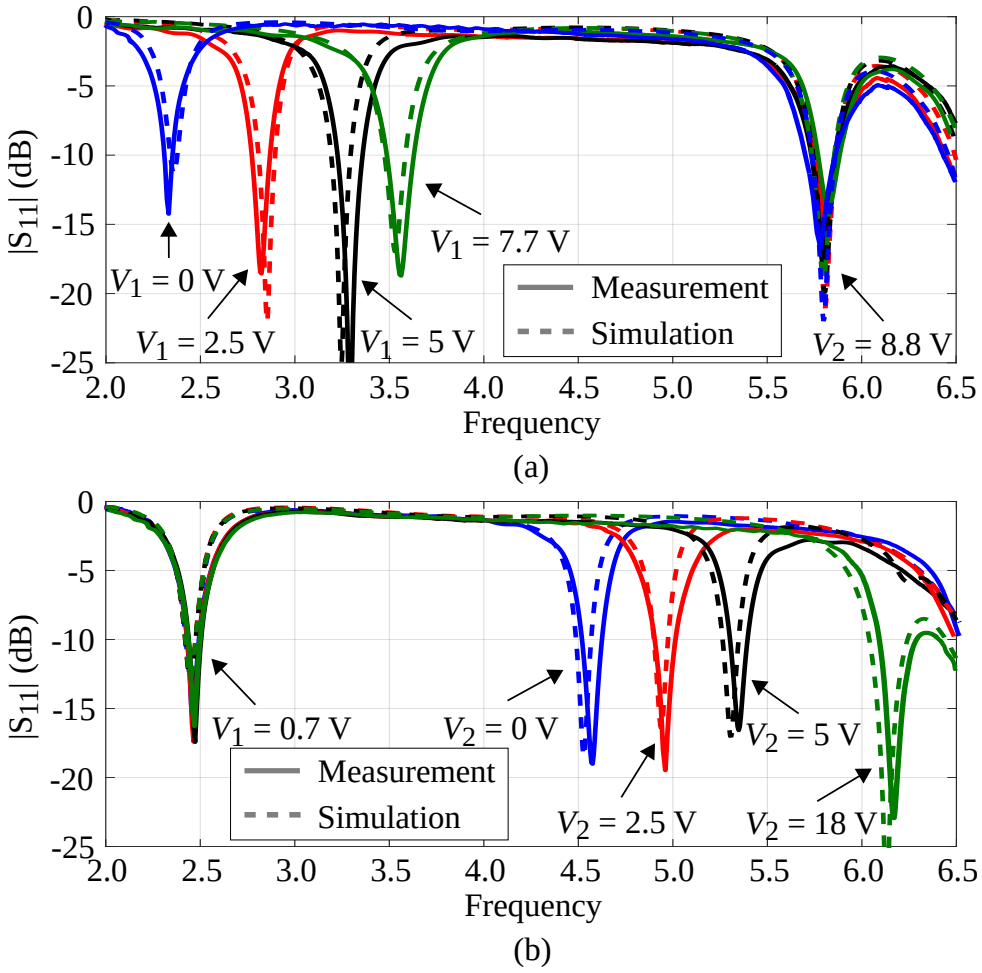

Figure 6.4. Reflection coefficients of the proposed antenna. Simulated (dashed lines) and measured (solid lines) reflection coefficient of the proposed antenna. Tuning the operation frequency at (a) the low band and (b) the high band.

that the polarization of the two modes are normal to each other, since the co-polarized orientations of the lower band and higher band are following x and y directions, respectively.

Figure 6.6 shows a satisfactory agreement between the simulated and measured realized gains of the proposed antenna. At the lower band, when increasing the resonance frequency from 2.34 to 3.55 GHz, the measured realized gain rises from 0.52 to 5.97 dBi. At the higher band, the measured realized gain increases from 2.42 to 6.71 dBi when the resonance frequency shifts from 4.55 to 6.15 GHz. The simulated antenna efficiency obtained rises from 51.7% to 87.5% at the lower band, while at the higher band the simulated efficiency increases from 41.8% to 86.6%. Thus, based on the measured gain, the

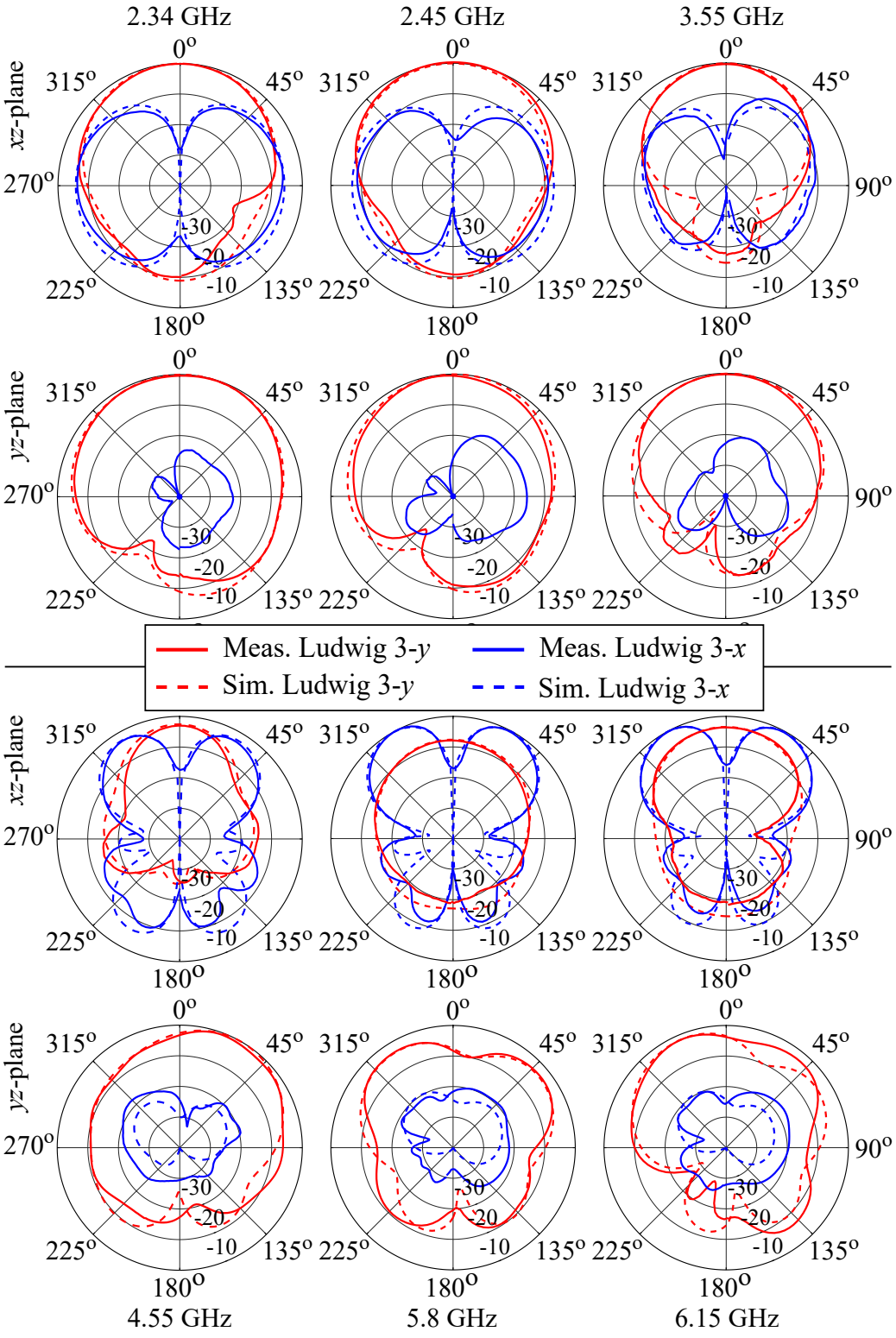

Figure 6.5. Normalized radiation patterns of the proposed antenna. Simulated and measured normalized radiation patterns (in Ludwig third definition) of the proposed antenna in the *xz*- and *yz*-planes at 2.26, 2.45, 3.56, 5.01, 5.8 and 6.27 GHz.

actual antenna efficiency is estimated to be between 49.1% and 84.1% at the lower band, and from 34.7% to 87.8% for the higher band.

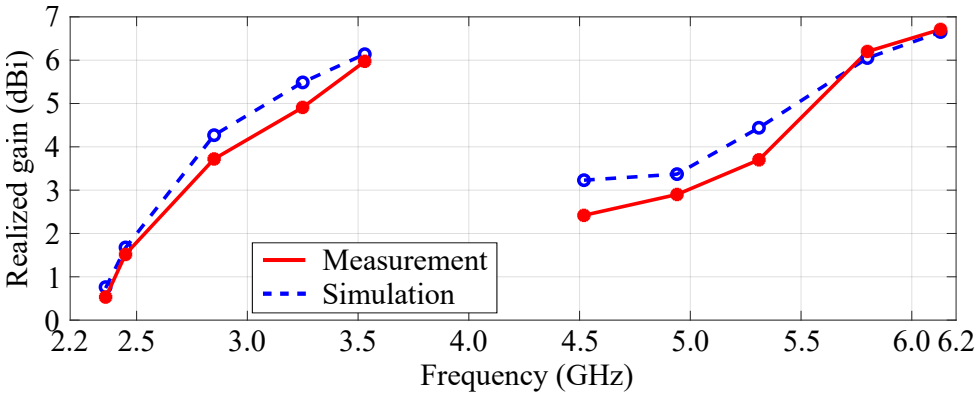

Figure 6.6. Realized gains of the proposed antenna. Simulated and measured realized gain of the proposed antenna when tuned for operation at 2.34, 2.45, 2.85, 3.25, 3.55, 4.55, 4.94, 5.31, 5.8 and 6.15 GHz.

6.3.4 Impact of bending

To investigate the impact on the antenna performance due to bending, the antenna is tuned to operate at 2.45 and 5.8 GHz simultaneously, with bias voltages of V_1 = 0.7 V and V_2 = 8.8 V. The antenna is then affixed onto two 3D printed cylindrical bases (with a 30 mm bending radius) and bent along the *x*- or *y*-axis, respectively. The measured reflection coefficients for these two bending configurations are shown in Fig. 6.7. When the antenna is bent along the *x*-axis, the resonance frequency at the lower band is shifted to 2.37 GHz (3.3%) while the higher frequency is nearly unchanged as illustrated in Fig. 6.7 (a). This is because while the antenna is bent along the *x*-axis, the antenna physical width remains nearly unchanged. In contrast, the higher band is much more sensitive to bending along the *y*-axis, with the resonance frequency shifted by 8.5%, from 5.8 to 5.33 GHz as shown in Fig. 6.7 (b). This can be explained by the significant physical change in the patch width when bent in this direction.

6.3.5 Independent detuning compensation

The reconfigurability of the antenna makes it possible to individually compensate the detuning effects in both bands, such as the impact due to antenna bending exemplified in the previous section. Such frequency shifts can be independently compensated for

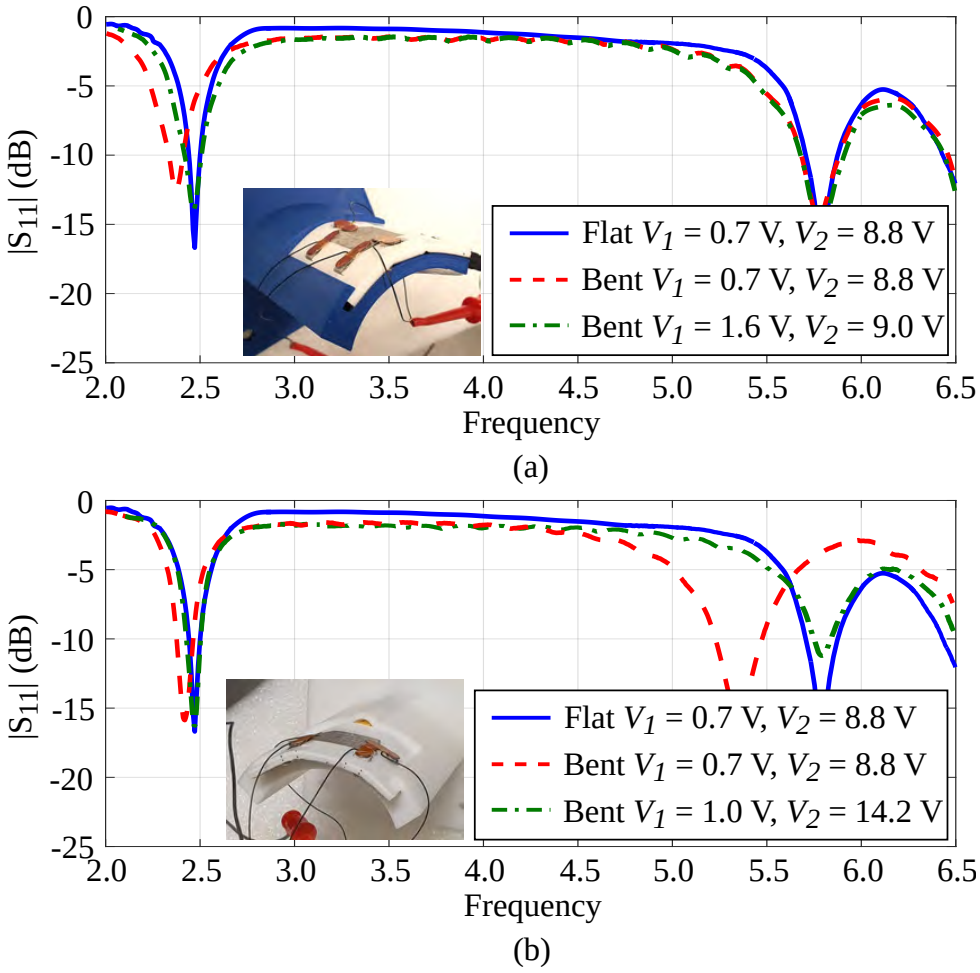

Figure 6.7. Reflection coefficients of the proposed antenna in conformal test. Measured reflection coefficients of the proposed antenna when it is flat, bent, and dynamically re-tuned to compensate the bending impact. Inset: bending measurement setup - the antenna was bent along (a) the *x*-axis and (b) the *y*-axis with a bending radius of 30 mm.

both bands by adjusting the bias voltages V_1 or V_2. Specifically, V_1 is tuned from 0.7 V to 1.6 V to recover the lower resonance frequency from 2.37 back to 2.45 GHz for the bending along *x*-axis. On the other hand, V_2 is tuned from 8.8 V to 14.2 V to bring the higher frequency from 5.33 back to 5.8 GHz for the other bending scenario. Such independent tunability will be useful for applications in very dynamic and complex surrounding environments such as wearable systems. Additionally, due to the good isolation provided by the full ground plane, the proposed antenna is insensitive to the wearer's body; this is also essential for wearable applications.

6.4 Conclusion

In this chapter, a frequency-reconfigurable flexible antenna with two independently tunable bands was presented for wearable applications. The proposed antenna made of conductive textile on a foam substrate is designed to cover two ISM bands centered at 2.45 and 5.8 GHz, with an independent frequency tuning range of 41.1% for the lower band and 29.9% for the higher band. The good agreement between the simulation and measurement results on a prototype validates its expected independent frequency tunability and the ability to individually compensate detuning in the two bands.

Chapter 7

Multi-Functional Wearable Textile Antennas

RECONFIGURABLE antennas with agility characteristics have been being increasingly developed to enhance versatility for various communications standards. A similar demand exists for body-worn antennas to keep the antenna operating stably in highly dynamic wearing conditions. A reconfigurable wearable antenna may not only be expected to have frequency agility, but potentially also to show a combination with pattern or polarization reconfigurability.

In this context, this chapter presents a multi-functional wearable antenna design, with two design variations. The first antenna provides frequency- and pattern-agility while the second antenna exhibits frequency- and polarization-reconfigurability. The antenna design principle is confirmed using equivalent circuit models before being validated by experimental results.

7.1 Introduction

As mentioned in Section 3.3, Chapter 3, in order to develop compact and versatile body-centric communications systems, it is desirable to develop body-worn flexible antennas that can switch between omnidirectional and broadside patterns at a fixed frequency band. Furthermore, in each of these radiation modes, frequency reconfigurability may be necessary to compensate frequency shifts due to deformation effects such as antenna bending or crumpling. Additionally, for linearly polarized antennas, the antenna polarization may need to be adaptable to maintain the communication links despite dynamic changes of on-body environment caused by wearers' daily activities and movements. Therefore, reconfigurable wearable textile antennas able to combine frequency-, polarization- or pattern-agility at a fixed frequency band are in high demand.

Several pattern-reconfigurable antennas were proposed in the literature [26,177–179] in which operation can be switched between broadside and monopole radiation modes. In [177, 179], the proposed antennas were able to change between different radiation patterns, however only at a fixed frequency. The antenna proposed in [26] was designed to not only provide broadside-to-omnidirectional switchability, but was also enhanced with frequency tunability with more than 20% of frequency tuning range for each mode. A number of polarization-reconfigurable antennas were also reported in the literature [21, 23, 148]. Reconfigurable antennas that can combine polarization- and frequency-agility were also investigated [22, 102] aiming to expand antenna functionalities. However, these antennas were implemented on rigid substrates, which are inappropriate for wearable applications.

Considering now reconfigurable flexible textile antennas, most of the reported designs aim at providing frequency reconfigurability [28, 29], while the number of practically demonstrated pattern-reconfigurable textile antennas has been very limited [30]. Utilizing PDMS substrate and PIN diodes, the antenna reported in [30] is able to switch between monopole-like and broadside radiation pattern at a fixed resonance frequency of 5.2 GHz. Regarding combination of frequency- and polarization-agility, there has not been any body-worn antenna reported in the literature to date.

In this chapter, an operation principle concept proposed for combining frequency- and pattern- or polarization-agility in one antenna design is presented. Based on the proposed strategy, two reconfigurable flexible textile antennas with multifunctionality are presented. The first antenna is able to switch between broadside and omnidirectional

radiation modes with frequency-agility enabled in each mode. The frequency fractional tuning ranges of the antenna at broadside and monopole-like modes are 57.3% and 27.2%, respectively. Frequency- and polarization-agility are embedded in the second antenna which is able to work in 0°, 120° or 240° linear polarizations. At each state of linear polarization, a wide frequency tuning range of 31.9% is provided.

7.2 Principle of operation

The antenna reconfigurability on a flexible wearable platform is implemented by considering a center-fed circular patch microstrip antenna inspired by a previously reported reconfigurable antenna [145]. In the considered antenna structure, a resonant patch is shorted to its ground plane by using three identical varactors placed at the patch circumference with 120° angular separation as shown in Fig. 7.1. The capacitance at the patch edge is changed by controlling the varactor bias voltage, which results in a change of effective dimensions of the patch and consequently a variation of the antenna radiation characteristics. It is expected that, simultaneous or individual tuning of the three hypothetical varactor capacitances (C_1, C_2 and C_3 corresponding to Varactor 1, 2 and 3 respectively) will lead to different changes in antenna radiation characteristics. Figure 7.2 displays three scenarios of varactor capacitance tuning which result in three promising antenna radiation states as described in the following.

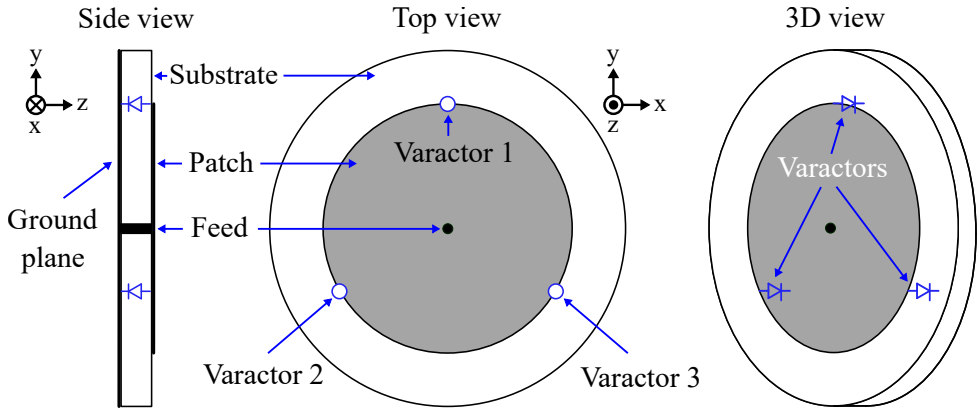

Figure 7.1. Antenna basis geometry. Ideal reconfigurable circular patch microstrip antenna structure.

In a first mode of operation, the three capacitances C_1, C_2 and C_3 are tuned simultaneously to achieve omnidirectional monopole patterns. It is well-known that a higher values of varactor capacitance leads to a higher RF current flowing through the varactors.

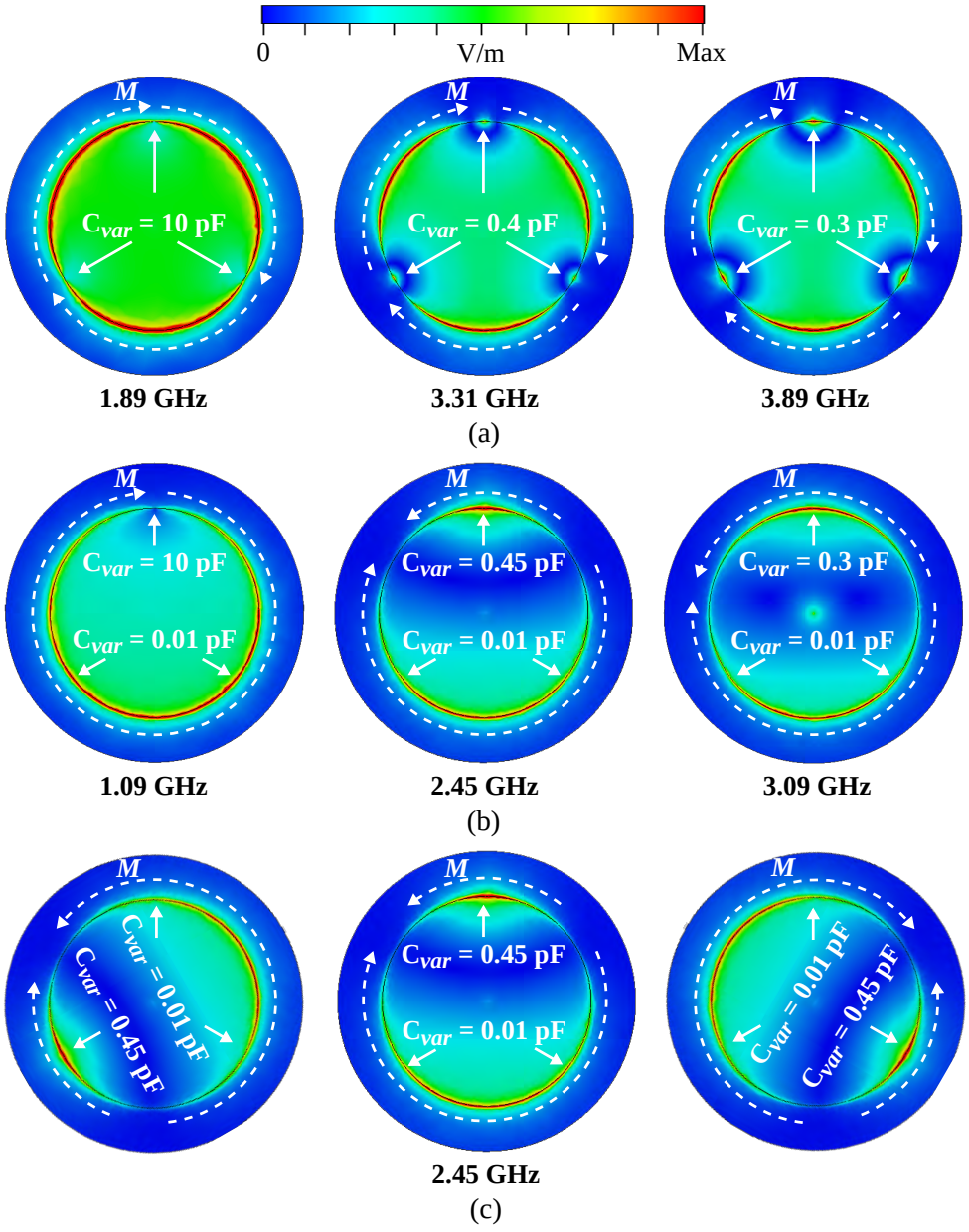

Figure 7.2. Electric field distribution of the considered antenna. Simulated instantaneous electric field distributions in the cavity of the considered antenna radiating in (a) omnidirectional mode, (b) broadside mode and (c) broadside mode with three linear polarization states.

In this case, the three varactors act as three vias which create three radiation apertures represented by three in-phase magnetic current elements, M, as shown in Figure 7.2 (a), left-hand side graph, where $C_1 = C_2 = C_3 = 10$ pF. When decreasing the three varactor junction capacitances, the effective length of the three radiation apertures is shortened which is illustrated in Figure 7.2 (a), center and right-hand side graphs. As a result, the resonance frequency of the antenna is increased. It is noticeable that, the values of

C_1, C_2 and C_3 have to be large enough to maintain the RF current flowing through the varactors and consequently maintain the RF connection between the resonant patch and the ground plane. It is also worth mentioning that, to maintain the omnidirectional monopole patterns, the distance in-between the centers of the magnetic current elements is limited to half of wavelength in free-space [123].

When the varactor capacitance is tuned to very low value, there is almost no current flowing through the varactor. In this case, there is effectively no connection between the antenna patch and the ground plane at the position of the low value varactor. Figure 7.2 (b) shows the electric field distribution of the antenna when the $C_2 = C_3 = 0.01$ pF and C_1 is varied from 10 pF to 0.3 pF. When the varactor capacitance C_1 is set to 10 pF, this creates a high-capacitance connection between the patch and the ground plane, and the antenna is working in a quarter-wave mode with one (effective) shorting point as shown on the left of Fig. 7.2 (b). When decreasing the value of C_1, the radiation mode is transitioning from the quarter-wave mode to a half-wave patch mode. However, when the value of C_1 is tuned to the very low value ($C_1 = C_2 = C_3 = 0.01$ pF), the will be no current flowing from the patch to the ground plane, the antenna is consequently working in a fundamental half-wave patch mode. By swapping the location of the higher value capacitance varactor, the linear polarization of the antenna working in broadside mode can be switched by 120° as shown in Fig. 7.2 (c).

In summary, by changing the tuning order of the three varactors, it is possible to realize a multi-functional antenna. The antenna radiation pattern can be switched between an omnidirectional pattern and a broadside pattern. While working in broadside mode, the antenna linear polarization can be tuned in steps of 120°. It is noticeable that, at each radiation mode mentioned, the resonance frequency of the antenna can be varied.

7.3 Reconfiguration analysis

An implementation of a reconfigurable wearable textile antenna based on the aforementioned operating principle is proposed with the structure as shown in Fig. 7.3. The proposed antenna configuration consists of a full ground plane, a flexible substrate, a circular radiation patch, three folded shorting stubs placed around the patch with a 120° angular separation. The reconfigurability is implemented by using the flexible coplanar reconfiguration module with varactors as presented in Chapter 5. Three

reconfiguration modules are used to connect the three folded shorting stubs to the antenna circular patch. Depending on a design requirement, an appropriate feeding technique can be selected. Based on the proposed structure, the antenna operation principle while working either in omnidirectional or broadside modes is analyzed using an equivalent circuit model.

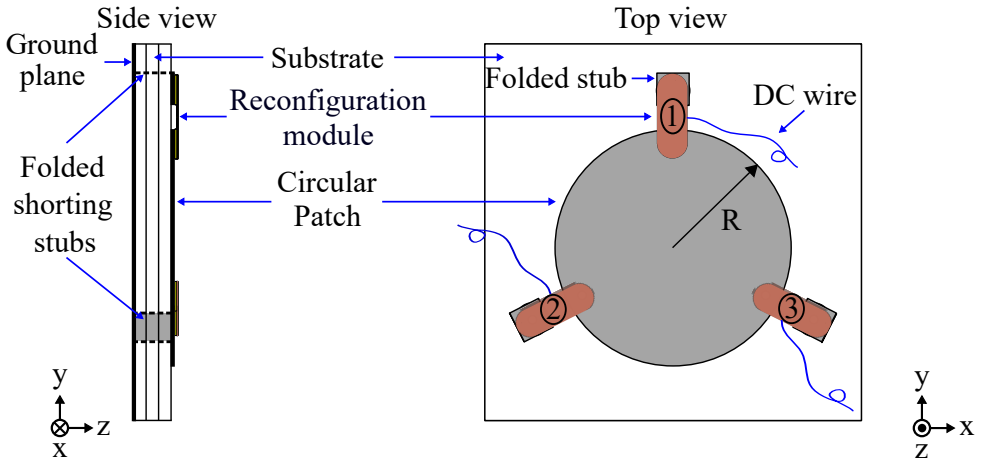

Figure 7.3. Multi-functional wearable antenna structure. General structure of the proposed multi-functional wearable textile antenna.

7.3.1 Resonance frequency for the broadside mode

As discussed in Section 5.2.3, at the lowest value of the varactor junction capacitance, the dedicated circuit in the reconfiguration module is nearly open. In this stage, there is almost no connection between the antenna patch and the folded shorting stubs. Therefore, when the varactor capacitance of module ② and ③ are tuned to 0.15 pF (corresponding to the bias voltage of 18V), these two modules can be considered as disconnected. The antenna structure is then simplified as shown in Fig. 7.4 (a) where the module ② and ③ are removed. Since the antenna resonant patch is a circle, it is necessary to transform it it to an equivalent rectangular shape before calculating a resonance frequency using transmission line theory. The equivalent rectangular patch with identical area to the circular patch shown in Fig. 7.4 (b) where the patch length (l_{pb}) and width (w_{pb}) can be estimated as follow

$$l_{pb} \approx 2R \tag{7.1}$$

$$w_{pb} \approx \frac{\pi R^2}{l_{pb}} \tag{7.2}$$

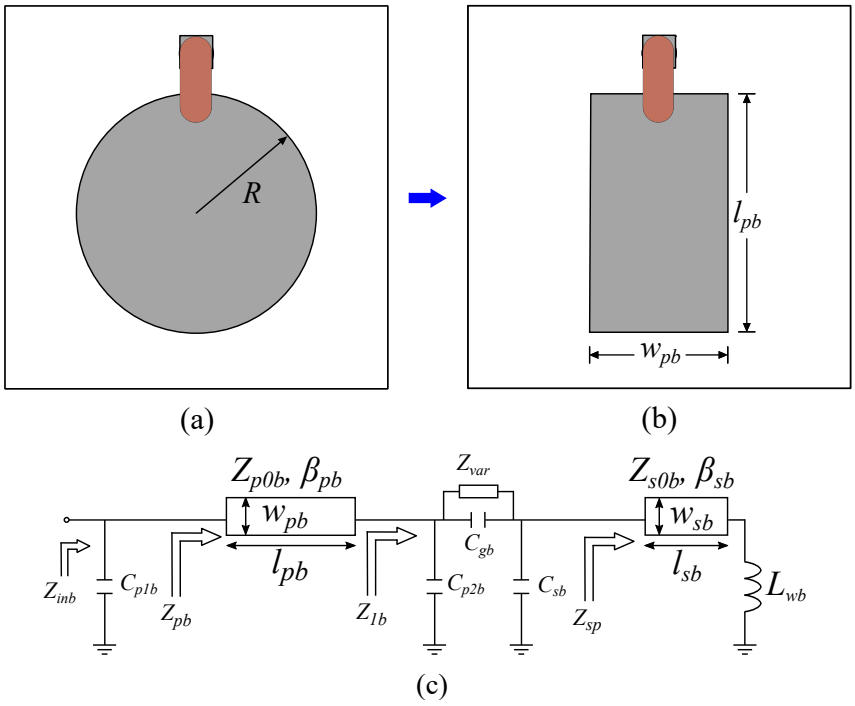

Figure 7.4. Calculation process for the antenna working in the broadside mode. Approximated calculation process with the antenna operating in its broadside mode. (a) Simplified antenna without modules 2 and 3, (b) equivalent rectangular patch antenna with identical area and (c) equivalent circuit model of equivalent rectangular patch antenna.

where R is the circular patch radius. Once the patch length and width of the equivalent rectangular patch are estimated, it can be analyzed using a circuit model as shown in Fig. 7.4 (c). The antenna resonance frequency as a function of a hypothetical varactor junction capacitance C_{var} can be calculated following the method presented in Section 5.2.3. As a result, for the case of the the antenna operating in broadside mode, the resonance frequency obtained from the equivalent circuit analysis and CST full-wave simulation according to different hypothetical values of C_{var} from 0.001 to 1000 pF can be calculated as displayed in Fig. 7.5.

7.3.2 Resonance frequency for the omnidirectional mode

As discussed in Section 7.2, when all the junction capacitance of the three varactors in their reconfiguration modules are tuned simultaneously with the same bias voltage, the antenna is working in omnidirectional radiation mode. Since the antenna patch is shorted to the ground through the three folded shorting stubs, three radiation apertures are created from the patch to the ground, defining three virtual cavities. These

7.3.2 Resonance frequency for the omnidirectional mode

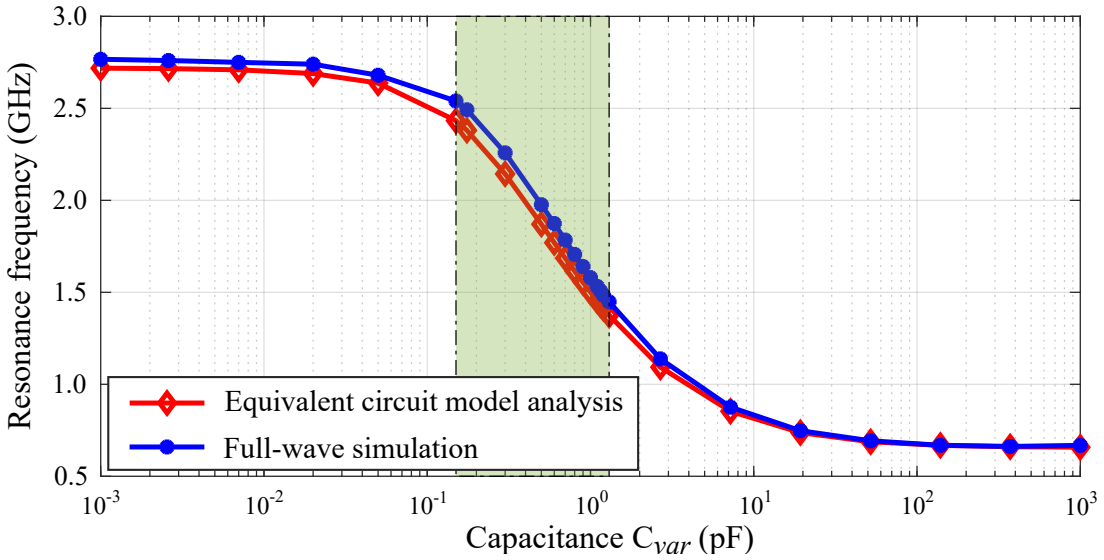

Figure 7.5. Analysis and simulation results of the resonance frequency in the broadside mode. Equivalent circuit model analysis and full-wave simulation of the resonance frequency across different hypothetical values of varactor capacitance for the antenna working in the broadside mode. Green area: Single varactor capacitance range (from 0.15 to 1.3 pF).

apertures are similar to thin slots which can be described as equivalent magnetic current elements as shown in Fig. 7.6 (a). Since the effective length of one resonant cavity determines the resonance frequency of the omnidirectional mode, one resonant cavity will be considered in the calculation as shown in Fig. 7.6 (b). The considered resonant cavity consists of one-third of the antenna resonant patch area, one half of reconfiguration module on each side of the patch, two folded shorting strips with a half width. An equivalent circuit of this resonant cavity can be obtained as described in the following.

As mentioned in Section 5.2.3, Chapter 5, the folded shorting stubs and the patch can be represented as two transmission lines with the corresponding impedance Z_s and Z_p obtained from transmission line theory. The impedance Z_s is calculated at the varactor position and Z_p is calculated at the start of the line (at feeding position, in the center of the circuit). The impedance Z_s can be calculated based on the characteristic impedances Z_{0s}, the phase constant β_s and the lengths l_s. It is noticeable that, the width of the new folded stub is a half of the original folded shorting stub ($w_{s1} = w_{s2} = W_2/2$). The impedance Z_p can be calculated based on Z_{0p}, β_p, w_p and l_p. However, since the considered patch is one third of a disk, this shape need to be approximately transformed to an equivalent rectangular shape with a length ($2l_p$) and width (w_p). We assume l_p to be a distance from the center of the resonant cavity to the edge as shown in Fig. 7.6 (b). To calculate the width w_p, the equivalent rectangular shape is assumed

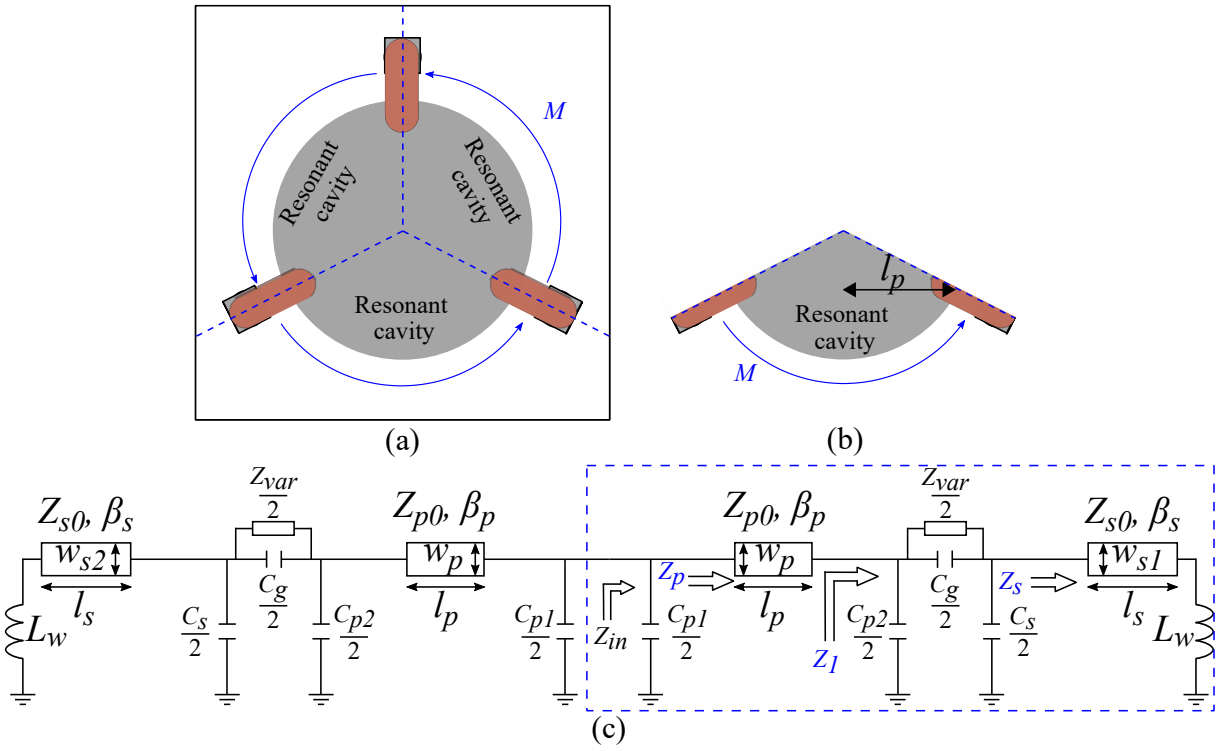

Figure 7.6. Calculation process for the antenna working in the monopole mode. Approximated calculation process for the antenna working in the monopole mode. (a) Antenna with three equivalent cavities and three magnetic current elements, (b) one aperture with one magnetic current and (c) equivalent circuit model of one resonant cavity.

to have equal area as the one third of a disk patch. Thus, l_p and w_p can be calculated as follow

$$l_p = sin(\frac{\pi}{3})R \tag{7.3}$$

$$w_p \approx \frac{\pi R^2}{6 l_p} \tag{7.4}$$

where R is the patch radius. Again, when the estimation values of l_p and w_p are obtained, the values of Z_{0p}, β_p can be calculated and hence Z_p can now be obtained using transmission line theory. Based on the transformation of this one-third of the resonant disk cavity to an equivalent rectangular shape, an equivalent circuit model of one resonant cavity can be obtained as shown in Fig. 7.6 (c). Because the feeding position is placed at the center of the cavity, the equivalent circuit of the resonant cavity can be divided into two identical branches. The input impedance Z_{in} can be calculated as a

function of a hypothetical varactor junction capacitance C_{var} on one branch as highlighted in Fig. 7.6 (c). Using the method presented in Section 5.2.3 the relation between the resonance frequency and the hypothetical varactor junction capacitance C_{var} can be obtained. A good agreement between the antenna resonance frequency calculated from the equivalent circuit analysis and the one obtained from the CST full-wave simulation for different hypothetical values of C_{var} is shown in Fig. 7.7. It is noticeable that, based on full-wave simulation, it is found that the lowest value of C_{var} should be limited to approximately 0.55 pF. This is because if C_{var} is smaller than 0.55 pF, the difference between the maximum and minimum gain for the antenna radiation in xy-plane is more than 3 dB which breaks the monopole-like pattern.

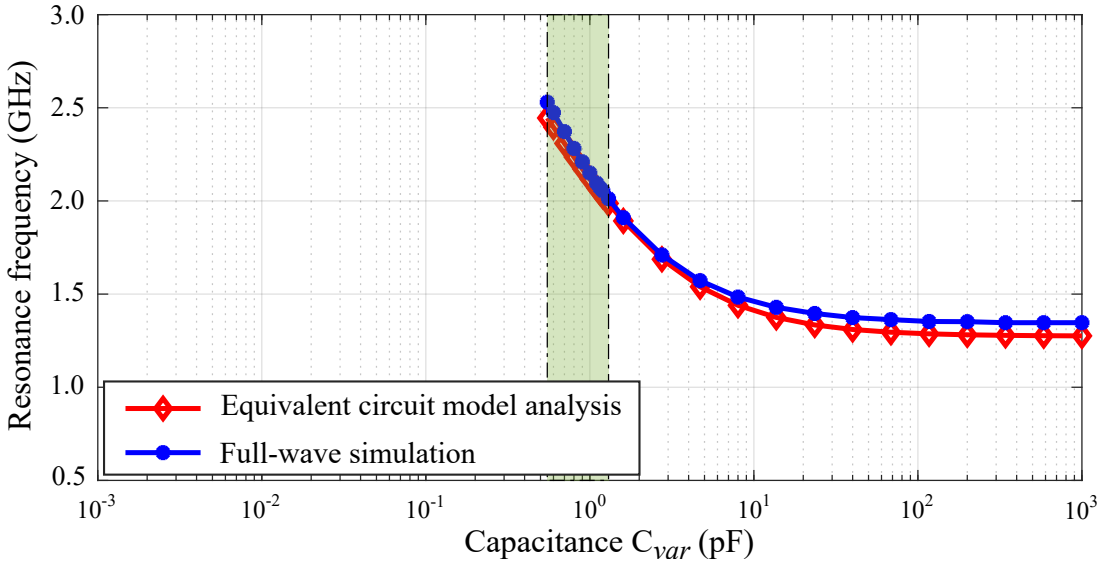

Figure 7.7. Analysis and simulation results of the resonance frequency in the omnidirectional mode. Equivalent circuit model analysis and full-wave simulation of the resonance frequency across different hypothetical values of varactor capacitance while antenna is working in the omnidirectional mode. Green area: Single varactor capacitance range (from 0.15 to 1.3 pF).

7.4 Antenna designs

It is worth mentioning that, a single antenna with frequency-, pattern- and polarization reconfigurabilities is in principle realizable. To achieve this reconfigurability, a centered probe feed is required to maintain the radial symmetry of the antenna. However, obtaining antenna matching in all the radiation modes fed by the probe

feed is a challenging task. Therefore, two reconfigurable antennas based on combinations of two of the aforementioned reconfigurability modalities are designed instead. The first antenna has frequency- and pattern-reconfigurability with the ability to switch between omnidirectional and broadside patterns. The second one is a frequency- and polarization-reconfigurable antenna with operation in broadside radiation mode where the linear polarization can be switched in steps of 120°. At each radiation mode, the two antennas also exhibit frequency reconfigurability.

7.4.1 Frequency- and pattern-reconfigurable antenna

The general structure of the proposed frequency- and pattern-reconfigurable antenna is shown in Fig. 7.8 with the dimensions given in the caption. The antenna consists of a full ground plane, three layers of substrate, a stepped proximity-coupled feed, a circular patch and three folded shorting strips. The three folded shorting strips are placed around the patch with 120° angular separation. Three reconfiguration modules are used to connect the 3 shorting strips to the antenna circular patch.

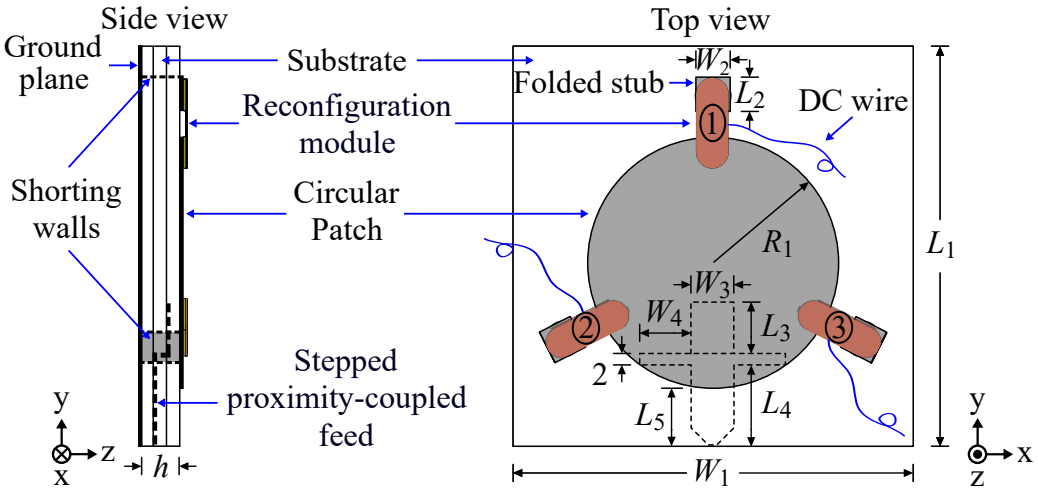

Figure 7.8. First antenna configuration. Frequency- and pattern-reconfigurable antenna configuration. Dimensions (mm): $L_1 = 70.0$, $L_2 = 6.0$, $L_3 = 9.0$, $L_4 = 14.0$, $L_5 = 10.0$, $L_6 = 10.2$, $W_1 = 70.0$, $W_2 = 6.0$, $W_3 = 7.5$, $W_4 = 9.0$, $R_1 = 22.0$ and $h = 4.8$.

The antenna is designed to provide frequency- and pattern-agility by switching between omnidirectional and broadside radiation modes. A proximity-coupled feed is selected to provide flexibility in optimization of the antenna impedance matching, since there are several degrees of freedom in the feed dimensions. Furthermore, the

feed is modified to a stepped proximity-coupled feed to also excite a higher-order mode resonating at 5.8 GHz, aiming to enhance the antenna functionalities (as mentioned in Chapter 5). However, since the proximity-coupled feed is realized on one side of the antenna, which breaks the antenna symmetry, this configuration does not allow realization of polarization agility as discussed in Section 7.2.

As shown in the highlighted areas in Fig. 7.5 and Fig. 7.7 for the two modes, it can be observed that the widest tuning range is achieved while using one single varactor MA120H46 with the capacitance ranging from 0.15 to 1.3 pF. Therefore, a reconfiguration module used in the antenna design is similar to the one employed in Chapter 5.

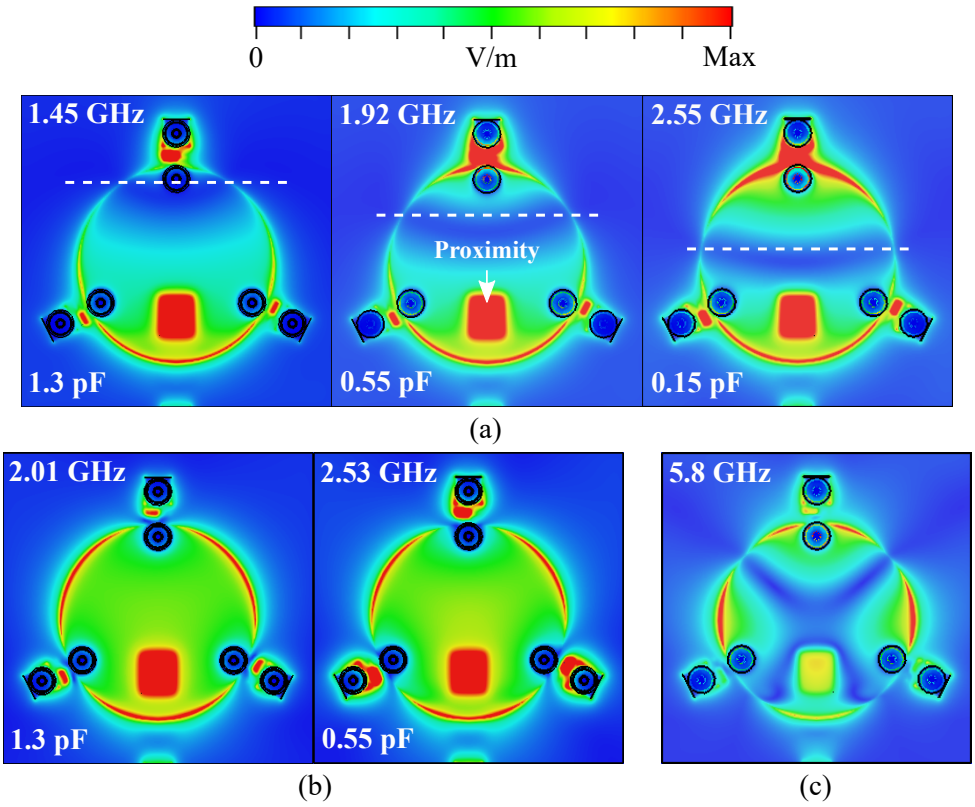

Figure 7.9. Electric field distributions of the first antenna. Simulated instantaneous electric field distribution of the frequency- and pattern-reconfigurable antenna in (a) broadside, (b) omnidirectional and (c) higher-order modes.

The electric field distributions of the proposed antenna operating in broadside and omnidirectional modes at different values of the varactor capacitance are shown in Fig. 7.9. When the antenna is working in broadside mode, the transition from a quarter-wave radiation mode to a half-wave patch mode is illustrated in Fig. 7.9 (a). Through this transition, a wide frequency tuning range of 55% (from 1.45 to 2.55 GHz) is achieved.

When the varactor capacitance of the three modules are tuned simultaneously with the same voltage, the omnidirectional radiation mode is excited with the three radiation apertures as displayed in Fig. 7.9 (b). As mentioned, the lowest value of the varactor capacitance is limited to 0.55 pF to maintain acceptable monopole-like pattern, which limits the highest resonance frequency in monopole mode to 2.53 GHz. The frequency tuning range when the antenna is operating in omnidirectional mode is 22% (from 2.1 to 2.53 GHz). The electric field distribution at the fixed frequency of 5.8 GHz corresponds to a higher-order mode, and is shown in Fig. 7.9 (c).

7.4.2 Frequency- and polarization-reconfigurable antenna

The geometry structure of the proposed frequency- and polarization-reconfigurable antenna is shown in Fig. 7.10 with the antenna dimensions given in the caption. It can be observed that, the antenna structure is broadly similar to the proposed frequency- and pattern-reconfigurable antenna, with the notable difference that a centered probe feed is utilized instead of the proximity-coupled feed. The antenna is designed to operate in the broadside radiation with 0°, 120° and 240° linear polarization. Specifically, when the varactor junction capacitance of module pairs (②, ③), (①, ②) and (①, ③) are set to 0.15 pF, the 0°, 120° and 240° linear polarization operation is achieved, respectively. The antenna resonance frequency is tuned by varying the varactor capacitance of the remaining (third) module. By using the probe feed fixed at the center of the radiating patch, the antenna is radially symmetrical which allows identical repetition of the linear polarization in all the three directions.

Since the antenna probe feed is fixed at the center of the radiation patch, it is difficult to achieve input impedance matching. Based on the given range of the single varactor capacitance, the antenna dimensions are optimized to achieve the widest frequency tuning range corresponding to a $|S_{11}|$ parameters of less than -10 dB. As a result of this optimization, the simulated resonance frequency of the proposed antenna can be tuned from 1.92 to 2.63 GHz (or 31.2%) corresponding to varactor junction capacitances ranging from 0.94 to 0.45 pF.

7.5 Experimental results

To validate the proposed reconfigurable concepts, the two proposed reconfigurable textile antennas are fabricated. Flexible and light-weight conductive and non-conductive

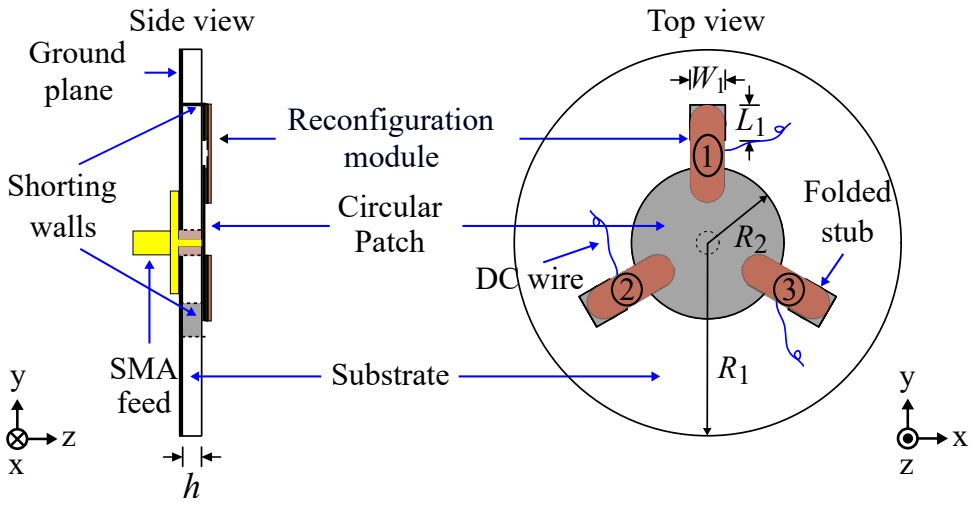

Figure 7.10. Second antenna configuration. Frequency- and polarization-reconfigurable antenna configuration. Dimensions (mm): $L_1 = 6.0$, $W_1 = 6.0$, $R_1 = 33.0$, $R_2 = 14.5$ and $h = 3.2$.

materials are used to construct the proposed body-worn antennas. A Cumming Microwave PF-4 foam with a loss tangent of $\tan\delta = 0.0001$, a relative permittivity $\varepsilon_r = 1.06$ and 1.6 mm of thickness is selected for the antenna substrates. All antenna conductors are made form a silver-coated nylon Rip-stop fabric (Shieldex Nora-RS) with a sheet resistance of 0.01 Ω/square. The antenna parts are glued together using fabric glue, while the SMA connector is connected to the feed and the ground plane using conductive epoxy. The two fabricated antennas are displayed in Fig. 7.11.

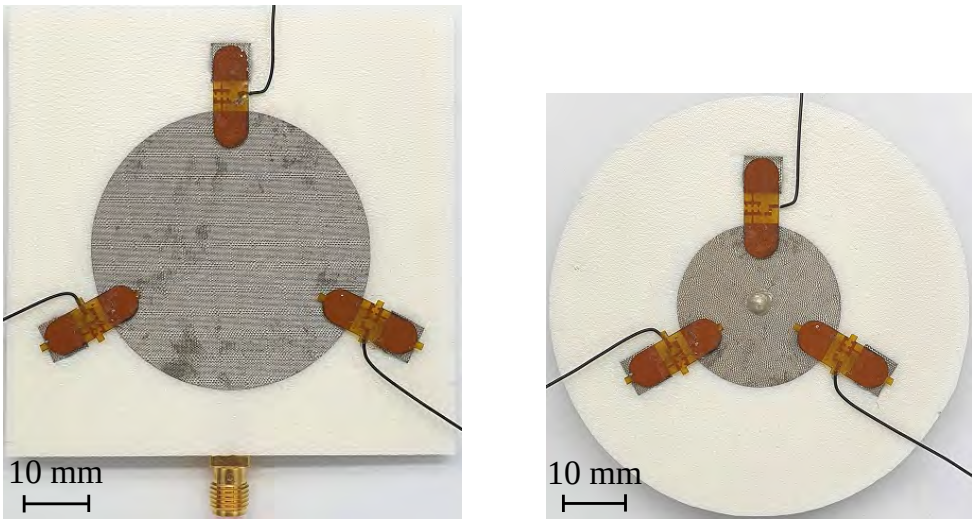

Figure 7.11. Fabricated multi-functional wearable textile antennas. Two fabricated antennas with (a) frequency and pattern reconfigurability and (b) frequency and polarization reconfigurability.

7.5.1 Frequency- and pattern-reconfigurable antenna

The simulated and measured $|S_{11}|$ parameters of the proposed frequency- and pattern-reconfigurable antenna operating in the broadside and omnidirectional modes are displayed in Fig. 7.12 (a) and (b), respectively.

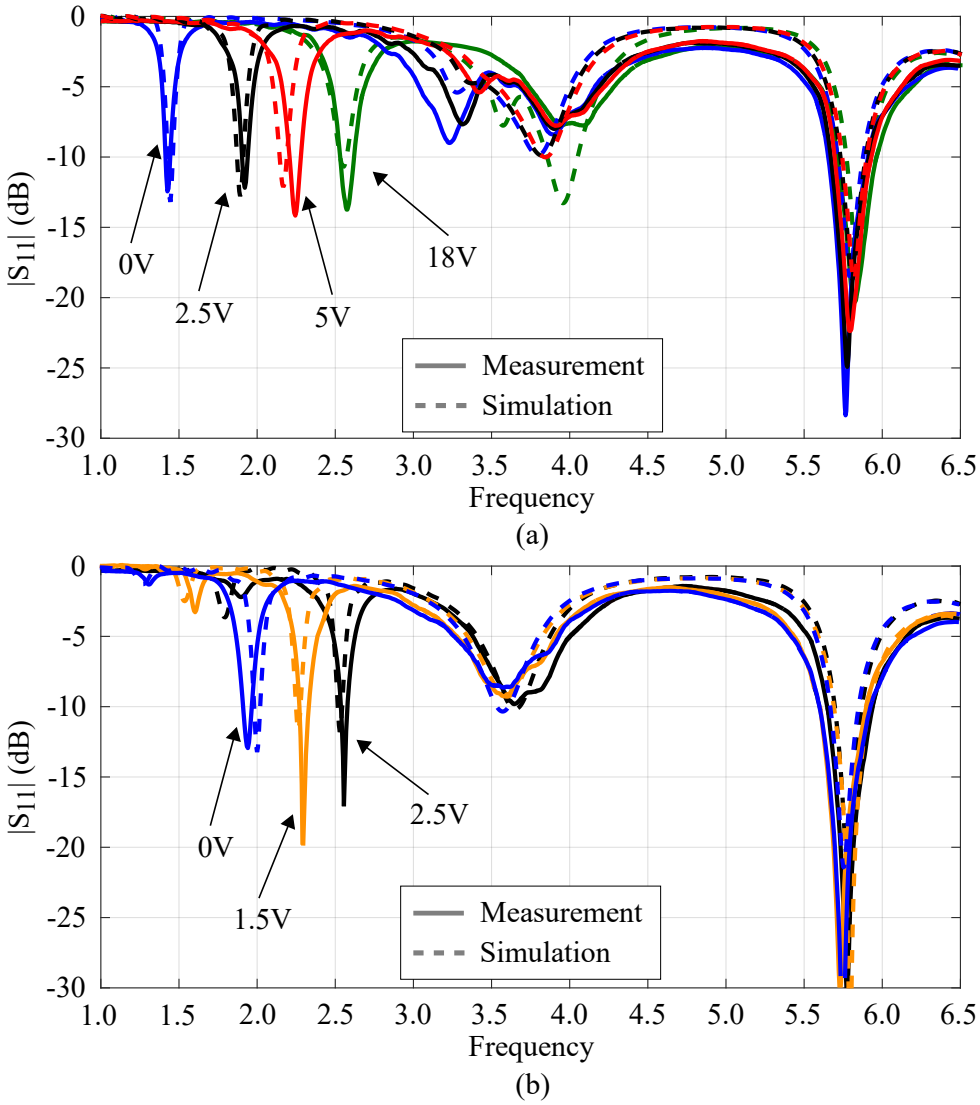

Figure 7.12. Reflection coefficients of the frequency- and pattern-reconfigurable antenna. Simulated and measured reflection coefficients of the proposed frequency- and pattern-reconfigurable antenna for selected values of the bias voltage applied to the varactor in (a) the broadside mode and (b) the omnidirectional mode.

At the lower band in the two radiation modes, a slight discrepancy is observed, which can be explained by the antenna fabrication tolerances. As expected, when the antenna operates in broadside mode, the measured frequency tuning range varies from 1.43 to

2.58 GHz (57.3% fractional tuning range) corresponding to the bias voltage of module ① tuned from 0 to 18 V. In omnidirectional mode, a fractional tuning range of 27.2% is achieved while simultaneously varying the three bias voltages from 0 to 2.5 V, to control the three modules. For the higher-order mode at 5.8 GHz, a relatively large discrepancy between simulated and measured $|S_{11}|$ parameters is observed, however with the target bandwidth (5.275 − 5.875 GHz) still fully covered.

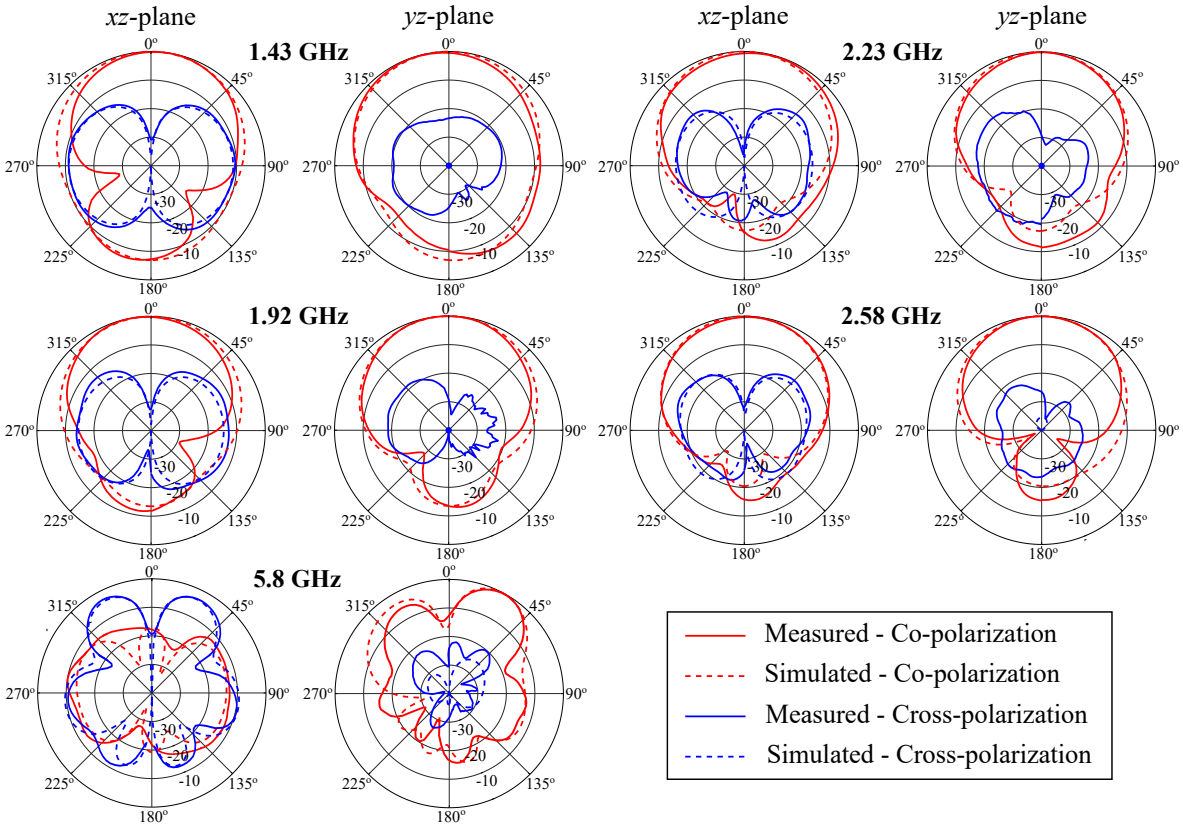

Figure 7.13. Radiation patterns of the frequency- and pattern-reconfigurable antenna in broadside mode. Simulated and measured normalized radiation patterns of the frequency- and pattern-reconfigurable antenna in broadside mode.

The simulated and measured normalized radiation patterns in the *xz*-plane (H-plane) and the *yz*-plane (E-plane) at 1.43, 1.92, 2.23, 2.58, and 5.8 GHz while the antenna is operating in broadside mode are displayed in Fig. 7.13. Across the lower band from 1.43 to 2.58 GHz, maximum radiation toward broadside direction is obtained. A conical monopole pattern with a tilt angle of 70° is also observed at 5.8 GHz. Figure 7.14 shows simulated and measured radiation patterns in the *xy*-plane and the *xz*-plane at 2.0, 2.28, 2.53 and 5.8 GHz for the state where the antenna is operating in omnidirectional mode. Because the antenna is fed by the proximity-coupled feed from its side,

an asymmetrical pattern in the lower band is observed in *xy*-plane. A stable radiation pattern at the higher-band resonance frequency of 5.8 GHz can be observed when the antenna switches from broadside to monopole modes.

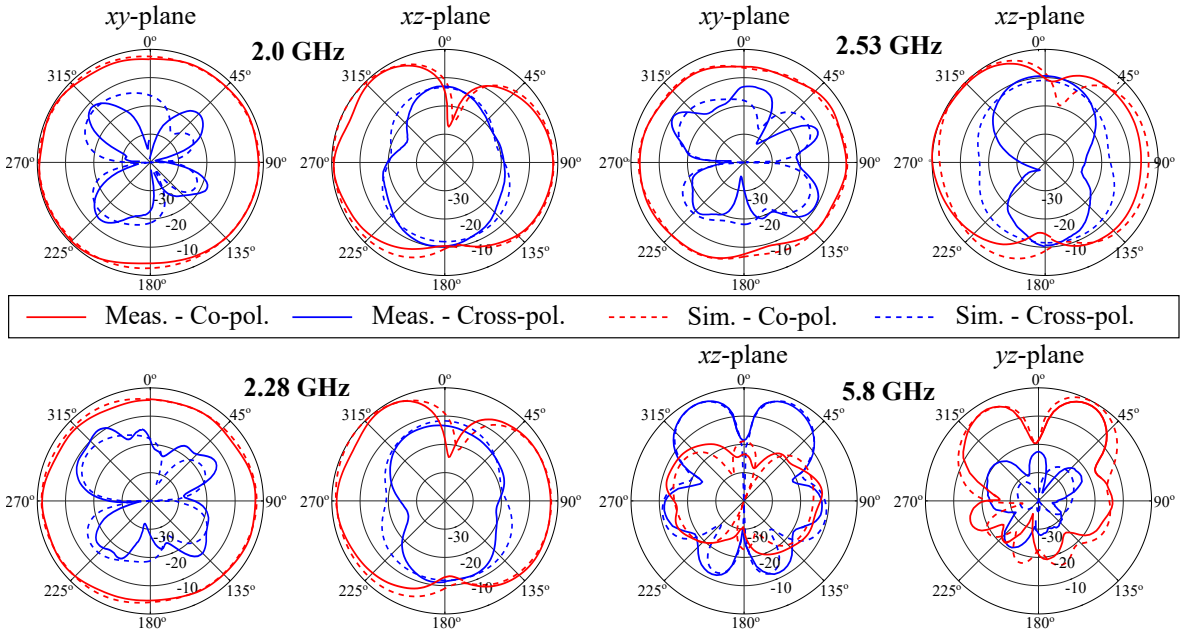

Figure 7.14. Radiation patterns of the frequency- and pattern-reconfigurable antenna in omnidirectional mode. Simulated and measured normalized radiation patterns of the frequency- and pattern-reconfigurable antenna in omnidirectional mode.

The simulated and measured realized gains of the proposed antenna in broadside and omnidirectional modes are shown in Fig. 7.15. When the antenna is operating in its broadside mode, the measured realized gain increases from -0.2 to 6.5 dBi. This is consistent with the transition from the quarter-wave mode to the half-wave patch while decreasing the varactor junction capacitance in broadside mode. The antenna simulated radiation efficiency increases from 40.1% to 96.3% in lower band and reaches 97.6% in higher band at 5.8 GHz. Radiation efficiencies estimated from measurements of the antenna in broadside mode in the lower band is between 33.2% and 90.3% and reach a value of 93.2% in the higher band at 5.8 GHz.

Switching to the omnidirectional mode, the significantly lower realized gain compared to the broadside mode is due to the inherent drawback of low gain of this type of radiation mode. This is also because of a higher power loss in the varactor at the higher value of its junction capacitance (0.55 to 1.3 pF in the omnidirectional mode) and the relative small size of the antenna. The antenna simulated radiation efficiency while

operating in omnidirectional mode increases from 32.2% to 39.4% while the efficiency estimated from measurements is between 28.6% and 41.5%.

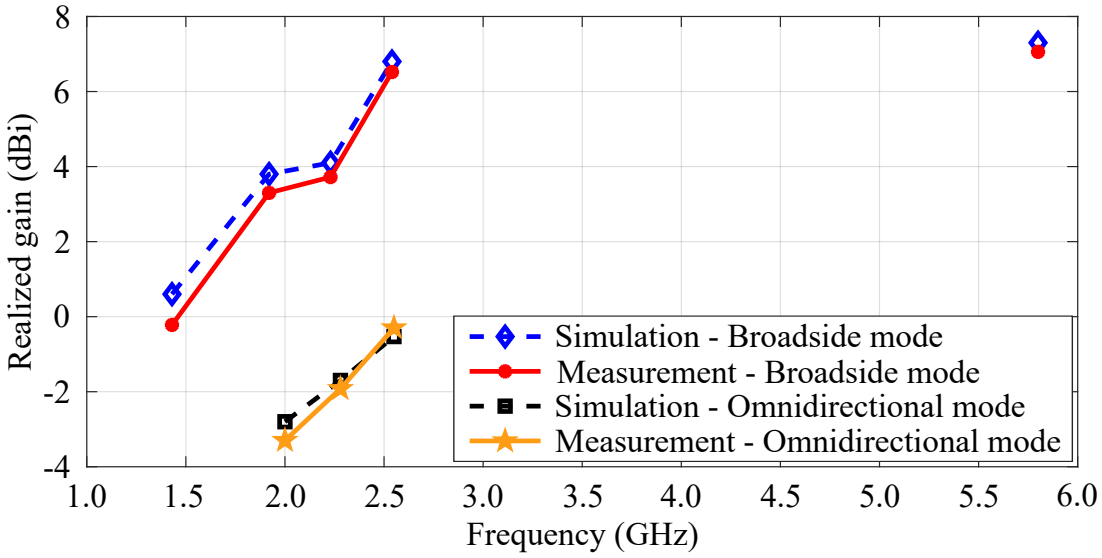

Figure 7.15. Realized gains of the frequency- and pattern-reconfigurable antenna. Simulated and measured realized gains of the frequency- and pattern-reconfigurable antenna in broadside and omnidirectional modes at various resonance frequencies.

7.5.2 Frequency- and polarization-reconfigurable antenna

A good agreement between the simulated and measured reflection coefficients for 0°, 120° and 240° linear polarization at different values of bias voltage is shown in Fig. 7.16. Due to the difficulties in obtaining $S_{11} < -10$ dB impedance matching in all polarization angles, the bias voltage is limited within the range of 1 to 3.8 V which corresponds to a resonance frequency tuning range from 1.9 to 2.62 GHz (31.9%).

The simulated and measured normalized radiation patterns of the proposed antenna in broadside modes for 0° linear polarization at 1.9, 2.34, 2.45 and 2.62 GHz are shown in Fig. 7.17. The typical PIFA radiation pattern with wide beamwidth toward broadside direction across all resonance frequencies is observed. The simulated and measured realized gains of the antenna for 0° linear polarization at 1.9, 2.34, 2.45 and 2.62 GHz are shown in Fig. 7.18. Based on the simulated antenna efficiency ranging from 41.6% to 72.7%, the radiation efficiency estimated from measurement of the antenna increases from 38.2% to 64.6%.

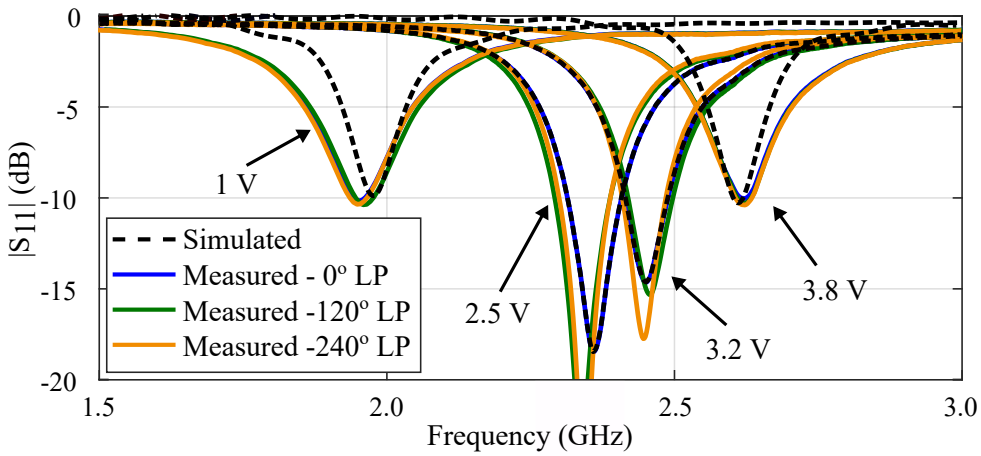

Figure 7.16. Reflection coefficients of the frequency- and polarization-reconfigurable antenna. Simulated (dash lines) and measured (solid lines) reflection coefficients of the frequency- and polarization-reconfigurable antenna for selected values of the bias voltage applied to the varactor.

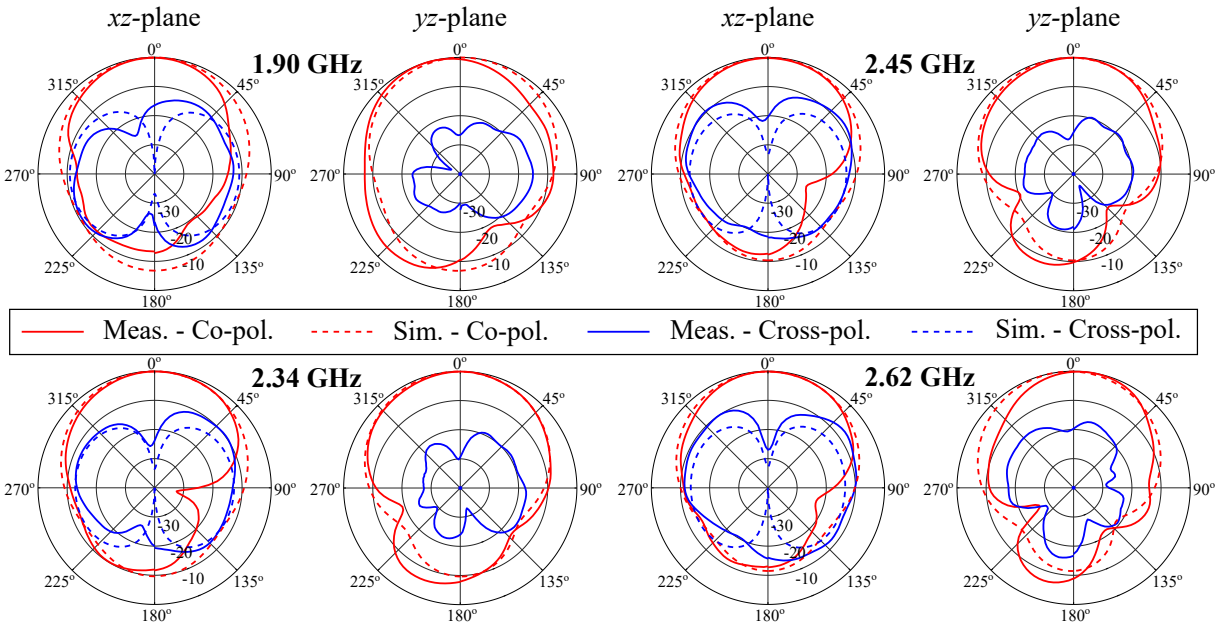

Figure 7.17. Radiation patterns of the frequency- and polarization-reconfigurable antenna. Simulated and measured normalized radiation patterns of the proposed frequency- and polarization-reconfigurable antenna for 0° linear polarization at 1.9, 2.34, 2.45 and 2.62 GHz.

Using a linearly polarized receiver antenna, the proposed antenna polarization reconfigurability can be experimentally characterized. The proposed antenna is mechanically fixed on a turn table before its linear polarization is switched by tuning the bias voltage to control the varactors on the three reconfiguration modules. For each angle

7.5.2 Frequency- and polarization-reconfigurable antenna

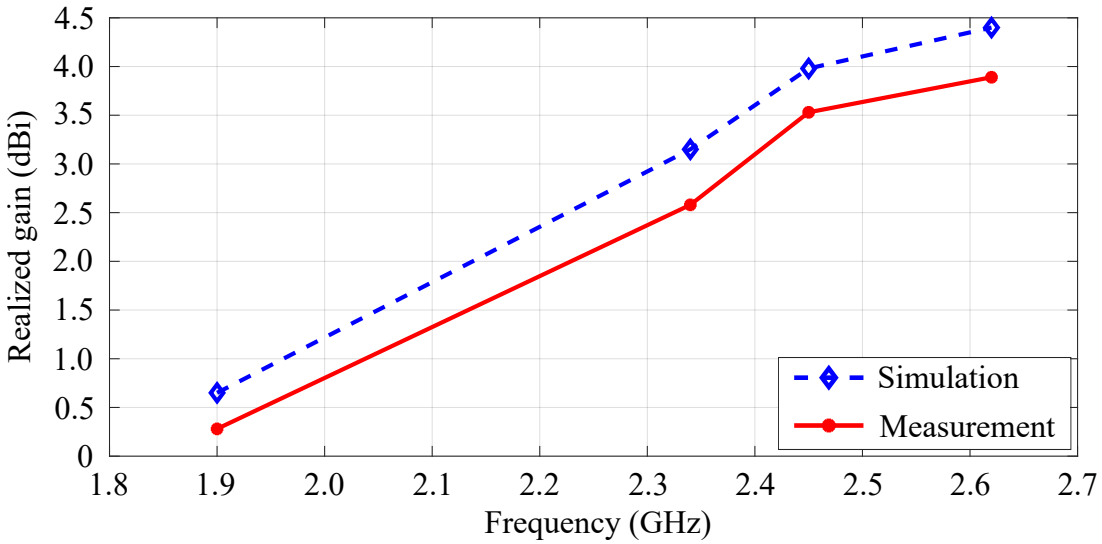

Figure 7.18. Realized gains of the frequency- and polarization-reconfigurable antenna. Simulated and measured realized gain of the frequency- and polarization-reconfigurable antenna for 0° linear polarization.

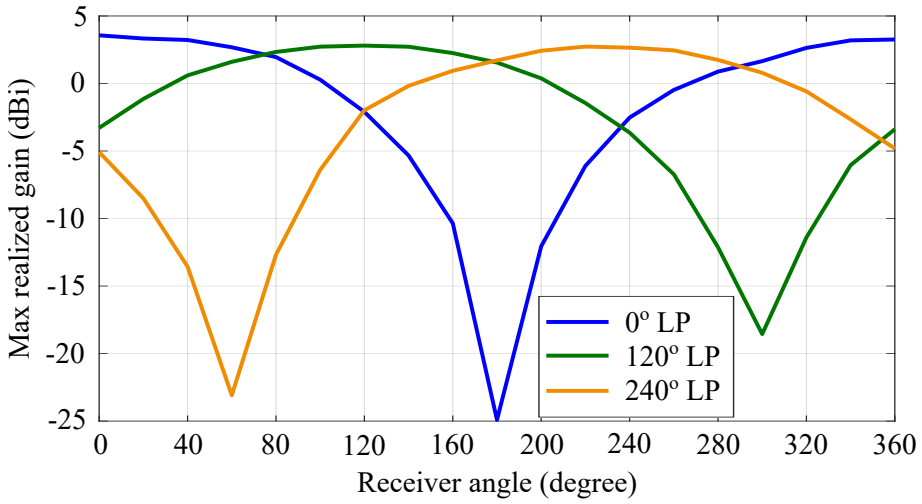

Figure 7.19. Measured maximum realized gains of the frequency- and polarization-reconfigurable antenna for all linear polarization angles. Measured maximum realized gains of the proposed antenna for 0°, 120° and 240° linear polarization at different receiver angles.

of linear polarization, the receiving antenna is rotated by 360° in steps of 20°. The maximum realized gain of the proposed antenna for 0°, 120° and 240° linear polarization at different receiver angles are shown in Fig. 7.19. As expected, the maximum realized gain appears when the receiver is rotated to the angle that matches the corresponding linear polarization states. The slight difference at the peak gain between the linear polarization states can be explained by the imperfection of measurement setup.

7.6 Conclusion

In this chapter, two multi-functional reconfigurable wearable textile antennas have been proposed. The first antenna can switch its pattern between broadside and omnidirectional radiation patterns, and in each of these radiation modes, the frequency of operation can be reconfigured as well. The fractional tuning range of the first antenna working in broadside and omnidirectional modes are 57.3% and 27.2%, respectively. It also excites a fixed higher-order mode with its resonance frequency at 5.8 GHz. This higher band operation in the 5.8 GHz ISM band extends the antenna functionality. The second antenna exhibits a broadside radiation pattern with the ability to switch between 0°, 120° and 240° linear polarization. In each state of linear polarization, the resonance frequency can be also reconfigured over a tuning range of approximately 31.9%. Equivalent circuit models have been used to elucidate the proposed antenna working principle. The two proposed antennas have been designed, fabricated and experimentally characterized to validate the operation concepts.

Chapter 8

Modular Integration of an RFID Sensor with Wearable Antennas

THIS chapter initially presents a novel integration and modularization solution for a passive computational radio frequency identification (RFID) module dedicated for wireless patient monitoring. In the proposed integrated configuration, all the electronic components are encapsulated within the cavity of a textile antenna. This forms a compact protected embodiment suitable for concealment in a hospital garment, with the aim of being unobtrusive to older patients. In addition, modularization of the sensor and textile antenna is introduced through a convenient snap-on attachment method for the computational RFID module. Several wearable modular antennas with a wide -10dB bandwidth aiming to cover the UHF band from 920 to 926 MHz are fabricated and measured. The completed sensors with a combination of the wearable antennas and the RFID module are implemented and tested to validate the design concepts.

In the second part, the effect of the gap in-between a wearer and a wearable antenna operating at 923 MHz is investigated. Due to a high isolation provided by a ground plane, the resonance frequency of the antenna is only slightly altered. The antenna gain and communication range increase to the highest value at a quarter-wave length gap between the antenna and the human body, then decrease when the antenna is moved further.

8.1 Introduction

Modern RFID technology is taking an increasingly important role in a wide range of applications such as structural monitoring [180], item tracking [181] and health care [182]. An important application domain is the use of computational RFID technologies such as the Wireless Identification and Sensing Platform (WISP) and Wearable WISP (W^2ISP) [183] that integrate sensors such as accelerometers with on-board computing capability for wireless monitoring of hospitalized older patients. This approach can be deployed to address concerns such as real-time bed-egress for falls prevention, location tracking and gait analysis [184–189]. Computational RFID technologies enable overcoming some of the most prevalent obstacles in older patient care applications using traditional sensors: Firstly, battery-powered sensor packages are bulky since the battery elements add significantly to their size and weight. Secondly, batteries require maintenance tasks such as replacements or recharging to enable continuous wireless patient monitoring [190–193].

Constructing a practicable computational RFID based batteryless, wearable sensor is challenging. This demands a robust and secure integration of a RFID circuitry module comprising of computing and sensing components with a flexible antenna. Typically the antenna is comparatively larger in size due to the low operating frequency and high performance demands. Ideally, the integration should lead to a compact, small form factor system-in-package capable of meeting wearable application requirements.

There have been several methods reported to integrate the electronics and the antenna together to realize an RF system in a single rigid package [38–40, 194–196]. These solutions usually deployed a stacked structure where the antenna was located immediately on top of the electronics, as shown in Fig. 8.1 (a). In order to provide shielding to the integrated circuit (IC) components from unwanted interactions with the radiators, various approaches have been proposed including additional ground planes combined with fences of vias [38–40, 194, 195] (see Fig. 8.1 (b)) or stacked patch configurations [196]. However, these integration methods increase the overall profile of the device and the complexity of fabrication and maintenance.

For wearable electronic systems, flexible UHF-RFID antennas capable of meeting wearability requirements have been designed [87,197,198], however, they are generally suitable for integration with millimeter-scale ASIC (Application Specific Integrated Circuit) RFID modules used in identification applications. Extending these designs with connection strategies to couple to a significantly larger computational RFID module,

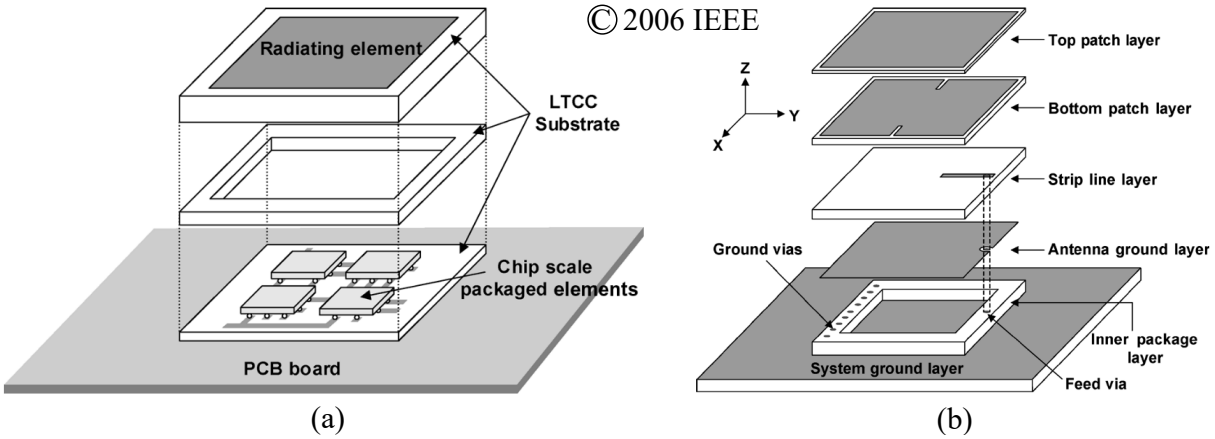

Figure 8.1. Package-level integrated antennas based on LTCC technology. Package-level integrated antennas based on LTCC technology (a) integration configuration and (b) expanded view of the proposed antenna. The images were adopted from [38].

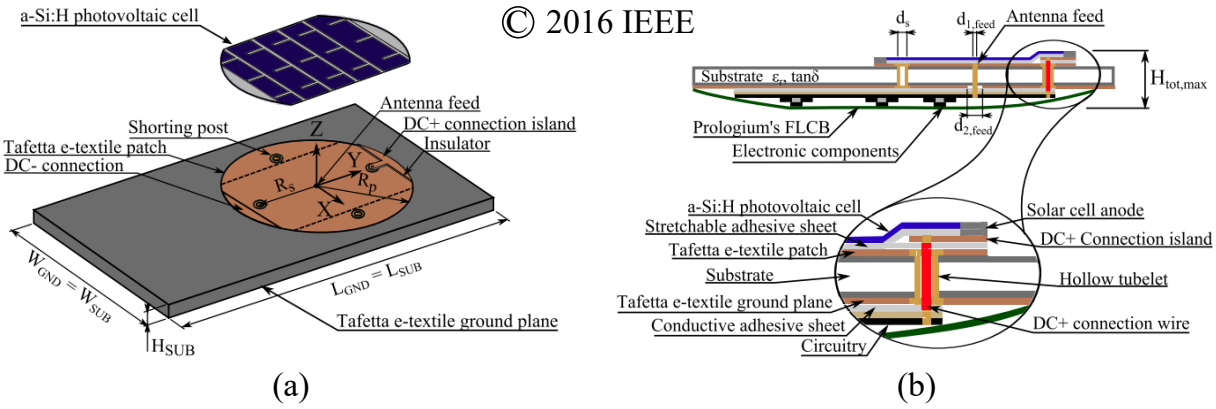

Figure 8.2. Wearable flexible antenna with integrated energy harvester. Wearable flexible antenna with integrated energy harvester (a) top 3-D view and (b) cross-view of the tag including wearable antenna and sensor. The images were adopted from [132].

such as in W^2ISP, leads to sensor packaging prone to be problematic for daily on-body wearing conditions whilst the electronics require separate protections. Although integration approaches for flexible antennas and electronics were reported in [132, 199], they usually placed the electronic components on the immediate periphery of the wearable antennas. An example of a wearable flexible antenna with an integrated energy harvester integrated circuit [132] is shown in Fig. 8.2. As a consequence, the electronics

remained exposed under on-body working conditions and required further protections whilst adding to increase the overall form factor of the device. Additionally, the electronics were bonded permanently to the antennas, which limited the capability for re-using, recycling or appropriately disposing of components. It is therefore highly desirable to co-develop a wearable antenna and a corresponding antenna-electronics integration method to realize a system-in-package solution providing: (i) compactness; (ii) robust connections between the antenna and the electronics; and (iii) secure protections for the electronics module.

In the first part of this chapter, a novel integration strategy to fully integrate a computational RFID module with relatively large size into an antenna resonant cavity is proposed. This helps to securely protect the RFID module while using in the harsh on-body operating environment. Additionally, since the large electronic components are unobtrusive, the wearer's comfort is enhanced [200]. Furthermore, based on an interchangeability of metallic snap-on buttons as presented in Chapter 3, modularization of the sensor and textile antenna is introduced. This is in harmony with simple assembly techniques and facilitates maintenance. Importantly, the resulting customizable configurations, for example, in terms of antenna form factor and materials, can be tailored to suit application requirements, such as performance and disposability. The experimental results demonstrate that the proposed wireless wearable sensor can operate with an antenna broadside gain of 2.74 dBi within a wide bandwidth extending over 893–964 MHz to support seamless worldwide operation across the ultrahigh-frequency (UHF) ISM bands. The wearable sensor embodiment characterized in the context of a monitoring system attains excellent performance in terms of received signal strength, data read rate, and batteryless operational range.

Utilizing the wearable antenna and the complete sensor proposed in the first part, the effect of air gap in-between the antenna and a wearer is investigated in the second part of the chapter. The change of antenna resonance frequency with human body phantom in vicinity is firstly considered. The antenna gains according to different gaps in-between the antenna and the phantom are simulated and measured in an anechoic chamber. Based on the measured antenna gains, the communication ranges of the antenna with integrated RFID module are estimated and measured to confirm the body-to-antenna gap effect of the antenna gain. It is found that, the antenna gain is increased with the wider gap in-between the antenna and human body and reaches the highest value at a quarter-wave length gap.

8.2 Modular integration of a passive RFID sensor with wearable textile antennas

In this first part of this chapter, a system-in-package wearable sensor construction based on a new integration and modularization method is conceptualized for a wearable textile antenna and electronics. The concept, as shown in Fig. 8.3, provides two key unique advantages. First, the novel integration method allows the computational RFID module to be completely integrated into the resonant cavity of a flexible textile planar inverted-F antenna (PIFA). This permits embedded and secure protection for the electronics from the dynamically changing wearing conditions. The second noticeable feature of the concept is the modularization, which facilitates robust interchangeable electrical and mechanical snap-on connections between the electronics and different antenna modules. This enables various configurations with customizable modular antenna designs for meeting different application requirements such as convenient reuse, recycling or disposal of components. It is believed that, these two main distinctive advantages have not been investigated before in literature. The results presented in this section have been published in [48].

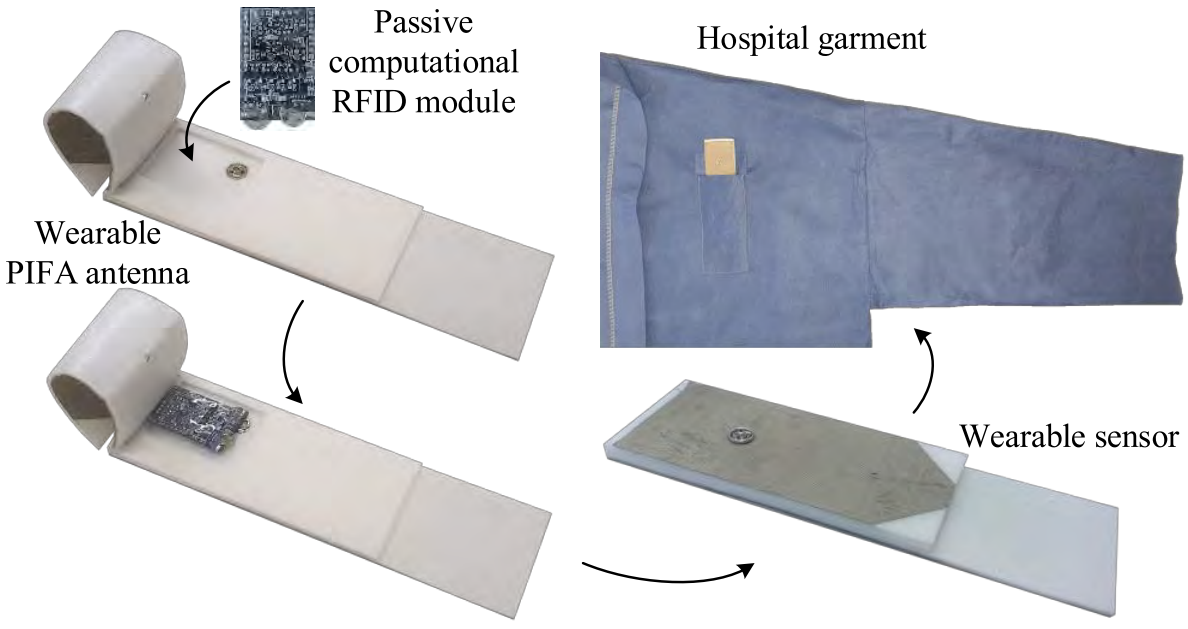

Figure 8.3. The proposed integration and modularization concept. The proposed integration and modularization concept and one of its practical application: encapsulating the computational RFID module into a flexible textile antenna to form a compact wearable sensor, which can be inserted into a hospital garment pocket.

8.2.1 Monitoring system requirements

System configuration

A typical patient monitoring system configuration based on a wearable RFID sensor is shown in Fig. 8.4 [185]. The three primary components of the system include a batteryless wearable sensor containing a computational RFID module (referred to as "RFID module" henceforth for simplicity) and its antenna, a reader with transceiving antennas and a back-end-system. The focus of this work is on the integration and modularization of the RFID module and its antenna.

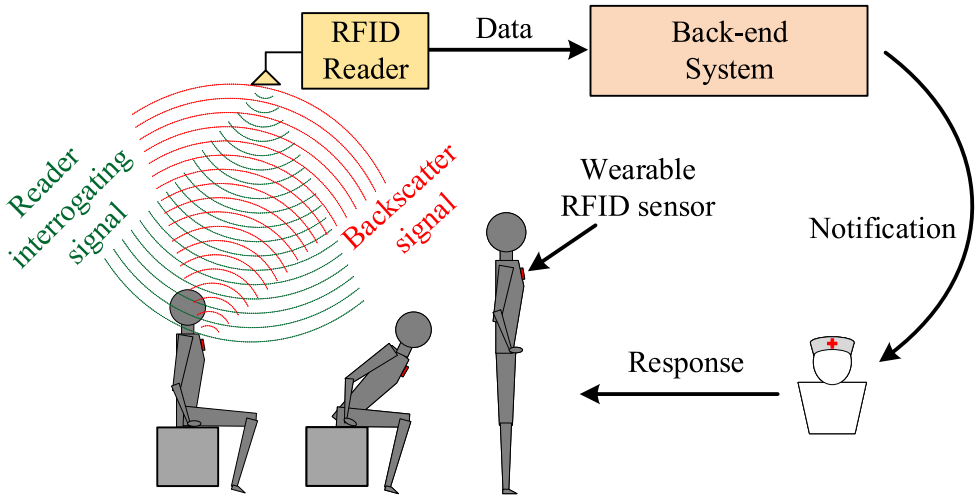

Figure 8.4. Patients monitoring system based on wearable RFID sensor. Patients monitoring system based on wearable RFID sensor for bed-egress and chair-egress movements detection of older patients in hospital ward rooms.

In a patient monitoring application, the wearable sensor is used to detect bed-egress and chair-egress movements of older patients in hospital ward rooms [185, 186]. The RFID module includes an accelerometer for capturing patient movement information such as lying to sitting, sitting to lying, or sitting to standing. The RFID reader interrogates and energizes the sensor and receives the reflected signal with the movement information from the wearer. The received signals are processed and stored in the back-end system. It is important to carefully select the RFID reader antenna position to maximize the coverage of the sensor in the monitored room.

Wearable sensor design requirements

As reported in [201] and [202], for an effective deployment where sensors are likely to be accepted by older people, wearable sensors are expected to be small, flexible, lightweight and preferably batteryless. Therefore, several important requirements need to be considered while identifying an appropriate integration solution and designing a corresponding modular antenna for the RFID module [203].

- **Materials**: Flexible and light-weight materials are chosen to realize the antenna for the RFID module. This is paramount to wearability for older patients, with the sensor being preferably mounted on the clothes or integrated as a part of them. A low cost of the antenna is also required for mass deployment in hospital environments.

- **Form factor**: The size of the antenna is expected to be as compact as possible, however keeping in mind a favorable trade-off between antenna miniaturization and acceptable performance.

- **Form factor**: The size of the antenna is expected to be as compact as possible, however keeping in mind a favorable trade-off between antenna miniaturization and acceptable performance.

- **Reliability**: The wearable sensor is required to maintain acceptable performances under different operation conditions such as bending of its antenna to follow body movements. Thus, it is highly desirable to protect the RFID module in a secure way. Additionally, the connection between the antenna and the RFID module needs to be robust. Last but not least, a wideband antenna is preferable to maintain satisfactory operation under bending conditions.

- **Operation frequency**: The sensor is working in the UHF band of the ISM band, which extends from 920 to 926 MHz in Australia (as regulated by the Australian Communications and Media Authority).

- **Antenna input impedance**: The RFID module's input impedance is $78 + 16j\ \Omega$, hence its antenna should be ideally designed to have a conjugate input impedance of 78 - 16j Ω. For simplicity of design and simulations, the input impedance at the feeding port can be approximated at 78 Ω instead of $78 - 16j\ \Omega$ since the impedance mismatch is inconsequential.

- **Read range**: The proposed antenna needs to enable an appropriate read range for patient monitoring. The read range can be estimated for impedance-matched antennas by using the classical Friis transmission equation [204]

$$P_R = P_T - 20log(\frac{4\pi d}{\lambda}) + G_T + G_R - L_P, \tag{8.1}$$

where P_T = 30 dBm is the power transmitted by the reader antenna, λ = 324.8 mm is the wavelength in free space at 923 MHz, G_T = 6 dBi is the realized gain of the reader antenna, G_R is the realized gain of the tag antenna, and L_P = 3 dB is the polarization loss which is caused by the polarization mismatch between the circularly polarized (CP) reader antenna and linearly polarized (LP) sensor antennas. P_R = −9.5 dBm is the minimum power required to turn the sensor on. Compared to achieved read ranges of 3 and 4 m demonstrated in [88] and [65] respectively, a competitive read range of at least 4 m is targeted here.

8.2.2 Integration and modularization

Integration approach

The main idea of the proposed integration solution is to co-design a low-profile low-Q-cavity-based antenna and an appropriate embedding approach for the electronics, aiming to integrate the RFID module totally inside the antenna cavity. By doing this, a compact sensor structure promoting sturdy protection for the electronics as well as robust antenna-to-electronics connection can be achieved. A low-Q antenna is required so that it is insensitive to and does not affect the embedded electronics. The detailed configuration of the proposed integration solution is illustrated in Fig. 8.5, and described in the following.

The RFID module is fully integrated inside the resonant cavity of the textile antenna and excites the antenna using metallic snap-on button connections. Commercial snap-on buttons have proven to be suitable as mechanical and RF connectors for textile antennas, with demonstrations showing that they can maintain satisfactory performance up to 10 GHz [28, 133]. As illustrated in Fig. 8.5, two male snap-on buttons are directly soldered to the two terminals of the antenna port of the RFID module. The top terminal is electrically connected to the antenna top layer by engaging the male button with its female counterpart, whereas the bottom terminal connects to the antenna ground plane in the same way. This configuration allows a detachable and attachable antenna-to-electronics connection. The antenna substrate thickness should be sufficiently large

to accommodate the RFID module. The bottom female snap-on button is sewed onto the ground plane using conductive threads for a permanent RF connection. The top female button is firmly affixed to the antenna top metal layer through the pull force from the engaged male button on the RFID module, noting that the required disengaging force is approximately 3 N [88].

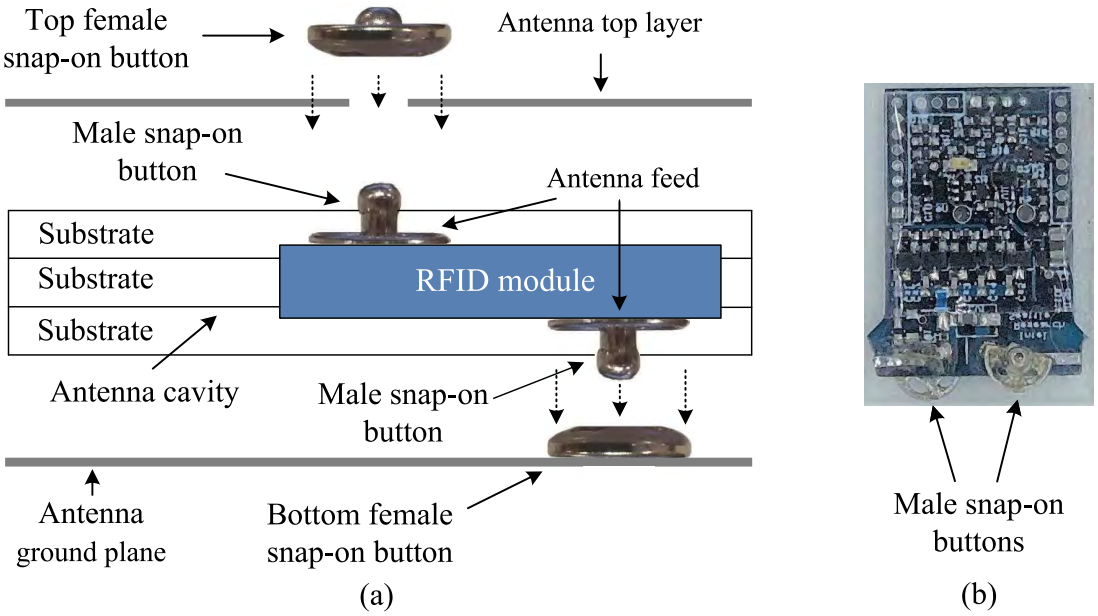

Figure 8.5. Configuration of the proposed integration solution. (a) Configuration of the proposed integration solution, and (b) the RFID module with two male snap-on buttons soldered as the antenna feed.

Antenna design

The chosen antenna topology is a PIFA which has a low-Q cavity with open boundaries on its sides. Importantly, it combines compactness, low profile and wide bandwidth features [135]. Additionally, a PIFA rests on a ground plane which is critical to minimize back radiation and interaction with the human body [64].

A general structure of the proposed antenna is illustrated in Fig. 8.6, showing the ground plane, a substrate with 3 layers of foam, a quarter-wave patch and a shorting wall. A highly flexible and light-weight Cumming Microwave PF-4 foam with a thickness of 1.6 mm, relative permittivity ε_r = 1.06 and loss tangent tanδ = 0.0001 is selected as substrate material. A biocompatible, flexible and highly electrically conductive silver-coated nylon Rip-stop fabric with a sheet resistance of 0.01 Ω/square

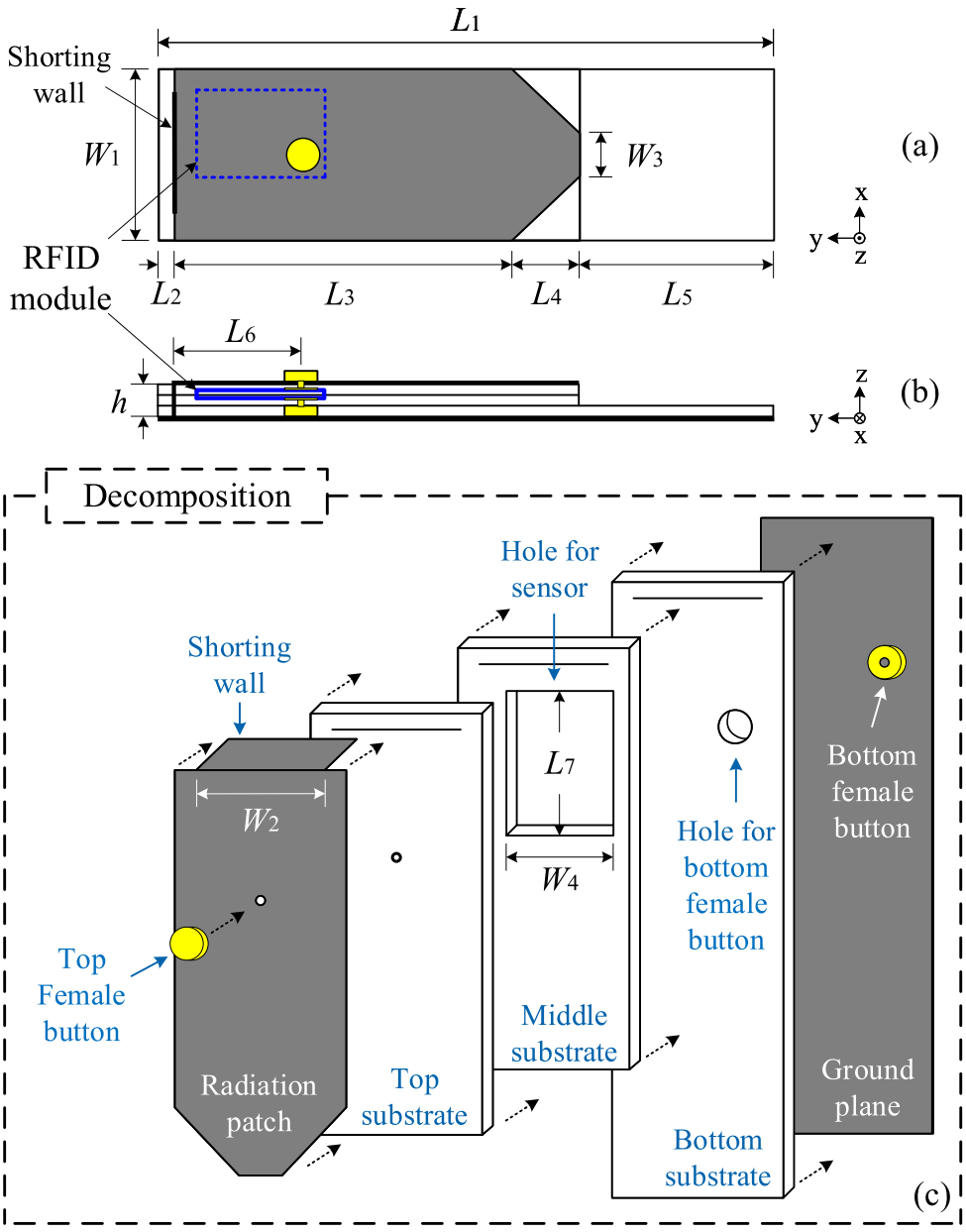

Figure 8.6. General structure of the proposed antenna. General structure of the proposed antenna. (a) Top view, (b) side view, and (c) antenna configuration. Dimensions (mm): $L_1 = 115.0$, $L_2 = 3.0$m, $L_3 = 63.0$, $L_4 = 12.0$, $L_5 = 36.3$, $L_7 = 25.0$, $W_1 = 32.0$, $W_2 = 24.0$, $W_3 = 8.0$, $W_4 = 20.0$ and $h = 4.8$.

is adopted to realize the ground plane, quarter-wave patch and shorting wall. The proposed antenna is simulated using CST Microwave Studio 2018.

A rectangular hole is cut in the middle substrate to tightly fit the RFID module. This hole combined with the two female snap-on buttons help to perfectly maintain the

module immobile inside the antenna. The top substrate and quarter-wave patch both have matching holes for the top male snap-on button pin to go through.

The resonance frequency of a PIFA can be approximately calculated as [85]

$$f = \frac{c_0}{4(L_3 + L_4 + W_1 - W_2 - h)\sqrt{\varepsilon_r}} \tag{8.2}$$

where c_0 is the velocity of light in free space, L_3 and W_1 are the length and width of resonant patch, W_2 is the width of the shorting wall, h and ε_r are the thickness and relative permittivity of the substrate. Equation (8.2) indicates that the resonance frequency is broadly inversely related to the radiation patch size and the square-root of the relative permittivity. It is also noted that reducing the shorting wall width decreases the resonance frequency. In this concept, the shorting wall is designed slightly narrower than the antenna width by 8 mm (4 mm on each side), as displayed in Fig. 8.6 (c) to decrease the patch area while still providing a strong mechanical support for the antenna. Considering the trade-off between antenna gain and size, this antenna has been parametrically optimized using CST to the dimensions listed in the caption of Fig. 8.6.

- **Feeding design**: In simulation, a discrete voltage port vertically connected between the patch and the ground is used to feed the antenna. As one of the most fundamental criteria for our antenna design, an appropriate antenna feeding point to achieve approximate impedance matching at the operating frequency at 923 MHz is found through simulation and it sets the locations of the snap-on buttons.

- **RFID module integration position**: The best location to load the RFID module as shows in Fig. 8.6, is determined based on several reasons. Firstly, placing the electronics close to the shorting wall contributes to the robustness of the sensor, due to the mechanical support offered by the shorting wall. Secondly, the length orientation of the module is the same as the one of the antenna which minimizes the space requirement for integration. Finally and most importantly, the chosen location close to the shorting wall lowers the risk of interference between the antenna and the module within the antenna cavity. This is illustrated in Fig. 8.7: the E-field strength becomes weaker when it is closer to the shorting wall. Taking advantage of this feature of PIFAs removes the need for further shielding methods to protect the RFID module from interferences. Figure 8.8 shows the simulated

antenna reflection coefficients with and without the module in the cavity, illustrating that the IC has an insignificant effect on the matching. The IC position and the detailed connection between the antenna and the RFID module is shown in Fig. 8.9.

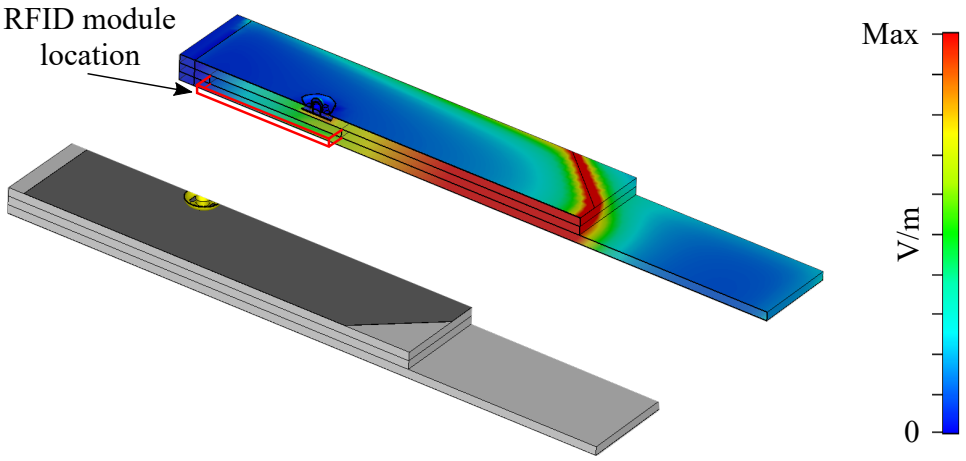

Figure 8.7. Exploded view of the electric field distribution inside the antenna cavity. Exploded view of the electric field distribution inside the antenna cavity.

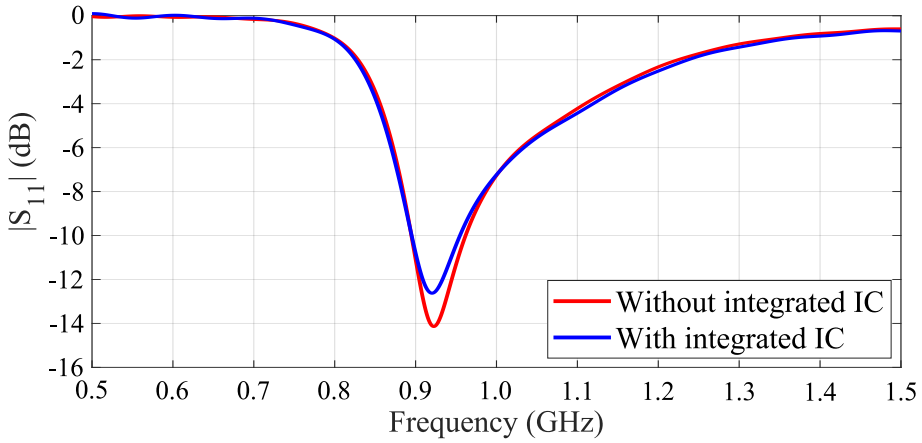

Figure 8.8. Simulated reflection coefficients of the antenna. Simulated reflection coefficients of the antenna with and without the integrated IC.

– **Patch geometry**: The antenna is designed to have a rather elongated shape so that it can be easily fitted in a small pocket. Furthermore, the corners near the open patch aperture are cut for practical considerations as explained in the following: In order to allow attaching/detaching the module into/out of the antenna, the top substrate needs to be opened, as shown in Fig. 8.9 (a).

In practice, the use of fabric glue to connect the top substrate to the middle one is therefore not appropriate, as it prohibits the electronics from being interchangeable. Therefore, the antenna patch is cut at its two open corners to leave the space to accommodate two pairs of plastic snap-on buttons. These plastic buttons provide a detachable/attachable fastening fixture for the antenna cavity without affecting the antenna performance. The practical sensor with these snap-on buttons as fixture is shown in Fig. 8.10.

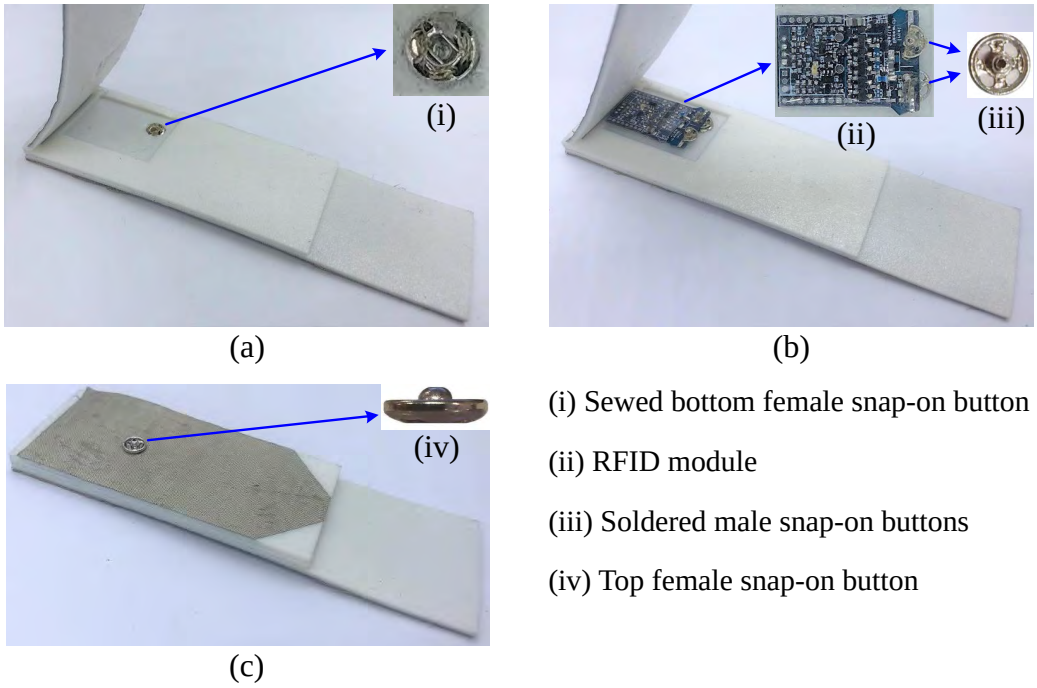

Figure 8.9. Integrated sensor implementation. Integrated sensor implementation: (a) An antenna without a RFID module, (b) integrating the RFID module into the antenna, and (c) completed sensor with the top substrate closed.

- **Extended ground plane**: Besides an effect of isolating the antenna from the body [205], an extended antenna ground plane can also contribute significantly to widen the bandwidth of PIFAs [206]. As illustrated in Fig. 8.11, the longer the extended ground plane is chosen, the wider the antenna bandwidth becomes. A sufficiently wide bandwidth is desirable to ensure that the antenna will operate within the system-specific bandwidth under different working conditions. However, considering the trade-off between the bandwidth and the antenna size, an extended ground with a length L_5 = 36.3 mm has been selected for this typical

8.2.2 Integration and modularization

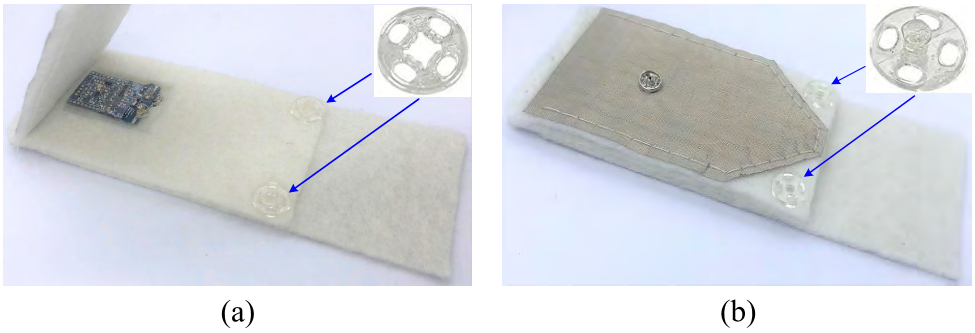

Figure 8.10. Modular antenna fabricated using a felt substrate. Modular antenna fabricated using a felt substrate. (a) The top substrate is open showing the two plastic female snap-on buttons, and (b) completed sensor with the top substrate closed with plastic male snap-on buttons as mechanical fixtures.

modular antenna design, which provides an impedance bandwidth of approximately 7.6%, thus generously covering the required bandwidth of 0.65%.

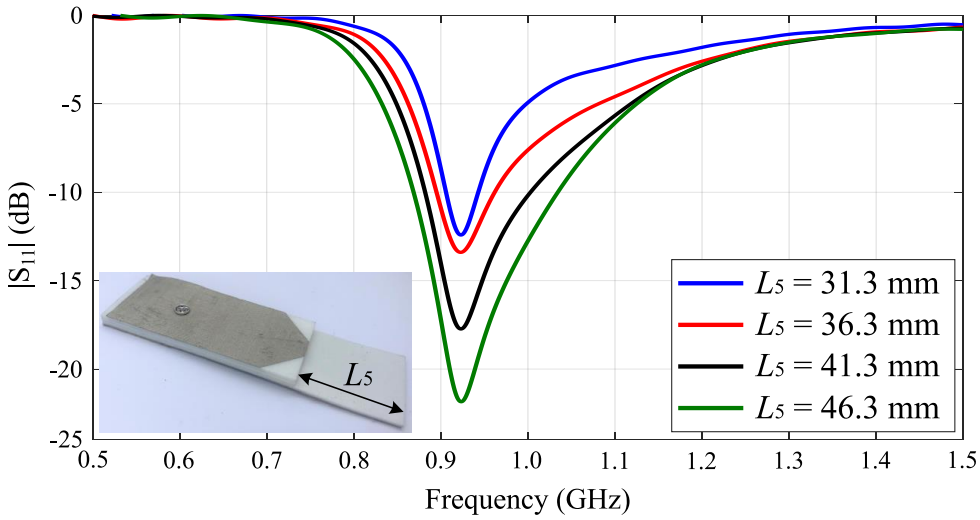

Figure 8.11. Reflection coefficients with different extended ground plane length. Simulated antenna reflection coefficients with different extended ground plane length (L_5).

- **Specific Absorption Rate (SAR)**: The simulated SAR of the proposed antenna for 500 mW input power at 923 MHz is 1.24 W/kg which is below the limit of 2 W/kg for 10 g of tissue [207]. Furthermore, considering that the output power of a 16-bit low power microcontroller (MSP430F2132) inside the RFID module is 0.55 mW [208], the effect of back radiation to the wearer is deemed to be negligible.

Modularization

An utilization of snap-on buttons in the integration process allows to easily and repeatedly attach/detach the rigid electronics into/out of the flexible antenna [37]. It therefore allows convenient interchange of customized antennas for different system requirements. To demonstrate the modularity of the concept, we have considered three alternative ways to apply the sensor to a disposable hospital garment, with two realizations based on a reusable antenna while the other considers disposable antennas. This section describes the pros and cons of each method.

- **Reusable antenna**: For reusable implementation of the antenna, a purpose-made pocket is added to the garment to accommodate the sensor. Figure 8.12 shows the integration of the sensor in such a pocket for chest area placement [5]. It is emphasized that the pocket can also be sewed on other locations of the garment such as the shoulder area. Figure 8.13 illustrates two typical on-body cases with the sensor placed either on the chest or the shoulder where the reader antenna is mounted on side wall or on the ceiling respectively. When the garment is changed daily, the sensor can be removed from its pocket and placed into new clothes. This method is simple as it only requires a pocket with appropriate dimensions sewed onto the garment. However, the number of sensor re-usage will be limited as it can be damaged by manipulation or patient's movements.

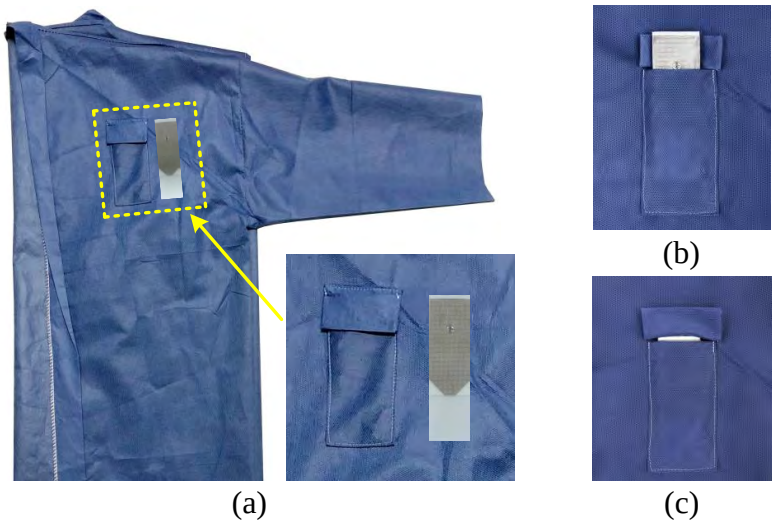

Figure 8.12. Sensor in a hospital gown. Sensor in a hospital gown. (a) Disposable hospital garment with the pocket for sensor, (b) sensor inserted in to and (c) completely in the pocket.

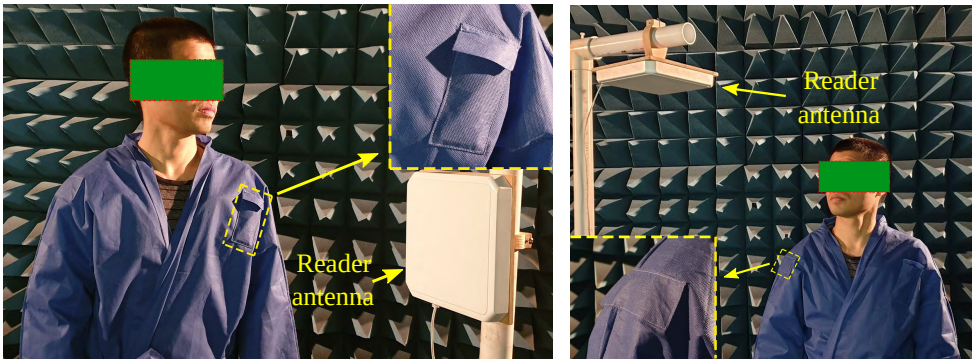

(a) (b)

Figure 8.13. Two practical on-body cases of using the sensor. On-body cases: (a) Sensor placed on the garment chest area while the reader antenna is mounted on the side wall, and (b) Sensor placed on the garment shoulder area while the reader antenna is mounted on the ceiling.

- **High gain antenna**: The practical RFID system setups available in this project have been previously shown in [209] with two different room sizes 3.3 m $\times$ 4 m and 4 m $\times$ 5 m. A minimum of three RFID reader antennas has been proven to fully cover the larger room. A solution to reduce the number of RFID reader antennas, or alternatively to expand usage to larger rooms is to increase the read range of the RFID sensor by improving the antenna gain. For demonstration, we aim to achieve a read range of 5.5 m corresponding to common hospital room sizes. Based on equation 8.1 the required antenna gain is then approximately 3.7 dBi. To achieve this gain in the considered topology, an antenna with nearly double width is necessary. It is noticeable that even with the larger area of 125 mm $\times$ 60 mm, the sensor remains more compact than the one reported in [65] which required a 200 mm $\times$ 200 mm extended ground plane.

- **Disposable antenna**: An alternative solution is utilizing disposable antennas. In this scenario, the antenna can become part of the disposable hospital garments by being sewed directly onto the garment. After daily use, only the RFID module will be detached and re-used with a new antenna on a new garment. To ensure the disposability, the antenna materials need to be as low-cost as possible while maintaining acceptable antenna performance.

  Felt has been proven to be an appropriate substrate combining low cost, flexibility and robustness [64, 136, 210]. It can therefore be an economical replacement for PF-4 foam. The selected felt substrate has a thickness of 1.8 mm, relative

permittivity ε_r = 1.2 and loss tangent tanδ = 0.025. Due to the overall thicker substrate, a wider bandwidth can be achieved, however at the cost of a slightly more voluminous antenna compared to the counterpart using PF-4 foam.

8.2.3 Experimental results

For demonstration of interchangeability of the proposed integration solution, three typical modular antennas with different size, gain and materials are experimentally characterized. These antennas include a narrow foam antenna designed for small hospital rooms, a wide foam antenna with a higher gain for large rooms, and an antenna made of felt for disposability, as depicted in Fig. 8.14. These three wearable antennas are characterized in isolation first, before being tested with the RFID module to assess their system performance.

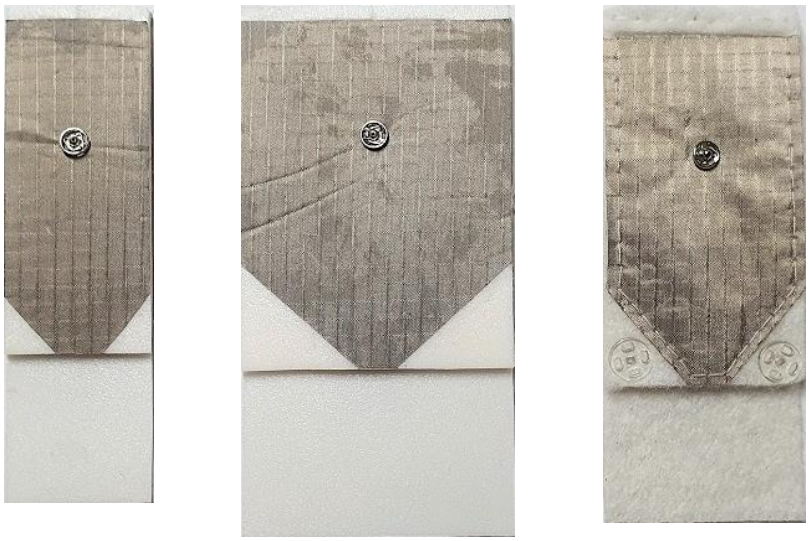

(a) (b) (c)

Figure 8.14. Three fabricated modular antennas. Three different fabricated modular antennas. (a) Narrow foam antenna (b) wide foam antenna, and (c) felt antenna.

Modular antennas fabrication

The antenna conductive parts are accurately cut from the metallized fabric using a laser milling machine (LPKF: Protolaser S). To ensure seamless electrical patch-to-ground connection with mechanical robustness, the antenna patch, shorting wall and ground

plane are realized as one piece of conductive fabric. This conductive piece is then precisely folded (as shown in Fig. 8.15) before being attached to the substrates to form a completed antenna. Slits are cut through the three substrates to allow the shorting wall to go through. For antennas using smooth-surface foam material, all antenna parts are able to be glued together using fabric glue (Tiger Grip from Helmar). In contrast, due to the rough surface of felt material, the various antenna parts are sewed together using cotton threads, except for the top substrate which is attached to the rest of antenna using plastic snap-on buttons.

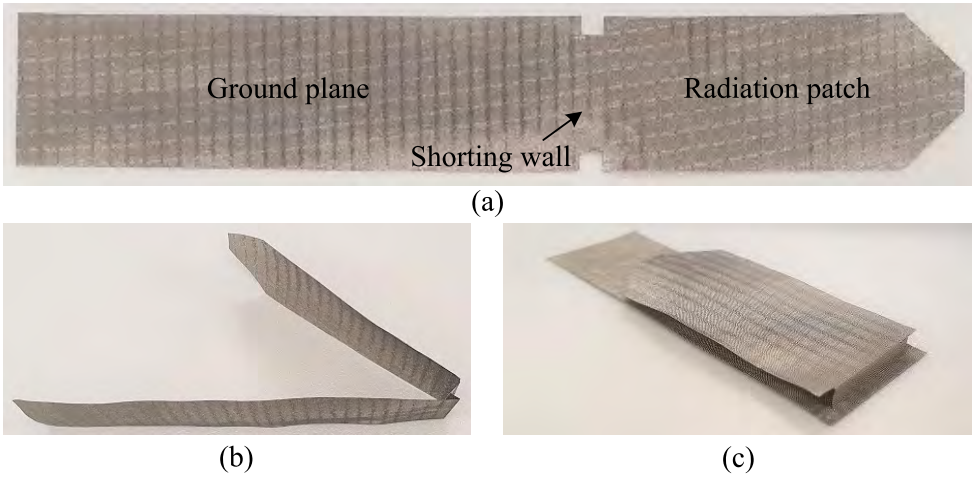

Figure 8.15. Fabrication process of the antenna conductive parts. Fabrication process of the antenna conductive parts: (a) the antenna conductive parts are cut as one piece of metallized fabric, (b) folding process, and (c) completed antenna conductive layers.

Antennas performance

The antenna performance measurements were carried out by connecting the center pin and the outer conductor of a 50 Ω coaxial cable to the patch and ground plane respectively using a pair of male snap-on buttons. By using this feeding method, the antenna top substrate and radiation patch are consequently lifted up to accommodate the coaxial cable (see an inset in Fig. 8.16). It is confirmed by simulations that, with the 50 Ω coaxial cable feeding the antenna from the side, the operating frequency is slightly shifted to 927 MHz compared to 923 MHz while using 78 Ω discrete port (as shown in Fig. 8.16). It is therefore appropriate to experimentally characterize the antenna performance using the 50 Ω coaxial cable without changing the antenna dimension. For brevity, only the results for the narrow foam antenna are explicitly presented in full, while the other results are summarized in tables.

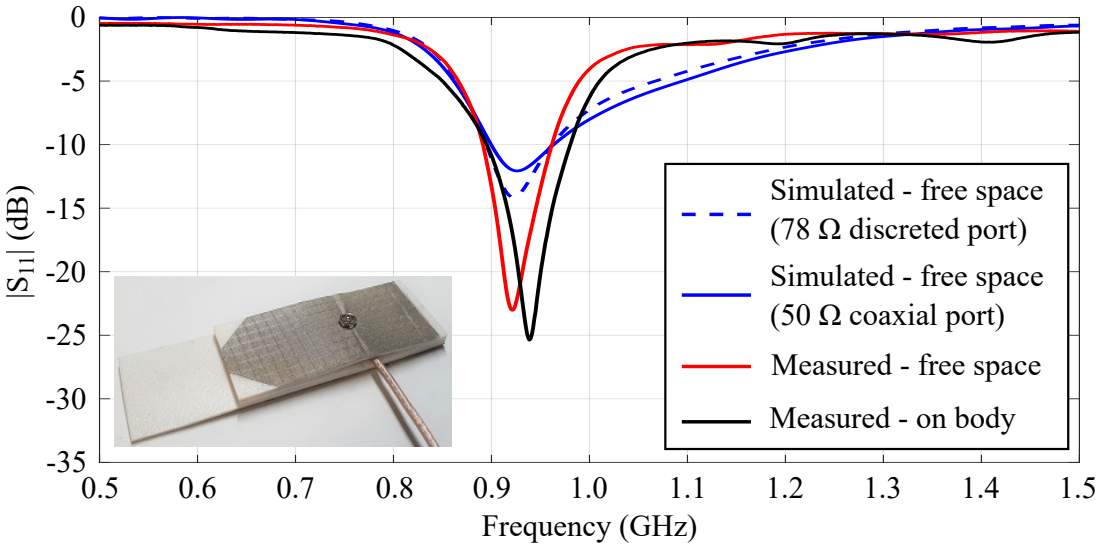

Figure 8.16. Reflection coefficents of the smallest foam antenna. Measured and simulated reflection coefficients of the smallest foam antenna. Inset: Antenna under test with a coaxial cable connected to a VNA.

Table 8.1. Reflection coefficients of the three antennas. Reflection coefficients of the three considered antennas

Antennas	Measured frequency (MHz)		Bandwidth (MHz)	
	Free-space	On-body	Free-space	On-body
Narrow foam	921	938	893 – 964	895 – 980
Wide foam	922	930	877 – 966	882 – 970
Felt	923	935	860 – 1051	877 – 1065

- **Reflection coefficient**: The simulated and measured reflection coefficients of the smallest foam antenna are displayed in Fig. 8.16. The measured center frequency and impedance bandwidth of three antennas are listed in Table 8.1, showing that the antennas in free-space cover the UHF ISM Australian band (920 - 926 MHz). A discrepancy occurs when placing the antenna on the human body, with the 10-dB impedance bandwidth being shifted upward. Nevertheless the whole required frequency band is still covered with sufficient margin.

- **Radiation pattern and gain**: The simulated and measured radiation patterns of the narrow foam antenna in the xz-plane (H-plane) and yz-plane (E-plane) at 923 MHz under free-space and on-body conditions are shown in Fig. 8.17. In

on-body condition simulation, a human body model with relative permittivity ε_r = 26 and loss tangent tanδ = 0.3 is employed. These material characteristics are similar to those of a human body phantom TORSO-OTA-V5.1 from SPEAG, as used in measurement. The antennas are placed at the distance of 5 mm from the human body which is slightly larger than the usual 3 mm distance. This is to take into account the fact that one-size-fit-all hospital gowns are normally larger than the patient body size for comfort and simple supply. The simulated and measured gain of three antennas in free space and on-body conditions are listed in Table 8.2. The discrepancies between simulation and measurement results are due to the imperfection of fabrication and experimental uncertainties.

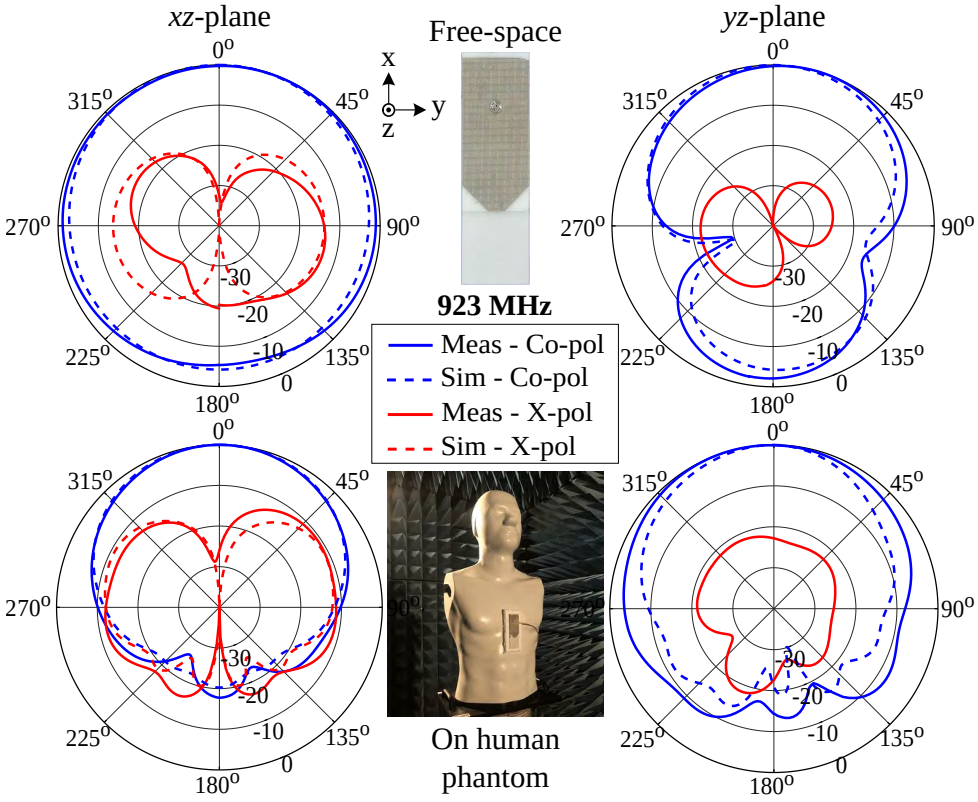

Figure 8.17. Radiation patterns the smallest foam antenna. Measured and simulated normalized radiation patterns the smallest foam antenna in free space and on a human phantom.

Sensor performance

Section 8.2.3 has illustrated that the proposed antenna performance is acceptable when measured without an integrated RFID module. In this section, the performance of

Table 8.2. Realized gains of the three antennas. Simulated and measured realized gains of the three considered antennas

Antennas	Free space gain (dBi)		On-body gain (dBi)	
	Simulated	Measured	Simulated	Measured
Narrow foam	2.94	2.74	2.17	2.33
Wide foam	3.81	3.75	3.41	3.23
Felt	2.70	2.61	1.92	1.75

the modular antennas with its integrated electronics in practical applications is investigated to validate the design. Several important system parameters measuring the wearable sensor performance are evaluated, namely the received signal strength indicator (RSSI), read rate and read range. These parameters are obtained using an Impinj Speedway R420 RFID reader. To minimize the environmental effects on the device performance, the measurements are conducted in the controlled environment of an anechoic chamber. For comparison, we also measure the sensor reported in [65] in identical test conditions.

- **Receive signal strength indicator**: The RSSI indicates the power level of the returned signal from the sensor detected by the reader. The RSSI values are measured at different distances between the reader and the sensor from 0.5 to 2.0 m without human body in its vicinity. The RSSI values of the three proposed sensors and the design in [65] are compared in Fig. 8.18. The results indicate that all of the three proposed sensors receive stronger signals than that of the previous sensor.

- **Read rate**: The sensor read rate is the number of successful individual read by the RFID reader per second. The read rate will vary with the level of transmitted power. A read-rate measurement is taken at a fix distance of 1 m between the antenna and RFID reader. As clearly seen in Fig. 8.19, all the three considered antennas provide significantly better read rates than the previous design when the transmit RF power level is higher than 18 dBm. It is noted that all of the sensors are unreadable when the transmit power level is below 18 dBm for the chosen distance.

8.2.3 Experimental results

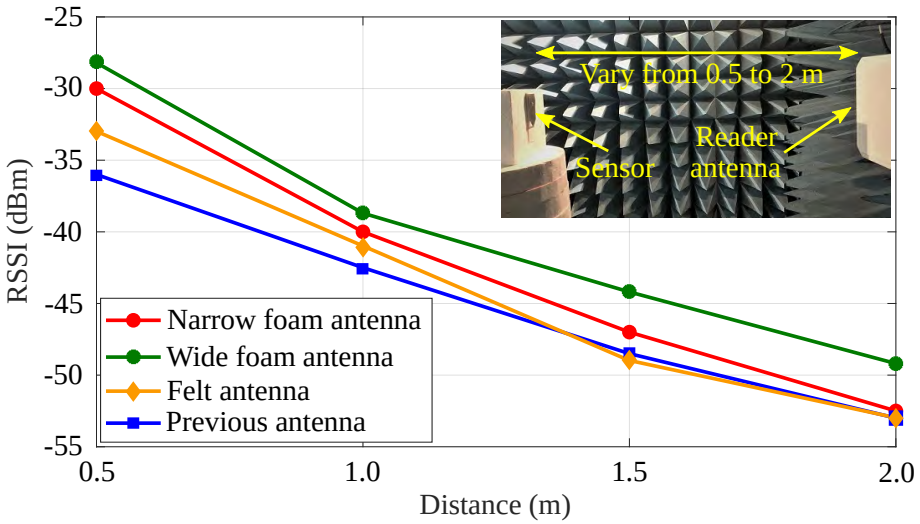

Figure 8.18. RSSI versus distance in the anechoic chamber. Measured RSSI versus distance in the anechoic chamber without a human body in vicinity. Inset: Measurement setup.

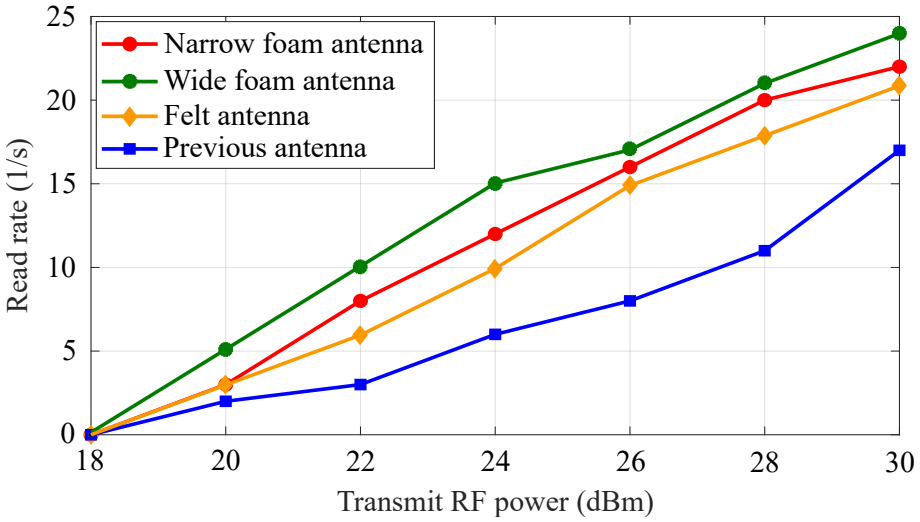

Figure 8.19. Read rates versus transmitted power. Measured read rates versus transmitted power at a fixed distance of 1 meter in the anechoic chamber without a human body in the vicinity.

- **Read range**: The sensor read range is defined as the maximum distance from the RFID reader to the sensor for which successful communication between them is established. In this study, the read range is measured when the sensor is operated with and without the human body in proximity. The read range is also tested under two different measurement setups where the reader is either mounted on the chamber wall or its ceiling, denoted as Case 1 and Case 2 respectively. These two cases correspond to two most suitable positions for the sensor on the human

body, which are on the chest and on the shoulder areas. The measurement setups and the corresponding maximum measured read ranges of the narrow foam antenna are shown in Fig. 8.20(a) and Fig. 8.20(b). As shown in Fig. 8.20(a) for Case 1, the measured maximum read ranges are 4.5 and 4.2 m for the free-space and on-body conditions, respectively. These results are in good agreement with the calculated read ranges based on (8.1). For Case 2 as depicted in Fig. 8.20(b), the sensor is measured while the reader antenna is mounted on the ceiling at a height of 2.2 m above. In this case, the maximum read range suggests that the sensor can function within a circle of 2.5-m and 2.1-m radius centered at the reader antenna, for the free-space and on-body conditions respectively. The detailed read range values of all three antennas for these two measurement setup cases are listed in Table 8.3.

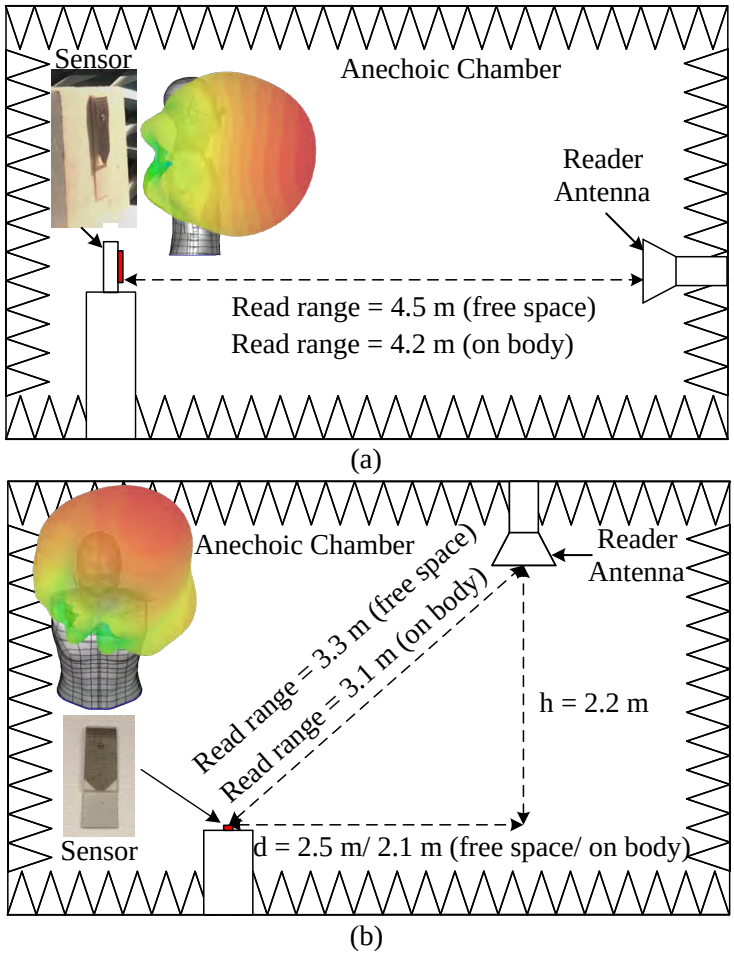

Figure 8.20. Read range measurement setup. Read range measurement setup. The reader antenna is mounted on (a) the side wall and (b) the ceiling of the chamber. Typical 3D radiation patterns of the antenna worn on the body for corresponding scenarios are displayed in the insets.

Table 8.3. Read range of the three antennas. Read range results of the three considered antennas

Antennas	Read range in case 1 (m)		Function circle radius (d) in case 2 (m)	
	Free space	On body	Free space	On body
Narrow foam	4.5	4.2	2.5	2.1
Wide foam	5.4	5.2	3.7	3.5
Felt	4.1	3.7	2.2	2.0

8.2.4 Summary on a modular antennass with integrated RFID sensor

The first part of this chapter has proposed a solution to fully integrate a computational RFID module into a modular wearable textile antenna. Compared to the designs where the electronics are placed on the periphery of the antenna, the proposed configuration with the electronics completely inside the antenna cavity leads to a smaller and more robust sensor. Additionally, the modularized design allows conveniently interchanging customized antennas for different applications. To validate the integration and modularization concept, three different modular antennas dedicated for three typical applications have been modeled, fabricated and experimentally characterized. As expected, all the fabricated sensors have demonstrated excellent performance in the system, either integrated into a reusable or a disposable antenna. The proposed concept enables a concealed integration of the whole sensor into the garment, which can contribute to improve end-users' perception and technology acceptance by the patients.

8.3 Body-to-antenna gap effect on the wearable antenna performance

The UHF textile antenna and the completed sensor proposed in Section 8.2 are highly promising to be used in hospitals as patient monitoring devices due to their advantageous features. The monitoring sensor can be easily integrated into a hospital garment as demonstrated in Section 8.2.2. However, UHF antennas are affected more significantly by the human body than the antennas operating at higher frequencies, because the free-space wavelength is comparable with the human body parts on which the antennas are mounted [136].

Considering the dynamic nature of wearing operation conditions, the performance of wearable antennas is impacted by a number of detuning effects including bending or crumpling as well as moisture effects [210, 211]. For health-care monitoring in a hospital environment, patients typically wear gowns which are usually one-size-fit-all. This will cause the spacing between the antennas and the patient's body to vary significantly with body movement. This motivates the study of the effect of the gap between the antenna and the wearer.

In this part of the chapter, the influence on the antenna performance owing to the gaps in-between the wearable antenna and the human body is investigated. Importantly, the considerations are not limited to the resonance frequency variations but also include the gain of the antenna and the communication range. The results presented in this section have been presented as a conference contribution in [49].

8.3.1 Experiment setup

The wearable antenna used in the experiment is a modular textile antenna reported in Section 8.2. The salient advantage of the concept is the complete integration of the RFID module into the tag antenna. Using this particular antenna in the present investigation allows not only to measure the reflection coefficient and gain in various conditions, but also to characterize the communication range of the antenna by connecting it with a batteryless RFID module.

A square homogeneous human body phantom and a human body phantom TORSO-OTA-V5.1 from SPEAG are used in the measurement of reflection coefficient and antenna gain, respectively. The distance between the wearable antenna and the phantom is varied in a controlled manner by using a white foam (with properties similar to air) with different thicknesses as spacer.

8.3.2 Experimental results

Figure 8.21 illustrates the measured reflection coefficients when the gap between the human body and the wearable antenna is varied. Although a high isolation from the antenna to the human body is provided by a ground plane, the values of measured $|S_{11}|$ parameters are slightly changed for all the considered distances. This can be explained by the long wavelength of the UHF band and the limited extent of the ground

plane, which exhibits an identical width to the radiating patch and the substrate. However, the bandwidth is sufficiently wide (895 - 980 MHz) to cover the required bandwidth for all the considered gaps between the antenna and the phantom.

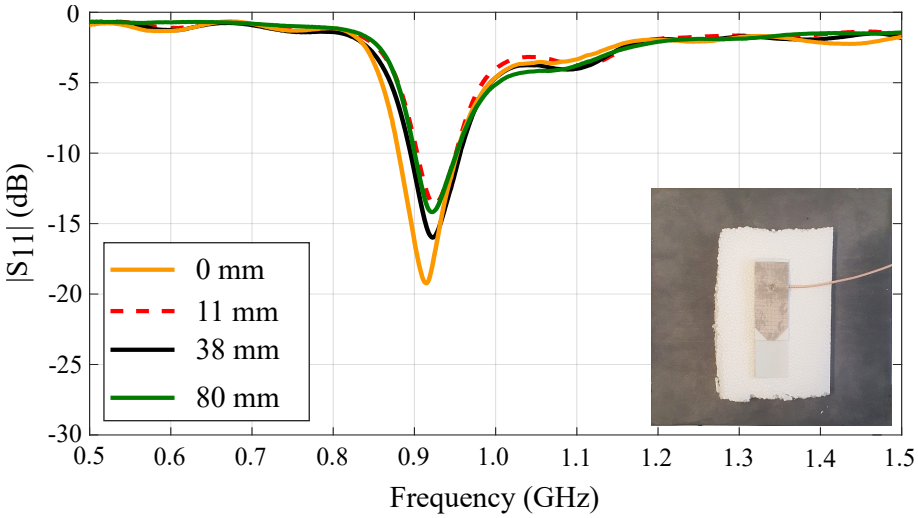

Figure 8.21. Reflection coefficients of the antenna with different gaps. Measured reflection coefficients of the wearable antenna with different gaps between antenna and human body. Inset: the measurement setup.

The variation of antenna gain corresponding to the different distances between the phantom and the wearable antenna is shown in Fig. 8.22. It is observed that the antenna gain is increasing with the spacing from antenna to the phantom. The highest gain is achieved when the phantom-antenna gap is 80 mm, which is approximately a quarter-wavelength distance with resulting in-phase transmitted and reflected waves towards broadside. The gain decreases when the distance is further increased.

In order to validate the effect of the phantom-antenna distance on the antenna gain, a battery-less RFID module is integrated into the wearable host antenna to measure the communication range. Based on the measured antenna gain, the read range can be estimated by using the Friis equation Eq. 8.1 [204]. A good agreement between the estimated and measured read range is illustrated in Fig. 8.23. This further validates the variation of antenna gain along with the distance of the phantom and the wearable antenna.

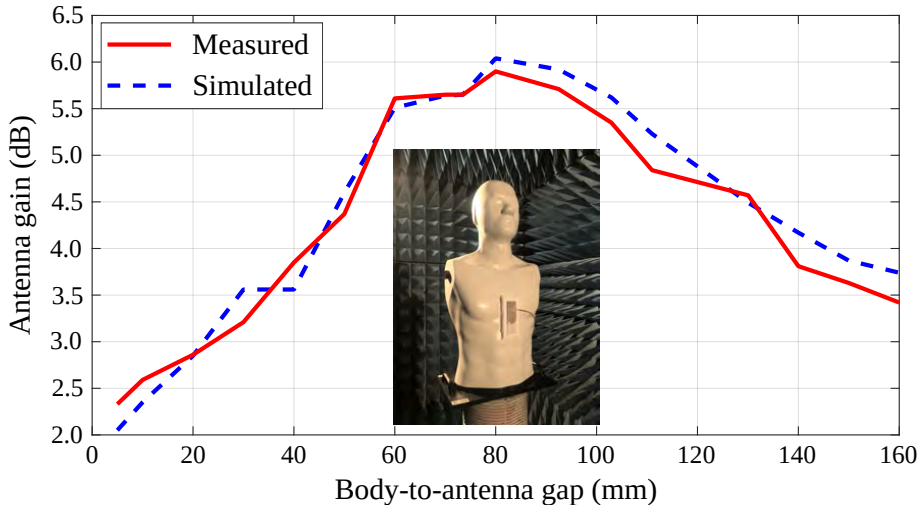

Figure 8.22. Realized gains of the antenna with different gaps. Measured and simulated realized gains of the wearable antenna with different gaps between antenna and human body. Inset: the measurement setup.

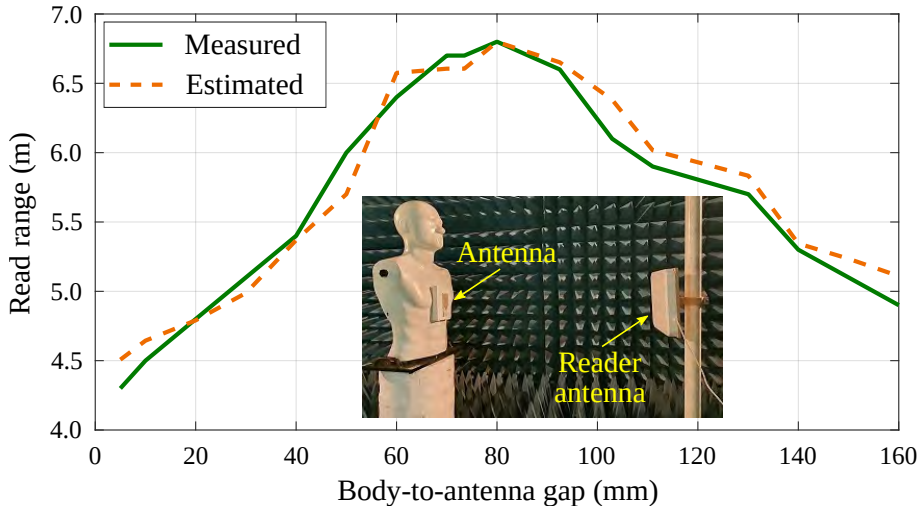

Figure 8.23. Communication range of the antenna with different gaps. Measured and estimated communication range of the wearable antenna with different body-to-antenna gaps. Inset: the measurement setup.

8.3.3 Summary on the body-to-antenna gap effects investigation

The effects of the distance between the human body and the proposed UHF wearable antenna have been assessed. With the isolation provided by a limited ground plane,

the antenna's resonance frequency is however only slightly changed with the variation of the wearer-antenna gap. The antenna gain and consequently the communication distance are increased with spacing, up to an approximate quarter wavelength at 923 MHz.

8.4 Conclusion

In this chapter, the method to fully integrate the computational RFID module inside the antenna resonant cavity has been proposed. Utilizing the interchangeability of metallic snap-on button and the PIFA structure, the computational battery-less RFID sensor has been securely protected inside the wearable antenna. Additionally, the design concept also provide a practical feature of modularization with excellent support form mechanic and RF connection of snap-on buttons. In the second part of the chapter, the effects of the gap between the wearers and body-worn antenna have been investigated. It is found that, when the body-to-antenna gap is increased up to approximately quarter-wave length, the antenna gain is increased.

Chapter 9

Reconfigurable Wearable Antennas for UHF Applications

As evolution of the antenna design proposed in the previous chapter, two variations of reconfigurable body-worn antennas for UHF applications are proposed in this chapter. The two antennas are designed with dual-band resonance frequencies centered at 923 MHz and 2.45 GHz to cover a RFID band as well as Bluetooth-like data transfer. The frequency-agility is implemented on the lower band while the higher band remains unchanged. The antenna is initially designed with a single feeding port with the frequency tuning range of 59.6% in the lower band. The alternative design with two feeding ports is then developed aiming to efficiently utilize the fixed frequency at higher band. The antenna is optimized to have the good isolation level between two ports, which should amount to at least 15 dB. At the lower band, the fractional tuning range is approximately 36.9%. The two antennas are fabricated and measured to validate the design concepts.

9.1 Introduction

As mentioned in Chapter 2, the dynamic physical changes of the human body usually cause mechanical deformation of body-worn antennas such as bending or crumpling. Considering wearable antennas operating in UHF bands, the negative effects of on-body operating conditions are typically even more severe than at higher frequencies. This is because the UHF antennas are usually physically large, therefore the bending or crumpling effects are more pronounced than for smaller antennas operating at higher frequencies. Furthermore, since the free-space wavelength of the UHF antennas is comparable with the physical size of wearers, it becomes challenging to keep the antenna performance stable with the human body in vicinity [136]. For the aforementioned reasons, implementation of reconfigurability for UHF wearable textile antennas using in body-centric communications, is even more desirable than for body-worn antennas operating in higher frequency bands.

Several reconfigurable antennas were reported in the literature targeting UHF radio bands [17, 156]. However, they are all realized on rigid materials, which is not applicable for wearable applications. Regarding body-worn antennas, there have not been any reconfigurable textile antennas covering UHF bands proposed in the literature to date.

In this context, this chapter presents two designs of frequency-reconfigurable flexible antennas for UHF applications. The first antenna is designed with one feeding port aiming to cover dual frequency bands with frequency-agility in its lower band ranging from 0.87 to 1.57 GHz corresponding to a 57.4% tuning range, while the resonance frequency of 2.45 GHz in higher band remains unchanged. Based on the first antenna, a second one is designed with two separated feeding ports, aiming to efficiently employ the fixed resonance frequency in the higher band at 2.45 GHz. In this case, the antenna port excites lower frequency which can be used for RFID application as mentioned in Chapter 8, while the other port working in the higher band is dedicated for other applications such as Bluetooth or communications to mobile devices. The frequency tuning range in the lower band is shrunk to 35% due to the requirement of 15 dB of isolation level between the two feeding ports.

9.2 Single-port frequency reconfigurable wearable antenna

9.2.1 Antenna design

The proposed single-port antenna configuration is shown in Fig. 9.1 with the antenna dimensions detailed in the caption. The proposed antenna concept is inspired by the modular antenna for RFID module presented in Chapter 8, while the reconfigurability is implemented following the antenna concept presented in Chapter 5. The antenna is designed with full ground plane to enhance the human-to-antenna isolation. A three substrate layers structure is used, with the bottom substrate and ground plane extended to enhance the bandwidth at resonance frequency in the lower band centered at 923 MHz. An antenna resonant patch is divided into two parts, a small patch (Patch 1) and a bigger patch (Patch 2). Patch 1 is folded and then shorted to the ground plane to form a PIFA configuration. This first patch is also connected to Patch 2 by a flexible reconfiguration module presented in Chapter 5. A highly flexible and low loss PF-4 foam is selected as antenna substrate and conductive fabric from Shieldex® Nora-RS is used for the antenna conductive parts.

As mentioned, the flexible reconfiguration module presented in Chapter 5 is utilized to obtain frequency reconfigurability. The two metallic male snap-on buttons are placed on the two sides of the reconfiguration module and hence the two antenna conductor parts are contacted through varactors assembled on the module (see an inset in Fig. 9.1). To tune the antenna resonance frequency to the required operating band, three varactors MA46H120 from MACOM Technical Solutions are employed. The antenna is designed and optimized using CST Microwave Studio 2021.

9.2.2 Antenna operation principle

The antenna is designed targeting to simultaneously cover two frequency bands centered at 923 MHz and 2.45 GHz. The frequency reconfigurability is implemented on the lower band aiming to compensate a frequency shift which is likely be more detrimental in wearable operating conditions of the narrow lower-band operation, while the higher band at 2.45 GHz remains unchanged. Both radiation bands are based on the fundamental quarter-wave resonant mode ($TM^z_{0(0.5)0}$), however with different patch dimensions.

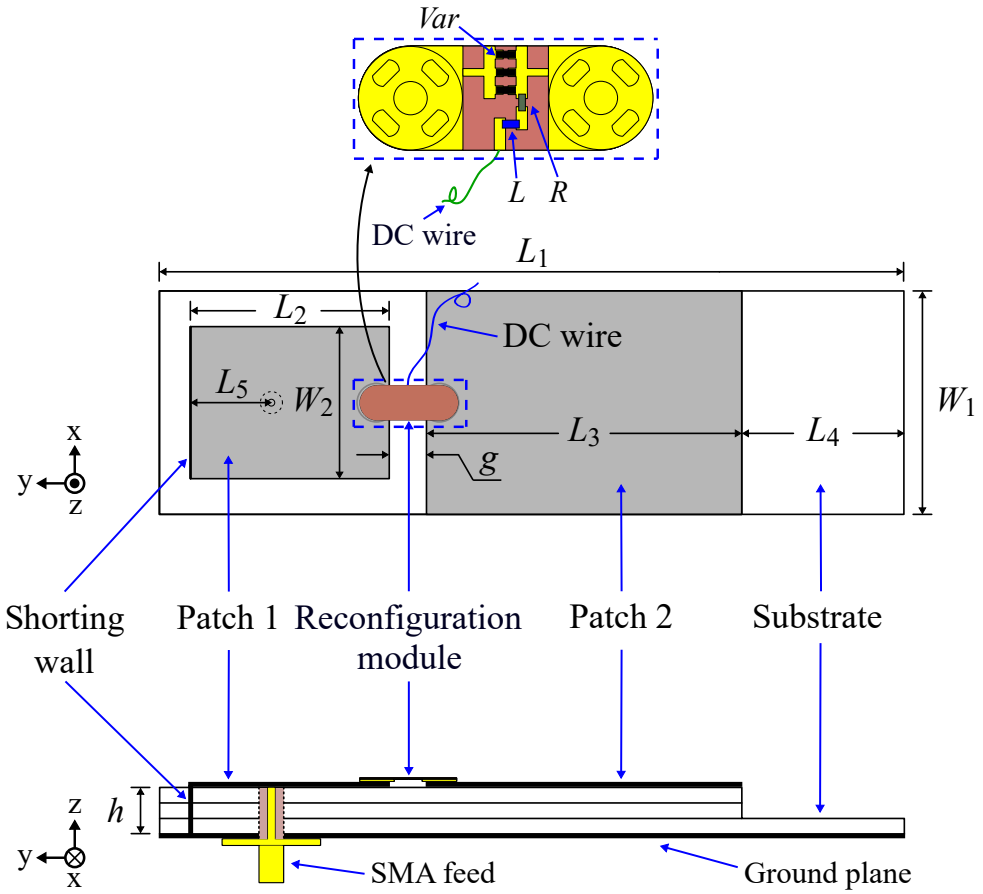

Figure 9.1. Single-port antenna structure. Single-port reconfigurable wearable antenna structure. Dimensions (mm): $L_1 = 120.0$, $L_2 = 32.0$, $L_3 = 50.5$, $L_4 = 26.5$, $L_5 = 13.0$, $W_1 = 36.0$, $W_2 = 24.5$, $g = 6.0$ and $h = 4.8$. Inset: Zoomed-in front side of the reconfiguration module.

The fixed resonance frequency at 2.45 GHz in the higher band is based on the fundamental quarter-wave mode ($TM^z_{0(0.5)0}$) of the small patch (Patch 1). It is initially excited by choosing an appropriate length of Patch 1 which is 30.6 mm (a quarter-wave length at 2.45 GHz). This value is then re-optimized to satisfy the required resonance frequencies at both bands.

The lower band centered at 923 MHz is based on the fundamental quarter-wave mode ($TM^z_{0(0.5)0}$) of the total length including the two patches shorted to the ground plane using the full folded shorting wall. Assuming firstly that the two patches are fully connected, the lowest resonance frequency in lower band can be approximated using the antenna dimensions relationship [85]

$$f = \frac{c_0}{4((L_2 + g + L_3) + W_1 - W_2 - h)\sqrt{\varepsilon_r}} \tag{9.1}$$

where c_0 is the speed of light in free space, ε_r is the substrate relative permittivity, L_2, g, L_3, W_1, W_2 and h are the antenna dimensions detailed in the caption of Fig. 9.1. As a result, the lowest resonance frequency in the lower band is estimated to be 760 MHz.

As mentioned, the reconfiguration module is placed in-between the two patches. In this topology, the resonance frequency can be tuned by changing the capacitance of the varactor inside the reconfiguration module. It is known that, the number of varactors used in the module influences the targeted resonance frequency tuning range [96]. Therefore, to cover the lower band center frequency of 923 MHz, it is necessary to select an appropriate number of varactors. The relation between achievable resonance frequency tuning range and a hypothetical value of varactor junction capacitance (from 0.001 to 1000 pF) can be simulated as shown in Fig. 9.2. When the varactor capacitance is 1000 pF, the resonance frequency nearly equal to the value calculated in equation 9.1. It can be observed that, while using three varactors, the lower band tuning range is approximately from 0.87 to 1.56 GHz which completely covers the required 923 MHz.

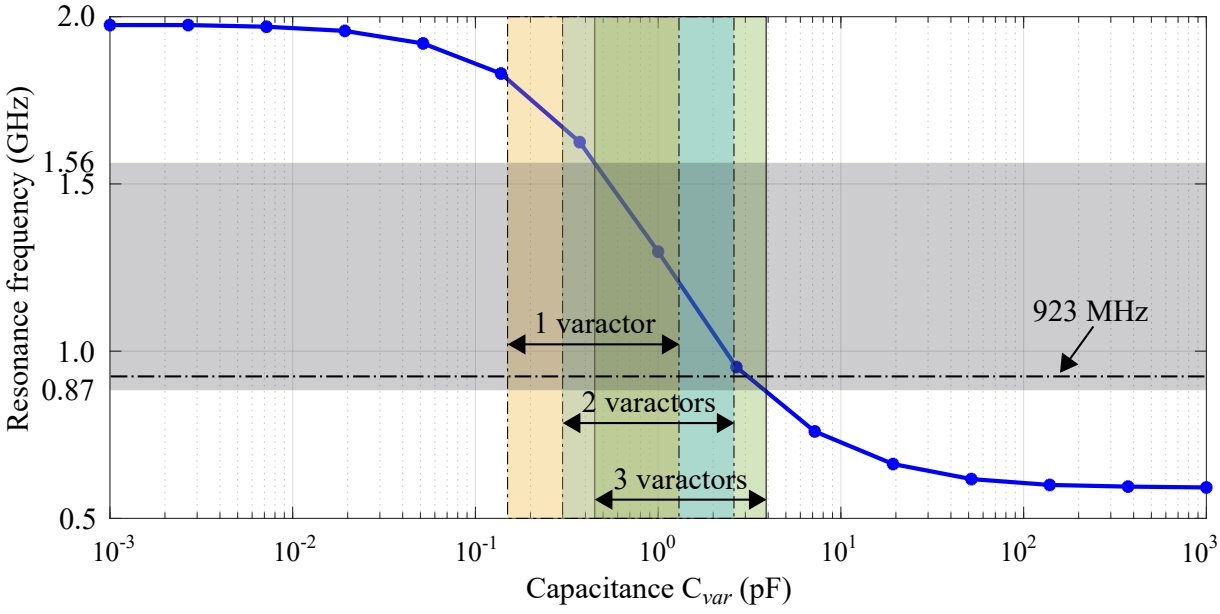

Figure 9.2. Frequency tuning range dependence on varactor capacitance. Simulated resonance frequencies across different values of varactor capacitance.

The simulated instantaneous electric field distributions in the cavity of the proposed antenna at three different values of the varactor capacitance (C_{var}) in the lower band centered at 923 MHz, and at 2.45 GHz in the higher band are shown in Fig. 9.3. When

decreasing the varactor junction capacitance, a null in the field distribution in the cavity (white dash line in Fig. 9.3 (a), (b) and (c)) is moving towards the center of the antenna which indicates the increase of the resonance frequency, as illustrated in Fig. 9.3 (a), (b) and (c). As a result, the frequency tuning range of approximately 57.3% is achieved. At the higher band, the electric field distribution of the small PIFA is nearly unchanged with different varactor capacitances, and the case when C_{var} = 0.36 pF is shown in Fig. 9.3 (d).

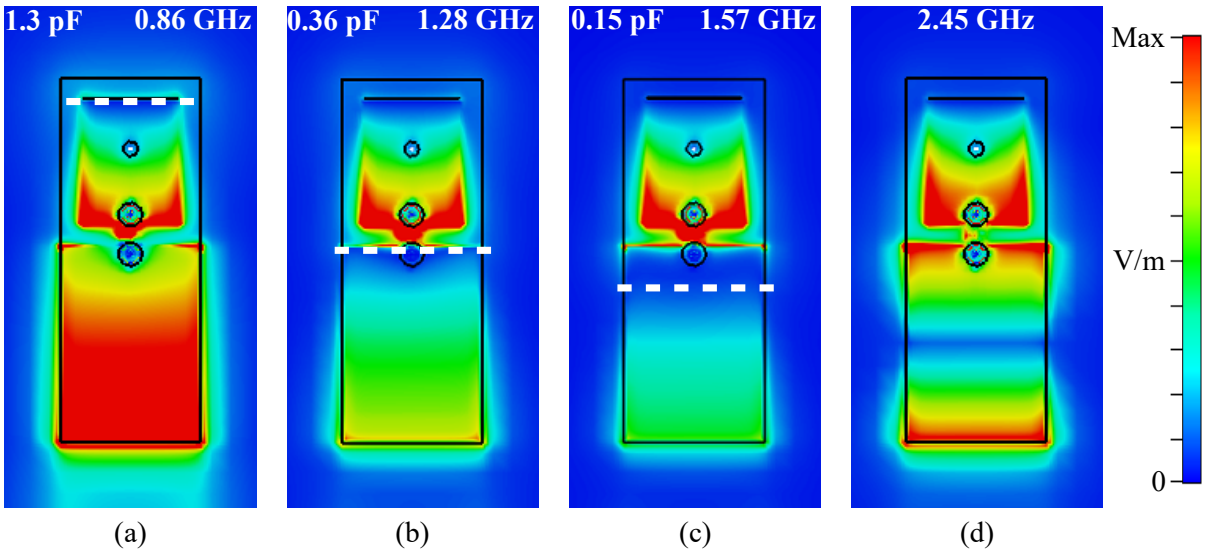

Figure 9.3. Electric field distributions of the proposed antenna. Simulated instantaneous electric field distributions in the cavity of the proposed antenna in (a), (b), (c) lower band at 0.86, 1.28, 1.57 GHz, respectively and (d) higher band at 2.45 GHz.

9.2.3 Experimental results

Antenna fabrication

In order to validate the operation concept, the proposed antenna has been fabricated and experimentally characterized. The antenna conductive parts are accurately cut using a laser milling machine. The antenna Patch 1, the shorting wall and the ground plane are realized as one piece of conductive textile, similarly as shown for the antenna proposed in Chapter 8. Two circular holes are trimmed on the top foam substrate to accommodate the two female snap-on buttons required to connect the reconfiguration

module to the antenna. The antenna substrate and conductors are glued together using fabric glue, while the SMA connector probe is connected to Patch 1 and the ground plane using conductive epoxy CW2400 from CircuitWorks. The top view of the fabricated antenna prototype is displayed in Fig. 9.4.

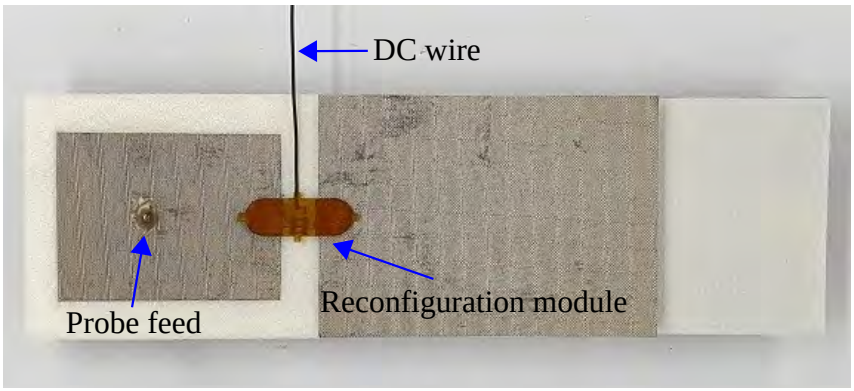

Figure 9.4. Single port antenna prototype. Top view of the single port antenna prototype.

Reflection coefficient

The antenna reflection coefficients obtained from simulation and measurement for different values of the bias voltage are shown in Fig. 9.5. An inconsequential discrepancy can be observed which is mainly due to the fabrication tolerances associated with flexible materials. It can be observed that, when the bias voltage is varied from 0 to 18 V, the measured resonance frequency changes from 0.86 to 1.59 GHz, corresponding to a fractional tuning range of 59.6%. Considering the wearable applications where the bias voltage would usually be limited to a maximum of 5 V, the achievable frequency tuning range remains appreciable at 40.7% (0.86 to 1.3 GHz). In the higher band, a stable resonance frequency at 2.45 GHz is observed for different values of the varactor capacitance.

Radiation pattern, gain and efficiency

Figure 9.6 displays the simulated and measured normalized radiation patterns of the proposed antenna at 0.86, 1.14, 1.30, 1.59 and 2.45 GHz in the xz-plane and the yz-plane. It can be observed that, the maximum gain is pointing to the broadside direction in both radiation bands, which is appropriate for off-body communications. The radiation patterns are stable in the lower band with a wide beamwidth and strong back radiation. This is because the antenna substrate, radiation patch and ground plane all

9.2.3 Experimental results

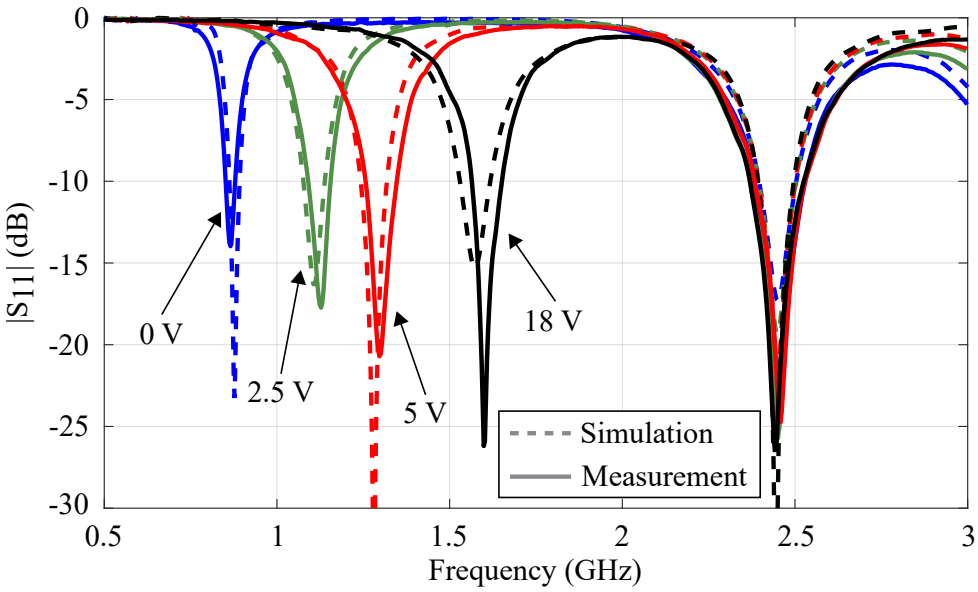

Figure 9.5. Reflection coefficients of the single-port antenna. Simulated and measured reflection coefficient $|S_{11}|$ of the proposed single-port antenna for selected values of the bias voltage applied to the varactors.

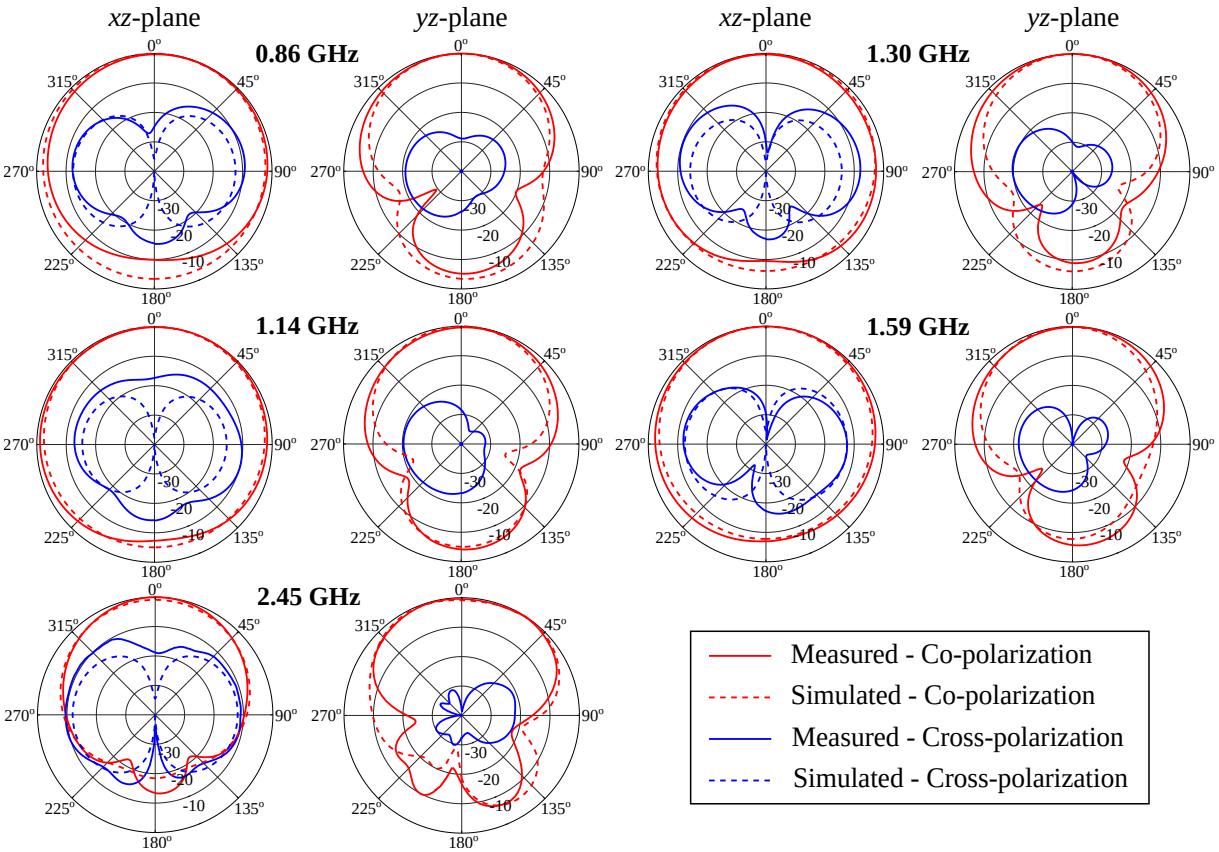

Figure 9.6. Radiation patterns of the single-port antenna. Simulated and measured normalized radiation patterns of the proposed single-port antenna in the *xz*- and *yz*-planes at 0.86, 1.14, 1.30, 1.59 and 2.45 GHz.

have a rather narrow electrical width, leading to an increase of fringing field in the x-direction. In the higher band, since the width of Patch 1 is smaller than the substrate and ground plane width, the radiation pattern is more directional with a narrower beamwidth and a smaller back radiation.

The simulated and measured realized gains of the proposed antenna are compared in Fig. 9.7 where a slight discrepancy is observed. This can be explained by the fabrication tolerances and unavoidable imperfection of measurement alignment. In the lower band, when the resonance frequency increases from 0.86 to 1.59 GHz, the measured realized gain rises from 1.72 to 4.46 dBi. The low gain at 0.86 GHz is due to the power losses in the three parallel varactors when they are tuned to their highest varactor junction capacitance of 1.3 pF. The measured realized gain of 4.71 dBi in the higher band at 2.45 GHz indicates that the antenna is working in PIFA mode with full shorting wall. Based on the antenna simulated efficiency and the measured gain, the actual radiation efficiency of the proposed antenna is ranging between 71.2% to 95% in the lower band and 94% in the higher band.

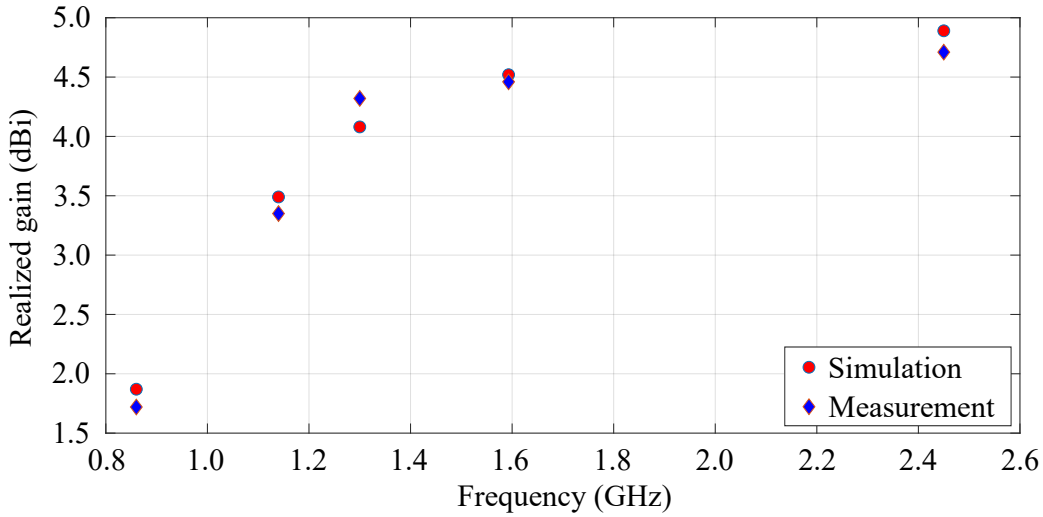

Figure 9.7. Realized gains of the single-port antenna. Simulated and measured realized gain of the proposed single-port antenna.

9.3 Dual-port frequency reconfigurable wearable antenna

The single-port dual-band reconfigurable wearable antenna presented in the previous section, can be used for dual-band systems, where the lower band with narrow operation bandwidth will benefit from being tunable whereas the less sensitive higher band

is fixed. In a particular use case, the lower band with the frequency tuning range from 0.86 to 1.59 GHz can be utilized for health care monitoring application using RFID sensors as mentioned in Chapter 8. The wide frequency tuning range is beneficial to compensate the frequency shift caused by the dynamic changes of on-body operation environment. The fixed resonance frequency at 2.45 GHz in the higher band, however, can be used for other applications such as Bluetooth or energy harvesting [212, 213]. However, the utilization of single port for RF transmission of two different applications may cause a significant power reduction. Therefore, an alternative design may be better suitable for this scenario, where a dual-port antenna is designed with each port is dedicated for each operation band.

In this section, a dual-port version of the reconfigurable wearable antenna presented in Section 9.2 is proposed. The antenna Port 1 is dedicated to excite a resonance frequency in the higher band at 2.45 GHz while the antenna Port 2 is used for tunable resonance frequency in the lower band centered at 923 MHz. The antenna is designed to have acceptable isolation level between the two ports which is specified to be at least 15 dB. The measured frequency tuning range in the lower band is 36.9% corresponding to the resonance frequency ranging from 0.84 to 1.22 GHz. The higher frequency is designed to remain unchanged at 2.45 GHz. The antenna has been fabricated and measured to validate the design concept.

9.3.1 Antenna design and operation

The dual-port antenna configuration is shown in Fig. 9.8 with the antenna dimensions listed in Table 9.1. As illustrated in Fig. 9.8, the antenna shares a similar structure with the single-port antenna presented in the Section 9.2, namely with full ground plane, three layers of substrate and two antenna patches. Two probe feeding ports are allocated underneath the two patches, Port 1 is connected to a small patch (Patch 1) and Port 2 is connected to a large patch (Patch 2). The flexible reconfiguration module with three varactors is used to connect the two patches to achieve frequency-reconfigurability. Two capacitive rectangular slots are introduced around the two probe feeds on the antenna patches as shown in Fig. 9.8.

The antenna operating principle is similar to the single-port antenna presented in the Section 9.2.2. The fundamental quarter-wave mode ($TM^{z}_{0(0.5)0}$) of the two patches with different sizes are used to excite two resonant bands simultaneously. Two rectangular

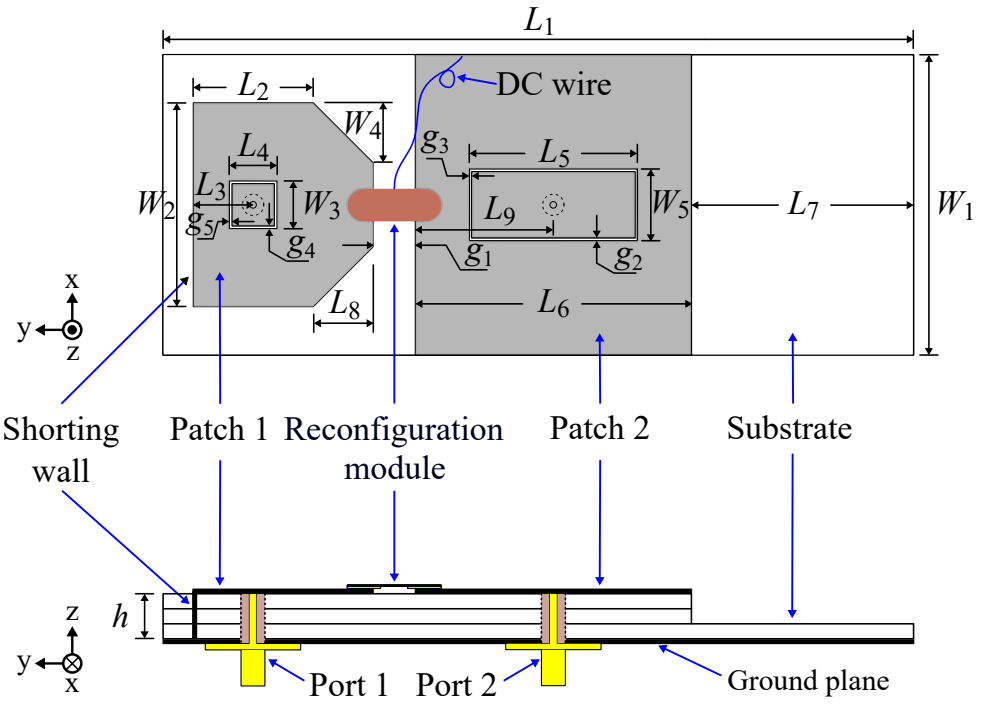

Figure 9.8. Dual-port antenna structure. Dual-port reconfigurable wearable antenna structure.

Table 9.1. Parameters of the dual-port antenna. Dimensions of the dual-port antenna (in mm)

Parameters	L_1	L_2	L_3	L_4	L_5	L_6	L_7	L_8	L_9	h
Values	125	20	10	8	28	46	37	10	23	4.8
Parameters	W_1	W_2	W_3	W_4	W_5	g_1	g_2	g_3	g_4	g_5
Values	50	34	8	10	12	7	0.5	0.4	0.5	0.5

slots are introduced on the patches around the two feeding pins to achieve isolation between the two ports. The slot dimensions and two port positions are optimized to achieve widest tuning range while maintaining the two-port isolation value above 15 dB.

9.3.2 Experimental results

The proposed antenna has been fabricated and experimentally characterized. The fabrication process is similar to the single-port antenna. However, this dual-port antenna requires higher accuracy while gluing the patches with thin slots on the top substrate. The front view of the fabricated antenna is illustrated in Fig. 9.9.

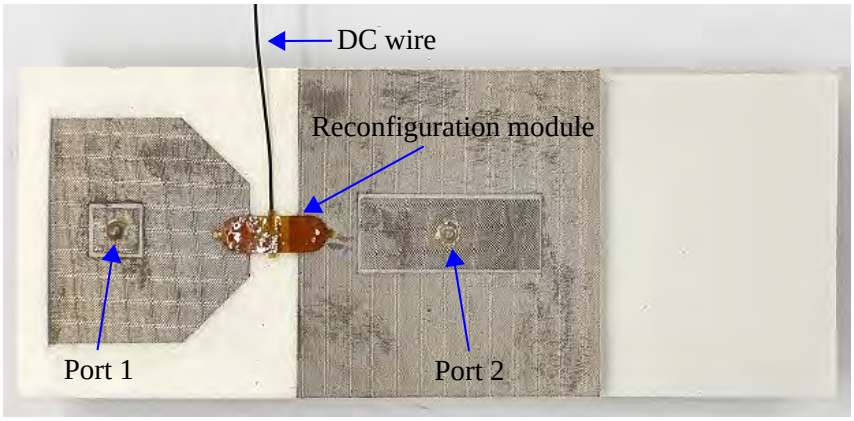

Figure 9.9. Dual-port antenna prototype. The top view of the dual-port antenna prototype.

S-parameters

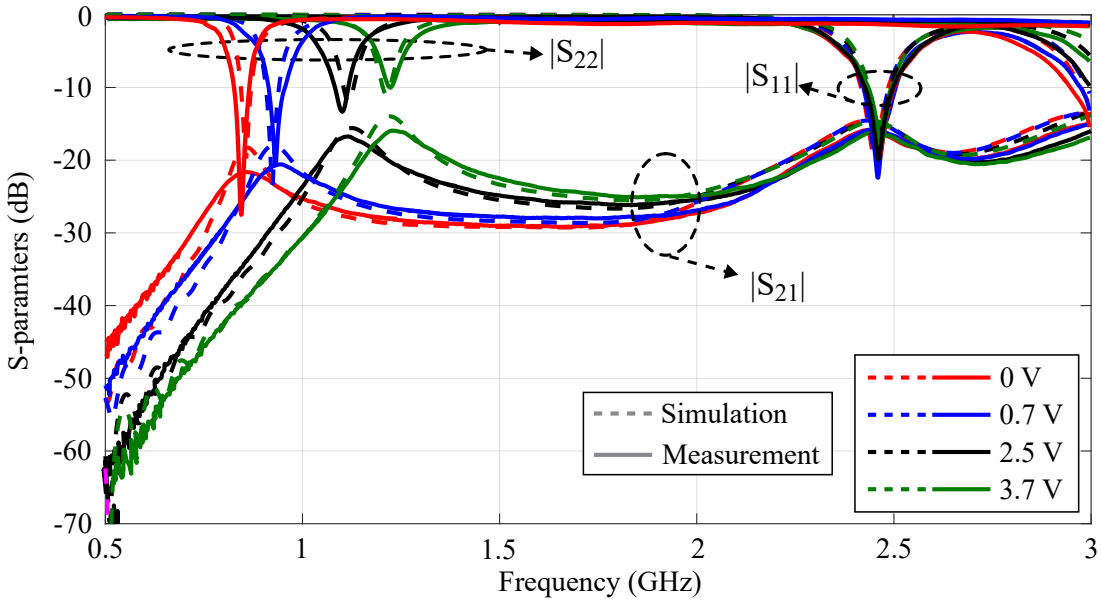

Figure 9.10. S-parameters of the dual-port antenna. Simulated and measured reflection and transmission coefficients of the proposed dual-port antenna for selected values of the bias voltage applied to the varactors.

The simulated and measured reflection coefficients of the proposed antenna for different values of the bias voltage are shown in Fig. 9.10. The slight discrepancy is mainly due to the antenna fabrication and measurement tolerances. The introduction of the rectangular slots makes the antenna matching more challenging. As a result, the measured resonance frequency can be tuned from 0.84 to 1.22 GHz (36.9% of fractional tuning range) when the bias voltage is varied from 0 to 3.7 V. The isolation between the two antenna ports progressively decreases while the resonance frequency is increased,

reaching the limit of approximately 15 dB at the highest frequency in the lower band. A fixed resonance frequency at 2.45 GHz in the higher radiation band can be observed.

Radiation pattern, gain and efficiency

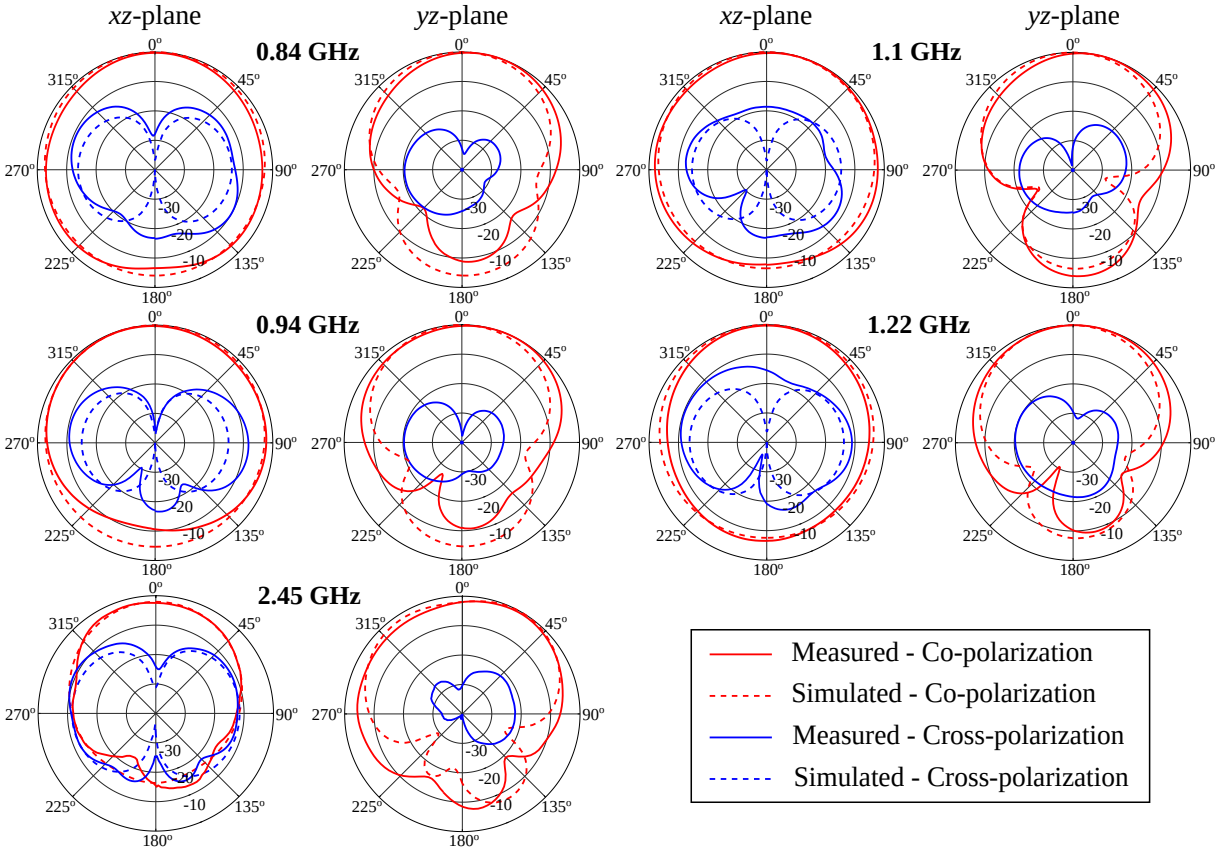

Figure 9.11. Radiation patterns of the dual-port antenna. Simulated and measured normalized radiation patterns of the proposed dual-port antenna in the *xz*- and *yz*-planes at 0.84, 0.94, 1.1, 1.22 and 2.45 GHz.

The simulated and measured normalized radiation patterns of the proposed antenna at 0.84, 0.94, 1.1, 1.22 and 2.45 GHz in the *xz*- and *yz*-plane are shown in Fig. 9.11 where an appreciable agreement is observed. Because the antenna shares the same structure as the single-port antenna, the same radiation pattern shapes is expected. The antenna is also appropriate for off-body communications with the maximum radiation direction towards the broadside in both bands.

The simulated and measured realized gains of the proposed antenna are shown in Fig. 9.12. Due to the imperfect measurement process, the discrepancy between the

simulation and measurement gains can be observed, with the measured data typically 0.5 − 1.0 dB lower than predicted in simulations. Because the antenna is working within the range of high values of the varactor junction capacitance (1.3 pF to 0.45 pF), the antenna gains are low in the lower band. This also leads to the low estimated antenna efficiency (compared with the single-port antenna) which is ranging from 59.7% to 72% in the lower band and 85% in the higher band.

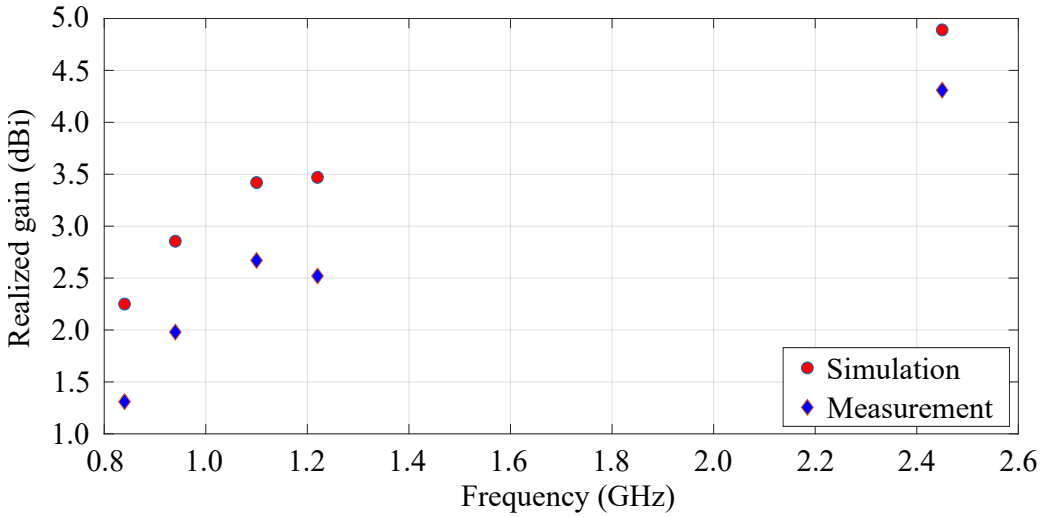

Figure 9.12. Realized gains of the dual-port antenna. Simulated and measured realized gains of the proposed dual port antenna.

9.4 Conclusion

In this chapter, two realizations of frequency-reconfigurable wearable antennas working in the UHF radio band have been presented. The two antennas are designed to simultaneously cover two radiation bands centered at 923 MHz and 2.45 GHz. Utilizing the flexible reconfiguration module introduced in Chapter 5, the frequency reconfigurability is implemented in the lower band, since it is more sensitive to the wearing operation conditions than the higher band. The first antenna is designed with a single feeding port while in the second design variation, a dual-port structure is utilized. The additional port is introduced to utilize the fixed resonance frequency at 2.45 GHz for other applications such as Bluetooth or energy harvesting. The single-port and the dual-port antenna exhibit wide frequency tuning range of 59.6% and 36.9% at the lower band, respectively. The two antennas have been fabricated and measured to validate the design concepts.

Chapter 10

Conclusion and Future Work

THIS thesis has proposed various passive and reconfigurable wearable textile antennas, with emphasis on the practicability for utilization in real applications. Several design techniques and components for active and passive wearable textile antenna designs have been proposed and investigated in the first part of the thesis. A number of reconfigurable wearable textile antennas with agility in resonance frequency, radiation pattern and polarization have been proposed in the second part of the dissertation. In the last part of the thesis, a flexible textile antenna which can be used in real application for patient monitoring has been presented, together with two of its variants with frequency-reconfigurability implemented. This chapter concludes by summarizing the original contributions of each aforementioned main part and suggests future works related to these topics.

The research work in this thesis has been described into three primary parts mainly focused on reconfigurable flexible textile antennas. In this chapter, the original contributions presented in these three main parts of the dissertation are summarized. Based on the research results obtained, different possible research pathways are then suggested.

10.1 Part I: Reconfigurable wearable antennas design techniques and components

The first part of this thesis is described in Chapter 3 and 4 where the design techniques and components used for reconfigurable textile antennas have been proposed. The shorting strategies, antenna design techniques and reconfiguration modules presented and investigated in this part are fundamental ingredients in all the antenna designs proposed in the thesis.

10.1.1 Summary of original contributions

- As the first contribution in Chapter 3, four shorting strategies commonly utilized in wearable textile antenna designs have been comprehensively analyzed. Based on the considered shorting methods, twelve wearable textile antennas categorized in three main groups including eight PIFAs and four shorted-patch monopole antennas have been designed, fabricated and experimentally characterized. It has been found that, none of the considered shorting strategies is perfect and fits all wearable antenna designs. Instead, each method exhibits its own advantageous and disadvantageous features considering simulation, fabrication, antenna performance, mechanical stability and modularity. The analysis results aim to guide wearable textile antenna designers with quick selection of appropriate shorting methods for the specific desired applications [41].

- The next contribution presented in Chapter 3 comes from the dual-band dual-mode design method of twelve wearable textile antennas using the four shorting methods. A design and optimization process of two wearable antennas aiming to simultaneously cover 2.45 and 5.8 GHz ISM bands for on-body and off-body

communications has been presented. The results indicate that dual-band characteristic can be achieved by simply optimizing antenna geometry or feeding structure, without utilizing complex techniques. The proposed design method helps to maintain antenna compactness, low profile and easy fabrication features while expanding antenna functionality [42].

- A dual-band wearable textile antenna with radiation pattern modularity for on-body and off-body communications at fixed resonance frequency has also been presented as another contribution in Chapter 3. The advantage of metallic snap-on buttons presented earlier in the chapter are exemplified in this design concept. Utilizing metallic snap-on fasteners to build a manual detachable RF connection, the proposed wearable textile antenna can be configured to operate in either omnidirectional or broadside patterns at 2.45 GHz.

- Aiming at investigating an alternative practical method to implement reconfigurability on wearable flexible textile antennas, a novel reconfiguration module has been proposed in Chapter 4. The module design is based on a small printed circuit board and a pair of metallic male snap-on buttons aiming to realize a robust electronics-to-textiles connection in coplanar setup. The simulation results have suggested a potentiality of the proposed module design in realization of practical reconfigurable wearable antennas [43].

- The other contribution presented in Chapter 4 is a demonstration of utilizing RF-switch ICs and PIN diodes to obtain reconfigurability for wearable textile antennas. Practically realizable solutions as well as a direct comparison of these switching components in reconfigurable wearable antenna designs have been proposed. The results have confirmed the great versatility of using reconfiguration modules to implement agility in body-worn textile antennas.

10.1.2 Future work

The utilization of switching components including RF-switch ICs and PIN diodes in reconfigurable wearable antennas has been demonstrated. Based on these components, several pattern- or polarization-reconfigurable textile antennas can be further investigated. One straightforward implementation is replacing the snap-on button connections in the modular pattern-interchangeable wearable antenna structure presented

in Chapter 3 by reconfiguration modules with RF switching components to realize a pattern-reconfigurable wearable antenna.

With an advantageous feature of having multi output ports which allows connecting and switching between multiple distinct tuning components, RF-switch IC is a promising component in multifunctional reconfigurable antenna designs. The application of RF-switch is not limited for wearable antennas but also to antennas realized on rigid materials.

10.2 Part II: Reconfigurable wearable antennas for body-centric communications

Utilizing the design techniques and the components presented in the first part, a wide range of reconfigurable textile antennas have been proposed in the second part of the thesis. These antennas have been presented in Chapter 5 through Chapter 7 with reconfigurability in operation frequency, polarization, radiation patterns and combination of these tunabilities. Folded strips of silver fabric have been used as shorting method in all the designs presented in this part to maximize the antenna performance as suggested in Chapter 3. The reconfigurability has been implemented in all the design concepts using a coplanar reconfiguration module based on the coplanar module design concept presented in Chapter 4, showcasing the versatility of the concept.

10.2.1 Summary of original contribution

- A frequency reconfigurable wearable patch antenna with very wide tuning range of approximately 70% have been proposed in Chapter 5. The operating principle of exploiting a continuous transition between a quarter-wave mode and a half-wave mode to obtain a very wide tuning range has been confirmed by using an equivalent circuit model. Although the reconfigurability is based on the coplanar module design concept proposed in Chapter 4, the actual module used in the design have been modified to enhance the practicality of the antenna. The proposed antenna have been optimized, fabricated and experimentally characterized to validate the operation concept. The prototype exhibits a very wide frequency tuning range of one octave extending from 1.82 to 3.77 GHz in free space

and also maintain good performance in bending and on human body/ phantom conditions [49].

- As an extended version of the antenna proposed in [49], a dual-band frequency-reconfigurable wearable flexible antenna that simultaneously covers 2.45 and 5.8 GHz ISM radio bands has been proposed in Chapter 5. Using the same structure as the antenna proposed in [49], the antenna dimensions have been re-optimized to operate in dual frequency bands. The proposed antenna has been fabricated and measured to validate the wide frequency tuning range in lower and higher bands which are 48.6% and 18.3%, respectively [45].

- Another contribution in Chapter 5 is the investigation of the thermal behavior of a frequency-reconfigurable textile antenna. The investigation is conducted on the frequency-reconfigurable textile antenna with one-octave tuning range proposed in [49]. The investigation results indicate the hottest position on the reconfigurable antennas is located at the active components. The relation between antenna input power and temperature has been also suggested [46].

- A frequency reconfigurable wearable flexible antenna with dual-band independent tuning capability has been proposed in Chapter 6. The proposed antenna is designed to operate simultaneously in two radiation modes that cover two ISM bands centered at 2.45 and 5.8 GHz ISM radio bands. The antenna reconfigurability is achieved using the coplanar reconfiguration module initially proposed in Chapter 4 and then practically modified in Chapter 5. The antenna concept has been fabricated and experimentally validated. It exhibits an independent frequency tuning range of 41.1% for the lower band and 29.9% for the higher band.

- In Chapter 7, two reconfigurable wearable antennas with tunability combination have been proposed. The first antenna is designed to simultaneously operate in 2.45 and 5.8 GHz ISM bands with frequency- and pattern-agility in the lower band while the higher band remains unchanged. In the lower band, the antenna frequency tuning range is 27.2% while working in a monopole mode and 57.3% when switched to a broadside mode. The antenna operation principle of switching between broadside and omnidirectional modes is analyzed using an equivalent circuit. The frequency- and polarization-reconfigurability have been implemented in a second antenna. The linear polarization direction of the antenna can

be switched between orientations at 0°, 120° and 240° over a wide frequency tuning range of approximately 31.9% in each polarization. The two proposed antennas have been optimized, fabricated and measured to validate the reconfigurable operation concepts.

10.2.2 Future work

The reconfigurable wearable antenna with very wide tuning range proposed in [44] demonstrates that, the very wide tuning range reconfigurable patch antenna is attainable by realizing a continuous transition between multi radiation modes. If the mode continuous transition in [44] can be combined with a higher-order radiation mode where the frequency-agility is available, a frequency-reconfigurable antenna with a tuning range of even more than 70% is potentially realizable.

The effective utilization of a flexible printed circuit board (PCB) in wearable textile antenna designs has been proven through an implementation of flexible reconfiguration modules proposed in Part II of the thesis. This opens another direction in reconfigurable flexible antenna design in which a broader flexible PCB is combined with conventional flexible material such as foam, silver fabric, to realize more compact reconfigurable flexible antennas.

10.3 Part III: Passive RFID sensor integration with wearable antennas

As mentioned, a main focus of the thesis is the practicability of reconfigurable textile antennas in real applications. To this aim, several wearable flexible antennas targeting healthcare applications for wireless patient monitoring have been proposed in Chapter 8 and 9.

10.3.1 Summary of original contribution

- A novel solution to realize a system-in-package sensor that consists of a wearable textile antenna and a computational RFID module has been proposed in Chapter 8. The distinctive advantage of the design concept is allowing the large-size

RFID module to be fully integrated into the resonant cavity of the flexible textile antenna. This remarkably enhances the practicality of the completed sensor since the RFID module is securely protected from the dynamic changes of wearing operation condition. Furthermore, the modularization of the concept allows an interchange of antenna modules according to different application requirements. Various antenna concepts have been designed, fabricated and measured to validate the desired antenna performance. After that, the completed sensors realized by integrating the RFID module to the modular antennas have been tested to prove the practicability in real application scenarios [48].

- Using the wearable textile antenna as well as the completed sensor proposed in [48], the effect of the distance between the human body and the wearable antenna has been investigated in Chapter 8. The good isolation between the antenna and the human body phantom regardless the different body-to-antenna gaps has been confirmed. The results also indicate that the antenna gain and consequently the communication range of the completed sensor are increased with spacing and reach maximum values at a gap of approximately quarter-wave length [49].

- Based on the UHF antenna structure proposed in [48], in combination with the coplanar reconfiguration module used in [44], two variations of dual-band frequency-reconfigurable wearable textile antennas have been proposed in Chapter 9. The two antennas have been designed with frequency-agility at their lower band centered at 923 MHz, while a resonance frequency in a higher band at 2.45 GHz remains fixed. The first proposed antenna was excited by a single port while the second antenna utilized dual-port to independently operate at the fixed frequency of 2.45 GHz. The two antennas have been fabricated an measured to validate the design concepts. The single-port and dual-port reconfigurable antennas exhibit wide frequency tuning range of 59.6% and 36.9% in the lower band which are promising to be used in wearable UHF applications where the antenna resonance frequency can easily be shifted.

10.3.2 Future work

The practicality of proposed modular wearable textile antenna with integrated RFID module has been successfully demonstrated in laboratory test conditions. The further

step is testing the completed sensor in the real conditions, i.e., when it is mounted on hospital gowns for patient monitoring. At this stage, the feasibility of the product in real applications is not only evaluated by the ability of maintaining the required performance. In fact, the user perception and acceptance are also the key factors to access in the final product. It is also desirable to integrate real chips (e.g, RFID modules) into the resonant cavity of the frequency-reconfigurable textile antennas proposed in Chapter 9 to test the sensor performance in harsh operating conditions while having the frequency-ability implemented.

10.4 Concluding statement

In this thesis, several design techniques, components, passive and reconfigurable wearable textile antennas have been proposed to be key components for a realization of multi-functional and/or smart wearable systems. Although the operation principle of all the proposed antennas in the thesis have been confirmed though either equivalent circuit analysis or full-wave simulation, the practical implementation and deployment of the proposed antennas in real applications have been always emphasized. All the passive and active wearable antennas presented in the dissertation exhibit robust experimentally validated performance in either various bending configurations or interactions with human body/phantom. It is of prime importance for all the future wearable textile antenna investigations to consider the practicability of the designs as one of the most crucial priorities.

Bibliography

[1] N. H. M. Rais, P. J. Soh, F. Malek, S. Ahmad, N. Hashim, and P. Hall, "A review of wearable antenna," in *2009 Loughbrgh. Antennas Propag. Conf.* IEEE, Nov. 2009, pp. 225–228.

[2] S. Agneessens, M. Bozzi, R. Moro, and H. Rogier, "Wearable textile antenna in substrate integrated waveguide technology," *Electron. Lett.*, vol. 48, no. 16, pp. 985–987, Aug. 2012.

[3] M. Grilo, M. Hiroaki Seko, and F. Salete Correra, "Wearable textile patch antenna fed by proximity coupling with increased bandwidth," *Microw. Opt. Technol. Lett.*, vol. 58, no. 8, pp. 1906–1912, Aug. 2016.

[4] S. J. Chen and C. Fumeaux, "Highly efficient graphite antennas for conformal applications," in *2018 Aust. Microw. Symp.* IEEE, Feb. 2018, pp. 61–62.

[5] A. Jayatilaka, Q. H. Dang, S. J. Chen, R. Visvanathan, C. Fumeaux, and D. C. Ranasinghe, "Designing batteryless wearables for hospitalized older people," in *Proc. 23rd Int. Symp. Wearable Comput. - ISWC '19*. New York, New York, USA: ACM Press, 2019, pp. 91–95.

[6] S. Zhu and R. Langley, "Dual-band wearable textile antenna on an EBG substrate," *IEEE Trans. Antennas Propag.*, vol. 57, no. 4, pp. 926–935, Apr. 2009.

[7] S. Agneessens and H. Rogier, "Compact half diamond dual-band textile HMSIW on-body antenna," *IEEE Trans. Antennas Propag.*, vol. 62, no. 5, pp. 2374–2381, May. 2014.

[8] S. Velan, E. F. Sundarsingh, M. Kanagasabai, A. K. Sarma, C. Raviteja, R. Sivasamy, and J. K. Pakkathillam, "Dual-band EBG integrated monopole antenna deploying fractal geometry for wearable applications," *IEEE Antennas Wirel. Propag. Lett.*, vol. 14, pp. 249–252, 2015.

[9] M. Wagih, G. S. Hilton, A. S. Weddell, and S. Beeby, "Dual-band dual-mode textile antenna/rectenna for simultaneous wireless information and power transfer (SWIPT)," *IEEE Trans. Antennas Propag.*, 2021.

[10] P. B. Samal, P. J. Soh, and G. A. E. Vandenbosch, "UWB all-textile antenna with full ground plane for off-body WBAN communications," *IEEE Trans. Antennas Propag.*, vol. 62, no. 1, pp. 102–108, Jan. 2014.

[11] S. J. Chen, T. Kaufmann, R. Shepherd, B. Chivers, B. Weng, A. Vassallo, A. Minett, and C. Fumeaux, "A compact, highly efficient and flexible polymer ultra-wideband antenna," *IEEE Antennas Wirel. Propag. Lett.*, vol. 14, pp. 1207–1210, 2015.

[12] L. A. Yimdjo Poffelie, P. J. Soh, S. Yan, and A. E. Vandenbosch, "A high-fidelity all-textile UWB antenna with low back radiation for off-body WBAN applications," *IEEE Trans. Antennas Propag.*, vol. 64, no. 2, pp. 757–760, Feb. 2016.

[13] R. B. Simorangkir, A. Kiourti, and K. P. Esselle, "UWB wearable antenna with a full ground plane based on PDMS-embedded conductive fabric," *IEEE Antennas Wirel. Propag. Lett.*, vol. 17, no. 3, pp. 493–496, Mar. 2018.

[14] X. Lin, Y. Chen, Z. Gong, B. C. Seet, L. Huang, and Y. Lu, "Ultrawideband textile antenna for wearable microwave medical imaging applications," *IEEE Trans. Antennas Propag.*, vol. 68, no. 6, pp. 4238–4249, Jun. 2020.

[15] H. A. Majid, M. K. Abdul Rahim, M. R. Hamid, N. A. Murad, and M. F. Ismail, "Frequency-reconfigurable microstrip patch-slot antenna," *IEEE Antennas Wirel. Propag. Lett.*, vol. 12, pp. 218–220, 2013.

[16] Lei Ge and Kwai-Man Luk, "Frequency-reconfigurable low-profile circular monopolar patch antenna," *IEEE Trans. Antennas Propag.*, vol. 62, no. 7, pp. 3443–3449, Jul. 2014.

[17] N. Nguyen-Trong, A. Piotrowski, and C. Fumeaux, "A frequency-reconfigurable dual-band low-profile monopolar antenna," *IEEE Trans. Antennas Propag.*, vol. 65, no. 7, pp. 3336–3343, Jul. 2017.

[18] Y. P. Selvam, M. Kanagasabai, M. G. N. Alsath, S. Velan, S. Kingsly, S. Subbaraj, Y. V. Ramana Rao, R. Srinivasan, A. K. Varadhan, and M. Karuppiah, "A low-profile frequency- and pattern-reconfigurable antenna," *IEEE Antennas Wirel. Propag. Lett.*, vol. 16, pp. 3047–3050, Oct. 2017.

[19] M. S. Alam and A. M. Abbosh, "Wideband pattern-reconfigurable antenna using pair of radial radiators on truncated ground with switchable director and reflector," *IEEE Antennas Wirel. Propag. Lett.*, vol. 16, pp. 24–28, 2017.

[20] Z. Ding, R. Jin, J. Geng, W. Zhu, and X. Liang, "Varactor loaded pattern reconfigurable patch antenna with shorting pins," *IEEE Trans. Antennas Propag.*, vol. 67, no. 10, pp. 6267–6277, Jun. 2019.

[21] C. Y. D. Sim, Y. J. Liao, and H. L. Lin, "Polarization reconfigurable eccentric annular ring slot antenna design," *IEEE Trans. Antennas Propag.*, vol. 63, no. 9, pp. 4152–4155, Sep. 2015.

[22] H. Wong, W. Lin, L. Huitema, and E. Arnaud, "Multi-polarization reconfigurable antenna for wireless biomedical system," *IEEE Trans. Biomed. Circuits Syst.*, vol. 11, no. 3, pp. 652–660, Jun. 2017.

[23] A. Bhattacharjee, S. Dwari, and M. K. Mandal, "Polarization-reconfigurable compact monopole antenna with wide effective bandwidth," *IEEE Antennas Wirel. Propag. Lett.*, vol. 18, no. 5, pp. 1041–1045, May. 2019.

[24] H. A. Majid, M. K. A. Rahim, M. R. Hamid, and M. F. Ismail, "Frequency and pattern reconfigurable slot antenna," *IEEE Trans. Antennas Propag.*, vol. 62, no. 10, pp. 5339–5343, Oct. 2014.

[25] D. Rodrigo, B. A. Cetiner, and L. Jofre, "Frequency, radiation pattern and polarization reconfigurable antenna using a parasitic pixel layer," *IEEE Trans. Antennas Propag.*, vol. 62, no. 6, pp. 3422–3427, Jun. 2014.

[26] N. Nguyen-Trong, L. Hall, and C. Fumeaux, "A Frequency- and Pattern-Reconfigurable Center-Shorted Microstrip Antenna," vol. 15, pp. 1955–1958, 2016.

[27] N. Nguyen-Trong, A. Piotrowski, L. Hall, and C. Fumeaux, "A frequency- and polarization-reconfigurable circular cavity antenna," *IEEE Antennas Wirel. Propag. Lett.*, vol. 16, pp. 999–1002, 2017.

[28] S. J. Chen, D. C. Ranasinghe, and C. Fumeaux, "A robust snap-on button solution for reconfigurable wearable textile antennas," *IEEE Trans. Antennas Propag.*, vol. 66, no. 9, pp. 4541–4551, Sep. 2018.

[29] R. B. V. B. Simorangkir, Y. Yang, K. P. Esselle, and B. A. Zeb, "A method to realize robust flexible electronically tunable antennas using polymer-embedded conductive fabric," *IEEE Trans. Antennas Propag.*, vol. 66, no. 1, pp. 50–58, Jan. 2018.

[30] B. Mohamadzade, R. B. Simorangkir, R. M. Hashmi, R. Gharaei, A. Lalbakhsh, S. Shrestha, M. Zhadobov, and R. Sauleau, "A conformal, dynamic pattern-reconfigurable antenna using conductive textile-polymer composite," *IEEE Trans. Antennas Propag.*, vol. 69, no. 10, pp. 6175–6184, Oct. 2021.

[31] G. Deschamps, "Microstrip microwave antennas," presented at the third USAF Symppsium on Antennas, 1953.

[32] J. Q. Howell, "Microstrip antennas1," *IEEE Trans. Antennas Propag.*, vol. 23, no. 1, pp. 90–93, 1975.

[33] P. K. Agrawal and M. C. Bailey, "An analysis technique for microstrip antennas," *IEEE Trans. Antennas Propag.*, vol. 25, no. 6, pp. 756–759, 1977.

[34] Y. T. Lo, D. Solomon, and W. F. Richards, "Theory and experiment on microstrip antennas," *IEEE Trans. Antennas Propag.*, vol. 27, no. 2, pp. 137–145, 1979.

[35] T. Kaufmann and C. Fumeaux, "Wearable textile half-mode substrate-integrated cavity antenna using embroidered vias," *IEEE Antennas Wirel. Propag. Lett.*, vol. 12, pp. 805–808, 2013.

[36] S. P. Pinapati, D. C. Ranasinghe, and C. Fumeaux, "Textile multilayer cavity slot monopole for UHF applications," *IEEE Antennas Wirel. Propag. Lett.*, vol. 16, pp. 2542–2545, Aug. 2017.

[37] S. J. Chen, T. Kaufmann, D. C. Ranasinghe, and C. Fumeaux, "A modular textile antenna design using snap-on buttons for wearable applications," *IEEE Trans. Antennas Propag.*, vol. 64, no. 3, pp. 894–903, Mar. 2016.

[38] S. H. Wi, Y. B. Sun, I. S. Song, S. H. Choa, I. S. Koh, Y. S. Lee, and J. G. Yook, "Package-level integrated antennas based on LTCC technology," *IEEE Trans. Antennas Propag.*, vol. 54, no. 8, pp. 2190–2197, Aug. 2006.

[39] Y. P. Zhang, "Integrated circuit ceramic ball grid array package antenna," *IEEE Trans. Antennas Propag.*, vol. 52, no. 10, pp. 2538–2544, Oct. 2004.

[40] S. Brebels, J. Ryckaert, B. Côme, S. Donnay, W. De Raedt, E. Beyne, and R. P. Mertens, "SOP integration and codesign of antennas," *IEEE Trans. Adv. Packag.*, vol. 27, no. 2, pp. 341–351, May. 2004.

[41] Q. H. Dang, S. J. Chen, B. Zhu, and C. Fumeaux, "Shorting strategies for wearable textile antennas: A review of four shorting methods," *IEEE Antennas Propag. Mag.*, vol. 64, no. 1, pp. 84–98, Feb. 2022.

[42] Q. H. Dang, S. Jammy Chen, B. Zhu, and C. Fumeaux, "Dual-band dual-mode wearable textile antennas for on-body and off-body communications," *2021 IEEE Asia-Pacific Microw. Conf.*, pp. 64–66, Nov. 2021.

[43] Q. H. Dang, S. J. Chen, D. C. Ranasinghe, and C. Fumeaux, "A reconfiguration module with coplanar snap-on connection for wearable textile antennas," in *2019 Asia-Pacific Microw. Conf.*, 2019, pp. 12–14.

[44] ——, "A frequency-reconfigurable wearable textile antenna with one-octave tuning range," *IEEE Trans. Antennas Propag.*, vol. 69, no. 12, pp. 8080–8089, Dec. 2021.

[45] Q. H. Dang, S. J. Chen, and C. Fumeaux, "Dual-band frequency-reconfigurable flexible wearable textile antenna," *2022 IEEE Int. Symp. Antennas Propag. Usn. Radio Sci. Meet.*, Jul. 2022.

[46] ——, "Thermographic investigation of frequency-reconfigurable wearable antennas," *2022 16th Eur. Conf. Antennas Propag.*, pp. 1–4, Mar. 2022.

[47] Q. H. Dang, S. J. Chen, D. C. Ranasinghe, and C. Fumeaux, "Dual-band reconfigurable flexible antenna with independent frequency tunability," *IEEE Antennas Wirel. Propag. Lett.*, pp. 1–5, 2022.

[48] ——, "Modular integration of a passive RFID sensor with wearable textile antennas for patient monitoring," *IEEE Trans. Components, Packag. Manuf. Technol.*, vol. 10, no. 12, pp. 1979 – 1988, 2020.

[49] ——, "Body-to-antenna gap effect on a UHF wearable textile antenna performance," *2021 IEEE Int. Symp. Antennas Propag. Usn. Radio Sci. Meet.*, pp. 1271–1272, Dec. 2021.

[50] K. Koski, A. Vena, L. Sydänheimo, L. Ukkonen, and Y. Rahmat-Samii, "Design and implementation of electro-textile ground planes for wearable UHF RFID patch tag antennas," *IEEE Antennas Wirel. Propag. Lett.*, vol. 12, pp. 964–967, 2013.

[51] Z. Wang, L. Z. Lee, D. Psychoudakis, and J. L. Volakis, "Embroidered multiband body-worn antenna for GSM/PCS/WLAN communications," *IEEE Trans. Antennas Propag.*, vol. 62, no. 6, pp. 3321–3329, Jun. 2014.

[52] S. Yan, P. J. Soh, and G. A. E. Vandenbosch, "Wearable dual-band magneto-electric dipole antenna for WBAN/WLAN applications," *IEEE Trans. Antennas Propag.*, vol. 63, no. 9, pp. 4165–4169, Sep. 2015.

[53] S. Cichos, J. Haberland, and H. Reichl, "Performance analysis of polymer based antenna-coils for RFID," *2nd Int. IEEE Conf. Polym. Adhes. Microelectron. Photonics, POLYTRONIC 2002 - Conf. Proc.*, pp. 120–124, 2002.

[54] T. Kaufmann, A. Verma, V.-T. Truong, B. Weng, R. Shepherd, and C. Fumeaux, "Efficiency of a compact elliptical planar ultra-wideband antenna based on conductive polymers," *Int. J. Antennas Propag.*, vol. 2012, pp. 1–11, May. 2012.

[55] A. Tsolis, W. Whittow, A. Alexandridis, J. Vardaxoglou, A. Tsolis, W. G. Whittow, A. A. Alexandridis, and J. C. Vardaxoglou, "Embroidery and related manufacturing techniques for wearable antennas: challenges and opportunities," *Electronics*, vol. 3, no. 2, pp. 314–338, May. 2014.

[56] F.-X. Liu, T. Kaufmann, Z. Xu, and C. Fumeaux, "Wearable applications of quarter-wave patch and half-mode cavity antennas," *IEEE Antennas Wirel. Propag. Lett.*, vol. 14, pp. 1478–1481, 2014.

[57] S. Pinapati, T. Kaufmann, D. Ranasinghe, and C. Fumeaux, "Wearable dual-band stripline-fed half-mode substrate-integrated cavity antenna," *Electron. Lett.*, vol. 52, no. 6, pp. 424–426, 2016.

[58] A. S. Alqadami, N. Nguyen-Trong, B. Mohammed, A. E. Stancombe, M. T. Heitzmann, and A. Abbosh, "Compact unidirectional conformal antenna based on flexible high-permittivity custom-made substrate for wearable wideband electromagnetic head imaging system," *IEEE Trans. Antennas Propag.*, vol. 68, no. 1, pp. 183–194, Jan. 2020.

[59] A. S. M. Sayem, R. B. Simorangkir, K. P. Esselle, R. M. Hashmi, and H. Liu, "A Method to Develop Flexible Robust Optically Transparent Unidirectional Antennas Utilizing Pure Water, PDMS, and Transparent Conductive Mesh," *IEEE Trans. Antennas Propag.*, vol. 68, no. 10, pp. 6943–6952, Oct. 2020.

[60] Sang-Jun Ha and C. Won Jung, "Reconfigurable beam steering using a microstrip patch antenna with a U-slot for wearable fabric applications," *IEEE Antennas Wirel. Propag. Lett.*, vol. 10, pp. 1228–1231, 2011.

[61] R. B. V. B. Simorangkir, Y. Yang, L. Matekovits, and K. P. Esselle, "Dual-band dual-mode textile antenna on PDMS substrate for body-centric communications," *IEEE Antennas Wirel. Propag. Lett.*, vol. 16, pp. 677–680, 2017.

[62] H. Lee, J. Tak, and J. Choi, "Wearable antenna integrated into military berets for indoor/outdoor positioning system," *IEEE Antennas Wirel. Propag. Lett.*, vol. 16, pp. 1919–1922, 2017.

[63] P. S. Hall, Y. Hao, Y. I. Nechayev, A. Alomalny, C. C. Constantinou, C. Parini, M. R. Kamarudin, T. Z. Salim, D. T. Hee, R. Dubrovka, A. S. Owadally, W. Song, A. Serra, P. Nepa, M. Gallo, and M. Bozzetti, "Antennas and propagation for on-body communication systems," *IEEE Antennas Propag. Mag.*, vol. 49, no. 3, pp. 41–58, 2007.

[64] P. J. Soh, G. A. E. Vandenbosch, S. L. Ooi, and N. H. M. Rais, "Design of a broadband all-textile slotted PIFA," *IEEE Trans. Antennas Propag.*, vol. 60, no. 1, pp. 379–384, Jan. 2012.

[65] T. Kaufmann, D. C. Ranasinghe, M. Zhou, and C. Fumeaux, "Wearable quarter-wave folded microstrip antenna for passive UHF RFID applications," *Int. J. Antennas Propag.*, vol. 2013, pp. 1–11, Jun. 2013.

[66] S. Pranonsatit, D. Worasawate, and P. Sritanavut, "Affordable ink-jet printed antennas for RFID applications," *IEEE Trans. Components, Packag. Manuf. Technol.*, vol. 2, no. 5, pp. 878–883, 2012.

[67] W. G. Whittow, A. Chauraya, J. C. Vardaxoglou, Y. Li, R. Torah, K. Yang, S. Beeby, and J. Tudor, "Inkjet-printed microstrip patch antennas realized on textile for wearable applications," *IEEE Antennas Wirel. Propag. Lett.*, vol. 13, pp. 71–74, 2014.

[68] S. Genovesi, F. Costa, F. Fanciulli, and A. Monorchio, "Wearable inkjet-printed wideband antenna by using miniaturized AMC for sub-GHz applications," *IEEE Antennas Wirel. Propag. Lett.*, vol. 15, pp. 1927–1930, 2016.

[69] R. N. Simons and R. Q. Lee, "Feasibility study of optically transparent microstrip patch antenna," *IEEE Antennas Propag. Soc. AP-S Int. Symp.*, vol. 4, pp. 2100–2103, 1997.

[70] R. F. Solberg and P. J. Siemsen, "Development of a conductive-polymer, composite, direction-finding antenna," *IEEE Antennas Propag. Soc. Int. Symp. Wirel. Technol. Inf. Networks, APS 1999 - Held conjunction with Usn. Natl. Radio Sci. Meet.*, vol. 3, pp. 1966–1969, 1999.

[71] T. Leng, X. Huang, K. Chang, J. Chen, M. A. Abdalla, and Z. Hu, "Graphene nanoflakes printed flexible meandered-line dipole antenna on paper dubstrate for low-cost RFID and sensing applications," *IEEE Antennas Wirel. Propag. Lett.*, vol. 15, pp. 1565–1568, 2016.

[72] T. Thanh Tung, S. J. Chen, C. Fumeaux, T. Y. Kim, and D. Losic, "N-doped reduced graphene oxide-PEDOT nanocomposites for implementation of a flexible wideband antenna for wearable wireless communication applications," *Nanotechnology*, vol. 32, no. 24, p. 245711, Mar. 2021.

[73] T. T. Tung, S. J. Chen, C. Fumeaux, and D. Losic, "Scalable realization of conductive graphene films for high-efficiency microwave antennas," *J. Mater. Chem. C*, vol. 4, no. 45, pp. 10 620–10 624, Nov. 2016.

[74] I. Locher, M. Klemm, T. Kirstein, and G. Trster, "Design and characterization of purely textile patch antennas," *IEEE Trans. Adv. Packag.*, vol. 29, no. 4, pp. 777–788, Nov. 2006.

[75] D. L. Paul, C. Jayatissa, G. S. Hilton, and C. J. Railton, "Conformability of a textile antenna for reception of digital television," *2010 Loughbrgh. Antennas Propag. Conf. LAPC 2010*, pp. 225–228, 2010.

[76] Y. Hong, J. Tak, and J. Choi, "An all-textile SIW cavity-backed circular ring-slot antenna for WBAN applications," *IEEE Antennas Wirel. Propag. Lett.*, vol. 15, pp. 1995–1999, 2016.

[77] B. Hu, G. P. Gao, L. L. He, X. D. Cong, and J. N. Zhao, "Bending and on-arm effects on a wearable antenna for 2.45 GHz body area network," *IEEE Antennas Wirel. Propag. Lett.*, vol. 15, pp. 378–381, 2016.

[78] G. P. Gao, C. Yang, B. Hu, R. F. Zhang, and S. F. Wang, "A wide-bandwidth wearable all-textile PIFA with dual resonance modes for 5 GHz WLAN applications," *IEEE Trans. Antennas Propag.*, vol. 67, no. 6, pp. 4206–4211, Jun. 2019.

[79] H. Yang and X. Liu, "Wearable dual-band and dual-polarized textile antenna for on- And off-body communications," *IEEE Antennas Wirel. Propag. Lett.*, vol. 19, no. 12, pp. 2324–2328, Dec. 2020.

[80] S. Hage-Ali, N. Tiercelin, P. Coquet, R. Sauleau, H. Fujita, V. Preobrazhensky, and P. Pernod, "A millimeter-wave microstrip antenna array on ultra-flexible micromachined polydimethylsiloxane (PDMS) polymer," *IEEE Antennas Wirel. Propag. Lett.*, vol. 8, pp. 1306–1309, 2009.

[81] Z. Wang, L. Zhang, Y. Bayram, and J. L. Volakis, "Embroidered conductive fibers on polymer composite for conformal antennas," *IEEE Trans. Antennas Propag.*, vol. 60, no. 9, pp. 4141–4147, 2012.

[82] A. S. M. Alqadami, M. F. Jamlos, P. J. Soh, and G. A. Vandenbosch, "Assessment of PDMS Technology in a MIMO Antenna Array," *IEEE Antennas Wirel. Propag. Lett.*, vol. 15, pp. 1939–1942, 2016.

[83] C. Cibin, P. Leuchtmann, M. Gimersky, R. Vahldieck, and S. Mosclbroda, "A flexible wearable antenna," *IEEE Antennas Propag. Soc. AP-S Int. Symp.*, vol. 4, pp. 3589–3592, 2004.

[84] S. J. Chen, D. C. Ranasinghe, and C. Fumeaux, "A polarization/frequency interchangeable patch for a modular wearable textile antenna," in *2017 11th Eur. Conf. Antennas Propag.* IEEE, Mar. 2017, pp. 2483–2486.

[85] C. A. Balanis, *Antenna theory: analysis and design*. Wiley Interscience, 2005.

[86] T. Kaufmann, I.-M. Fumeaux, and C. Fumeaux, "Comparison of fabric and embroidered dipole antennas," in *7th Eur. Conf. Antennas Propag.* IEEE, 2013.

[87] G. Ginestet, N. Brechet, J. Torres, E. Moradi, L. Ukkonen, T. Björninen, and J. Virkki, "Embroidered antenna-microchip interconnections and contour antennas in passive UHF RFID textile tags," *IEEE Antennas Wirel. Propag. Lett.*, vol. 16, pp. 1205–1208, 2017.

[88] S. J. Chen, C. Fumeaux, D. C. Ranasinghe, and T. Kaufmann, "Paired snap-on buttons connections for balanced antennas in wearable systems," *IEEE Antennas Wirel. Propag. Lett.*, vol. 14, pp. 1498–1501, 2015.

[89] M. Klemm and G. Troester, "Textile UWB antennas for wireless body area networks," *IEEE Trans. Antennas Propag.*, vol. 54, no. 11, pp. 3192–3197, 2006.

[90] H. T. Friis, C. B. Feldman, and W. M. Sharpless, "The determination of the direction of arrival of short radio waves," *Proc. Inst. Radio Eng.*, vol. 22, no. 1, pp. 47–78, 1934.

[91] E. BRUCE and A. C. BECK, "Experiments with directivity steering for fading reduction," *Proc. Inst. Radio Eng.*, vol. 23, no. 4, pp. 357–371, 1935.

[92] H. T. Friis and C. B. Feldman, "A multiple unit steerable antenna for short-wave reception," *Bell Syst. Tech. J.*, vol. 16, no. 3, pp. 337–419, 1937.

[93] S. L. S. Yang, A. A. Kishk, and K. F. Lee, "Frequency reconfigurable U-slot microstrip patch antenna," *IEEE Antennas Wirel. Propag. Lett.*, vol. 7, pp. 127–129, 2008.

[94] M. N. M. Kehn, O. Quevedo-Teruel, and E. Rajo-Iglesias, "Reconfigurable loaded planar inverted-F sntenna using varactor diodes," *IEEE Antennas Wirel. Propag. Lett.*, vol. 10, pp. 466–468, May. 2011.

[95] N. Nguyen-Trong, T. Kaufmann, L. Hall, and C. Fumeaux, "Analysis and design of a reconfigurable antenna based on half-mode substrate-integrated cavity," *IEEE Trans. Antennas Propag.*, vol. 63, no. 8, pp. 3345–3353, Aug. 2015.

[96] N. Nguyen-Trong and C. Fumeaux, "Tuning range and efficiency optimization of a frequency-reconfigurable patch antenna," *IEEE Antennas Wirel. Propag. Lett.*, vol. 17, no. 1, pp. 150–154, Jan. 2018.

[97] J. S. Row, W. L. Liu, and T. R. Chen, "Circular polarization and polarization reconfigurable designs for annular slot antennas," *IEEE Trans. Antennas Propag.*, vol. 60, no. 12, pp. 5998–6002, 2012.

[98] P.-Y. Qin, Y. J. Guo, A. R. Weily, and C.-H. Liang, "A pattern reconfigurable U-slot antenna and its applications in MIMO systems," *IEEE Trans. Antennas Propag.*, vol. 60, no. 2, pp. 516–528, Feb. 2012.

[99] W. Lin, H. Wong, and R. W. Ziolkowski, "Wideband pattern-reconfigurable antenna with switchable broadside and conical beams," *IEEE Antennas Wirel. Propag. Lett.*, vol. 16, pp. 2638–2641, 2017.

[100] S. L. Chen, P. Y. Qin, W. Lin, and Y. J. Guo, "Pattern-reconfigurable antenna with five switchable beams in elevation plane," *IEEE Antennas Wirel. Propag. Lett.*, vol. 17, no. 3, pp. 454–457, Mar. 2018.

[101] S. Nikolaou, R. Bairavasubramanian, C. Lugo, I. Carrasquillo, D. C. Thompson, G. E. Ponchak, J. Papapolymerou, and M. M. Tentzeris, "Pattern and frequency reconfigurable annular slot antenna using pin diodes," *IEEE Trans. Antennas Propag.*, vol. 54, no. 2, pp. 439–448, Feb. 2006.

[102] N. Nguyen-Trong, L. Hall, and C. Fumeaux, "A frequency- and polarization-reconfigurable stub-Loaded microstrip patch antenna," *IEEE Trans. Antennas Propag.*, vol. 63, no. 11, pp. 5235–5240, Nov. 2015.

[103] S. N. M. Zainarry, N. Nguyen-Trong, and C. Fumeaux, "A frequency- and pattern-reconfigurable two-element array antenna," *IEEE Antennas Wirel. Propag. Lett.*, vol. 17, no. 4, pp. 617–620, Apr. 2018.

[104] S. Yan and G. A. E. Vandenbosch, "Radiation pattern-reconfigurable wearable antenna based on metamaterial structure," *IEEE Antennas Wirel. Propag. Lett.*, vol. 15, pp. 1715–1718, 2016.

[105] S. Manzari, C. Occhiuzzi, S. Nawale, A. Catini, C. Di Natale, and G. Marrocco, "Humidity sensing by polymer-loaded UHF RFID antennas," *IEEE Sens. J.*, vol. 12, no. 9, pp. 2851–2858, Sep. 2012.

[106] Z. Hamouda, J. L. Wojkiewicz, A. A. Pud, L. Kone, B. Belaabed, S. Bergheul, and T. Lasri, "Dual-band elliptical planar conductive polymer antenna printed on a flexible substrate," *IEEE Trans. Antennas Propag.*, vol. 63, no. 12, pp. 5864–5867, Dec. 2015.

[107] M. Akbari, M. W. A. Khan, M. Hasani, T. Björninen, L. Sydänheimo, and L. Ukkonen, "Fabrication and characterization of graphene antenna for low-cost and environmentally friendly RFID tags," *IEEE Antennas Wirel. Propag. Lett.*, vol. 15, pp. 1569–1572, 2016.

[108] P. Kopyt, B. Salski, M. Olszewska-Placha, D. Janczak, M. Sloma, T. Kurkus, M. Jakubowska, and W. Gwarek, "Graphene-based dipole antenna for a UHF RFID tag," *IEEE Trans. Antennas Propag.*, vol. 64, no. 7, pp. 2862–2868, Jul. 2016.

[109] H. Li, S. Sun, B. Wang, and F. Wu, "Design of compact single-layer textile MIMO antenna for wearable applications," *IEEE Trans. Antennas Propag.*, vol. 66, no. 6, pp. 3136–3141, Jun. 2018.

[110] D. L. Diedhiou, O. De Sagazan, R. Sauleau, and A. V. Boriskin, "Contactless microstrip transition for flexible microfluidic circuits and antennas," *IEEE Antennas Wirel. Propag. Lett.*, vol. 14, pp. 1502–1505, 2015.

[111] Zhan Li, Yahya Rahmat-Samii, and Teemu Kaiponenz, "Bandwidth study of a dual band PIFA on a fixed substrate for wireless communication," in *IEEE Antennas Propag. Soc. Int. Symp. Dig. Held conjunction with Usn. North Am. Radio Sci. Meet. (Cat. No.03CH37450)*, vol. 1. IEEE, pp. 435–438.

[112] H. T. Chen, K. L. Wong, and T. W. Chiou, "PIFA with a meandered and folded patch for the dual-band mobile phone application," *IEEE Trans. Antennas Propag.*, vol. 51, no. 9, pp. 2468–2471, Sep. 2003.

[113] L. Sun, Y. Li, Z. Zhang, and M. F. Iskander, "Low-cost compact circularly polarized dual-layer PIFA for active RFID reader," *IEEE Trans. Antennas Propag.*, vol. 67, no. 1, pp. 681–686, Jan. 2019.

[114] H. Gharibi and F. H. Kashani, "Design of a compact circularly polarized dual-mode monopulse cavity-backed substrate integrated waveguide antenna," *IEEE Antennas Wirel. Propag. Lett.*, vol. 14, pp. 519–522, 2015.

[115] H. Lee, Y. Sung, C. T. M. Wu, and T. Itoh, "Dual-band and polarization-flexible cavity antenna based on substrate integrated waveguide," *IEEE Antennas Wirel. Propag. Lett.*, vol. 15, pp. 488–491, 2016.

[116] K. Kumar and S. Dwar, "Substrate integrated waveguide cavity-backed self-Triplexing slot antenna," *IEEE Antennas Wirel. Propag. Lett.*, vol. 16, pp. 3249–3252, Nov. 2017.

[117] K. Dhwaj, J. M. Kovitz, H. Tian, L. J. Jiang, and T. Itoh, "Half-mode cavity-based planar filtering antenna with controllable transmission zeroes," *IEEE Antennas Wirel. Propag. Lett.*, vol. 17, no. 5, pp. 833–836, May. 2018.

[118] X. Yang, L. Ge, Y. Ji, X. Zeng, and K. M. Luk, "Design of low-profile multi-band half-mode substrate-integrated waveguide antennas," *IEEE Trans. Antennas Propag.*, vol. 67, no. 10, pp. 6639–6644, Oct. 2019.

[119] J. S. Row and S. H. Chen, "Wideband monopolar square-ring patch antenna," *IEEE Trans. Antennas Propag.*, vol. 54, no. 4, pp. 1335–1339, Apr. 2006.

[120] S.-J. Lin and J.-S. Row, "Monopolar patch antenna with dual-band and wideband operations," *IEEE Trans. Antennas Propag.*, vol. 56, no. 3, pp. 900–903, Mar. 2008.

[121] J. Liu, Q. Xue, H. Wong, H. W. Lai, and Y. Long, "Design and analysis of a low-profile and broadband microstrip monopolar patch antenna," *IEEE Trans. Antennas Propag.*, vol. 61, no. 1, pp. 11–18, 2013.

[122] Juhua Liu, Shaoyong Zheng, Yuanxin Li, and Yunliang Long, "Broadband monopolar microstrip patch antenna with shorting vias and coupled ring," *IEEE Antennas Wirel. Propag. Lett.*, vol. 13, pp. 39–42, 2014.

[123] T. Kaufmann and C. Fumeaux, "Low-profile magnetic loop monopole antenna based on a square substrate-integrated cavity," *Int. J. Antennas Propag.*, vol. 2015, pp. 1–6, Jan. 2015.

[124] N. Nguyen-Trong, S. P. Pinapati, D. Hall, A. Piotrowski, and C. Fumeaux, "Ultralow-profile and flush-mounted monopolar antennas integrated into a metallic cavity," *IEEE Antennas Wirel. Propag. Lett.*, vol. 17, no. 1, pp. 86–89, Jan. 2018.

[125] H. Nakano, H. Iwaoka, K. Morishita, and J. Yamauchi, "A wideband low-profile antenna composed of a conducting body of revolution and a shorted parasitic ring," *IEEE Trans. Antennas Propag.*, vol. 56, no. 4, pp. 1187–1192, Apr. 2008.

[126] L. Zhang, Z. Wang, and J. L. Volakis, "Textile antennas and sensors for body-worn applications," *IEEE Antennas Wirel. Propag. Lett.*, vol. 11, pp. 1690–1693, 2012.

[127] A. Kiourti and J. L. Volakis, "High-geometrical-accuracy embroidery process for textile antennas with fine details," *IEEE Antennas Wirel. Propag. Lett.*, vol. 14, pp. 1474–1477, 2015.

[128] S. J. Chen, T. Kaufmann, and C. Fumeaux, "Shorting strategies for a wearable L-slot planar inverted-F antenna," in *2014 Int. Work. Antenna Technol. Small Antennas, Nov. EM Struct. Mater. Appl.* IEEE, Mar. 2014, pp. 18–21.

[129] D. Van Baelen, S. Lemey, J. Verhaevert, and H. Rogier, "A novel manufacturing process for compact, low-weight and flexible ultra-wideband cavity backed textile antennas," *Materials (Basel).*, vol. 11, no. 1, p. 67, Jan. 2018.

[130] S. Agneessens, S. Lemey, T. Vervust, and H. Rogier, "Wearable, small, and robust: the circular quarter-mode textile antenna," *IEEE Antennas Wirel. Propag. Lett.*, vol. 14, pp. 1482–1485, 2015.

[131] O. Caytan, S. Lemey, S. Agneessens, D. Vande Ginste, P. Demeester, C. Loss, R. Salvado, and H. Rogier, "Half-mode substrate-integrated-waveguide cavity-backed slot antenna on cork substrate," *IEEE Antennas Wirel. Propag. Lett.*, vol. 15, pp. 162–165, 2016.

[132] S. Lemey, S. Agneessens, P. Van Torre, K. Baes, J. Vanfleteren, and H. Rogier, "Wearable flexible lightweight modular RFID tag with integrated energy harvester," *IEEE Trans. Microw. Theory Tech.*, vol. 64, no. 7, pp. 2304–2314, Jul. 2016.

[133] S. J. Chen, D. C. Ranasinghe, and C. Fumeaux, "Snap-on buttons as detachable shorting vias for wearable textile antennas," in *2016 Int. Conf. Electromagn. Adv. Appl.* IEEE, Sep. 2016, pp. 521–524.

[134] S. Zhang, A. Chauraya, W. Whittow, R. Seager, T. Acti, T. Dias, and Y. Vardaxoglou, "Embroidered wearable antennas using conductive threads with different stitch spacings," in *2012 Loughbrgh. Antennas Propag. Conf.* IEEE, Nov. 2012, pp. 1–4.

[135] P. Salonen, L. Sydänheimo, M. Keskilammi, and M. Kivikoski, "A small planar inverted-F antenna for wearable applications," in *Dig. Pap. Third Int. Symp. Wearable Comput.* IEEE Comput. Soc, pp. 95–100.

[136] P. Nepa and H. Rogier, "Wearable antennas for off-body radio links at VHF and UHF bands: challenges, the state of the art, and future trends below 1 GHz," pp. 30–52, Oct. 2015.

[137] K. Paramayudha, S. J. Chen, W. Withayachumnankul, and C. Fumeaux, "Low-profile monopole antenna with via-less shorting," in *2018 Aust. Microw. Symp.* IEEE, Feb. 2018, pp. 11–12.

[138] S. P. Pinapati, D. Ranasinghe, and C. Fumeaux, "Characterization of conductive textiles for wearable RFID applications," in *2016 Int. Conf. Electromagn. Adv. Appl.* IEEE, Sep. 2016, pp. 341–344.

[139] R. Seager, S. Zhang, A. Chauraya, W. Whittow, Y. Vardaxoglou, T. Acti, and T. Dias, "Effect of the fabrication parameters on the performance of embroidered antennas," *IET Microwaves, Antennas Propag.*, vol. 7, no. 14, pp. 1174–1181, 2013.

[140] T. Kellomäki, "Snaps to connect coaxial and microstrip lines in wearable systems," *Int. J. Antennas Propag.*, vol. 2012, 2012.

[141] K. N. Paracha, S. K. Abdul Rahim, P. J. Soh, and M. Khalily, "Wearable antennas: a review of materials, structures, and innovative features for autonomous communication and sensing," pp. 56 694–56 712, 2019.

[142] X. Yin, S. J. Chen, and C. Fumeaux, "Wearable dual-band dual-polarization button antenna for WBAN applications," *IEEE Antennas Wirel. Propag. Lett.*, vol. 19, no. 12, pp. 2240–2244, Dec. 2020.

[143] C. Hertleer, H. Rogier, L. Vallozzi, and L. Van Langenhove, "A textile antenna for off-body communication integrated into protective clothing for firefighters," *IEEE Trans. Antennas Propag.*, vol. 57, no. 4, pp. 919–925, Apr. 2009.

[144] X. Tong, C. Liu, X. Liu, H. Guo, and X. Yang, "Switchable ON-/OFF-body antenna for 2.45 GHz WBAN applications," *IEEE Trans. Antennas Propag.*, vol. 66, no. 2, pp. 967–971, Feb. 2018.

[145] P. Bhartia and I. Bahl, "A frequency agile microstrip antenna," in *1982 Antennas Propag. Soc. Int. Symp.*, vol. 20. Institute of Electrical and Electronics Engineers, pp. 304–307.

[146] P.-Y. Qin, A. R. Weily, Y. J. Guo, and C.-H. Liang, "Polarization reconfigurable U-slot patch antenna," *IEEE Trans. Antennas Propag.*, vol. 58, no. 10, pp. 3383–3388, Oct. 2010.

[147] P. Y. Qin, Y. J. Guo, Y. Cai, E. Dutkiewicz, and C. H. Liang, "A reconfigurable antenna with frequency and polarization agility," *IEEE Antennas Wirel. Propag. Lett.*, vol. 10, pp. 1373–1376, 2011.

[148] P. Y. Qin, Y. Jay Guo, and C. Ding, "A dual-band polarization reconfigurable antenna for WLAN systems," *IEEE Trans. Antennas Propag.*, vol. 61, no. 11, pp. 5706–5713, 2013.

[149] MACOM-Technology-Solutions, *Product: MA4FCP300*, 2017. [Online]. Available: https://www.macom.com/products/product-detail/MA4FCP300

[150] R. L. Haupt and M. Lanagan, "Reconfigurable antennas," *IEEE Antennas Propag. Mag.*, vol. 55, no. 1, pp. 49–61, Feb. 2013.

[151] J. Costantine, Y. Tawk, S. E. Barbin, and C. G. Christodoulou, "Reconfigurable antennas: design and applications," *Proc. IEEE*, vol. 103, no. 3, pp. 424–437, Mar. 2015.

[152] J. T. Rayno and S. K. Sharma, "Wideband frequency-reconfigurable spirograph planar monopole antenna (SPMA) operating in the UHF band," *IEEE Antennas Wirel. Propag. Lett.*, vol. 11, pp. 1537–1540, 2012.

[153] X. Jiang, Z. Zhang, Y. Li, and Z. Feng, "A novel null scanning antenna using even and odd modes of a shorted patch," *IEEE Trans. Antennas Propag.*, vol. 62, no. 4, pp. 1903–1909, 2014.

[154] Xue-Xia Yang, Bing-Cheng Shao, Fan Yang, A. Z. Elsherbeni, and Bo Gong, "A polarization reconfigurable patch antenna with loop slots on the ground plane," *IEEE Antennas Wirel. Propag. Lett.*, vol. 11, pp. 69–72, 2012.

[155] B. Babakhani, S. K. Sharma, and N. R. Labadie, "A frequency agile microstrip patch phased array antenna with polarization reconfiguration," *IEEE Trans. Antennas Propag.*, vol. 64, no. 10, pp. 4316–4327, Oct. 2016.

[156] H. Li, J. Xiong, Y. Yu, and S. He, "A simple compact reconfigurable slot antenna with a very wide tuning range," *IEEE Trans. Antennas Propag.*, vol. 58, no. 11, pp. 3725–3728, Nov. 2010.

[157] N. Behdad and K. Sarabandi, "Dual-band reconfigurable antenna with a very wide tunability range," *IEEE Trans. Antennas Propag.*, vol. 54, no. 2, pp. 409–416, Feb. 2006.

[158] L. Pazin and Y. Leviatan, "Reconfigurable slot antenna for switchable multiband operation in a wide frequency range," *IEEE Antennas Wirel. Propag. Lett.*, vol. 12, pp. 329–332, 2013.

[159] J. S. Row and J. F. Tsai, "Frequency-reconfigurable microstrip patch antennas with circular polarization," *IEEE Antennas Wirel. Propag. Lett.*, vol. 13, pp. 1112–1115, 2014.

[160] H. Gu, J. Wang, and L. Ge, "Circularly polarized patch antenna with frequency reconfiguration," *IEEE Antennas Wirel. Propag. Lett.*, vol. 14, pp. 1770–1773, 2015.

[161] K. Gupta, R. Garg, and I. Bahl, "Microstrip lines and slotlines," *Artech house*, 1979.

[162] N. G. Alexopoulos and S. C. Wu, "Frequency-independent equivalent circuit model for microstrip open-end and gap discontinuities," *IEEE Trans. Microw. Theory Tech.*, vol. 42, no. 7, pp. 1268–1272, 1994.

[163] P. Silvester and P. Benedek, "Equivalent capacitances of microstrip open circuits," *IEEE Trans. Microw. Theory Tech.*, vol. 20, no. 8, pp. 511–516, 1972.

[164] E. Hammerstad and O. Jensen, "Accurate models for microstrip computer-aided design," in *IEEE MTT-S Int. Microw. Symp. Dig.*, May. 1980, pp. 107–409.

[165] M. Kirschning, R. H. Jansen, and N. H. Koster, "Accurate model for open end effect of microstrip lines," *Electron. Lett.*, vol. 17, no. 3, pp. 123–125, Feb. 1981.

[166] E. O. Hammerstad, "Equations for microstrip circuit design." Institute of Electrical and Electronics Engineers (IEEE), Nov. 2007, pp. 268–272.

[167] Q. Bai, R. Singh, K. L. Ford, T. O'Farrell, and R. J. Langley, "An independently tunable tri-band antenna design for concurrent multiband single chain radio receivers," *IEEE Trans. Antennas Propag.*, vol. 65, no. 12, pp. 6290–6297, Dec. 2017.

[168] S. P. Pinapati, S. J. Chen, D. Ranasinghe, and C. Fumeaux, "Detuning effects of wearable patch antennas," *Asia-Pacific Microw. Conf. Proceedings, APMC*, vol. 1, pp. 162–165, 2018.

[169] S. J. Chen, D. C. Ranasinghe, and C. Fumeaux, "Reconfigurable wearable antenna for compensation of detuning effects," 2019.

[170] F. C. Henriques, Jr., and A. R. Moritz, "Studies of thermal injury: I. the conduction of heat to and through skin and the temperatures attained therein. A theoretical and an experimental investigation*," *Am. J. Pathol.*, vol. 23, no. 4, p. 530, Jul. 1947.

[171] G. S. Baird, "The effect of circuit loading on electrical problem temperature," vol. 0780, no. 11, pp. 47–49, May. 1987.

[172] H. F. Abutarboush, R. Nilavalan, S. W. Cheung, and K. M. Nasr, "Compact printed multiband antenna with independent setting suitable for fixed and reconfigurable wireless communication systems," *IEEE Trans. Antennas Propag.*, vol. 60, no. 8, pp. 3867–3874, 2012.

[173] R. O. Ouedraogo, J. Tang, K. Fuchi, E. J. Rothwell, A. R. Diaz, and P. Chahal, "A tunable dual-band miniaturized monopole antenna for compact wireless devices," *IEEE Antennas Wirel. Propag. Lett.*, vol. 13, pp. 1247–1250, 2014.

[174] A. Boukarkar, X. Q. Lin, J. W. Yu, P. Mei, Y. Jiang, and Y. Q. Yu, "A highly integrated independently tunable triple-band patch antenna," *IEEE Antennas Wirel. Propag. Lett.*, vol. 16, pp. 2216–2219, 2017.

[175] F. A. Asadallah, J. Costantine, and Y. Tawk, "A multiband compact reconfigurable PIFA based on nested slots," *IEEE Antennas Wirel. Propag. Lett.*, vol. 17, no. 2, pp. 331–334, Feb. 2018.

[176] K. Paramayudha, S. J. Chen, T. Kaufmann, W. Withayachumnankul, and C. Fumeaux, "Triple-band reconfigurable low-profile monopolar antenna with independent tunability," *IEEE Open J. Antennas Propag.*, vol. 1, pp. 47–56, Mar. 2020.

[177] I. Lim and S. Lim, "Monopole-like and boresight pattern reconfigurable antenna," *IEEE Trans. Antennas Propag.*, vol. 61, no. 12, pp. 5854–5859, 2013.

[178] P. K. Li, Z. H. Shao, Q. Wang, and Y. J. Cheng, "Frequency- and pattern-reconfigurable antenna for multistandard wireless applications," *IEEE Antennas Wirel. Propag. Lett.*, vol. 14, pp. 333–336, 2015.

[179] C. Y. Chiu, S. Shen, B. K. Lau, and R. Murch, "The design of a trimodal broadside antenna element for compact massive MIMO arrays: utilizing the theory of characteristic modes," *IEEE Antennas Propag. Mag.*, vol. 62, no. 6, pp. 46–61, Dec. 2020.

[180] E. DiGiampaolo, A. DiCarlofelice, and A. Gregori, "An RFID-enabled wireless strain gauge sensor for static and dynamic structural monitoring," *IEEE Sens. J.*, vol. 17, no. 2, pp. 286–294, Jan. 2017.

[181] B. Gao and M. M. Yuen, "Passive UHF RFID packaging with electromagnetic band gap (EBG) material for metallic objects tracking," *IEEE Trans. Components, Packag. Manuf. Technol.*, vol. 1, no. 8, pp. 1140–1146, Aug. 2011.

[182] H. Gholamhosseini, M. M. Baig, M. J. Connolly, and M. Linden, "A multifactorial falls risk prediction model for hospitalized older adults," in *2014 36th Annu. Int. Conf. IEEE Eng. Med. Biol. Soc. EMBC 2014*. Institute of Electrical and Electronics Engineers Inc., Nov. 2014, pp. 3484–3487.

[183] J. R. Smith, "Wirelessly powered sensor networks and computational RFID," Springer New York Heidelb. Dordr. London, 2013.

[184] T. E. Lockhart, A. T. Barth, X. Zhang, R. Songra, E. Abdel-Rahman, and J. Lach, "Portable, non-invasive fall risk assessment in end stage renal disease patients on hemodialysis," in *Wirel. Heal. 2010 - WH '10*. New York, New York, USA: ACM Press, 2010, p. 84.

[185] R. L. Shinmoto Torres, R. Visvanathan, D. Abbott, K. D. Hill, and D. C. Ranasinghe, "A battery-less and wireless wearable sensor system for identifying bed and chair exits in a pilot trial in hospitalized older people," *PLoS One*, vol. 12, no. 10, Oct. 2017.

[186] A. Wickramasinghe, D. C. Ranasinghe, C. Fumeaux, K. D. Hill, and R. Visvanathan, "Sequence learning with passive RFID sensors for real-time bed-egress recognition in older people," *IEEE J. Biomed. Heal. Informatics*, vol. 21, no. 4, pp. 917–929, Jul. 2017.

[187] D. Ranasinghe, R. Shinmoto Torres, K. Hill, and R. Visvanathan, "Low cost and batteryless sensor-enabled radio frequency identification tag based approaches to identify patient bed entry and exit posture transitions," *Gait Posture*, vol. 39, no. 1, pp. 118–123, Jan. 2014.

[188] M. Kangas, A. Konttila, I. Winblad, and T. Jamsa, "Determination of simple thresholds for accelerometry-based parameters for fall detection," in *2007 29th Annu. Int. Conf. IEEE Eng. Med. Biol. Soc.* IEEE, Aug. 2007, pp. 1367–1370.

[189] F. Hussain, M. Ehatisham-ul Haq, M. A. Azam, and A. Khalid, "Elderly assistance using wearable sensors by detecting fall and recognizing fall patterns," in *Proc. 2018 ACM Int. Jt. Conf. 2018 Int. Symp. Pervasive Ubiquitous Comput. Wearable Comput. - UbiComp '18*. New York, New York, USA: ACM Press, 2018, pp. 770–777.

[190] Shaopeng Liu, R. X. Gao, D. John, J. W. Staudenmayer, and P. S. Freedson, "Multisensor data fusion for physical activity assessment," *IEEE Trans. Biomed. Eng.*, vol. 59, no. 3, pp. 687–696, Mar. 2012.

[191] D. Karantonis, M. Narayanan, M. Mathie, N. Lovell, and B. Celler, "Implementation of a real-time human movement classifier using a triaxial accelerometer for ambulatory monitoring," *IEEE Trans. Inf. Technol. Biomed.*, vol. 10, no. 1, pp. 156–167, Jan. 2006.

[192] M. Narayanan, S. Redmond, M. Scalzi, S. Lord, B. Celler, and N. Lovell, "Longitudinal falls-risk estimation using triaxial accelerometry," *IEEE Trans. Biomed. Eng.*, vol. 57, no. 3, pp. 534–541, Mar. 2010.

[193] A. Godfrey, A. Bourke, G. Ólaighin, P. van de Ven, and J. Nelson, "Activity classification using a single chest mounted tri-axial accelerometer," *Med. Eng. Phys.*, vol. 33, no. 9, pp. 1127–1135, Nov. 2011.

[194] S. H. Wi, J. S. Kim, N. K. Kang, J. C. Kim, H. G. Yang, Y. S. Kim, and J. G. Yook, "Package-level integrated LTCC antenna for RF package application," *IEEE Trans. Adv. Packag.*, vol. 30, no. 1, pp. 132–141, Feb. 2007.

[195] S. H. Wi, Y. P. Zhang, H. Kim, I. Y. Oh, and J. G. Yook, "Integration of antenna and feeding network for compact UWB transceiver package," *IEEE Trans. Components, Packag. Manuf. Technol.*, vol. 1, no. 1, pp. 111–118, 2011.

[196] R. L. L. Li, G. DeJean, M. Maeng, K. Lim, S. Pinel, M. M. Tentzeris, and J. Laskar, "Design of compact stacked-patch antennas in LTCC multilayer packaging modules for wireless applications," *IEEE Trans. Adv. Packag.*, vol. 27, no. 4, pp. 581–589, Nov. 2004.

[197] A. Ali Babar, T. Björninen, V. A. Bhagavati, L. Sydänheimo, P. Kallio, and L. Ukkonen, "Small and flexible metal mountable passive UHF RFID tag on high-dielectric polymer-ceramic composite substrate," *IEEE Antennas Wirel. Propag. Lett.*, vol. 11, pp. 1319–1322, 2012.

[198] S. Shao, A. Kiourti, R. J. Burkholder, and J. L. Volakis, "Broadband textile-based passive UHF RFID tag antenna for elastic material," *IEEE Antennas Wirel. Propag. Lett.*, vol. 14, pp. 1385–1388, 2015.

[199] S. Lemey, F. Declercq, and H. Rogier, "Dual-band substrate integrated waveguide textile antenna with integrated solar harvester," *IEEE Antennas Wirel. Propag. Lett.*, vol. 13, pp. 269–272, 2014.

[200] Y. L. Zheng, X. R. Ding, C. C. Y. Poon, B. P. L. Lo, H. Zhang, X. L. Zhou, G. Z. Yang, N. Zhao, and Y. T. Zhang, "Unobtrusive sensing and wearable devices for health informatics," *IEEE Trans. Biomed. Eng.*, vol. 61, no. 5, pp. 1538–1554, 2014.

[201] R. Steele, A. Lo, C. Secombe, and Y. K. Wong, "Elderly persons' perception and acceptance of using wireless sensor networks to assist healthcare," *Int. J. Med. Inform.*, vol. 78, no. 12, pp. 788–801, Dec. 2009.

[202] G. Mountain, S. Wilson, C. Eccleston, S. Mawson, J. Hammerton, T. Ware, H. Zheng, R. Davies, N. Black, N. Harris, T. Stone, and H. Hu, "Developing and testing a telerehabilitation system for people following stroke: Issues of usability," *J. Eng. Des.*, vol. 21, no. 2-3, pp. 223–236, Apr. 2010.

[203] K. Rao, P. Nikitin, and S. Lam, "Antenna design for UHF RFID tags: a review and a practical application," *IEEE Trans. Antennas Propag.*, vol. 53, no. 12, pp. 3870–3876, Dec. 2005.

[204] A. Sample, D. Yeager, P. Powledge, A. Mamishev, and J. Smith, "Design of an RFID-based battery-free programmable sensing platform," *IEEE Trans. Instrum. Meas.*, vol. 57, no. 11, pp. 2608–2615, Nov. 2008.

[205] G. A. Casula, A. Michel, P. Nepa, G. Montisci, and G. Mazzarella, "Robustness of wearable UHF-band PIFAs to human-body proximity," *IEEE Trans. Antennas Propag.*, vol. 64, no. 5, pp. 2050–2055, May. 2016.

[206] N. L. Bohannon and J. T. Bernhard, "Design guidelines using characteristic mode theory for improving the bandwidth of PIFAs," *IEEE Trans. Antennas Propag.*, vol. 63, no. 2, pp. 459–465, Feb. 2015.

[207] IEEE International Committee on Electromagnetic Safety., Institute of Electrical and Electronics Engineers., and IEEE-SA Standards Board., *IEEE standard for safety levels with respect to human exposure to radio frequency electromagnetic fields, 3kHz to 300 GHz*. IEEE, 2006.

[208] D. C. Ranasinghe, R. L. Shinmoto Torres, A. P. Sample, J. R. Smith, K. Hill, and R. Visvanathan, "Towards falls prevention: A wearable wireless and battery-less sensing and automatic identification tag for real time monitoring of human movements," in *2012 Annu. Int. Conf. IEEE Eng. Med. Biol. Soc.* IEEE, Aug. 2012, pp. 6402–6405.

[209] R. L. Shinmoto Torres, Q. Shi, A. van den Hengel, and D. C. Ranasinghe, "A hierarchical model for recognizing alarming states in a batteryless sensor alarm intervention for preventing falls in older people," *Pervasive Mob. Comput.*, vol. 40, pp. 1–16, Sep. 2017.

[210] D. Ferreira, P. Pires, R. Rodrigues, and R. F. Caldeirinha, "Wearable textile antennas: examining the effect of bending on their performance." *IEEE Antennas Propag. Mag.*, vol. 59, no. 3, pp. 54–59, Jun. 2017.

[211] M. Toivonen, T. Björninen, L. Sydänheimo, L. Ukkonen, and Y. Rahmat-Samii, "Impact of moisture and washing on the performance of embroidered UHF RFID tags," *IEEE Antennas Wirel. Propag. Lett.*, vol. 12, pp. 1590–1593, 2013.

[212] B. S. Yildirim, B. A. Cetiner, G. Roqueta, and L. Jofre, "Integrated bluetooth and UWB antenna," *IEEE Antennas Wirel. Propag. Lett.*, vol. 8, pp. 149–152, 2009.

[213] Y. W. Chong, W. Ismail, K. Ko, and C. Y. Lee, "Energy harvesting for wearable devices: a Review," *IEEE Sens. J.*, vol. 19, no. 20, pp. 9047–9062, Oct. 2019.

Biography

Quoc Hung Dang was born in Hanoi, Vietnam, in 1986. He received his Bachelor in Electrical & Electronic Engineering from Le Quy Don Technical University, Vietnam in 2010. In 2018, he received his Master of Electronic Engineering from The University of Adelaide, Adelaide, Australia. He was awarded the Adelaide Graduate Research Scholarship to pursue his Ph.D in the School of Electrical & Electronic Engineering, The University of Adelaide in Nov. 2018, under the supervisions of Prof. Christophe Fumeaux, Dr. Shengjian Jammy Chen and Assoc. Prof. Damith Chinthana Ranasinghe. His research interests include wearable, reconfigurable textile antennas, RFID-based wearable applications and material characterization.

During his candidature, he received a number of scholarship, travel grand including Adelaide Graduate Research Scholarship, the 2022 IEEE AP-S C. J. Reddy Travel Grant for Graduate Students and some Supplementary Scholarships. He was also the recipient of the Best Student Paper Award at the 2022 International Symposium on Antennas and Propagation (ISAP 2022). He has been student member of the Institute of Electrical and Electronic Engineers (IEEE), IEEE Young Professionals, IEEE Antennas and Propagation Society, and IEEE Microwave Theory and Techniques Society Membership since Feb. 2019. During Ph.D candidature, he has been involved in a sponsored project in partnership with a multi-national company (u-blox, based on Switzerland).

Quoc Hung Dang has served as a reviewer for a number of recognized journals and conference including *IEEE Transactions on Antennas and Propagation*, *IEEE Sensors Journal*, *Microwave and Optical Technology Letters* and the 2022 International Symposium on Antennas and Propagation Conference (ISAP2022).

Quoc Hung Dang
quochung.dang@adelaide.edu.au